frontiers | Research Topics

Advances in bacteriophage research & development with therapeutic applications

Edited by
Mercedes Gonzalez Moreno, Derry Keith Mercer and Silke Alt

Published in
Frontiers in Cellular and Infection Microbiology

ISSN 1664-8714
ISBN 978-2-8325-7318-1
DOI 10.3389/978-2-8325-7318-1

Generative AI statement
Any alternative text (Alt text) provided alongside figures in the articles in this ebook has been generated by Frontiers with the support of artificial intelligence and reasonable efforts have been made to ensure accuracy, including review by the authors wherever possible. If you identify any issues, please contact us.

About Frontiers

Frontiers is more than just an open access publisher of scholarly articles: it is a pioneering approach to the world of academia, radically improving the way scholarly research is managed. The grand vision of Frontiers is a world where all people have an equal opportunity to seek, share and generate knowledge. Frontiers provides immediate and permanent online open access to all its publications, but this alone is not enough to realize our grand goals.

Frontiers journal series

The Frontiers journal series is a multi-tier and interdisciplinary set of open-access, online journals, promising a paradigm shift from the current review, selection and dissemination processes in academic publishing. All Frontiers journals are driven by researchers for researchers; therefore, they constitute a service to the scholarly community. At the same time, the *Frontiers journal series* operates on a revolutionary invention, the tiered publishing system, initially addressing specific communities of scholars, and gradually climbing up to broader public understanding, thus serving the interests of the lay society, too.

Dedication to quality

Each Frontiers article is a landmark of the highest quality, thanks to genuinely collaborative interactions between authors and review editors, who include some of the world's best academicians. Research must be certified by peers before entering a stream of knowledge that may eventually reach the public - and shape society; therefore, Frontiers only applies the most rigorous and unbiased reviews. Frontiers revolutionizes research publishing by freely delivering the most outstanding research, evaluated with no bias from both the academic and social point of view. By applying the most advanced information technologies, Frontiers is catapulting scholarly publishing into a new generation.

What are Frontiers Research Topics?

Frontiers Research Topics are very popular trademarks of the *Frontiers journals series*: they are collections of at least ten articles, all centered on a particular subject. With their unique mix of varied contributions from Original Research to Review Articles, Frontiers Research Topics unify the most influential researchers, the latest key findings and historical advances in a hot research area.

Find out more on how to host your own Frontiers Research Topic or contribute to one as an author by contacting the Frontiers editorial office: frontiersin.org/about/contact

Advances in bacteriophage research & development with therapeutic applications

Topic editors

Mercedes Gonzalez Moreno — Leibniz Institute for Natural Product Research and Infection Biology, Hans Knoll Institute, Germany

Derry Keith Mercer — INCATE, Switzerland

Silke Alt — German Center for Infection Research (DZIF), Germany

Citation

Gonzalez Moreno, M., Mercer, D. K., Alt, S., eds. (2026). *Advances in bacteriophage research & development with therapeutic applications*. Lausanne: Frontiers Media SA. doi: 10.3389/978-2-8325-7318-1

Table of contents

frontiers | Frontiers in Cellular and Infection Microbiology

TYPE Editorial
PUBLISHED 10 December 2025
DOI 10.3389/fcimb.2025.1751637

OPEN ACCESS

EDITED AND REVIEWED BY
Costas C. Papagiannitsis,
University of Thessaly, Greece

*CORRESPONDENCE
Derry Mercer
derry.mercer@incate.net

RECEIVED 21 November 2025
ACCEPTED 26 November 2025
PUBLISHED 10 December 2025

CITATION
Gonzalez Moreno M, Alt S and Mercer D (2025) Editorial: Advances in bacteriophage research & development with therapeutic applications.
Front. Cell. Infect. Microbiol. 15:1751637.
doi: 10.3389/fcimb.2025.1751637

Editorial: Advances in bacteriophage research & development with therapeutic applications

Mercedes Gonzalez Moreno[1,2], Silke Alt[1,3] and Derry Mercer[1]*

[1]INCubator for Antibiotic Therapies Europe (INCATE), Basel, Switzerland, [2]Leibniz Institute for Natural Product Research and Infection Biology, Hans Knöll Institute, Jena, Germany, [3]Translational Project Management Office (TPMO), German Center for Infection Research (DZIF), Braunschweig, Germany

KEYWORDS

phage therapy, antimicrobial resistance, bacteriophage research, endolysin, artificial intelligence

Editorial on the Research Topic
Advances in bacteriophage research & development with therapeutic applications

Introduction

In response to the global crisis of antimicrobial resistance, phage therapy (PT) is emerging as alternative and complementary therapy to treat bacterial infections. Advances in genomics, synthetic biology and AI play a role in elevating the clinical potential of PT and phage-encoded proteins. The challenge of PT needs to progress beyond compassionate and individual use and address issues including standardized guidelines for phage susceptibility testing, dosing, manufacturing, storage requirements and regulations for clinical trials, to become an established and more broadly used therapeutic option. We are witnessing progress on some aspects, including formation of a working group by the European Committee on Antimicrobial Susceptibility Testing (EUCAST) to develop standardized guidelines for phage susceptibility testing.[1] Additionally, the European Medicines Agency (EMA) is preparing new guidelines on the development and manufacture of human medicinal products specific for PT.[2] In 2024 the Portuguese National Authority of Medicines and Health Products, announced the approval of a regulatory framework allowing administration of personalized phage products, following the Belgian model.[3,4]

1 https://www.eucast.org/ast-of-phages

2 https://www.ema.europa.eu/en/development-and-manufacture-human-medicinal-products-specifically-designed-phage-therapy-scientific-guideline

3 https://www.infarmed.pt/documents/15786/9697484/2024-11-15_Delibera%C3%A7%C3%A3o_112_CD_2024/d0424242-a103-1256-cd7d-526aaf12dfac

4 Jean-Paul Pirnay, Gilbert Verbeken, Magistral Phage Preparations: Is This the Model for Everyone?, Clinical Infectious Diseases, Volume 77, Issue Supplement_5, 1 November 2023, Pages S360–S369, https://doi.org/10.1093/cid/ciad481

The growing momentum in phage research over the last two decades is contributing to this progress and is paving the way for PT to become a reality.

This Research Topic brings together eleven articles and one correction that collectively contribute to expanding the evidence and understanding of several critical aspects of PT to advance its implementation.

Structural and functional phage biology

Understanding phage structure, host specificity, lytic mechanisms and the functional role of phage-derived proteins (e.g. endolysins) should contribute to the development of effective phage-based therapies. Three articles in this Research Topic contribute key insights into these crucial aspects.

Khan et al. provides structural analysis of the *Salmonella*-infecting phage Epsilon15, offering detailed characterization of its DNA packaging system and injection apparatus, alongside the functional analysis of its encoded endolysin LysSA05. Bioinformatic and machine learning analyses identified an amphipathic α-helical region within LysSA05 with antimicrobial peptide-like properties, likely responsible for mediating outer membrane interaction and translocation of the catalytic domain to peptidoglycan, a dual function potentially enhancing the enzyme's efficacy against Gram-negative pathogens. LysSA05 demonstrated antibacterial activity against multidrug-resistant clinical isolates of *E. coli* and *Salmonella* spp., supporting its therapeutic potential.

Ning et al. addressed the evolutionary dynamics of *E. coli* phage BW-1, investigating whether this phage can expand their host range through experimental evolution. Their findings suggest that host-switching is limited, and when adaptation occurs, it is genetically constrained, and may come with fitness costs (infectivity or virulence). The authors suggest that there is a reduced risk of therapeutic phages evolving to infect non-target or beneficial gut bacteria.

Alsaadi et al. performed a prophage analysis of 44 P. *aeruginosa* isolates, revealing high diversity with most prophages classified as novel genera and lacking antimicrobial resistance or virulence genes. Many encoded different anti-phage defence mechanisms. This demonstrates prophage genomics can help to predict resistance trends and optimize treatment strategies.

Selection, optimization, and production

The success of PT depends on identification of effective phages rational cocktail design, and scalable production and optimization strategies, amongst others. Four articles in this Research Topic highlight advances and challenges in these areas.

Rieper et al. tackled the challenge of phage selection, aiming to determine the best strategies for evaluating their therapeutic potential. Their study compared double agar overlay plaque assay and planktonic killing assay to assess the host range and lytic efficacy of a diverse range of lytic phages against clinical *P. aeruginosa*. Their findings highlight the need for standardised and rigorous testing protocols and the integration of *in silico* tools for optimal phage selection.

Doud et al. offer a forward-looking perspective, exploring how AI can be leveraged to improve PT. The authors discuss recent AI advances that enable the prediction of phage-host compatibility, discovery of functional phage genes, and rational engineering of synthetic phages, but emphasize the need for experimental validation.

Ramirez-Garcia et al. present a novel antimicrobial approach base on P4 and P2 bacteriophages engineered as phage-like transducing particles that carry a genetically encoded multi-lysin cassette instead of viral DNA. These virus-free particles cannot replicate and offer controllable expression of lytic proteins inside bacteria. The authors achieved high-yield production through bioprocess optimization and showed antimicrobial activity against *E. coli* in pure culture and a co-culture infection model.

Kulkarni et al. contribute a perspective that proposes synthetic cells as programmable and modular platforms for bacteriophage production, control and delivery, moving beyond the constraints of traditional bacterial hosts. The authors further envision the integration of these synthetic cells within smart antimicrobial materials, and outline the direction toward AI and microfluidics-driven platforms that could enable predictive phage–host modelling, high-throughput screening and personalized PT workflows.

Preclinical and clinical applications

Current knowledge gaps exist on different clinical aspects in PT such as appropriate dosage, route and frequency of administration, concomitant use of antibiotics, phage resistance, immunogenicity and phage pharmacokinetic properties to better guide clinical implementation. Together, three studies in this Research Topic offer a view of PT's translational journey.

Zhu et al. assessed the combined efficacy of the lytic phage HZJ31 with tigecycline against carbapenem-resistant *K. pneumoniae in vitro* and in *Galleria mellonella* larvae, demonstrating synergistic effects, significantly enhancing bacterial suppression and improving survival outcomes *in vivo*. Characterization of phage-resistant bacteria revealed trade-offs leading to reduced virulence and increased sensitivity to piperacillin and gentamicin, supporting the potential of phage-antibiotic combination therapies.

Peez et al. investigated the application of phage in a sheep model of fracture-related infection caused by *S. aureus*, comparing intravenous versus local phage delivery. This study revealed key pharmacokinetic aspects in this preclinical model, especially the challenges of phage neutralization and rapid bloodstream clearance, that can limit therapeutic efficacy.

Wahl et al. reported a clinical case of co-administration of phages for successful antibiotic suppression therapy in a

periprosthetic hip and knee joint infection caused by MRSA. Infection persistence led to consideration of PT. Successful outcomes illustrated PT as a valuable adjunct to suppress infection but exposed the logistical challenges in facilitating therapy.

Regulatory perspectives

The increasing body of clinical data on PT is driving progress in adapting regulatory frameworks and creating new pathways that address specific characteristics of phage therapeutics.

Fürst-Wilmes et al. provided a comprehensive overview of the current regulatory landscape for PT in Europe, highlighting key developments on manufacturing standards, quality criteria and adaptations of pharmaceutical legislation to PT.

Conclusions

Collectively, these articles reflect the diverse and rapidly advancing landscape of PT and underscore the multidisciplinary and collaborative effort needed to bring it to clinical reality.

Author contributions

MM: Writing – review & editing, Investigation, Supervision, Formal analysis, Project administration, Writing – original draft, Conceptualization. SA: Supervision, Investigation, Conceptualization, Writing – original draft, Writing – review & editing, Formal analysis, Project administration. DM: Supervision, Conceptualization, Writing – review & editing, Writing – original draft, Formal analysis, Project administration.

Conflict of interest

The author(s) declared that this work was conducted in the absence of any commercial or financial relationships that could be construed as a potential conflict of interest.

Generative AI statement

The author(s) declared that generative AI was not used in the creation of this manuscript.

Any alternative text (alt text) provided alongside figures in this article has been generated by Frontiers with the support of artificial intelligence and reasonable efforts have been made to ensure accuracy, including review by the authors wherever possible. If you identify any issues, please contact us.

Publisher's note

frontiers | Frontiers in Cellular and Infection Microbiology

TYPE Original Research
PUBLISHED 04 April 2025
DOI 10.3389/fcimb.2025.1547250

OPEN ACCESS

EDITED BY
Mercedes Gonzalez Moreno,
Hans Knoll Institute, Germany

REVIEWED BY
Catherine Maylin Loc-Carrillo,
The University of Utah, United States
Malgorzata Barbara Lobocka,
Polish Academy of Sciences, Poland

*CORRESPONDENCE
T. Fintan Moriarty
fintan.moriarty@aofoundation.org

†These authors have contributed equally to this work and share first authorship

RECEIVED 18 December 2024
ACCEPTED 19 March 2025
PUBLISHED 04 April 2025

CITATION
Peez C, Chen B, Henssler L, Chittò M, Onsea J, Verhofstad MHJ, Arens D, Constant C, Zeiter S, Obremskey W, Trampuz A, Raschke MJ, Zalavras C, Metsemakers W-J and Moriarty TF (2025) Evaluating the safety, pharmacokinetics and efficacy of phage therapy in treating fracture-related infections with multidrug-resistant *Staphylococcus aureus*: intravenous versus local application in sheep. *Front. Cell. Infect. Microbiol.* 15:1547250. doi: 10.3389/fcimb.2025.1547250

Evaluating the safety, pharmacokinetics and efficacy of phage therapy in treating fracture-related infections with multidrug-resistant *Staphylococcus aureus*: intravenous versus local application in sheep

Christian Peez[1,2†], Baixing Chen[2,3,4†], Leopold Henssler[2,5], Marco Chittò[2], Jolien Onsea[3,4], Michael H. J. Verhofstad[6], Daniel Arens[2], Caroline Constant[2], Stephan Zeiter[2], William Obremskey[7], Andrej Trampuz[8], Michael J. Raschke[9], Charalampos Zalavras[10], Willem-Jan Metsemakers[3,4] and T. Fintan Moriarty[2*]

[1]Department of Trauma, Hand and Reconstructive Surgery, University Hospital Münster, Münster, Germany, [2]AO Research Institute Davos, Davos, Switzerland, [3]Department of Trauma Surgery, University Hospitals Leuven, Leuven, Belgium, [4]Department of Development and Regeneration, KU Leuven, Leuven, Belgium, [5]Department of Trauma Surgery, University Hospital Regensburg, Regensburg, Germany, [6]Trauma Research Unit, Department of Surgery, Erasmus MC, University Medical Center Rotterdam, Rotterdam, Netherlands, [7]Center for Musculoskeletal Research, Vanderbilt University Medical Center, Nashville, TN, United States, [8]Queensland University of Technology, Brisbane, QLD, Australia, [9]Department of Trauma, Hand and Reconstructive Surgery, University Hospital Muenster, Muenster, Germany, [10]Department of Orthopaedic Surgery, Los Angeles General Medical Center & Keck School of Medicine, University of Southern California, Los Angeles, CA, United States

Background: Fracture-related infections (FRI), particularly those caused by antibiotic resistant *Staphylococcus aureus*, present significant clinical challenges due to the formation of biofilm on the implanted device, and reduced options for conventional antibiotic treatment. Bacteriophage (phage) therapy (PT) offers a targeted approach to managing such infections, however, evidence for pharmacokinetics and optimal route of administration is limited for FRI. This study aimed to evaluate safety, phage distribution kinetics, phage neutralization, and antibacterial efficacy after intravenous or local administration in a sheep model.

Methods: The study was conducted in two phases: Phase 1 assessed the safety and distribution of two successive rounds of intravenous and local phage administration in non-infected sheep, while Phase 2 evaluated the therapeutic efficacy of intravenous versus local phage administration in combination with intravenous vancomycin in treating MRSA-induced FRI (tibial osteotomy with plate fixation). The specific pathogen and phage used in the sheep were both taken from a human FRI patient treated with PT. Phage neutralization and phage distribution were the primary outcomes measured in both phases of the sheep study.

Results: Both intravenous and local phage administration were well-tolerated in non-infected sheep. Phages were cleared rapidly from circulation after intravenous administration, with no phage detected after 240 minutes. Phage neutralization increased during PT, peaking at 99.9% in non-inoculated sheep by the end of the second phage treatment (day 50). In infected sheep, phage neutralization levels reached a maximum of 99.9% earlier (day 13), with no significant differences between intravenous and local administration. The bacterial load was not significantly changed by PT, either IV or locally applied.

Conclusions: PT is a safe adjunct to antibiotic treatment for FRI, however, phage neutralization developed rapidly and was accelerated in infected hosts. Further research is required to optimize phage selection, dosing, and delivery methods to enhance its therapeutic potential as an adjunct to conventional antibiotic therapy, particularly in the face of challenges such as rapid clearance and phage neutralization.

KEYWORDS

bacteriophage, fracture related infection, MRSA, pharmacokinetics, administration, neutralization, osteomyelitis, *Staphylococcus aureus*

1 Introduction

Fracture-related infection (FRI) represents a significant clinical challenge, particularly in the presence of antibiotic-resistant bacteria and biofilms, leading to prolonged hospital stays, repeated surgeries, high recurrence rates and, in severe cases, amputation or even death (Moriarty et al., 2022; Metsemakers et al., 2023a). Methicillin-resistant *Staphylococcus aureus* (MRSA) is an important causative pathogen in these infections, further complicating treatment and worsening patient outcomes (Morgenstern et al., 2021). Central to the treatment of FRI are biofilms, which are complex communities of bacteria that adhere to surfaces and are encased in a self-produced protective extracellular matrix (Khatoon et al., 2018). Growth in biofilm helps bacteria evade immune defenses and exhibit tolerance to antibiotics (Masters et al., 2019). Standard procedures for managing FRI involve surgical debridement, irrigation, implant removal, and prolonged antibiotic administration (Metsemakers et al., 2020). Despite these extensive efforts, the recurrence rates remain high, necessitating the exploration of alternative and adjunctive therapies (Lebeaux et al., 2014).

Bacteriophages, or phages, are viruses that specifically infect and lyse bacterial cells, offering a targeted approach to eradicating infections (Onsea et al., 2020). Recent case reports and small-scale clinical studies have shown encouraging results for phage therapy (PT), including for antibiotic-resistant infections and orthopaedic device-related infection (Uyttebroek et al., 2022). A review of 137 human patients who received phage therapy for orthopedic infections reported that direct local instillation was the most commonly used method (35.0%). This is followed by combined intravenous and intra-articular delivery (16.1%), combined intra-articular and direct local delivery (16.1%), and intravenous delivery alone (15.3%) (Young et al., 2024). While local administration ensures high concentrations of phages directly at the infection site, this approach increases the risk of superinfection when percutaneous drains are left *in situ* for multiple days to facilitate repeat dosing (Onsea et al., 2019). In contrast, local administration may delay some of the potential side effects associated with IV administration, such as immune-mediated neutralization (Suh et al., 2022; Le et al., 2023).

The titer of phage reaching infected musculoskeletal tissues is poorly understood for both modes of administration. There is also uncertainty on how antibacterial efficacy compares between local and IV administration of PT. To address these knowledge gaps, we performed a series of PT investigations in a large animal model of FRI. The phage and pathogen (more information can be found in the Methods section) were selected from a successful PT case in a human patient (Onsea et al., 2021b) and transferred to a large animal model to provide the best possible recapitulation of the key factors involved in PT in FRI: size of the animal, volume of phage applied, and use human implants to fix an osteotomy. The large animal study was performed in two phases, both of which compared IV with local administration: Phase 1 focusing on safety and distribution in non-infected sheep, and Phase 2 focusing on therapeutic efficacy in sheep with established MRSA FRI. Primary outcome measures were phage distribution and phage neutralization, with secondary outcome being antibacterial efficacy in phase 2. The overall goal is to provide more evidence and data for PT in FRI, contributing to more effective and safer PT protocols for clinical use.

2 Methods

2.1 Bacterial strains and inoculum preparation

This patient from whom the pathogen was cultured was included in the PHAGEFORCE study (NCT06368388) which aims to standardize PT and prospectively collect data on patients (Onsea et al., 2021b). In brief, the patient suffered from an FRI after a Gustilo-Anderson type II open tibia fracture. Despite multiple surgical revision procedures and multiple courses of antibiotic treatment, the infection persisted. Deep tissue cultures showed the presence of MRSA (MRSA MSI-003), resistant to oxacillin, levofloxacin, gentamicin, tobramycin, erythromycin, clindamycin, minocycline, and rifampicin. The Coordination group for Bacteriophage therapy Leuven (CBL) considered previous surgical and antibiotic treatments as adequate and maximal, thereby deeming the patient eligible for PT. During a surgical debridement, a draining system was placed and based on susceptibility testing, the patient received 20 mL of single phage ISP (10^7 PFU/mL) three times per day for 10 days postoperatively. The patient simultaneously received antibiotic treatment for a total duration of three months. No adverse events were reported during PT. After cessation of treatment and over three years in follow-up, the infection did not recur.

Given the successful clinical outcome observed in the patient treated with single phage ISP, this study aimed to further investigate the safety, pharmacokinetics and efficacy of PT using a large animal model with the same pathogen and phage. MRSA MSI-003 was kept at -20°C in a 25% glycerol solution for long-term storage. Bacteria were grown on tryptic soy agar (TSA, Sigma-Aldrich, Steinheim, Germany) and an overnight culture of MRSA MSI-003 was prepared in 20 ml tryptic soy broth (TSB, Sigma-Aldrich, Steinheim, Germany) at 37°C one day before animal surgery. A fresh logarithmic phase culture was prepared in TSB from the overnight culture. Bacteria were centrifuged at 3220 × g for 10 min (Thermo fisher) and washed twice in phosphate buffered saline (PBS, Sigma-Aldrich, St. Louis, MO, USA) 1.5h prior to surgery and diluted in PBS to obtain a target inoculum of 2.0×10^6 CFU/mL. A total of 1mL of this suspension was used to inoculate the osteotomy site and induce infection. The bacteria were applied within 30 minutes of the inoculum preparation. Immediately after inoculum preparation, the number of bacteria present in each inoculum was quantified by plating a dilution series into TSB at 37°C.

2.2 Overview of animal study

Institutional review board approval for the animal study was granted by the Ethical Committee of the Canton of Grisons in Switzerland (approval number: GR 10_2023). The experiments were conducted in an Association for Assessment and Accreditation of Laboratory Animal Care (AAALAC) approved facility, adhering to Swiss laws and regulations for animal protection. A total of 16 skeletally mature (2 to 4 years old) female Swiss Alpine sheep were included in this study. Prior to enrolment, each sheep underwent a physical examination and radiographic screening to ensure the tibial canal accommodated the intramedullary nail. In addition, a complete blood count was obtained from the internal jugular vein to exclude the presence of preoperative inflammation. The sheep were group housed for at least 2 weeks before surgery to acclimatize to the housing conditions. They were kept in an environment with daily cycles of 12 hours of light and dark and were fed twice per day with hay fed ad libitum, a mineral lick, and hand-fed grain.

The study was conducted in two phases: Phase 1 assessed phage tolerability, pharmacokinetics, and neutralization in non-infected sheep, while Phase 2 evaluated all of the above plus the safety and efficacy of PT in treating MRSA-induced FRI. An overview of the study design is shown in Figure 1.

Sheep in Phase 1 did not have any fracture or infection but had a filtration probe to collect fluids in the intramedullary canal of the tibia. Twenty mL of phage ISP (10^9 PFU/mL) suspension was administered in two rounds, three times per day, each lasting 10 days, with a 28-day interval between each round. The phage titer was adapted from previous studies of PT in *S. aureus* infections in rabbit and mouse models (Wills et al., 2005; Capparelli et al., 2007; Kishor et al., 2016). Group 1 (n=3) received phages intravenously (IV), and Group 2 (n=3) received phages by instillation through drainage (local). All sheep received an identical total phage titer regardless of route of administration. The animals were housed for an additional 2 days (a total of 50 days) after the cessation of the second PT to continue drawing serum samples and measuring residual phage and phage neutralization after euthanasia.

Sheep in Phase 2 had an FRI of the tibia (in the setting of plate fixation) caused by a human-isolated *S. aureus* (MRSA MSI-003). After three weeks, a revision surgery was conducted, which involved debridement and irrigation, as well as the placement of filtration probes within the intramedullary canal of the tibia. Following the revision surgery (on day 21), all sheep in phase 2 received systemic treatment with vancomycin administered as an intravenous infusion over the course of one hour, three times daily, for a duration of ten days (1g per sheep, Sandoz Pharmaceuticals AG, Rotkreuz, Switzerland). Sheep in phase 2 were divided into 3 groups, (n=3 per group): Group 3 received 20 mL of phage ISP (10^9 PFU/mL) intravenously; Group 4 received 20 mL of phage ISP (10^9 PFU/mL) locally; group 5 served as the control group without any phage application. Both groups 3 and 4 received phages three times daily for 10 days. After a two-day washout period to prevent false negatives, the sheep were euthanized 33 days after the first surgery which involved the induction of the FRI.

2.3 Surgical procedure and group allocation

2.3.1 Phase 1

After anaesthesia and aseptic preparation of the right tibia, the intramedullary (IM) canal was exposed through an intramedullary nailing approach medial to the patellar ligament. A guide wire was

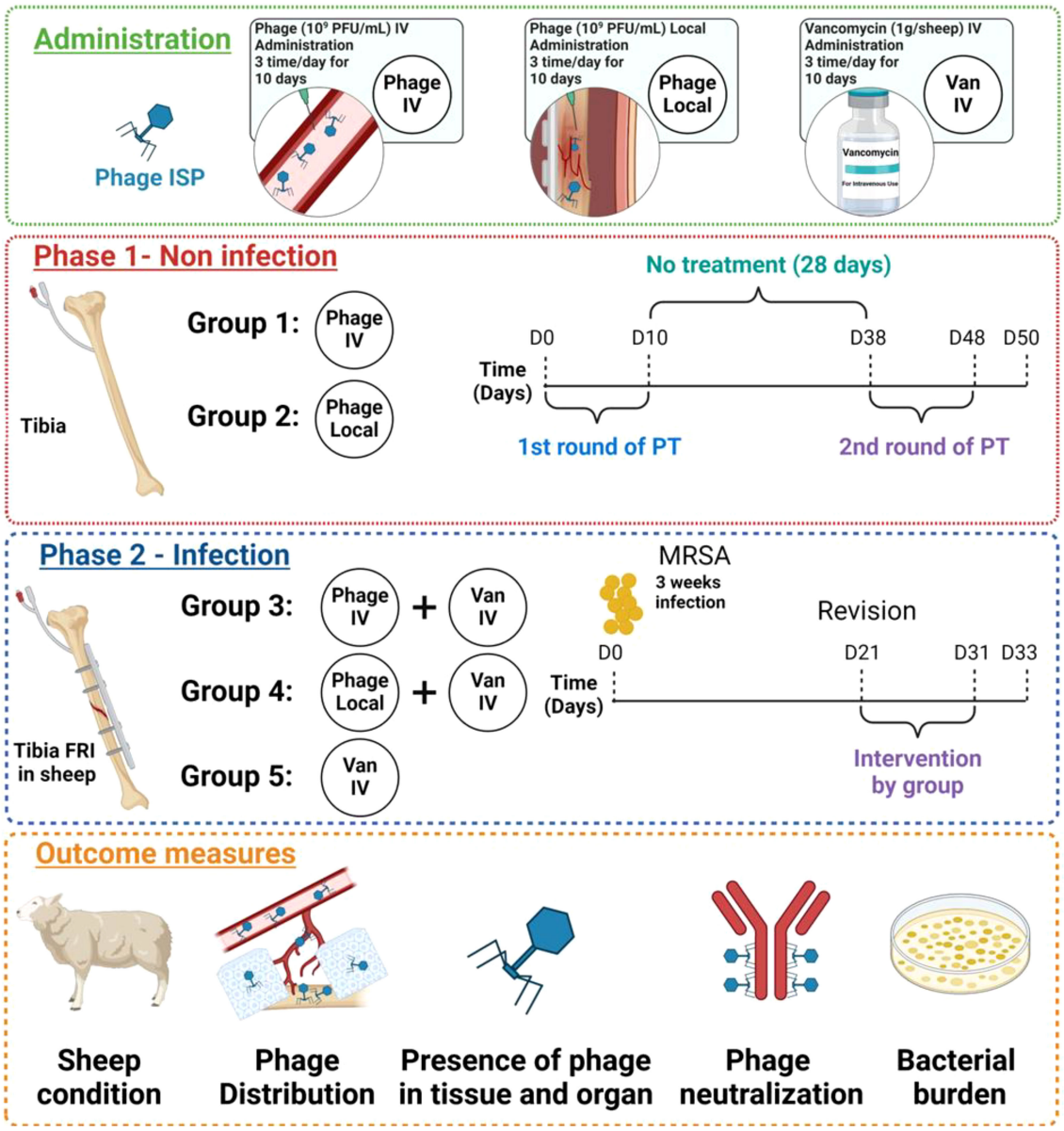

FIGURE 1
Overview of study design. Phased experimental protocol for administering phage therapy (PT) and vancomycin (Van) in sheep, depicting both non-infection and infection phases. The green box describes three treatments, including phage intravenous administration, phage local administration, and vancomycin intravenous administration. The red box is Phase 1 (Non-infection): Groups receive treatments by specific administration routes, Group 1 received intravenous phage administration, and Group 2 received phage instillation through a drainage tube (local). Groups 1 and 2 initially received 10 days of PT (1st round), followed by a subsequent 28-day no-treatment interval. This is then succeeded by a second 10 days of PT (2nd round), concluding on Day 50. The blue box is Phase 2 (Infection): The sheep included in this phase received osteotomy, plate and screw osteosynthesis, and were infected with MRSA MSI-003 at day 0. Revision surgery was performed at day 21 after which they received a combination of intravenous phage and intravenous vancomycin for group 3, a combination of local phage and intravenous vancomycin for group 4, and intravenous vancomycin only for group 5. These treatments continued for 10 days, followed by a two-day wash-out period, leading up to a final evaluation through euthanasia and sample collection at day 33. The orange box is outcome measures, including the general condition of the sheep, the distribution of phage within the body, the presence of phage in tissues and organs, the bacterial burden in infected areas, and the level of phage neutralization.

inserted at the anterior edge of the tibial plateau, aiming down the tibial crest and thus the centre of the IM canal. The tibial cortex was opened using a cannulated awl over the previously placed guide wire, followed by insertion of a custom-sized filtration probe (Bioanalytical Systems, West Lafayette, IN) into the in IM canal under fluoroscopic guidance (Supplementary Figure S1). For those sheep receiving local PT, a separate drainage system (Bioanalytical Systems, West Lafayette, IN) was installed through the same incision and tunneled to exit laterally. The probes were secured with Chinese finger trap sutures, and the area was closed in three layers with absorbable suture material (#3-0 non-cutting and cutting Monocryl, Ethicon), followed by protective gauze and

bandages. Group 1 (n=3) received phage ISP (20 mL, 10^9 PFU/mL) intravenously, and Group 2 (n=3) received phage ISP (20 mL, 10^9 PFU/mL) locally, both treatments being administered three times daily for 10 days. The first round of PT involved replacing the collection drainage bottle of the ultrafiltration probe three times daily for 10 days, followed by storage at 4°C. Post-therapy, all devices were removed, followed by bacterial quantification to exclude bacterial contamination. After four weeks, revision surgery was performed, involving similar preparatory steps to re-expose the tibial area and adjust or reinstall the necessary medical devices. This phase included two 10-day rounds of PT, separated by a 28-day interval without treatment, spanning from Day 0 to Day 50.

2.3.2 Phase 2

The preparatory steps for Phase 2 were similar to those in Phase 1, with additional surgical procedures to secure a 10-hole, 5.5 mm steel plate (DePuy Synthes) on the tibia with locking screws and perform a transverse osteotomy with a 2 mm gap, which was inoculated with 1mL of MRSA MSI-003 ($2x10^6$ CFU/mL) to induce infection (Siverino et al., 2023). Post-surgery, sheep were supported in slings to reduce stress on the tibia. After 21 days, the surgical site was reopened, a formal debridement was performed to remove infected tissue for analysis, and the plate was retained. The bone and implant were flushed with 1 L of saline (0.9%) and fluid was collected for bacteriological culture. The filtration probe and drainage system setup (Supplementary Figure S1), as described in Phase 1, was applied to Group 3 (n=3) and Group 4 (n=3). Group 3 received a combination of intravenous phage ISP (20 mL, 10^9 PFU/mL, 3 times) and intravenous vancomycin (1g per sheep every 8 hours). Group 4 received local phage ISP (20 mL, 10^9 PFU/mL, 3 times) with intravenous vancomycin (1g per sheep every 8 hours), while Group 5 (control, n=3) received only intravenous vancomycin (1g per sheep every 8 hours). PT was scheduled 21 days after initial surgery, and assessments were conducted until Day 33.

2.4 Phage preparation

ISP, a single phage targeting *S. aureus* was used with permission from the Eliava Institute, Georgia. The ability of ISP to infect MRSA MSI-003 was confirmed. Phage preparation was conducted using the double-agar overlay method. Initially, the bacterial strain was cultured overnight in TSB broth at 37°C. Bacteriophages were then diluted in Dulbecco phosphate buffer saline (DPBS, [2.7 mM Potassium Chloride (KCl), 1.5 mM Potassium Phosphate monobasic (KH2PO4), 137.9 mM Sodium Chloride (NaCl), 8.1 mM Sodium Phosphate dibasic (Na2HPO4-12H2O)]) buffer and 100 µL of the phage dilution was mixed with 100 µL of bacterial suspension (MRSA MSI-003), combined with 4 mL of TSA soft agar (3% TSB and 0.6% agar), and poured onto TSA plates. These plates were incubated at 37°C overnight. After incubation, the phages were harvested by covering the top layer of the plates with 5 mL of DPBS and placing them overnight at 4°C. The upper liquid layer was then transferred into a 50 mL Falcon tube. The suspension was centrifuged at 3260 rpm, 4°C for 10 minutes, and the supernatant was subsequently filtered through 0.45 µm and then 0.22 µm filters (Millex, Merck Millipore, Ireland). To further purify and concentrate the phages, the supernatant was filled in Spectra/Por® 7 dialysis membranes with 100,000 Da molecular weight cutoff (Spectrum Laboratories, Inc., Rancho Dominguez, CA, USA) to dialyze over three days at 4°C. Ultrafiltration was then performed using an Amicon filter (Millipore Sigma) with a 100 kDa cut-off. The phage titer was finally determined using a double agar overlay method to ensure the titer was appropriate (10^{10} PFU/mL) for subsequent experimental applications.

2.5 Phage pharmacokinetics and quantification *in vivo*

For Phase 1, blood samples (10ml) from Groups 1 and 2 were collected at 5, 30, 60, 120, 240, and 360 minutes after phage administration on days 1, 5, and 10 during first round of PT, and on days 38, 42, and 47 during second round of PT via a central venous catheter in the internal jugular vein. For Phase 2, blood samples from Groups 3, 4 and 5 were collected at 5, 30, 60, 120, 240, and 360 minutes after phage administration on days 1, 5, and 10 during PT. The active phage titer was determined by the double agar overlay method. Briefly, an aliquot of blood was centrifuged at 3220 × g for 10 min at 4°C to pellet cells and debris. The plasma was collected and filtered through a 0.45 µm filter and then through a 0.22 µm to remove debris and bacteria. Subsequently, 100 µL of the filtrate was mixed with 100 µL of bacterial suspension (MRSA MSI-003) and added to 4 ml of soft agar. The mixture was transferred to the TSA plate after gently mixing and we counted the plaque-forming units after overnight incubation in a 37 °C incubator. All experiments were performed in triplicate.

Routine evaluation of phage titer entailed the daily collection of plasma and draining fluid samples each morning prior to the commencement of daily PT to monitor baseline phage titers. At euthanasia, additional titers were taken from tissues as outlined below. Sheep were euthanized at day 50 for Phase 1 and at day 33 for Phase 2. The bone (i.e. osteotomy, proximal bone, distal bone and bone marrow), soft tissue and organs, including lung, kidney, liver, spleen, iliac lymph nodes, and popliteal lymph nodes were harvested (approximately 20g total for each sample). Three samples were randomly taken from each organ and homogenized (Omni TH, tissue homogenizer TH-02/TH21649) in 20 mL of sterile PBS. The plate and screws were removed from the bone, transferred into a glass tube containing 20 ml PBS and sonicated in an ultrasonic water bath (Model RK 510H, Bandelin electronic GmbH & Co. KG, Berlin, Germany) for 10 min. An aliquot of each tissue sample and sonication fluid from the implant was centrifuged at 3220 × g for 10 min at 4°C to pellet cells and debris. The plasma, draining fluid and supernatant were collected and filtered through a 0.45 µm filter and

then through a 0.22 μm filter (Millex, Merck Millipore, Ireland) to remove debris, bacteria and small contaminants. The active phage titer was determined by the double agar overlay method as mentioned above.

2.6 Phage neutralization assay

Phage neutralization in the serum was determined by a modified version of the phage-neutralization assay as previously described (Chen et al., 2023). Briefly, 900 μL of serum, diluted at a 1:100 ratio, was mixed with 100 μL of phage ISP (10^7 PFU/ml). This mixture was incubated at 37 °C for 30 minutes. Following incubation, the mixture was further diluted by a factor of 1000 using 0.9% saline. The phage titer was then determined using the double-agar overlay technique as outlined above. The percentage of phage particles neutralized was calculated using the formula: (P0 - P1)/P0 × 100%, where 'P1' represents the phage titer post-serum incubation at the time of euthanasia, and 'P0' was the titer after incubation with serum obtained before the initial surgery.

2.7 Bacterial quantification

The bone (i.e. osteotomy, proximal bone, distal bone and bone marrow), soft tissue adjacent to the plate and bone and organs, including lung, kidney, liver, spleen, iliac lymph nodes, and popliteal lymph nodes were collected in Phase 2 at euthanasia to quantify bacterial load. In particular, the bacterial load was examined for the FRI site separately for its subdivisions - soft tissue, osteotomy, and implant - to assess the overall effect of the phage therapy and its efficacy in different tissues/materials. These samples underwent ten-fold serial dilutions and plated on 5% horse blood agar plates (BA, Oxoid Ltd., Hampshire, United Kingdom). The plates were incubated at 37°C, and bacterial colonies were quantified after 24 hours. Plates were also monitored at room temperature for another 24 hours to check for slow-growing colonies or potential contaminants by Staphaurex plus latex agglutination test (Thermo Scientific).

2.8 Statistical analysis

All experiments were conducted in triplicate, with each test being repeated three times, and the results were expressed as mean ± standard deviation. Descriptive and statistical data analysis was performed and visualized using GraphPad Prism 9 (GraphPad Software). The Shapiro-Wilk test was employed to assess the normality of continuous data, while the homogeneity of variances was evaluated using Levene's test. For parametric data, group differences were analyzed using Student's t-test or a one-way ANOVA. For nonparametric data, the Kruskal-Wallis test or Mann-Whitney U test was applied. Tukey posttest was performed to compare more than two groups. For all tests, p-value < 0.05 was considered statistically significant.

3 Results

3.1 Phase 1: phage therapy for non-infected sheep

3.1.1 Animal welfare and safety

Six sheep were included in Phase 1. Postoperatively, the sheep recovered well after each surgery. In general, there was no significant difference in weight change between the two groups. Both groups maintained stable weights throughout the study, with no notable weight loss observed (Supplementary Figure S2A). Moreover, no distinct pattern could be observed for white blood cell counts (WBC) between two groups at each time point (Supplementary Figure S2B).

3.1.2 Phage titer in plasma in healthy sheep

In case of intravenous administration, a rapid decline (4 $\log_{10}$ reduction) was observed within the first 5 minutes and this rapid decrease continued, leading to undetectable levels within 6 hours (Figure 2). A similar trend of phage distribution was observed in the second round of PT given intravenously, although phages reached undetectable levels sooner, within 4 hours (Figure 2). The decrease in active phage particles was even more pronounced after several administrations had been performed in the second round of applications (Figure 2).

The distribution of the phage in the serum was also analyzed following local administration, however, no active phage was detected in the serum at any time over a period of 6 hours.

3.1.3 Phage titers in tissue in healthy sheep

No viable phages were detected in the draining fluid or plasma collected before daily PT administration for either intravenous or local administration during the first and second rounds of therapy, as determined by the double agar method. Additionally, during the final evaluation after euthanasia, no viable phages were found in the soft tissue, bone, implant, lung, kidney, liver, spleen, iliac lymph nodes, or popliteal lymph nodes for either intravenous or local administration, as confirmed by the double agar method.

3.1.4 Phage neutralization in healthy sheep

Initially, the serum from healthy sheep with both intravenous and local administrations showed a rapid increase in presumptive anti-phage antibodies (indicated by neutralized phage particles) after the first round of PT, with levels peaking at approximately 60% by day 10. During the subsequent 28-day no-treatment period, local administration showed a significant decline ($p<0.05$) in phage neutralization, dropping to approximately 30% by day 24 and further decreasing to approximately 20% by day 38. In contrast, the intravenous administration maintained a relatively stable phage neutralization during the no-treatment period, stabilizing at approximately 50% by day 38.

The second round of PT, beginning at day 38, showed a rapid increase in phage neutralization for both administration routes, from days 38 to 42, with IV administration demonstrating a

significantly faster increase in phage neutralization compared to local administration. It rose to approximately 99.9% by the end of the second round on day 48 and was broadly equivalent for both local and IV at this time (Figure 3).

3.2 Phase 2: phage therapy for infected Sheep

3.2.1 Animal welfare and safety

Nine sheep were planned for inclusion in Phase 2. One sheep from the vancomycin-only control group died due to oesophageal obstruction, and a replacement sheep was introduced. All sheep recovered well postoperatively after each surgery. In general, there was no consistent difference regarding weight change or WBC counts among the 3 groups throughout the study duration (Supplementary Figure S3). However, a slight increase in WBC counts was observed at the revision time point (d21) in animals that received phage IV and vancomycin IV, as shown in Supplementary Figure S3B. This increase was not statistically significant, though it may indicate a response to the surgical procedure or the infection status at that point (Supplementary Figure S3B).

3.2.2 Infection burden after phage therapy

The bacterial load at euthanasia was assessed across different tissue locations: soft tissue, osteotomy, and implant, for each animal. In the soft tissue, osteotomy site and implant, both PT routes achieved variable bacterial load reduction when compared to sheep receiving vancomycin only, however, the differences were not statistically significant (Figure 4). Additionally, bacterial load was evaluated across distinct anatomical segments of bone, including the proximal and distal regions as well as the bone marrow. However, no significant difference was observed across different bone locations (Supplementary Figure S4).

3.2.3 Phage titer in plasma in infected sheep

The phage titer in the plasma of sheep subjected to local PT combined with intravenous vancomycin, as well as sheep administered intravenous PT combined with intravenous vancomycin, was assessed to determine the distribution of phages. There was a significant reduction in phage concentration (4 $\log_{10}$) within the first 5 minutes after intravenous PT, and a continued rapid decline in phage concentration within the first few hours post-therapy, leading to near-undetectable levels within 6 hours (Figure 5). There was no significant change in active phage count after repeated phage administration (day 5 and 10) compared with the first administration (day 1). Moreover, no active phage was detected in the plasma at any time during the 6 hours after local PT.

3.2.4 Phage titers in tissue in infected sheep

No viable phages were detected in the draining fluid or plasma collected before daily PT administration for either intravenous or

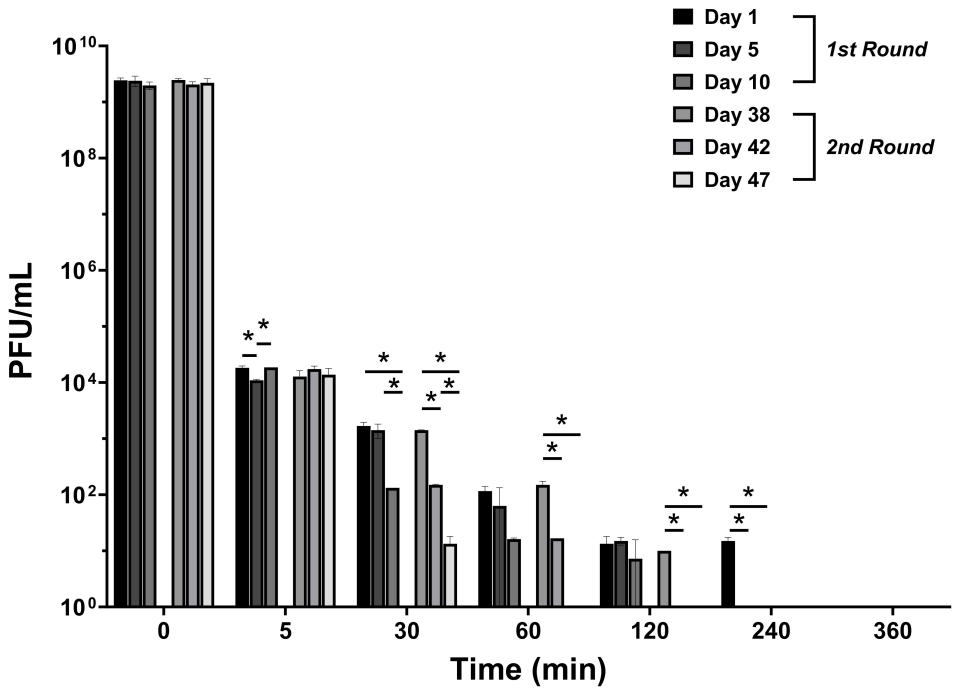

FIGURE 2
Phage distribution in serum after the first and the second round of intravenous administration. Measurements were taken at 5, 30, 60, 120, 240, and 360 minutes. The titer of phage administered intravenously and locally was 10^9 PFU/mL for both. PFU, Plaque-forming unit. The data were presented as mean ± standard deviation of results, and statistical significance was determined using a one-way ANOVA test followed by Tukey posttest, *$p < 0.05$. The data for the local administration are not shown in this figure as phage titers were below the detectable limit. The detection limit of the assay used to quantify active phage was 10 PFU/mL.

local administration during PT, as determined by the double agar method. Additionally, during the final evaluation after euthanasia, no viable phages were found in the soft tissue, bone, implant, lung, kidney, liver, spleen, iliac lymph nodes, or popliteal lymph nodes for either intravenous or local administration, as confirmed by the double agar overlay method.

3.2.5 Phage neutralization in infected sheep

Initially, both administration routes resulted in a gradual increase in phage neutralization. By day 3, local administration reached approximately 16.4% neutralization, while intravenous administration reached approximately 7.2%. As the experiment progressed, both administration routes resulted in an increase in phage neutralization. By day 7, local administration reached approximately 53.7% neutralization, and intravenous administration approximately 57.2%. The trends continued upward, with local administration reaching about 93.7% and IV administrations at about 90.5% by day 10 at the end of PT. After a 3-day hiatus without any treatment, both administrations reached their peak in phage neutralization by day 13: local administration reached approximately 99.4% neutralization, while intravenous administration reached approximately 99.5%. No statistical differences were observed between the two administrations at each time point throughout the experiment (Figure 6).

4 Discussion

This study mimicked a challenging human case of FRI treated with PT in a controlled *in vivo* preclinical study, using the same pathogen and phage used in PT. In human cases, significant clinical improvement has been observed, underscoring the potential of PT as a valuable adjunct to conventional antibiotic treatment. However, although such positive clinical outcomes exist for PT in human patients, there are still unanswered questions regarding the optimal application, safety, pharmacokinetics, and efficacy of PT. The large animal study was, therefore, designed to answer some of these fundamental open questions.

Overall, our findings revealed some important information about PT and how it performs in a controlled preclinical model. PT was found to be safe, as evidenced by the stable weight of sheep across the study, the absence of significant differences in WBC counts among the treatment groups, the lack of observable side effects, and the absence of active phages in organs. The rapid elimination of phage from the circulating plasma and an inability to detect active phage locally during treatment were primary outcomes. The lower-than-expected titers of phages may be a result of a combination of factors including rapid induction of neutralizing antibodies, and dilution in a large animal as will be discussed below. Secondly, we did not see any significant additional

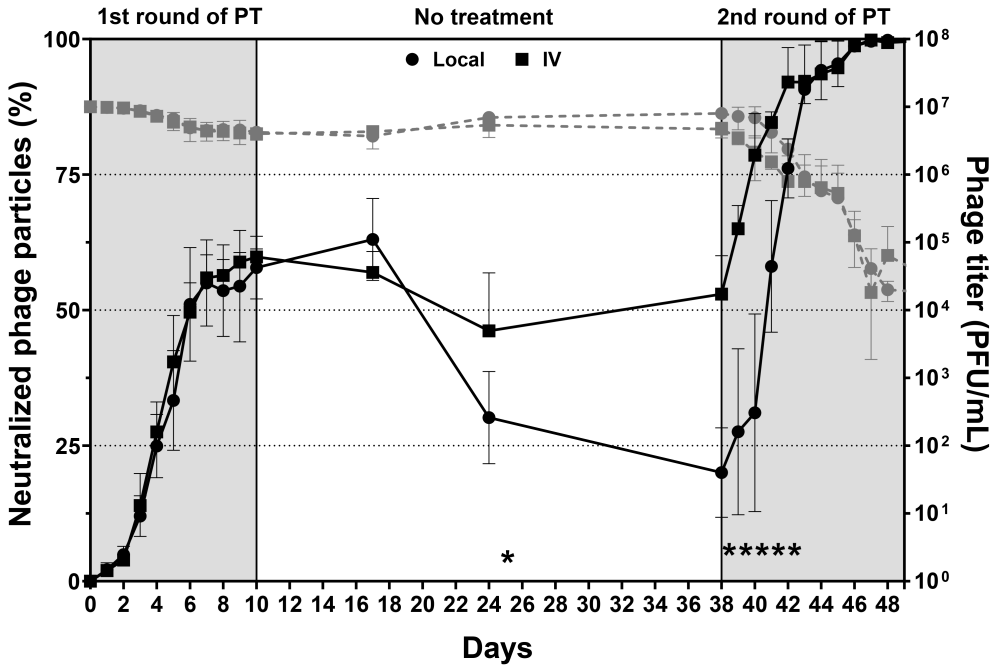

FIGURE 3
Phage neutralization between intravenous and local administrations. The black solid line represented the percentage of phage neutralization and should be read on the left Y-axis. The grey dashed line represented the phage titer of phage neutralization and should be read on the right Y-axis. PT was administered over two 10-day treatment periods separated by a 28-day no-treatment period. Higher neutralization values indicated reduced phage activity. The data are presented as mean ± standard deviation, and statistical significance was determined using a student's t-test (*$p < 0.05$). The detection limit of the assay used to quantify active phage was 10 PFU/mL.

10.3389/fcimb.2025.1547250

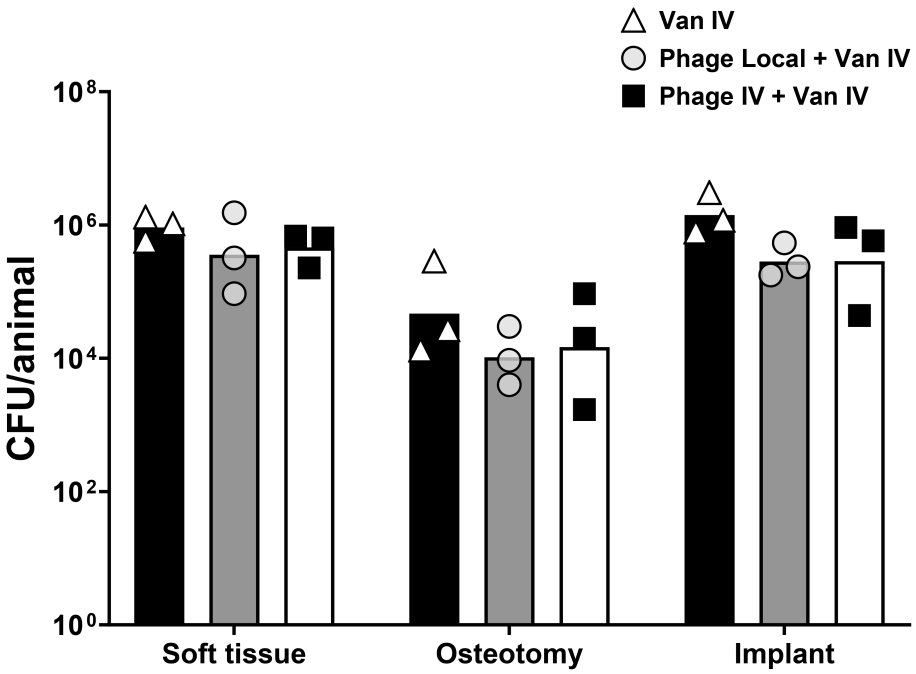

FIGURE 4
Bacterial load in soft tissue, osteotomy, implant, and total bacterial load. Sheep were treated with either vancomycin alone, intravenous phage therapy combined with intravenous vancomycin, or local phage therapy combined with intravenous vancomycin. Data represent the mean ± standard deviation, and statistical significance was determined using a Kruskal-Wallis test followed by Tukey post test. CFU, colony forming units.

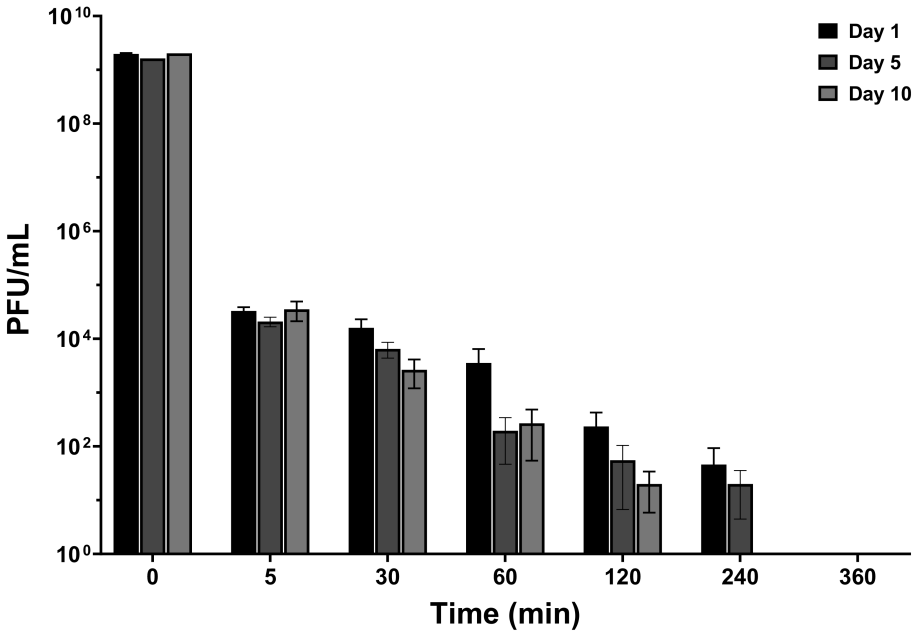

FIGURE 5
Phage distribution in plasma after intravenous administration and local administration. Measurements were taken at 5, 30, 60, 120, 240, and 360 minutes on days 1, 5, and 10 post-PT. The titer of phage administered intravenously and locally was10^9 PFU/mL. The data were presented as mean ± standard deviation of results and error bars represent standard deviation, and statistical significance was determined using a one-way ANOVA test followed by Tukey posttest. The detection limit of the assay used to quantify active phage was 10 PFU/mL.

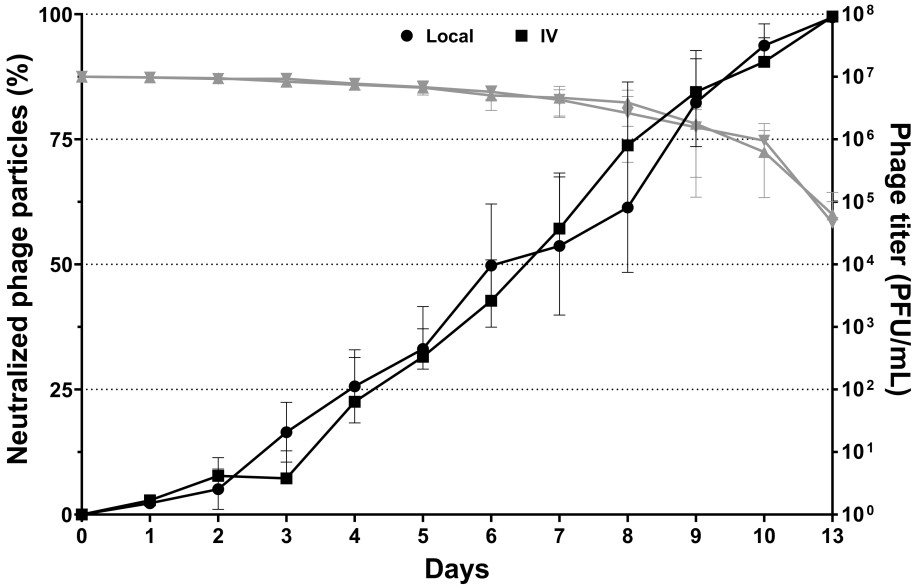

FIGURE 6
Phage neutralization between intravenous and local administrations over a 13-day period. Error bars indicate the standard deviation of the measurements. The black solid line represented the percentage of phage neutralization and should be read on the left Y-axis. The grey dashed line represented the phage titer of phage neutralization and should be read on the right Y-axis. The data were presented as mean ± standard deviation of results and error bars represent standard deviation, and statistical significance was determined using a student's t-test (*$p < 0.05$). The detection limit of the assay used to quantify active phage was 10 PFU/mL.

antibacterial benefit in adding phages to systemic antibiotic therapy. Although trends were observed for a reduction in CFU, the effect was insufficient to eradicate the infection.

Intravenous administration is efficient and very fast in terms of phage delivery. However, our results demonstrated a rapid decline in phage titer in the plasma following intravenous administration. This rapid clearance suggests that phages may be diluted in plasma or quickly removed from circulation. It was observed in a rabbit study that immediately after injection (within 2.5 minutes), the phage concentration in rabbit blood was 100 times lower than the expected titer, which was calculated based on the dose and expected dilution in the blood volume (Sulkin et al., 1957). In the context of our study, using sheep which most closely approximate the human scale, the expected phage titer following intravenous injection was calculated to provide a theoretical baseline for comparison. For example, in a sheep weighing 70 kg, the blood volume was estimated based on a standard value of 60 mL/kg of body weight (Gillett and Halmagyi, 1966), resulting in a total blood volume of approximately 4200 mL. Given an initial phage dose of 20 mL $\times 10^9$ PFU, then the expected phage titer was determined to be approximately 4×10^6 PFU/mL. However, the phage titer in the blood immediately after injection (5 minutes) is approximately 10^4 PFU/mL. This is markedly less than expected from the hypothetical dilution of phage in body volume (100-fold lower) and it suggests a very rapid mechanism of capturing or neutralizing the phages in sheep.

Liver and spleen are the most commonly reported organs that accumulate phage delivered systemically (Dabrowska and Abedon, 2019). As important elements of the mononuclear phagocytic system (MPS), they filter many foreign objects traveling in circulation, including phages (Van Belleghem et al., 2018). Typically, the spleen is the organ where active phages can be detected for the longest time, even for 12 days after administration in rabbit (Reynaud et al., 1992). However, in our study, no active phage was observed in the sections of organs that were tested at euthanasia. It is possible that phages were present in untested areas or remained below the detection limit of our assay. It could indicate that the phages were rapidly cleared or inactivated by the host immune system before they could accumulate in these organs. The rapid phage clearance, seen in plasma, suggests that the immune system played a major role in this process. Furthermore, the absence of detectable phages could be attributed to the utilization of the double agar overlay method, which exclusively identifies active phages. In contrast, polymerase chain reaction (PCR) techniques are capable of detecting both active and inactive phages. Given that PCR was not employed in this study, it is plausible that inactive phages were present in the organs. Moreover, considering that three days had passed without any PT prior to euthanasia, it is plausible that the phages had been eradicated within the body during this washout period. This is more relevant for the non-inoculated sheep, where the bacterial host is absent so replication of phage was not possible, and only the introduced phage could be expected to be present.

Not only was the phage titer in plasma lower than may have been expected, phages were the not even detected in draining fluid and bone 72 hours after last administration upon euthanasia. This may be attributed to suboptimal distribution resulting from delivery via the drainage. In the sheep model, phages were administered locally through this tube to concentrate them at the infection site. However, this method might not have allowed adequate dispersal throughout the target tissue. This is likely a limitation of the

experimental setup, rather than a broader issue with phage therapy itself. Improvements in phage delivery systems, such as for example via the use of continuous infusion or application in biomaterials, could enhance tissue penetration in future studies.

One of the key host responses influencing the outcome of PT is the induction of a specific immune response to the phage itself. In healthy sheep, phage neutralization reached approximately 60% by day 10 and dropped significantly after the first PT round but surged to 99.9% upon re-exposure in the second round. This suggests that the immune system retains memory of the phages and can respond robustly upon subsequent exposure, even without infection. In the presence of bacteria as modelled in phase 2 with MRSA infection, neutralization rose even more quickly, reaching 99% by day 13 at the end of PT. This indicates that ongoing bacterial presence boosts immune activity against phages and was not different for local or IV administered phages.

Rapid induction of phage neutralization may cause a rapid decline in phage titer, which leads to an insufficient bacterial load reduction. Phage neutralization levels in our sheep FRI models peaked at 99% by day 10. In contrast, previous studies in human patients showed phage neutralization occurring between 6 and 35 days after starting therapy in 38.5% of cases, particularly with invasive phage administrations (Pirnay et al., 2024). Two case reports found no phage neutralization in patients with FRI during local phage treatment (Onsea et al., 2021a; Eskenazi et al., 2022). Similarly, Cano et al. observed IgG anti-phage antibodies in periprosthetic joint infection patients but saw no significant changes in IgG levels over time (Cano et al., 2021). The difference in phage neutralization between humans and sheep, despite identical administration and therapy duration, is possible due to variations in the immune response. Many patients suffered from long-term osteomyelitis before receiving PT, possibly altering the immune response (Surendar et al., 2024). In chronic infections, immune tolerance and exhaustion involve regulatory mechanisms that suppress the immune response to minimize inflammation and tissue damage (Rogovskii, 2020). This creates a less aggressive immune environment, potentially allowing therapeutic agents like phages to act with less interference from the host's defenses. In contrast, sheep models, with their shorter infection duration, perhaps had a more active and less tolerant immune system, that could result in higher phage neutralization due to a vigorous immune response to both bacterial pathogens and therapeutic phages (Nishitani et al., 2016). This could also explains why the efficacy outcome is not positive. Conversely, in humans with chronic infections and associated suppressed or reduced immune responses, phage neutralization might be less of an issue, as evidenced by improved bacterial clearance and therapeutic outcomes (Onsea et al., 2021b; Uyttebroek et al., 2022; Metsemakers et al., 2023b). For instance, in one case study, a 15-year-old lung transplant patient, likely due to rituximab treatment, did not develop phage neutralization (Dedrick et al., 2019). Another patient on photopheresis, intravenous immunoglobulin, sirolimus, and prednisone also exhibited immune tolerance, likely lowering phage neutralization risk (Dan et al., 2023). This suggests that phage neutralization is a key consideration in PT, but its impact can vary significantly based on the immune status of the patient. To enhance PT outcomes for FRI, a tailored approach considering immune status is beneficial. Pre-therapy immune assessments could evaluate markers of tolerance and exhaustion to predict phage neutralization risks. Optimizing phage formulations with immune modulators, protective carriers, or selecting phages with inherently low immunogenicity can help reduce immune exposure and extend therapeutic effects based on these findings. By integrating these strategies, clinicians can enhance the efficacy of PT, particularly in patients whose immune systems may otherwise compromise the treatment's success.

One of the challenges associated with phage neutralization in human PT is the potential for neutralization to persist long after the therapeutic intervention. Łusiak-Szelachowska et al. reported that patients with bone infections undergoing PT can develop high levels of phage-neutraliziation. In their study, PT lasted between 24 to 54 days, and the antibodies persisted for several months to over a year after therapy, showing considerable variation in how long they took to decline (Lusiak-Szelachowska et al., 2022). In another study, Eskenazi et al. reported a 6-day course of PT for FRI caused by pan-drug-resistant *Klebsiella pneumoniae*. In their case, no phage neutralization was observed during the first 8 days. However, neutralizing antibodies began to develop between days 8 and 18 after phage administration, and by 161 days post-therapy, a significant neutralization rate of 87.13% was detected (Eskenazi et al., 2022). The researchers considered that phage-neutralizing antibodies were unlikely to have impeded the efficacy of the PT due to the short course of treatment. In this study, we assessed phage neutralization before the start of PT, with baseline levels recorded as 'Day 0.' These baseline measurements were compared to control phage titers to determine changes in phage neutralization over time. However, phage neutralization is expected to persist for an extended period and is an important factor to consider in PT as also confirmed in our sheep study.

The choice between local and intravenous phage administration remains a key question in phage therapy. Our study found no significant difference in efficacy between the two routes of administration. Although no significant therapeutic efficacy was observed for either route of phage administration, we did observe phage neutralization reaching high levels (>90%) for both groups, indicating the rapid immune response to phage treatment. Local administration offers the advantage of targeting the infection site directly. However, IV administration provides a rapid systemic approach to potentially address infections at multiple sites. Despite similar levels of phage neutralization between the two methods, local administration may still provide an advantage in cases where localized infections, such as FRI, are the primary concern. Local delivery may reduce the likelihood of rapid clearance or dilution in the bloodstream, though more research is needed to confirm this. There is no reason from this study to suggest that local administration should be avoided.

In terms of efficacy, our study revealed that while PT demonstrated some antibacterial activity, it fell short of eradicating the infection, even when PT was combined with systemic antibiotics. Several factors may have contributed to this

outcome. The rapid neutralization of phages by the host immune system likely played a significant role, as evidenced by the high phage-neutralizing antibody levels observed during treatment. The method of phage delivery, whether intravenous or local, may have influenced the distribution and availability of active phages at the infection site. The lack of detectable phages in both plasma and tissue further underscores the challenges of achieving sufficient therapeutic concentrations *in vivo*. This variability in immune response highlights the importance of considering different phage types in phage therapy. Phages, being highly specific to their bacterial targets, may interact with the immune system differently based on their structure, size, and other factors. Although few studies have compared immune responses to different phages or phage cocktails, it is not clear how other phages may be affected, but that it is an area requiring further research. Moreover, critical differences in treatment protocols must be considered. In this study, infection was treated with implant retention, which is known to be suboptimal compared to protocols involving implant removal. If the referenced patient underwent implant removal along with PT, the clinical context would differ significantly from the experimental conditions in our study. For these reasons, it is not appropriate to directly compare the results of our preclinical study to those of individual clinical cases. Instead, the study aims to address broader questions of PT efficacy, safety, pharmacokinetics, and immunogenicity within a controlled experimental framework.

Sheep were chosen as the large animal model due to their established compatibility with human clinical instrumentation and standardized infection induction and management protocols. While other large animals such as pigs offer greater phylogenetic similarity, their logistical demands and associated costs outweigh the potential gains in physiological relevance for this proof-of-concept study. Our selection of sheep prioritized translational feasibility, ethical efficiency, and alignment with existing experience in our facilities.

Despite the valuable insights provided by this study, several limitations need to be addressed. The relatively small sample size in both phases is a limitation. Nonetheless, intravenous vancomycin combined with local and intravenous PT resulted in a 66% and 52% reduction respectively, in the total bacterial load of a human isolated multi-resistant pathogen, which may still be considered clinically relevant, despite the lack of statistical significance. However, Larger studies, including those with increased group sizes, extended follow-up periods, better monitoring of human patients, and potentially additional animal models such as pigs or non-human primates, are necessary to confirm the trends observed and to establish more robust conclusions regarding the efficacy and safety of PT in FRI. Second, the study focused on monophage therapy (Alispahic et al., 2020) and a specific bacterial isolate (MRSA MSI-003). While this approach ensured consistency in the results, it may not fully represent the broader spectrum of phage-bacteria interactions seen in clinical settings. The findings might differ with other phage strains or bacterial species, suggesting the need for further studies involving multiple phages and pathogens to evaluate the general applicability of the results. Second, an acute FRI (Inoculum for 3 weeks) was simulated rather than a chronic infection. The increased immune response in the sheep models highlights the difficulty of using PT for acute infections, as the immune system may neutralize the phages prematurely. Conversely, in chronic infections with reduced or suppressed individual immune responses, phage neutralization may be less of an issue, improving bacterial clearance and therapeutic outcomes, as has been shown clinically. However, this would require dedicated and substantial studies to confirm these hypotheses (Onsea et al., 2021b; Uyttebroek et al., 2022; Metsemakers et al., 2023b). Finally, our study did not explore the impact of using phage cocktails or combinations of different phages, whereas phage cocktails are commonly employed in clinical PT to minimize the emergence of bacterial resistance and broaden efficacy. We did not assess whether bacteria isolated post-mortem developed phage resistance, which represents a limitation of this study and should be considered in future investigations.

This study contributes to the growing body of evidence on the safety and pharmacokinetics of PT in treating FRI caused by MRSA. The results demonstrate that both intravenous and local administration of phages are well-tolerated and result in similar levels of phage neutralization when treating implant-associated infections and resulting biofilms, although neither route provided a significant advantage over standard antibiotic therapy in reducing bacterial load. The findings highlight the complexity of PT, particularly the challenges posed by phage neutralization and rapid clearance from the bloodstream. While PT holds promise as a complementary approach to antibiotics, its clinical efficacy may require further optimization, including the selection of more effective phage strains, adjustment of dosing regimens, and improved delivery methods to overcome immune-mediated inactivation.

Data availability statement

The original contributions presented in the study are included in the article/Supplementary Material. Further inquiries can be directed to the corresponding author.

Ethics statement

The animal study was approved by Ethical Committee of the Canton of Grisons in Switzerland (approval number: GR 10_2023). The study was conducted in accordance with the local legislation and institutional requirements. Written informed consent was obtained from the individual(s) for the publication of any potentially identifiable images or data included in this article.

Author contributions

CP: Formal Analysis, Investigation, Methodology, Writing – review & editing. BC: Conceptualization, Formal Analysis,

Investigation, Methodology, Visualization, Writing – original draft, Writing – review & editing. LH: Investigation, Methodology, Writing – review & editing. MC: Investigation, Methodology, Writing – review & editing. JO: Resources, Writing – review & editing. MV: Writing – review & editing. DA: Investigation, Methodology, Writing – review & editing. CC: Investigation, Methodology, Writing – review & editing. SZ: Investigation, Methodology, Writing – review & editing. WO: Writing – review & editing. AT: Writing – review & editing. MR: Resources, Writing – review & editing. CZ: Writing – review & editing. WM: Conceptualization, Resources, Supervision, Writing – review & editing. TM: Conceptualization, Formal Analysis, Funding acquisition, Investigation, Methodology, Resources, Supervision, Visualization, Writing – review & editing.

Funding

The author(s) declare that financial support was received for the research and/or publication of this article. This project was funded by AO Innovation translation center via the Anti-infective Global Expert Committee of the AO Innovation Translation Center.

Acknowledgments

Virginia Post (AO Research Institute Davos, Switzerland) is acknowledged for technical support.

Conflict of interest

The authors declare that the research was conducted in the absence of any commercial or financial relationships that could be construed as a potential conflict of interest.

The handling editor MM declared a past co-authorship with the authors.

Generative AI statement

The author(s) declare that no Generative AI was used in the creation of this manuscript.

Publisher's note

Supplementary material

The Supplementary Material for this article can be found online at: https://www.frontiersin.org/articles/10.3389/fcimb.2025.1547250/full#supplementary-material

SUPPLEMENTARY FIGURE 1
The placement of the probe and the collection tube for the animals that received local administration. The left side is phase 1, animal without any osteotomy or fracture-related infection, and the right side is phase 2, where the animals received an osteotomy, plate ad screw fixation and fracture-related infection. The animals that received systemic administration (i.e. no PT) did not receive any tube for phage application.

SUPPLEMENTARY FIGURE 2
The measurements of **(A)** weight and **(B)** white blood cell (WBC) count in sheep receiving phage administration locally and intravenously. Weights were normalized to the preoperative weights at the primary surgery and set at 100%. 1st OP: The beginning of PT. 1st PT: D9 is the timepoint when PT of the first round has been administered for 10 days; 2nd OP: 28 days after the end of PT, the second operation started at Day 37; 2nd PT: D47 was the timepoint when PT of the second round has been administered for 10 days. Data points represented individual measurements, with horizontal lines indicating the mean values and statistical significance was determined using a student's t-test.

SUPPLEMENTARY FIGURE 3
The measurements of **(A)** weight and **(B)** white blood cell (WBC) count in sheep with fracture-related infection receiving local phage therapy (PT) combined with intravenous vancomycin, intravenous PT combined with intravenous vancomycin and intravenous vancomycin only. Weights were normalized to the preoperative weights at the primary surgery and set at 100%. Data points represented individual measurements, with horizontal lines indicating the mean values and statistical analysis was performed using a two-way ANOVA followed by *post hoc* Tukey's multiple comparisons test. The detection limit of the assay used to quantify bacteria was 10 CFU/mL.

SUPPLEMENTARY FIGURE 4
Bacterial load in different tissue locations: proximal bone, distal bone, and bone marrow for each animal. The treatments compared were local PT combined with intravenous vancomycin, intravenous PT combined with intravenous vancomycin, and vancomycin alone. Data represent the mean ± standard deviation, and statistical significance was determined using a Kruskal-Wallis test followed by Tukey's posttest. CFU, colony-forming units.

References

Alispahic, N., Brorson, S., Bahrs, C., Joeris, A., Steinitz, A., and Audigé, L. (2020). Complications after surgical management of proximal humeral fractures: A systematic review of event terms and definitions. *BMC Musculoskelet. Disord.* 21, 327. doi: 10.1186/s12891-020-03353-8

Cano, E. J., Caflisch, K. M., Bollyky, P. L., Van Belleghem, J. D., Patel, R., Fackler, J., et al. (2021). Phage therapy for limb-threatening prosthetic knee Klebsiella pneumoniae infection: case report and *in vitro* characterization of anti-biofilm activity. *Clin. Infect. Dis.* 73, e144–ee51. doi: 10.1093/cid/ciaa705

Capparelli, R., Parlato, M., Borriello, G., Salvatore, P., and Iannelli, D. (2007). Experimental phage therapy against Staphylococcus aureus in mice. *Antimicrob. Agents Chemother.* 51, 2765–2773. doi: 10.1128/AAC.01513-06

Chen, B., Benavente, L. P., Chitto, M., Wychowaniec, J. K., Post, V., D'Este, M., et al. (2023). Alginate microbeads and hydrogels delivering meropenem and bacteriophages to treat Pseudomonas aeruginosa fracture-related infections. *J. Control Release* 364, 159–173. doi: 10.1016/j.jconrel.2023.10.029

Dabrowska, K., and Abedon, S. T. (2019). Pharmacologically aware phage therapy: pharmacodynamic and pharmacokinetic obstacles to phage antibacterial action in

animal and human bodies. *Microbiol. Mol. Biol. Rev.* 83, e00012–19. doi: 10.1128/MMBR.00012-19

Dan, J. M., Lehman, S. M., Al-Kolla, R., Penziner, S., Afshar, K., Yung, G., et al. (2023). Development of host immune response to bacteriophage in a lung transplant recipient on adjunctive phage therapy for a multidrug-resistant pneumonia. *J. Infect. Dis.* 227, 311–316. doi: 10.1093/infdis/jiac368

Dedrick, R. M., Guerrero-Bustamante, C. A., Garlena, R. A., Russell, D. A., Ford, K., Harris, K., et al. (2019). Engineered bacteriophages for treatment of a patient with a disseminated drug-resistant Mycobacterium abscessus. *Nat. Med.* 25, 730–733. doi: 10.1038/s41591-019-0437-z

Eskenazi, A., Lood, C., Wubbolts, J., Hites, M., Balarjishvili, N., Leshkasheli, L., et al. (2022). Combination of pre-adapted bacteriophage therapy and antibiotics for treatment of fracture-related infection due to pandrug-resistant Klebsiella pneumoniae. *Nat. Commun.* 13, 302. doi: 10.1038/s41467-021-27656-z

Gillett, D. J., and Halmagyi, D. F. (1966). Results and limitations of blood volume measurements in sheep. *J. Surg. Res.* 6, 211–214. doi: 10.1016/s0022-4804(66)80018-5

Khatoon, Z., McTiernan, C. D., Suuronen, E. J., Mah, T. F., and Alarcon, E. I. (2018). Bacterial biofilm formation on implantable devices and approaches to its treatment and prevention. *Heliyon* 4, e01067. doi: 10.1016/j.heliyon.2018.e01067

Kishor, C., Mishra, R. R., Saraf, S. K., Kumar, M., Srivastav, A. K., and Nath, G. (2016). Phage therapy of staphylococcal chronic osteomyelitis in experimental animal model. *Indian J. Med. Res.* 143, 87–94. doi: 10.4103/0971-5916.178615

Le, T., Nang, S. C., Zhao, J., Yu, H. H., Li, J., Gill, J. J., et al. (2023). Therapeutic potential of intravenous phage as standalone therapy for recurrent drug-resistant urinary tract infections. *Antimicrob. Agents Chemother.* 67, e0003723. doi: 10.1128/aac.00037-23

Lebeaux, D., Ghigo, J. M., and Beloin, C. (2014). Biofilm-related infections: bridging the gap between clinical management and fundamental aspects of recalcitrance toward antibiotics. *Microbiol. Mol. Biol. Rev.* 78, 510–543. doi: 10.1128/MMBR.00013-14

Lusiak-Szelachowska, M., Miedzybrodzki, R., Rogoz, P., Weber-Dabrowska, B., Zaczek, M., and Gorski, A. (2022). Do anti-phage antibodies persist after phage therapy? A preliminary report. *Antibiotics (Basel)* 11, 1358. doi: 10.3390/antibiotics11101358

Masters, E. A., Trombetta, R. P., de Mesy Bentley, K. L., Boyce, B. F., Gill, A. L., Gill, S. R., et al. (2019). Evolving concepts in bone infection: redefining "Biofilm", "Acute vs. Chronic osteomyelitis", "the immune proteome" and "Local antibiotic therapy". *Bone Res.* 7, 20. doi: 10.1038/s41413-019-0061-z

Metsemakers, W. J., Morgenstern, M., Senneville, E., Borens, O., Govaert, G. A. M., Onsea, J., et al. (2020). General treatment principles for fracture-related infection: recommendations from an international expert group. *Arch. Orthop. Trauma Surg.* 140, 1013–1027. doi: 10.1007/s00402-019-03287-4

Metsemakers, W. J., Moriarty, T. F., Morgenstern, M., Marais, L., Onsea, J., O'Toole, R. V., et al. (2023a). The global burden of fracture-related infection: can we do better? *Lancet Infect. Dis.* 24, e386–e393. doi: 10.1016/S1473-3099(23)00503-0

Metsemakers, W. J., Onsea, J., Moriarty, T. F., Pruidze, N., Nadareishvili, L., Dadiani, M., et al. (2023b). Bacteriophage therapy for human musculoskeletal and skin/soft tissue infections. *Clin. Microbiol. Infect.* 29, 695–701. doi: 10.1016/j.cmi.2023.01.011

Morgenstern, M., Erichsen, C., Militz, M., Xie, Z., Peng, J., Stannard, J., et al. (2021). The Ao trauma Cpp bone infection registry: epidemiology and outcomes of Staphylococcus aureus bone infection. *J. Orthop. Res.* 39, 136–146. doi: 10.1002/jor.24804

Moriarty, T. F., Metsemakers, W. J., Morgenstern, M., Hofstee, M. I., Vallejo Diaz, A., Cassat, J. E., et al. (2022). Fracture-related infection. *Nat. Rev. Dis. Primers* 8, 67. doi: 10.1038/s41572-022-00396-0

Nishitani, K., Bello-Irizarry, S. N., de Mesy Bentley, K. L., Daiss, J. L., and Schwarz, E. M. (2016). The role of the immune system and bone cells in acute and chronic osteomyelitis. *Osteoimmunology*, 283–295. doi: 10.1016/B978-0-12-375670-1.10013-5

Onsea, J., Post, V., Buchholz, T., Schwegler, H., Zeiter, S., Wagemans, J., et al. (2021a). Bacteriophage therapy for the prevention and treatment of fracture-related infection caused by Staphylococcus aureus: A preclinical study. *Microbiol. Spectr.* 9, e0173621. doi: 10.1128/spectrum.01736-21

Onsea, J., Soentjens, P., Djebara, S., Merabishvili, M., Depypere, M., Spriet, I., et al. (2019). Bacteriophage application for difficult-to-treat musculoskeletal infections: development of a standardized multidisciplinary treatment protocol. *Viruses* 11, 891. doi: 10.3390/v11100891

Onsea, J., Uyttebroek, S., Chen, B., Wagemans, J., Lood, C., Van Gerven, L., et al. (2021b). Bacteriophage therapy for difficult-to-treat infections: the implementation of a multidisciplinary phage task force (the phageforce study protocol). *Viruses* 13, 1543. doi: 10.3390/v13081543

Onsea, J., Wagemans, J., Pirnay, J. P., Di Luca, M., Gonzalez-Moreno, M., Lavigne, R., et al. (2020). Bacteriophage therapy as a treatment strategy for orthopaedic-device-related infections: where do we stand? *Eur. Cell Mater.* 39, 193–210. doi: 10.22203/eCM.v039a13

Pirnay, J. P., Djebara, S., Steurs, G., Griselain, J., Cochez, C., De Soir, S., et al. (2024). Personalized bacteriophage therapy outcomes for 100 consecutive cases: A multicentre, multinational, retrospective observational study. *Nat. Microbiol.* 9, 1434–1453. doi: 10.1038/s41564-024-01705-x

Reynaud, A., Cloastre, L., Bernard, J., Laveran, H., Ackermann, H. W., Licois, D., et al. (1992). Characteristics and diffusion in the rabbit of a phage for Escherichia coli 0103. Attempts to use this phage for therapy. *Vet. Microbiol.* 30, 203–212. doi: 10.1016/0378-1135(92)90114-9

Rogovskii, V. (2020). Immune tolerance as the physiologic counterpart of chronic inflammation. *Front. Immunol.* 11. doi: 10.3389/fimmu.2020.02061

Siverino, C., Gens, L., Ernst, M., Buchholz, T., Windolf, M., Richards, G., et al. (2023). Debridement, antibiotics, irrigation, and implant retention in a sheep fracture-related infection model. *Orthop. Proc.* 105-B, 16–. doi: 10.1302/1358-992x.2023.17.016

Suh, G. A., Lodise, T. P., Tamma, P. D., Knisely, J. M., Alexander, J., Aslam, S., et al. (2022). Considerations for the use of phage therapy in clinical practice. *Antimicrob. Agents Chemother.* 66, e0207121. doi: 10.1128/AAC.02071-21

Sulkin, S. E., Finkelstein, R. A., and Rosenblum, E. D. (1957). Effect of zymosan on bacteriophage clearance. *Science* 125, 742–743. doi: 10.1126/science.125.3251.742

Surendar, J., Hackenberg, R. K., Schmitt-Sanchez, F., Ossendorff, R., Welle, K., Stoffel-Wagner, B., et al. (2024). Osteomyelitis is associated with increased anti-inflammatory response and immune exhaustion. *Front. Immunol.* 15. doi: 10.3389/fimmu.2024.1396592

Uyttebroek, S., Chen, B., Onsea, J., Ruythooren, F., Debaveye, Y., Devolder, D., et al. (2022). Safety and efficacy of phage therapy in difficult-to-treat infections: A systematic review. *Lancet Infect. Dis.* 22, e208–ee20. doi: 10.1016/S1473-3099(21)00612-5

Van Belleghem, J. D., Dabrowska, K., Vaneechoutte, M., Barr, J. J., and Bollyky, P. L. (2018). Interactions between bacteriophage, bacteria, and the mammalian immune system. *Viruses* 11, 10. doi: 10.3390/v11010010

Wills, Q. F., Kerrigan, C., and Soothill, J. S. (2005). Experimental bacteriophage protection against Staphylococcus aureus abscesses in a rabbit model. *Antimicrob. Agents Chemother.* 49, 1220–1221. doi: 10.1128/AAC.49.3.1220-1221.2005

Young, J., Lee, S. W., Shariyate, M. J., Cronin, A., Wixted, J. J., Nazarian, A., et al. (2024). Bacteriophage therapy and current delivery strategies for orthopedic infections: A scoping review. *J. Infect.* 88, 106125. doi: 10.1016/j.jinf.2024.106125

frontiers | Frontiers in Medicine

TYPE Case Report
PUBLISHED 25 April 2025
DOI 10.3389/fmed.2025.1564369

OPEN ACCESS

EDITED BY
Derry Keith Mercer,
INCATE, Switzerland

REVIEWED BY
Geetha Manivasagam,
VIT University, India
Kashif Haq,
Birmingham City University, United Kingdom

*CORRESPONDENCE
Lorenz Leitner
✉ lorenz.leitner@balgrist.ch

RECEIVED 21 January 2025
ACCEPTED 08 April 2025
PUBLISHED 25 April 2025

CITATION
Wahl P, Schläppi M, Loganathan A, Uçkay I, Hodel S, Fritz B, Scheidegger J, Djebara S, Leitner L and McCallin S (2025) Bacteriophage therapy created the necessary conditions for successful antibiotic suppression in a periprosthetic hip joint infection: a Case Report.
Front. Med. 12:1564369.
doi: 10.3389/fmed.2025.1564369

Bacteriophage therapy created the necessary conditions for successful antibiotic suppression in a periprosthetic hip joint infection: a Case Report

Peter Wahl[1,2], Michel Schläppi[1], Archana Loganathan[3], Ilker Uçkay[4], Sandro Hodel[5], Benjamin Fritz[6], Jens Scheidegger[3], Sarah Djebara[7], Lorenz Leitner[3]* and Shawna McCallin[3]

[1]Division of Orthopaedics and Traumatology, Cantonal Hospital Winterthur, Winterthur, Switzerland, [2]Faculty of Medicine, University of Bern, Bern, Switzerland, [3]Department of Neuro-Urology, Balgrist University Hospital, University of Zurich, Zürich, Switzerland, [4]Unit of Clinical and Applied Research, Infectiology, Balgrist University Hospital, University of Zurich, Zürich, Switzerland, [5]Department of Orthopedics, Balgrist University Hospital, University of Zurich, Zürich, Switzerland, [6]Department of Radiology, Balgrist University Hospital, University of Zurich, Zürich, Switzerland, [7]Center for Infectious Diseases, Queen Astrid Military Hospital, Brussels, Belgium

Introduction: Treatment failure remains an issue in periprosthetic joint infection (PJI). Bacteriophages offer new treatment options. However, there is still a lack of evidence to better define their usefulness and administration. We report a case in which antibiotic suppression was successful only after administration of bacteriophages.

Case description: Antibiotic suppression was the only option for a 94-year-old male with methicillin-resistant *Staphylococcus aureus* (MRSA) PJI of the hip and of the knee. As the hip PJI could not be suppressed adequately, bacteriophages were administered locally and systemically together with daptomycin. This combined approach led to sufficient clinical improvement for further oral antibiotic suppression, although without infection eradication.

Conclusion: The administration of bacteriophages may be a valuable, less-invasive adjunct therapy to successfully suppress PJI. Bacteriophage selection, preparation and administration, however, remains associated with administrative obstacles, greatly limiting availability and practicability. Nevertheless, research and developments in this domain should be pursued, particularly considering issues with future antibiotic limitations and cost associated with treatment failure in PJI.

KEYWORDS

periprosthetic joint infection, PJI, bacteriophages, antibiotic suppression, *Staphylococcus aureus*, MRSA

Introduction

Periprosthetic joint infection (PJI) remains a severe complication of arthroplasty, associated with a relevant morbidity and mortality (1–6). Despite many advances and standardizations in treatment, therapy failures remain a frequent issue, particularly when treatment options are limited by surgical aspects or by comorbidities (5, 7–11). Long-term

antibiotic suppression therapy remains an option in case of failure to eradicate PJI (9, 12, 13).

However, prolonged administration of antibiotics is associated with a relevant rate of adverse reactions, and suppression of the infection may not be successful (4, 12, 13). Bacteriophages offer new treatment options, particularly considering increasing evidence for a synergistic effect of bacteriophages and antibiotics (14–17). Though, there is still a lack of evidence to better define their appropriate use and therapeutic role of their administration as well as the posology in musculoskeletal infections (14, 15). In selected cases where curative surgery is not feasible, and infection persists despite standard treatment, bacteriophage therapy may offer a viable adjunctive option, particularly when microbiological data support its use (15, 17).

We report such a case in which the last option of suppressive antibiotic therapy was successful only after administration of bacteriophages.

Case description

A 94-year-old male with a complex medical history was hospitalized due to sepsis and new onset right hip pain. A therapeutic oral anticoagulation with apixaban had been maintained since a pulmonary embolism one year prior, and the patient suffered from chronic renal impairment (estimated clearance between 30 and 35 mL/min/1.7 m^2). Total hip arthroplasty (THA) had been performed 7 years and medial unicompartimental knee arthroplasty had been performed 14 years before, respectively, both on the right side. Since THA, the patient had been operated repeatedly on his lumbar spine. Because of the pain irradiating to the right hip, aspiration of the hip joint had been performed 1.5 years after THA, excluding PJI, based on a low cell count and sterile microbiologic workup.

The patient had undergone lumbopelvic stabilization surgery two years earlier. Since surgery, he had not regained the ability to walk, but he remained pain-free and was able to manage most aspects of personal hygiene independently. Separately, due to an oncologic subtotal penectomy performed 12 years earlier, permanent bladder drainage had been necessary. In recent years, he had received multiple courses of antibiotics due to recurrent urinary tract infections, a potential source for the selection of multidrug-resistant microorganisms.

Following the patient's request for therapeutic support, hemodynamic stabilization was performed, and an empiric parenteral antibiotic therapy with cefepime was introduced. Blood cultures returned positive within hours for *Staphylococcus aureus*, which was identified the next day as being methicillin-resistant (MRSA), prompting to switch the antimicrobial therapy to daptomycin at 8 mg/kg/day. This antibiotic was preferred over glycopeptides due to renal impairment with an estimated clearance of 30–35 mL/min and a hemodynamically unstable situation. The port and time of entry of this virulent pathogen remained unknown. Aspiration of the right hip, which was overtly inflamed, yielded pus with 108′400 leucocytes/µl and 91% polymorphonuclear cells. Cultures of the hip joint fluid confirmed the same strain of MRSA. Aspiration of the right knee was macroscopically not suspicious for infection, and the cell count was only at 160 leucocytes/µl. Both the hip and the knee presented a flexion contracture of more than 40°.

Considering the confirmed patient's desire for therapy, a rapidly positive response to the initial treatment, surgical treatment was aimed for on the third day to allow elimination of the oral anticoagulant. Shortly before surgery, cultures from the knee joint also yielded MRSA in low quantity. Considering the confirmed short duration of symptoms and as no component loosening was present, both joint replacements were therefore accessible to debridement and implant retention procedures. The alterations observed along the proximal femur could well be explained by mechanical issues associated with the line-to-line cementation of the stem (Figure 1) (18).

Surgical treatment began at the overtly more severely infected hip. Despite THA having been performed initially through an anterior approach, full exposure through the same approach was not feasible due to pronounced scar tissue formation around the deeply situated hip joint. The medial neocapsule remained inaccessible to debridement. Dislocation of the prosthesis was not possible, despite the use of a mobile traction table, rendering exchange of the modular components impossible. Finally, the surgery had to be aborted due to blood loss and increasing hemodynamic instability. Local application of antibiotic-loaded beads was not done due to the already poor renal failure and expected worsening following surgery.

Postoperatively, the patient stabilized rapidly. Considering the massive scar tissue formation around the hip, the infection was deemed chronic and the initial sepsis was most probably secondary. The PJI of the knee was likely secondary but had been diagnosed with a very low bacterial load. Considering age, comorbidities, as well as the surgical requirements for a cure of the PJI, the option of a suppressive antibiotic therapy was negotiated with the patient. He could be discharged back to his nursing facility on the 7th postoperative day with an oral antibiotic suppression with trimethoprim/sulfamethoxazole.

The patient never had low back pain, and there never were any clinical signs of infection in the lumbar region. One of the infectious episodes of the last years treated as recurrent urinary tract infection was probably a *S. aureus* sepsis causing PJI of the hip, as postoperative infection had been ruled out thanks to the aspiration performed about 1.5 years post-THA.

Over the following months, the patient remained pain-free, but the hip remained clinically inflamed, whereas the knee remained clinically inconspicuous. Serum C-reactive protein (CRP) levels stagnated initially but increased secondarily (Figure 2). As there were no treatment alternatives, particularly regarding oral suppression options, and as the patient still did not accept palliative treatment, this prompted investigations regarding possibilities for an adjunct treatment with bacteriophages. Bacteriophages were made available from the collection from Queen Astrid Military Hospital (Brussels, Belgium). Bacteriophage ISP had only a limited lytic activity against the MRSA strain of the patient (efficiency of plating: 0.1), but this was deemed sufficient as a small additive effect was observed *in vitro* in combination with daptomycin (Figure 3). Limited bacterial regrowth was observed after 10 h, which was not unexpected due to the use of rich growth media and was present to a lower degree when phage antibiotics were combined. The heat map of various concentrations of bacteriophages in combination with various concentrations of daptomycin is provided in Figure 4. Bacteriophage ISP is a frequently used staphylococcal phage in Magistral preparations at Queen Astrid Military Hospital and the specific batch underwent quality control by Sciesano for pH (mean 7.13; pass), identification (confirmed),

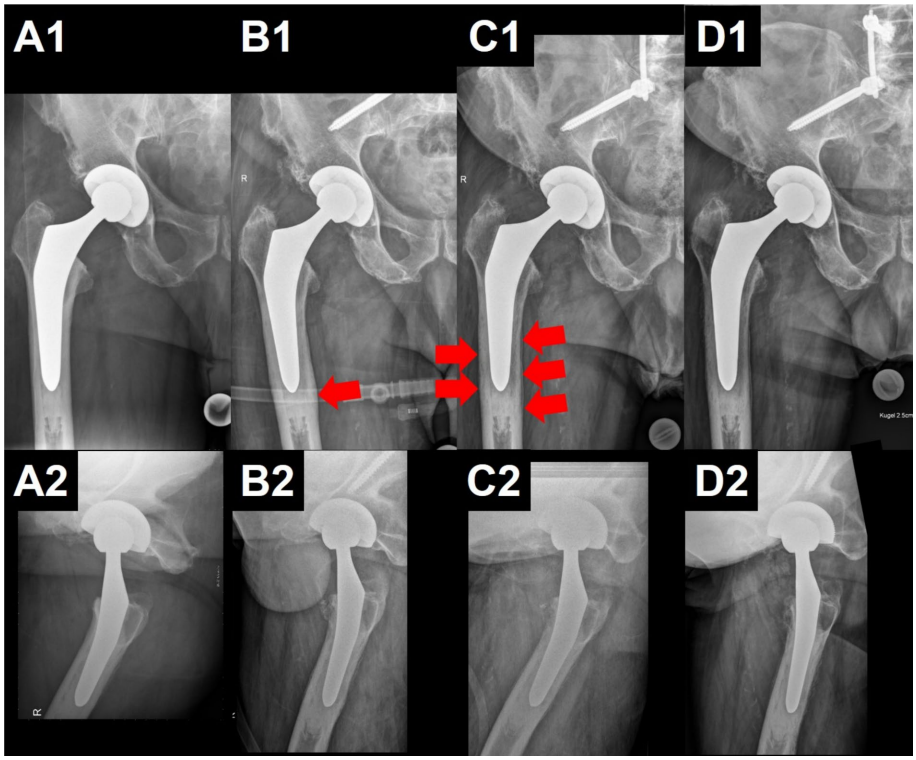

FIGURE 1
Radiographic follow-up of the patient described. The upper row shows the zone of interest of pelvic anteroposterior radiographs, illustrating the right hip. The lower row shows the corresponding axial views. Note the total hip arthroplasty (THA) with uncemented cup and cemented stem, as well as the partially illustrated material from the lumbopelvic fixation. In **(A)**, after THA. In **(B)**, regular follow-up 5 years after THA. Note the appearance of a cortical thickening at the tip of the stem (red arrow), most probably due to mechanical overload secondary to the line-to-line cementation. In **(C)**, 7 years after THA, when the patient was hospitalized due to the sepsis. Note the additional periosteal reaction (red arrows), which may still be caused by the above-mentioned mechanical issue and not necessarily by the infection. In **(D)**, the last radiographs, approximately 7 months after the revision. Technical differences in exposure of the radiograph explain differences in contrast, but no loosening is present.

microbial contamination (pass), and endotoxin quantification (<5 EU/mL).

The patient was hospitalized for this treatment about 6 months after the revision, as soon as the preparation could be made available, which took more than 3 months. Bacteriophages were applied parenterally as well as intraarticularly over a total of 10 days at a concentration of 10^7 plaque forming units (PFU)/mL (Table 1). During the bacteriophage treatment, the oral antimicrobial therapy with trimethoprim/sulfamethoxazole was substituted with parenteral daptomycin at 8 mg/kg/day again. The patient tolerated the repeated joint infiltrations well. Joint aspirations were obtained prior to the start of phage therapy and then before subsequent doses. No bacteriophage was detected in the synovial fluid of either joint at the start of therapy, but was then detected in the synovial fluid of the hip prior to subsequent administrations (average 2×10^4 PFU/mL), indicating prolonged presence at the site of infection. Low levels of MRSA were found in the hip synovial fluid throughout the treatment but no resistance to phage ISP was detected and there was no change in antibiotic susceptibility of the isolated MRSA strains. No more MRSA was detected in the knee.

The bacteriophage treatment was considered very successful by the patient. He noted an improvement of his general state and better mobility of his hip. Objectively, a disappearance of clinical signs of infection could be observed (Figure 5), as well as a regression of the CRP, even if a normalization was not reached (Figure 2). However, repeated aspirations of the hip joint proved persistence of the MRSA and leukocytes (Figure 2). Thus, the antimicrobial treatment with trimethoprim/sulfamethoxazole was maintained. Nevertheless, only small quantities of fluid could be aspirated, whereas initially large quantities of pus were present, and bacterial identification then required 5–8 days of culture.

The patient finally died in his nursing home about 6 months after the bacteriophage therapy, respectively 12 months after the revision, without presenting signs of infection or pain, although it was not possible to ascertain an ultimate cause of death. Obtaining follow-up samples to determine the presence of MRSA and bacteriophages, as well as phage neutralizing antibodies, was not possible due to the death of the patient shortly before the scheduled visit.

The patient had provided written informed consent for publication of anonymized data before the revision.

Discussion

In the reported case bacteriophage therapy was considered due to persistent MRSA infection despite standard treatment, limited oral antibiotic options, and the patient's comorbidities restricting further surgical interventions. Additionally, increased *in vitro* activity between

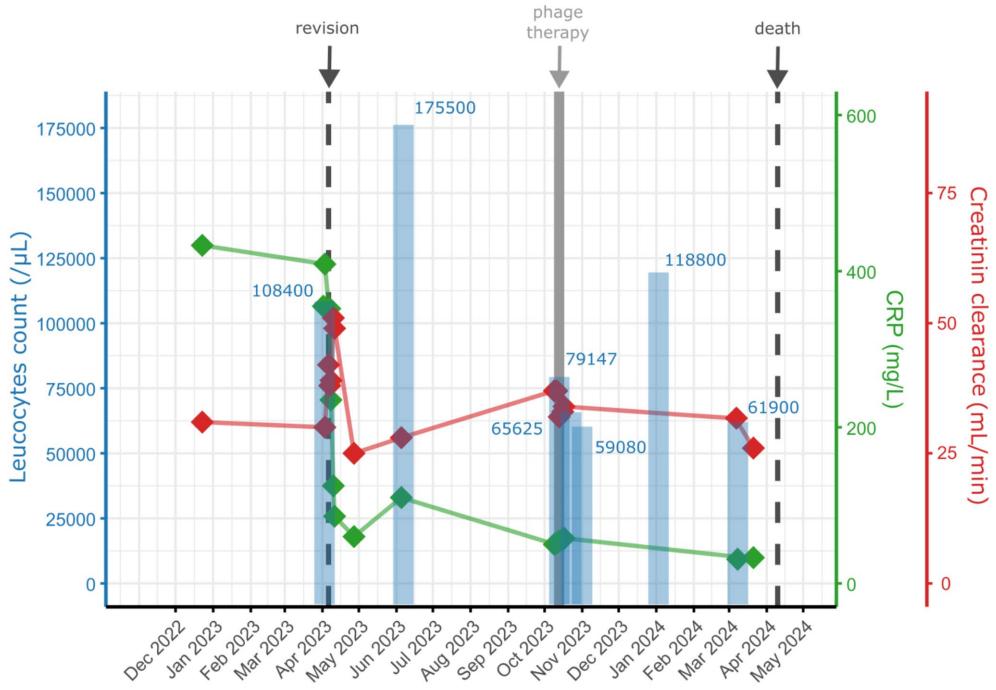

FIGURE 2
Overview of the serum CRP levels (green), the creatinine clearance (red) as estimated by the modification of diet in renal diseases (MDRD) formula, and of the leucocyte count from the hip joint aspirations (blue) over time from the patient described. Note the reduction of CRP following the phage treatment. Even if the leucocyte count from the joint aspiration remained elevated, there were no more clinical signs of infection and the bacterial growth in culture was notably delayed.

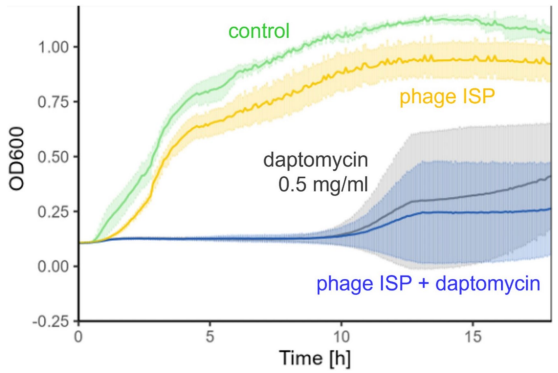

FIGURE 3
Phage susceptibility testing. Turbidity reduction assay of phage ISP on the patient's MRSA strain as measured by optical density (OD 600 nm) over time (h) showing the effect of phage ISP (yellow; 10^7 PFU/mL) and daptomycin (grey, 0.5 mg/L) alone and in combination (blue) on bacterial growth (control in green).

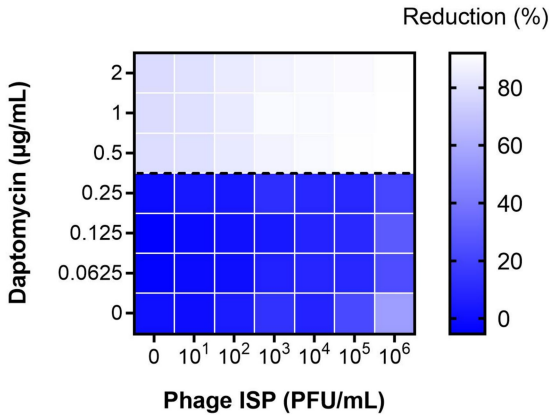

FIGURE 4
Heat map of phage-antibiotic synergy tested against the patient's isolate at 12 h. Effect of phage ISP in combination with daptomycin as shown as the mean reduction of each combination; Reduction (%) = $[(OD_{growth\ control} - OD_{treatment})/OD_{growth\ control}] \times 100$. The dotted line indicates the minimum inhibitory concentration (MIC) of the strain to daptomycin. The graph was plotted using GraphPad Prism version 8.0.2 for Windows.

daptomycin and the selected phage supported its use as a promising adjunctive strategy for infection control.

Classical surgical and antibiotic options may not be sufficiently effective or tolerable to treat successfully PJI, particularly when comorbidities limit therapeutic possibilities (4, 5, 7–11, 15, 19). Antibiotic suppression would be the classical option in case of treatment failure without surgical options (9, 12, 13). However, adequate drugs may not always be available or tolerated by the patient (4, 13), and antibiotic suppression may also not be sufficient to prevent overt recurrence of infection (12, 13, 20). As illustrated in this case, the administration of bacteriophages may be a valuable, less-invasive adjunct to successfully suppress the infection (12–14, 20). PJI persistence was proven by repeated aspirations (Figure 2). However, the bacteriophage-antibiotic synergy may have been decisive to obtain

TABLE 1 Overview of the administration scheme of the bacteriophages.

	Quantity\Day	1	2	3	4	5	6	7	8	9	10
Systemic	80 mL at 1×10^7 PFU/mL in 100 mL saline over 6 h	X	X	X	X	X	X	X	X	X	X
Hip	20 mL at 1×10^7 PFU/mL	X		X	X	X			X		
Knee	10 mL at 1×10^7 PFU/mL	X							X		

A solution containing 10^7 PFU/mL of the phage ISP was used. Bacteriophages were administered systemically as well as locally. For systemic application, 80 mL of phage ISP (1×10^7 PFU/mL) was diluted in 100 mL of sterile saline and administered intravenously via a perfusor over a 6-h period, corresponding to an infusion rate of 30 mL/h. Intra-articular phage therapy was administered as a bolus injection. Under sterile conditions in a radiologic intervention suite, joint aspiration was performed under fluoroscopic guidance. Following the removal of synovial fluid, the phage ISP (20 mL at 1×10^7 PFU/mL for the hip, 10 mL at 1×10^7 PFU/mL for the knee) was injected into the joint space using a single-use syringe. Daptomycin was administered concomitantly during the 10-day course.

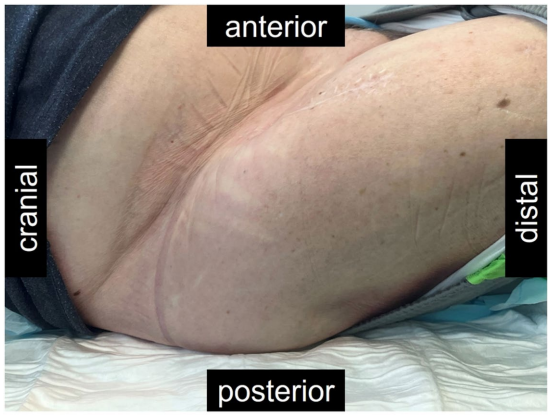

FIGURE 5
Picture of the right hip of the patient described, approximately 11 months after the revision, and 5 months after bacteriophage therapy. The scar from the anterior approach remained closed throughout. Fibrosis made the tissues around the hip hard and the hip remained fixated in the flexion illustrated. However, the patient had no more pain and the hyperemia nearly had disappeared after the treatment with bacteriophages.

the desire control of infection. In this case, the bacteriophage therapy was tolerated without side effects.

While objective parameters showed only a marginal response (Figure 2), clinically and subjectively, there was a major benefit of the bacteriophage therapy (Figure 5). Such soft outcomes are difficult to document, particularly in retrospective studies. Differences in outcome parameters, however, have major implications on the reported treatment effectiveness in PJI (21, 22). The Musculoskelettal Infection Society provided guidelines for tiered outcome reporting to better assess treatment success (22). While this classification is not yet widely known, the bacteriophages would have transformed a Tier 3 or 4 (overt failures) into a Tier 2 outcome (successful control of the infection with antibiotic suppression) (22). Standardization of outcome reporting in the treatment of musculoskeletal infections is encouraged, particularly as functional outcomes and infection control may by more important than eradication of infection (14, 15, 21–25). This case suffered no adverse events from the bacteriophage administration. Minor and mostly local reactions to bacteriophage administration are reported only rarely (14, 15, 26).

Beyond the clinical benefit for this one patient, this report may be useful for the technical details made available regarding posology (Table 1), as this remains an open topic in bacteriophage therapy (14, 15). Bacteriophage selection, preparation and administration remains associated with major obstacles, greatly limiting availability and practicability. In this case, the procedure required more than 3 months from the timepoint of indication until the preparations were available. While selection, culture and preparation of the bacteriophages invariably takes a certain amount of time, the issue is primarily administrative, particularly when cross-country delivery is required (27). Particularly if more than one country is involved, which usually is necessary in Europe to access the various bacteriophage libraries available. Beyond the administrative burden, which is out of proportion for clinical care and which requires a dedicated research team, such delays may be inacceptable if the evolution of the infection dictates faster treatment. Nevertheless, research and developments in this domain should be pursued, particularly considering issues with future antibiotic limitations, costs associated with treatment failure in PJI, and considering the very interesting results published so far (14, 15). While bacteriophages are used so far only as last-resort salvage, this may have to be reconsidered to attribute a role earlier in the treatment algorithms.

Finally, the duration of symptoms is recommended as a decisive parameter to indicated prosthesis-retaining treatment (7–9). While the duration of symptoms was short, this patient overtly presented a chronic PJI of his hip. Despite impossibility to perform the treatment of choice, i.e., full revision of the components, infection control could be obtained, representing an acceptable option in such an elderly and multimorbid patient (7–9, 12, 13, 22–25).

Data availability statement

Raw data supporting the conclusions of theis article will be shared with researchers submitting a methodologically sound proposal. Requests should be directed to the corresponding author.

Ethics statement

The study was conducted in accordance with local legislation and institutional requirements. Ethical approval for the reuse of medical data and biological material was obtained under a general consent

framework approved by the Kantonale Ethikkommission Zürich, Zürich, Switzerland. Written informed consent was obtained from the patient for the publication of this case report. Phage therapy was administered as an experimental treatment on a compassionate-use basis. The procedure adhered to the guidelines of the Swiss Academy of Medical Sciences (SAMS) regarding the distinction between standard and experimental therapy. A declaration of non-responsibility ("Nichtzuständigkeitserklärung") was obtained from the local ethics committee. Additionally, written informed consent was obtained from the patient prior to undergoing the experimental therapy.

Author contributions

PW: Conceptualization, Data curation, Formal analysis, Investigation, Project administration, Supervision, Writing – original draft, Writing – review & editing, Visualization. MS: Investigation, Visualization, Writing – original draft, Writing – review & editing, Methodology. AL: Investigation, Methodology, Visualization, Writing – original draft, Writing – review & editing, Data curation, Formal analysis, Supervision. IU: Investigation, Writing – original draft, Writing – review & editing. SH: Investigation, Writing – original draft, Writing – review & editing. BF: Investigation, Writing – original draft, Writing – review & editing. JS: Investigation, Writing – original draft, Writing – review & editing, Data curation, Formal analysis, Visualization. SD: Writing – original draft, Writing – review & editing, Methodology, Supervision. LL: Methodology, Supervision, Writing – original draft, Writing – review & editing, Conceptualization, Data curation, Formal analysis, Funding acquisition, Investigation, Project administration. SM: Conceptualization, Data curation, Formal analysis, Funding acquisition, Investigation, Methodology, Project administration, Resources, Software, Supervision, Validation, Visualization, Writing – original draft, Writing – review & editing.

Funding

The author(s) declare that financial support was received for the research and/or publication of this article. Funding was received from the Swiss Continence Foundation (www.swisscontinencefoundation.ch); The Swiss National Science Foundation (www.snsf.ch), Sinergia grant (CRSII5_189957); The LOOP Zurich, and the Monique Dornonville de la Cour-Stiftung.

Acknowledgments

The authors acknowledge the Phage Therapy Group and the Laboratory for Molecular and Cellular Technology at the Queen Astrid Military Hospital for testing and supplying the bacteriophages used in this case. We also thank the Swiss Continence Foundation (www.swisscontinencefoundation.ch), the Swiss National Science Foundation (www.snsf.ch), Sinergia grant (CRSII5_189957), The LOOP Zurich, and the Monique Dornonville de la Cour-Stiftung for their financial support of researchers involved in this work. Special thanks go to Sonja Milek and Oksana Chemych from the Phage Therapy Lab at Balgrist University Hospital, University of Zurich, Zürich, Switzerland for their invaluable contributions to on-site bacteriophage handling and sample processing and to Prof. Thomas M. Kessler for establishing the framework of the Phage Therapy Lab. We extend our sincere appreciation to the nursing staff at Balgrist University Hospital for their dedicated care of the patient and for embracing additional responsibilities throughout the experimental treatment. Most importantly, we thank the patient for his exceptional commitment, strict adherence to all instructions, and unwavering motivation during the entire course of therapy.

Conflict of interest

The authors declare that the research was conducted in the absence of any commercial or financial relationships that could be construed as a potential conflict of interest.

Generative AI statement

The authors declare that no Gen AI was used in the creation of this manuscript.

Publisher's note

References

1. Lum ZC, Natsuhara KM, Shelton TJ, Giordani M, Pereira GC, Meehan JP. Mortality during total knee periprosthetic joint infection. *J Arthroplast*. (2018) 33:3783–8. doi: 10.1016/j.arth.2018.08.021

2. Natsuhara KM, Shelton TJ, Meehan JP, Lum ZC. Mortality during total hip periprosthetic joint infection. *J Arthroplast*. (2019) 34:S337–42. doi: 10.1016/j.arth.2018.12.024

3. Shahi A, Tan TL, Chen AF, Maltenfort MG, Parvizi J. In-hospital mortality in patients with Periprosthetic joint infection. *J Arthroplast*. (2017) 32:948–52.e1. doi: 10.1016/j.arth.2016.09.027

4. Valour F, Karsenty J, Bouaziz A, Ader F, Tod M, Lustig S, et al. Antimicrobial-related severe adverse events during treatment of bone and joint infection due to methicillin-susceptible *Staphylococcus aureus*. *Antimicrob Agents Chemother*. (2014) 58:746–55. doi: 10.1128/AAC.02032-13

5. Resl M, Becker L, Steinbrück A, Wu Y, Perka C. Re-revision and mortality rate following revision total hip arthroplasty for infection. *Bone Joint J*. (2024) 106-B:565–72. doi: 10.1302/0301-620X.106B6.BJJ-2023-1181.R1

6. Reinhard J, Lang S, Walter N, Schindler M, Bärtl S, Szymski D, et al. In-hospital mortality of patients with periprosthetic joint infection. *Bone Jt Open*. (2024) 5:367–73. doi: 10.1302/2633-1462.54.BJO-2023-0162.R1

7. Zimmerli W, Trampuz A, Ochsner PE. Prosthetic-joint infections. *N Engl J Med*. (2004) 351:1645–54. doi: 10.1056/NEJMra040181

8. Osmon DR, Berbari EF, Berendt AR, Lew D, Zimmerli W, Steckelberg JM, et al. Diagnosis and management of prosthetic joint infection: clinical practice guidelines by the Infectious Diseases Society of America. *Clin Infect Dis*. (2013) 56:e1–e25. doi: 10.1093/cid/cis803

9. Tande AJ, Gomez-Urena EO, Berbari EF, Osmon DR. Management of Prosthetic Joint Infection. *Infect Dis Clin N Am*. (2017) 31:237–52. doi: 10.1016/j.idc.2017.01.009

10. Grammatopoulos G, Kendrick B, McNally M, Athanasou NA, Atkins B, McLardy-Smith P, et al. Outcome following debridement, antibiotics, and implant retention in hip periprosthetic joint infection-an 18-year experience. *J Arthroplast*. (2017) 32:2248–55. doi: 10.1016/j.arth.2017.02.066

11. Lora-Tamayo J, Senneville É, Ribera A, Bernard L, Dupon M, Zeller V, et al. The not-so-good prognosis of streptococcal periprosthetic joint infection managed by implant retention: the results of a large multicenter study. *Clin Infect Dis*. (2017) 64:1742–52. doi: 10.1093/cid/cix227

12. Sandiford NA, Hutt JR, Kendoff DO, Mitchell PA, Citak M, Granger L. Prolonged suppressive antibiotic therapy is successful in the management of prosthetic joint infection. *Eur J Orthop Surg Traumatol*. (2020) 30:313–21. doi: 10.1007/s00590-019-02559-4

13. Prendki V, Ferry T, Sergent P, Oziol E, Forestier E, Fraisse T, et al. Prolonged suppressive antibiotic therapy for prosthetic joint infection in the elderly: a national multicentre cohort study. *Eur J Clin Microbiol Infect Dis*. (2017) 36:1577–85. doi: 10.1007/s10096-017-2971-2

14. Clarke AL, De Soir S, Jones JD. The safety and efficacy of phage therapy for bone and joint infections: A systematic review. *Antibiotics*. (2020) 9:795. doi: 10.3390/antibiotics9110795

15. Geneviève J, McCallin S, Huttner A, Pham TT, Suva D. A systematic review of phage therapy applied to bone and joint infections: an analysis of success rates, treatment modalities and safety. *EFORT Open Rev*. (2021) 6:1148–56. doi: 10.1302/2058-5241.6.210073

16. Gordillo Altamirano FL, Kostoulias X, Subedi D, Korneev D, Peleg AY, Barr JJ. Phage-antibiotic combination is a superior treatment against *Acinetobacter baumannii* in a preclinical study. *EBioMedicine*. (2022) 80:104045. doi: 10.1016/j.ebiom.2022.104045

17. Łusiak-Szelachowska M, Międzybrodzki R, Drulis-Kawa Z, Cater K, Knežević P, Winogradow C, et al. Bacteriophages and antibiotic interactions in clinical practice: what we have learned so far. *J Biomed Sci*. (2022) 29:23. doi: 10.1186/s12929-022-00806-1

18. Beel W, Klaeser B, Kalberer F, Meier C, Wahl P. The effect of a distal centralizer on cemented femoral stems in arthroplasty shown on radiographs and SPECT/CT: a case report. *JBJS Case Connect*. (2021) 11:973. doi: 10.2106/JBJS.CC.20.00973

19. Li C, Renz N, Trampuz A. Management of periprosthetic joint infection. *Hip Pelvis*. (2018) 30:138–46. doi: 10.5371/hp.2018.30.3.138

20. Siqueira MB, Saleh A, Klika AK, O'Rourke C, Schmitt S, Higuera CA, et al. Chronic suppression of periprosthetic joint infections with oral antibiotics increases infection-free survivorship. *J Bone Joint Surg Am*. (2015) 97:1220–32. doi: 10.2106/JBJS.N.00999

21. Debbi EM, Khilnani T, Gkiatas I, Chiu YF, Miller AO, Henry MW, et al. Changing the definition of treatment success alters treatment outcomes in periprosthetic joint infection: a systematic review and meta-analysis. *J Bone Jt Infect*. (2024) 9:127–36. doi: 10.5194/jbji-9-127-2024

22. Fillingham YA, Della Valle CJ, Suleiman LI, Springer BD, Gehrke T, Bini SA, et al. Definition of successful infection management and guidelines for reporting of outcomes after surgical treatment of periprosthetic joint infection: from the workgroup of the musculoskeletal infection society (MSIS). *J Bone Joint Surg Am*. (2019) 101:e69. doi: 10.2106/JBJS.19.00062

23. Grammatopoulos G, Bolduc ME, Atkins BL, Kendrick BJL, McLardy-Smith P, Murray DW, et al. Functional outcome of debridement, antibiotics and implant retention in periprosthetic joint infection involving the hip: a case-control study. *Bone Joint J*. (2017) 99-B:614–22. doi: 10.1302/0301-620X.99B5.BJJ-2016-0562.R2

24. Dzaja I, Howard J, Somerville L, Lanting B. Functional outcomes of acutely infected knee arthroplasty: a comparison of different surgical treatment options. *Can J Surg*. (2015) 58:402–7. doi: 10.1503/cjs.017614

25. Herman BV, Nyland M, Somerville L, Mac Donald SJ, Lanting BA, Howard JL. Functional outcomes of infected hip arthroplasty: a comparison of different surgical treatment options. *Hip Int*. (2017) 27:245–50. doi: 10.5301/hipint.5000455

26. Uyttebroek S, Chen B, Onsea J, Ruythooren F, Debaveye Y, Devolder D, et al. Safety and efficacy of phage therapy in difficult-to-treat infections: a systematic review. *Lancet Infect Dis*. (2022) 22:e208–20. doi: 10.1016/S1473-3099(21)00612-5

27. Pirnay JP, Verbeken G. Magistral phage preparations: is this the model for everyone? *Clin Infect Dis*. (2023) 77:S360–9. doi: 10.1093/cid/ciad481

frontiers | Frontiers in Cellular and Infection Microbiology

TYPE Original Research
PUBLISHED 28 April 2025
DOI 10.3389/fcimb.2025.1563781

OPEN ACCESS

EDITED BY
Mercedes Gonzalez Moreno,
Leibniz Institute for Natural Product Research and Infection Biology, Hans Knoll Institute, Germany

REVIEWED BY
Jumpei Fujiki,
Rakuno Gakuen University, Japan
Ahmed Elfadadny,
Tokyo University of Agriculture and Technology, Japan

*CORRESPONDENCE
Ahlam Alsaadi
alsaadi-ahlam@hotmail.com

RECEIVED 20 January 2025
ACCEPTED 27 March 2025
PUBLISHED 28 April 2025

CITATION
Alsaadi A, Imam M, Alghamdi AA, Aljedani SS, Alsari A, Aljami H and Bosaeed M (2025) Genomic analysis of prophages in 44 clinical strains of *Pseudomonas aeruginosa* isolated in Saudi Arabia. *Front. Cell. Infect. Microbiol.* 15:1563781. doi: 10.3389/fcimb.2025.1563781

Genomic analysis of prophages in 44 clinical strains of *Pseudomonas aeruginosa* isolated in Saudi Arabia

Ahlam Alsaadi[1]*, Mohammed Imam[2], Abdulrahman A. Alghamdi[1], Safia S. Aljedani[1], Amal Alsari[1], Haya Aljami[1] and Mohammad Bosaeed[1,3]

[1]King Abdullah International Medical Research Center, King Saud Bin Abdulaziz University for Health Sciences, Riyadh, Saudi Arabia, [2]Department of Microbiology and Parasitology, Qunfudah College of Medicine, Umm Al-Qura University, Al-Qunfudah, Makkah, Saudi Arabia, [3]Department of Medicine, King Abdulaziz Medical City, Ministry of National Guard Health Affairs, Riyadh, Saudi Arabia

Prophages are bacteriophages that integrate their genomes into the bacterial chromosome. This research aimed to analyze and characterize prophages integrated into 44 *Pseudomonas aeruginosa* strains isolated from tertiary hospitals in Saudi Arabia. A total of 97 intact prophages were identified among clinical strains, with 16 prophages found present in more than one strain simultaneously. All prophages were found to have lengths ranging from 7.7 kb to 74.1 kb, and their GC content was found to be between 49.91% and 64.9%. Our findings show that prophages are present in the majority of the isolated *P. aeruginosa* strains (41 out of 44). Additionally, several proteins related to viral defense (toxin/antitoxin modules and proteins against restriction-modification enzymes) were identified, supporting the idea that prophages influence bacterial pathogenesis and anti-phage defenses.

KEYWORDS

***Pseudomonas aeruginosa*, prophages, multi-drug resistance, bacteriophages, Saudi Arabia**

Background

Pseudomonas aeruginosa is an opportunistic, Gram-negative pathogen and a member of the diverse and complex *Pseudomonas* genus (Pirnay et al., 2009). *P. aeruginosa* persists in both clinical and environmental settings and causes a wide spectrum of human infections, ranging from mild to life-threatening conditions (Diggle and Whiteley, 2020). The treatment of infections caused by *P. aeruginosa* presents one of the greatest therapeutic challenges (Pelegrin et al., 2021). Antibiotic resistance in *P. aeruginosa* can develop either through mutation that modify the expression or function of resistance-related genes or by

acquiring resistance genes via mobile genetic elements (MGEs) (Silby et al., 2011). The accessory genome in *P. aeruginosa* consists mainly of mobile genetic elements such as plasmids, transposons, and temperate bacteriophages (prophages) (Silby et al., 2011). *P. aeruginosa* is listed in the ESKAPE group of pathogens, a designation for six bacteria recognized for critical clinical importance due to their increased antimicrobial-resistance rates (Rice, 2008).

Bacteriophages, or phages for short, are bacterial viruses considered obligate intracellular parasites. Phages are highly abundant on earth (Ackermann, 2007). During host infection, typically phages undergo one of two different life cycles: the lysogenic or the lytic cycle (Penadés et al., 2015; Williams et al., 2008). For phage therapy, strictly lytic phages, which directly undergo the lytic life cycle and lyse the target bacterial cells are preferable. Phages that follow the lysogenic life cycle integrate their genomes into the genome of their bacterial host, thereby contributing to bacterial fitness and bacterial genomic diversity, including the acquisition of antibiotic resistance genes and virulence factors (Gandon, 2016). Phages that integrate their genomes into the bacterial host are referred to as "prophages" or "temperate" phages (Gandon, 2016; Gordon et al., 2017). Recent studies have shown that prophages interact with their bacterial host's regulatory cascade and interfere with the host's immune system, in addition to encoding toxins, lytic proteins, and antimicrobial-resistance genes (Cieślik et al., 2021). For instance, in clinical *P. aeruginosa* prophage were found to code complete type II toxin-antitoxin module, exhibiting homology to the BrnT toxin and a CopG family antitoxin while other encode for complete type II TA system YoeB/YefM that is related to antibiotic resistance, biofilm formation, serum survival and host infection (Heaton et al., 2012; Ma et al., 2021). Moreover, the type II toxin YafO and a type IV antitoxin AbiEi were found in P. aeruginosa prophages all in which counteract bacterial defenses or to compete against external phages targeting the host (González de Aledo et al., 2023; Leroux and Laub, 2025). Therefore, the impact of prophages on human health and disease are largely unexplored and is still under investigation.

Early estimates found that prophages account for 10 to 20% of the host's genome (Hatfull and Hendrix, 2011). The presence of prophages within the bacterial genome can provide the host with a selective advantage, for instance, the acquisition of prophages in clinical *P. aeruginosa* has been shown to reduce antibiotic susceptibility and enhance biofilm formation (Tariq et al., 2019). Among these, *P. aeruginosa* filamentous prophages Pf4 are highly upregulated and contributed to both biofilm formation and virulence (Hay and Lithgow, 2019; Platt et al., 2008; Rice et al., 2009). Additionally, prophages DMS3 and pp3 play distinct roles in host adaptation: DMS3 inhibits infection by phages that utilize the type IV pilus as a receptor, while pp3 promotes biofilm formation, facilitating bacterial persistence (Canchaya et al., 2004; Li et al., 2017; Little, 2005; Shah et al., 2021). Prophages can protect bacteria from environmental stressors and confer antibiotic resistance to bacterial cells by enhancing bacterial fitness through mechanisms such as, toxin-antitoxin systems, superinfection exclusion, biofilm formation and horizontal gene transfer (HGT) (Wang et al., 2010). These temperate phages significantly contribute to the extensive genomic diversity of bacteriophages through HGT and recombination (Dion et al., 2020).

Prophage-host interactions and dynamic adaptations over time have resulted in the acquisition of numerous defense mechanisms in response to selective pressures. These mechanisms including restriction-enzymes (RM) systems, clustered regularly interspaced short palindromic repeats (CRISPR) and CRISPR-associated (*cas*) genes, the abortive infection (Abi) systems, as well as the accumulation of a variety of mutations in surface receptor proteins (Ambroa et al., 2022; Labrie et al., 2010). As the evolutionary race between bacteria and their viral predators continue, new anti-viral mechanisms have been discovered and describes, such as the use of cyclic nucleotides as signaling molecules, such as the cyclic oligonucleotide-based antiphage signaling system, the pyrimidine cyclase system for antiphage resistance, and restriction by an adenosine deaminase acting on RNA (Cohen et al., 2019; Duncan-Lowey et al., 2023; Tal et al., 2021). Additionally, NAD+ depletion is a widespread bacterial defense response to viral infection (Garb et al., 2022; Tal and Sorek, 2022). As phages evolve, they have developed mechanisms such as anti-CRISPR (Acr) proteins and viral DNA methyltransferases. Acr proteins, first discovered in prophages infecting *P. aeruginosa* strains (Bondy-Denomy et al., 2013), are small peptides known to inhibit CRISPR-Cas activity. They function by binding to the different elements of the CRISPR machinery, thereby preventing DNA recognition, or inhibiting Cas protein activity once the protein complex has assembled around the target DNA (Pawluk et al., 2018).

Most *P. aeruginosa* strains have been identified to contain at least one prophage-like element; some are poly-lysogens, harboring several prophages in their genome (Knezevic et al., 2015; Silby et al., 2011). Lysogenic phages in *P. aeruginosa* have been shown to confer selective beneficial traits, such as O antigen conversion, biofilm development, and virulence (Hayashi et al., 1990; Kuzio and Kropinski, 1983; Rice et al., 2009). Additionally, prophages can serve as viable candidates for phage therapy, as they can be genetically engineered to be strictly lytic. For instance, in 2019, a patient with disseminated drug-resistant *Mycobacterium abscessus* was successfully treated with a cocktail of mutant phages engineered to eliminate lysogeny associated genes (Dedrick et al., 2019). Thus, identifying *P. aeruginosa* prophages provides valuable insight into the role of phages in *P. aeruginosa* fitness and pathogenicity.

Here, we investigate publicly available *P. aeruginosa* genomes from Saudi Arabia, which currently include 44 published clinical bacterial genomes, with a focus on temperate *P. aeruginosa* phages. This study aims to expand understanding of the nature, composition, and role of prophages found within a multicenter hospital *P. aeruginosa* strain collection from Saudi Arabia. Additionally, we analyze the genes these prophages harbor to overcome bacterial defenses and disseminate antibiotic resistance genes. Identifying prophages with no AMR or virulence factor genes in their genome is beneficial as they can hold potential as phage therapy candidates.

Materials and methods

Origin of *P. aeruginosa* isolated genomes

A total of 44 complete genomes of *P. aeruginosa* isolates from 44 patients were obtained from the National Center for Biotechnology Information (NCBI) database (https://www.ncbi.nlm.nih.gov/) (Last accessed on April 17, 2023). Demographic data of the patients were extracted from the original study's Supplementary Data and presented in the study (see Table 1; Supplementary Table 1), bacterial genomes were sequenced using the MiSeq Illumina platform with a 2 x 300 bp paired-end reads protocol, as previously described (Doumith et al., 2022). The whole genome extraction and sequencing methods are described (Doumith et al., 2022), and genomes were deposited in Genebank under the accession numbers PRJNA751257.

Identification of prophages in *P. aeruginosa* strains

Whole-genome sequences of *P. aeruginosa* clinical strains were used to identify and annotate prophages by submitting FASTA files via the web interface to PHASTER (PHAge Search Tool Enhanced Release) (https://phaster.ca/), a bioinformatics tool designed to rapidly identify and annotate putative prophage genomes sequences within the contigs of each bacterial genome. *P. aeruginosa* genomes were accessed on 23 04 2023. According to scoring criteria, PHASTER identifies prophages in three different categories: intact (score >90), questionable (score 70-90), and incomplete (score <70). Only intact prophages with scores of >90 were selected for this study. Additionally, PHASTER provides the location or insertion site of prophage within the bacterial genome, the number of coding DNA sequences (CDSs), and the GC% content of each prophage genome. Prophage genomes content were annotated using Prokka (https://github.com/tseemann/prokka) (last accessed on January 10, 2024) and the PHROGs database, which represents a library of families of different prokaryotic virus proteins generated using a new clustering approach based on remote homology detection, (https://phrogs.lmge.uca.fr/) (last accessed on January 10, 2024) (Terzian et al., 2021).

P. aeruginosa prophage classification based on genomic similarity

With the increasing amount of phage genomic data, phages are now classified based on their genome similarity, as defined by the International Committee on the Taxonomy of Viruses (ICTV). Taxonomic classification of dsDNA phage genomes was conducted using a recently published automated high-throughput computational tool (taxmyPHAGE) (https://github.com/amillard/tax_myPHAGE/tree/main) designed for genus- and species-level identification of bacteriophages (Millard et al., 2024). In this study, we searched for closely related phages based on their genome similarity to classify prophage genomes using taxmyPHAGE. Input phage genomes were prophages whole genome sequences as FASTA format files, and the output data included information on the phage genus and species, along with similarity scores. Based on the tool guidelines, dsDNA phage genomes with an average nucleotide identity (ANI) ≥95% are considered the same species, and bacteriophages with an ANI ≥ 70% over 100% of the genome are considered to belong to the same genus (Millard et al., 2024). Also, Genome-based phylogeny and tree construction was performed using the VICTOR web platform to compare Psedumonas prophage genomes from this study with three members of the *Casadabanvirus* genus, as currently recognized by the ICTV (https://ictv.global) (Meier-Kolthoff and Göker, 2017). Whole-genome amino acid sequences comparisons were conducted using the Genome-BLAST Distance Phylogeny method (GBDP) approach, applying the d0 distance formula (Meier-Kolthoff et al., 2013). The resulting intergenomic distances were used to construct a balanced minimum evolution phylogenetic tree using FASTME 2.0, incorporating subtree pruning and regrafting (SPR) optimization and supported by 100 pseudo-bootstrap replicates (Lefort et al., 2015). The final tree was midpoint-rooted and visualized using the ggtree package (Yu et al., 2017). Species, genus, and family demarcation thresholds were determined using the OPTSIL clustering algorithm (Göker et al., 2009). Applying standard parameters and an F value of 0.5, protein homology was assessed using HHPRED (Zimmermann et al., 2018) and PHYRE2 (Kelley et al., 2015), while domain architecture predictions were carried out using the SMART tool (Letunic et al., 2021).

Phylogenetic analysis of common *Pseudomonas* prophages

All identified complete prophage sequences were aligned using the MAFFT Version 7.0 program (https://maft.cbrc.jp/alignment/server/), using the strategy 'auto'. A phylogenetic tree of the genomes was subsequently constructed using the phylogeny program (https://maft.cbrc.jp/alignment/server/phylogeny.html) using the neighbor-joining method using bootstrap values of 1000 replicates. The generated phylogenetic tree was visualized using the iTOL program (Baliga et al., 2021).

Identification of virulence factors in prophage genomes

Prophage genomes were used to screen for virulence factor (VF) genes against the Virulence Factors of Pathogenic Bacteria Database (VFDB) (http://www.mgc.ac.cn/cgi-bin/VFs/v5/main.cgi, last accessed on November 20, 2023) (Liu et al., 2019). The VFDB was established in 2004 to provide up-to-date information about VFs from various bacterial pathogens and serves as a comprehensive repository system of bacterial virulence factors. Furthermore, VF genes were identified using VirulanceFinder 2.0

10.3389/fcimb.2025.1563781

TABLE 1 Characteristics of the 44 P. *aeruginosa* clinical strains.

Strain ID	MLST	β-lactamase	Origin	GenBank accession no.	Accession ID
RPA91	ST235	*bla*GES-15	Respiratory	DAHMLR000000000.1	SAMN20514488
RPA85	ST233	*bla*VIM-2, *bla*OXA-4	Respiratory	DAHMLQ000000000.1	SAMN20514487
RPA78	ST111	*bla*VIM-28	Urine	DAHMLP000000000.1	SAMN20514486
RPA66	ST235	*bla*VEB-16	Urine	DAHPTU000000000.1	SAMN20514485
RPA61	ST1076	-	Respiratory	DAHPTT000000000.1	SAMN20514484
RPA41	ST235	*bla*GES-5	Respiratory	DAHMLO000000000.1	SAMN20514483
RPA37	ST357	-	Blood	DAHMLN000000000.1	SAMN20514482
RPA32	ST235	*bla*GES-5	Urine	DAHMLM000000000.1	SAMN20514481
RPA23	ST235	*bla*GES-5	Blood	DAHMNH000000000.1	SAMN20514480
RPA226	ST357	*bla*OXA-10, *bla*VEB-9	Blood	DAHMMR000000000.1	SAMN20514479
RPA206	ST235	*bla*GES-5	Respiratory	DAHMMQ000000000.1	SAMN20514478
RPA185	ST235	*bla*GES-5	Respiratory	DAHMMP000000000.1	SAMN20514477
RPA135	ST357	*bla*VIM-2, *bla*OXA-10, *bla*VEB-9	Respiratory	DAHMLL000000000.1	SAMN20514476
RPA128	ST235	*bla*GES-5	Blood	DAHPTS000000000.1	SAMN20514475
RPA117	ST1659	-	Blood	DAHMMO000000000.1	SAMN20514474
RPA109	ST235	*bla*GES-5	Blood	DAHMNG000000000.1	SAMN20514473
RPA100	ST1076	-	Respiratory	DAHMNE000000000.1	SAMN20514472
RPA10	ST233	*bla*VIM-2, *bla*OXA-33	Respiratory	DAHPUN000000000.1	SAMN20514471
MPA91	ST773	*bla*NDM-1	Respiratory	DAHMMM000000000.1	SAMN20514470
MPA54	ST235	*bla*GES-5	Wound	DAHPTR000000000.1	SAMN20514469
MPA32	ST235	*bla*GES-5	Respiratory	DAHMNF000000000.1	SAMN20514468
MPA31	ST235	*bla*GES-5	Respiratory	DAHMLK000000000.1	SAMN20514467
MPA14	ST235	*bla*GES-5	Respiratory	DAHPTP000000000.1	SAMN20514466
MPA01	ST235	*bla*GES-5	Urine	DAHMMN000000000.1	SAMN20514465
JPAU94	ST235	*bla*GES-5	Urine	DAHPTO000000000.1	SAMN20514464
JPAU63	ST235	*bla*GES-5	Urine	DAHPTN000000000.1	SAMN20514463
JPAU54	ST308	-	Urine	DAHMLC000000000.1	SAMN20514462
JPAU51	ST1659	–	Urine	DAHMNB000000000.1	SAMN20514461
JPAU32	ST375	*bla*GES-5	Urine	DAHMMH000000000.1	SAMN20514460
JPAR79	ST235	*bla*GES-5	Respiratory	DAHMLJ000000000.1	SAMN20514459
JPAR65	ST235	*bla*GES-5	Respiratory	DAHPTM000000000.1	SAMN20514458
JPAR60	ST233	*bla*VIM-2, *bla*OXA-33, *bla*PER-1	Respiratory	DAHMNC000000000.1	SAMN20514457
JPAR31	ST235	*bla*GES-1	Respiratory	DAHPTL000000000.1	SAMN20514456
JPAR102	ST865	-	Respiratory	DAHPTK000000000.1	SAMN20514455
JPAO31	ST1020	-	Ear Swab	DAHMNA000000000.1	SAMN20514454
JPAB50	ST244	*bla*OXA-232	Blood	DAHPTY000000000.1	SAMN20514453
JPAB41	ST357	*bla*OXA-10, *bla*VEB-9	Blood	DAHPTX000000000.1	SAMN20514452
JPAB38	ST829	-	Blood	DAHPTV000000000.1	SAMN20514451

(Continued)

TABLE 1 Continued

Strain ID	MLST	β-lactamase	Origin	GenBank accession no.	Accession ID
JPAB28	ST233	*bla*OXA-33, *bla*PER-1	Blood	DAHPTW000000000.1	SAMN20514450
JPAB24	ST2374	-	Blood	DAHMLB000000000.1	SAMN20514449
JPAB21	–	-	Blood	DAHMNI000000000.1	SAMN20514448
HPA69	ST500	-	Urine	DAHPTQ000000000.1	SAMN20514447
DPA57	ST357	*bla*VIM-2, *bla*OXA-10, *bla*VEB-9	Respiratory	DAHMND000000000.1	SAMN20514446
DPA39	ST641	-	Blood	DAHPTJ000000000.1	SAMN20514445

Carbapenem-resistant *P. aeruginosa* were isolated between March 2018 and April 2019 from five different hospitals located in the eastern, western and, central regions of Saudi Arabia and various sites of infection (Doumith et al., 2022).

(https://cge.cbs.dtu.dk/services/VirulenceFinder/, last accessed on November 20, 2023).

Identification of antibiotic resistance genes in prophage genomes

All prophage genomes were screened for the presence of antibiotic resistance genes in the Comprehensive Antibiotic Resistance Database (CARD) (https://card.mcmaster.ca/, last accessed on November 20, 2023) (Alcock et al., 2020). CARD is a biological database integrating molecular and sequence data while collecting resistance determinants and associated antibiotics. Resistance genes were also assessed by screening for AMR genes using the ResFinder 4.1 database (https://cge.cbs.dtu.dk/services/ResFinder-4.1/, last accessed on November 20, 2023).

Statistical analysis

The Pearson's correlation coefficient (r) analysis was conducted using DATAtab: Online Statistics Calculator (DATAtab: DATAtabTeam, 2025) https://datatab.net. Pearson's correlation was computed with a two-tailed test, and a threshold of $p < 0.05$ was considered statistically significant. Additionally, scatter plots were generated using DATAtab's online tool, which provided visual representation of the relationships between variables. All statistical assumptions, including normality, were verified before analysis.

Results

Abundance of prophages in *P. aeruginosa* genomes

The genome sequences of 44 P. *aeruginosa* clinical isolates from 44 patients were screened for prophages. A total of 270 prophage-like elements were detected (Supplementary Table 2, 9), of which 97 were classified as intact, 96 as incomplete, and 77 as questionable (Figure 1). The number of intact bacteriophages found in each genome ranged from one to six, with a median of two, adding up to a final value of 97 prophages (Supplementary Table 2). The correlation between the prophage genome type and its distribution was investigated. The Pearson's correlation coefficients (R-values) were Total & Incomplete ($r = 0.79$, $p < 0.001$), Total & Intact ($r = 0.62$, $p < 0.001$) and Total & Questionable ($r = 0.4$, $p = 0.007$). This correlation reveals a significant correlation between the total category and all three subcategories, as the strongest relationship is with Incomplete, followed by Intact, while the weakest is with Questionable. The R-values for all categories were greater than 0.5, indicating a positive correlation between increased the total prophages count with intact and incomplete prophage count increase. In total, 41 P. *aeruginosa* clinical (93.1%) were found to harbor at least one to six prophages. However, in strains JPAB41, JPAU51, and RPA226, no intact prophages were found. This indicates that prophages are abundant in the genomes of *P. aeruginosa*.

AMR and virulence factors found in prophages

Prophages provide genomic plasticity and host adaptation for their bacteria (Shen et al., 2020), and act as important vehicles carrying virulence factor (VF) and antimicrobial resistance (AMR) genes (Colomer-Lluch et al., 2011). Among all prophages, only the prophage genome AA67 was found to carry a chloramphenicol resistance gene catB7_1 detected by ResFinder (Supplementary Table 10). There were no VF or AMR genes identified in other intact prophages in this study, this absence may be attributed to a complex decay process involving the accumulation of mutations, deletions or genetic rearrangements, leading to the loss of non-essential genes such as AMR genes. Additionally, carrying AMR genes can impose a metabolic burden on bacteria, especially in antibiotics-free environments, potentially reducing bacterial fitness. Thus, this selective pressure may favor retention of prophages lacking these genes (Kondo et al., 2021). However, VF genes were detected in the incomplete genomes of JPAO31R1in, JPAO31R7in, JPAR31R6in, JPAU63R6in, RPA10R10in, RPA41R7in, RPA109R8in, RPA128R6in, RPA135R4in, and MPA31R8in (Supplementary Table 3). In the clinical *P. aeruginosa* isolates, the presence of VF and/or AMR genes in incomplete prophages rather than intact prophages could be often associated with that intact prophages often retain genes essential for phage-related functions,

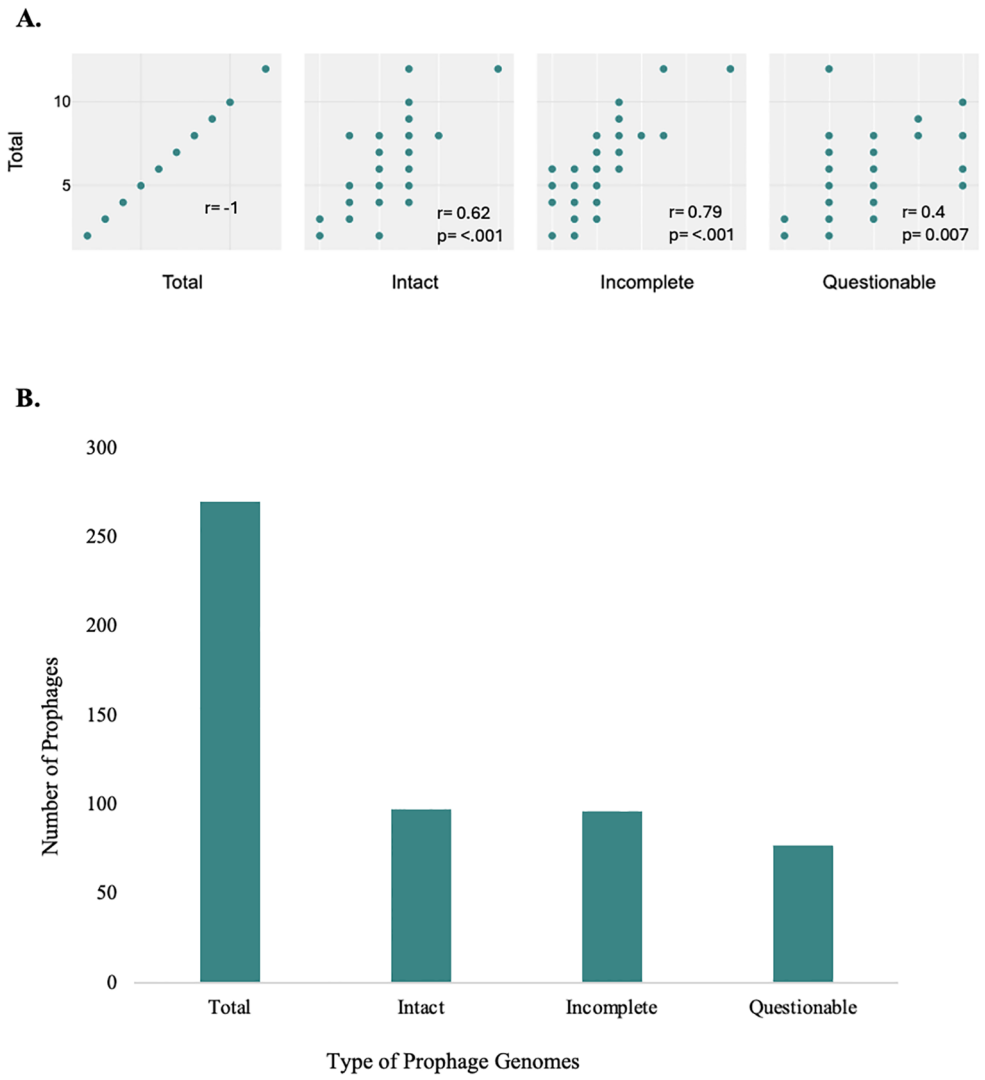

FIGURE 1
Prophage distribution in *P. aeruginosa* genomes. Illustration of the correlation coefficients between the total number of intact, incomplete, and questionable prophages **(A)**, and total number of prophages in *P. aeruginosa* genomes, categorized as intact, incomplete, and questionable **(B)**. Prophages were detected and classified using the PHASTER with default arguments and its scoring system. **(A)** Correlation and scatter plot of prophage genome types and their distribution. The analysis reveals a significant correlation between the total category and all three subcategories, as the strongest relationship is with Incomplete, followed by Intact, while the weakest is with Questionable, all with p-values <0.05; these correlations are statistically significant. **(B)** There were differences in the distribution of prophages of varying completeness on the chromosomes of *P. aeruginosa*. The integration of intact prophages in the bacterial genome indicates a recent infection with a temperate phage (Costa et al., 2018). There is a significantly high prevalence of defective phages (Figure 1, Supplementary Table 2).

whereas incomplete prophages may accumulate genes advantageous to bacterial survival. In the study by Kondo et al. (2021), they observed that AMR genes were frequently located near recombination-related genes, such as integrases and transposases, within prophage regions. In contrast, VF genes were less commonly associated with these recombination-related genes. The distinct distribution patterns imply that AMR and VF genes may be acquired and propagated through different evolutionary pathways within bacterial genomes (Kondo et al., 2021). In the genomes of nine different incomplete prophages, an annotated *Escherichia coli iss* gene was detected with 97.41% coverage (GenBank accession no. AF042279). The *iss2* gene contributes to bacterial survival and is not usually found in *Pseudomonas* spp., suggesting acquisition through horizontal gene transfer. The incomplete prophage genome JPAO31R1in was found to carry eight different VF genes, including *algL*, *algX*, *algG*, *algE*, *algK*, *alg44*, *alg8*, and *algD*). Some of these alginates represent key exopolysaccharides involved in biofilm formation and alginate production by *P. aeruginosa* (Monday and Schiller, 1996).

Genetic diversity of *P. aeruginosa* prophages

Among the identified prophages, some prophages were found to be present in more than one clinical strain, with 13 P. *aeruginosa*

genomes carrying the prophage AA18, 12 genomes harboring AA20 as the second most abundant prophage, and eight *P. aeruginosa* genomes carrying prophage AA19. The genomes of prophages AA13, AA08, and AA03 were found in six, five and four *P. aeruginosa* genomes, respectively (Figure 2). Four prophage genomes were present in three different genomes. In comparison, the other six common prophage genomes were only found twice in each bacterial genome (Supplementary Table 4; Figure 2). These common prophage genomes were distributed across a variety of strains with different sequence types and also had high percentages of integration on the chromosome. All prophage genome sizes ranged from 7.7 kb to 74.1 kb, and their GC% content was found to be between 49.91% and 64.9%, which is slightly lower than the host's GC content of 65-67% for *P. aeruginosa* (Klockgether et al., 2011) (Supplementary Table 5). The differences in GC content among prophages are considered an evolutionary trait, indicative of the recent acquisition of prophage regions with exogenous origins (Fortier and Sekulovic, 2013). The most common prophage among *P. aeruginosa* strains, AA18, with a GC content of 62.67% indicates its adaptation to its host; the more similar the GC content of a prophage is to its host, the better adapted the prophage is. Additionally, prophages with shorter genome lengths present higher GC content, such as prophages AA29, AA47, AA67, and AA5 (Supplementary Table 5). It is important to note that the genomes were divided into contigs, which implies that PHASTER may have underestimated the correct number of intact prophages. Some prophages may have split into different contigs and thus identified as incomplete or questionable prophages.

Analysis of prophage distribution according to taxonomic classification and genome size

Using TaxmyPHAGE, 97 prophage genomes were classified into distinct taxonomic groups (Supplementary Table 6). TaxmyPHAGE identified the genera and species of the input prophage genome sequences; genomes were found to differ based on their genomic analysis (Figure 3). Genomic comparisons revealed that 28.1% of the genomes were from known genera, while 71.8% were classified to be from novel and unknown genera, 39.58% and 32.29% respectively. The majority of phages belong to novel or uncharacterized taxa at both the genus and species levels, suggesting the discovery of new phage groups. From the genera and species contributed significantly, like *Casadabanvirus* (7.2%), *Lambdavirus* (8.3%), and *Citexvirus* (6.25%). While genera and species such as *Beetrevirus* (2.08%) and *Hollowayvirus* (2.08%) were less common, suggesting they may be less widespread or specialized. Unexpectedly, the presence of *Lambdavirus* lambda was reported among *Pseudomonas* phages, in prophages genomes AA29, AA52, and AA62. These genome sequence annotations were verified using BLAST against the NCBI database to ensure accuracy, that the prophage genome annotations indicated *Lambdavirus* lambda. The results show a high degree of prophage diversity among the *P. aeruginosa* clinical strains. The average genome size of the prophages was 41.3kb, which is consistent with values reported from other studies working on different bacteria (Bobay et al., 2014; Canchaya et al., 2003).

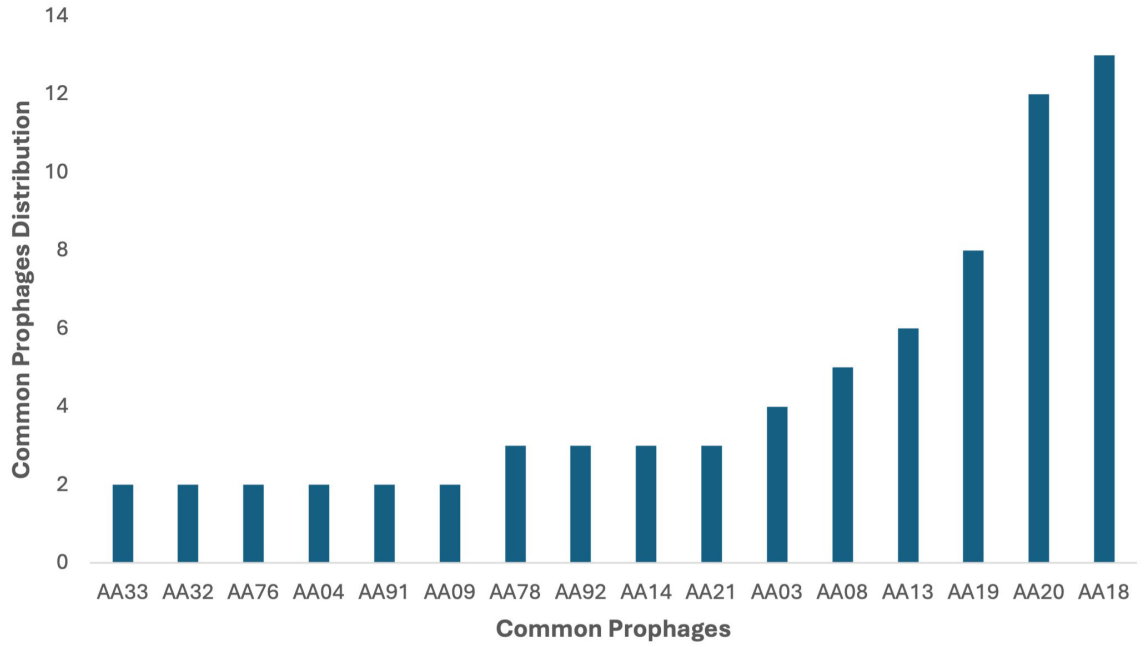

FIGURE 2
Distribution of intact prophages in the 44 P. *aeruginosa* strains. Among the identified prophages, AA18 was the dominant intact prophage in 13 P. *aeruginosa* genomes in the study, followed by AA20 in 12 genomes and AA19 in eight genomes. Prophages AA13, AA08, and AA03 were present in six, five, and four genomes, respectively. Four prophages were identified in three genomes each, while six other prophages were found in two genomes each.

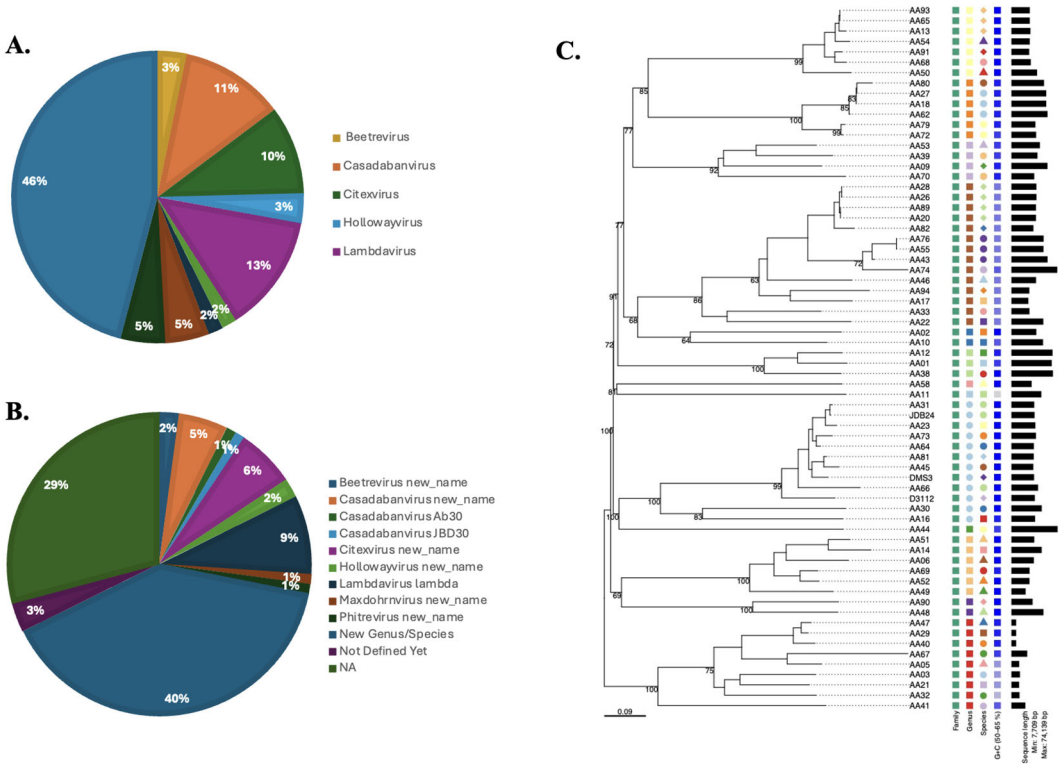

FIGURE 3
Taxonomic classification of prophage genomes. TaxmyPHAGE classified 97 prophage genomes, identifying 28.1% as belonging to known genera, and 71.8% as novel and unknown genera. Prominent taxa included *Casadabanvirus* (7.2%) and *Lambdavirus* (8.3%), while less frequent taxa, such as *Beetrevirus* (2.08%), were observed at both the genus **(A)** and species **(B)** levels. **(C)** Phylogeny of *Pseudomonas* prophages in current study and three different prophages (JDB24 (NC 020203), DMS3 (NC 008717), and D3112 (NC 005178) within the *Casadabanvirus* genus as listed by ICTV. The tree was inferred from the amino acid sequences using the VICTOR pipeline with the GBDP d0 formula.

Phylogenetic relationship between prophages

A phylogenetic tree was generated based on complete prophage sequences to evaluate diversity. The tree was constructed using the major capsid protein (MCP) as a reference (Figure 4). The phylogenetic analysis revealed that the prophages clustered according to their morphological family types, indicating that the predicted virion morphotypes correlate with the genomic phylogeny. This finding aligns with the new classification system of the International Committee on the Taxonomy of Viruses, which is based on genome and proteome data (Adriaenssens and Rodney Brister, 2017). Furthermore, phylogenetic analysis of the *P. aeruginosa* prophages investigated demonstrated a high diversity of evolutionary groupings and provided potential functional insights derived from the MCP sequences. Prophage genomes such as AA01, AA12, and AA09 are closely clustered, indicating lower genetic divergence and suggesting that their capsid structures may be highly conserved, which could imply a specific phage-host interaction. In contrast, prophages AA44, AA16, and AA73 share an evolutionary history, while the longer branches of AA45, AA09 with AA49, AA06, and AA92 suggest more distant relationships. These insights provide a framework for future studies on the diverse structural and functional roles of MCP in prophage adaptation. The tree was visualized using Interactive Tree of Life (iTOL) v6.

Sequence type distribution

In the sequence set consisting of 44 strains of *P. aeruginosa*, all strains had known sequence types (ST), except for one strain JPAB21 (Table 1), which were divided into 16 distinct types. The correlation between the *P. aeruginosa* ST and prophage harboring was studied (Supplementary Table 7). In the collection of 44 P. *aeruginosa* strains, ST235 was found to be the most prevalent type (n = 19), followed by ST233 (n = 5) and ST357 (n = 4), (Figure 5).

In ST235, prophage AA18 was found in 13 out of 19 strains, prophage AA20 in 12 out of 19, and prophage AA19 in 5 out of 19 strains; in ST233 2 out of 4, and in ST111, 1 out of 1 strain. *P. aeruginosa* strains with ST235 harbor the three most common prophages, which carry the GES-5 and GES-15 β-lactamases. The other three *P. aeruginosa* strains JPAB41, JPAU51, and RPA226, which did not harbor any of the three most common prophages, carried the GES-1 and GES-5 β-lactamases. In other ST, the distribution of these prophages was rare or even absent. This suggests that ST may relate to the types of prophages integrated into the chromosome.

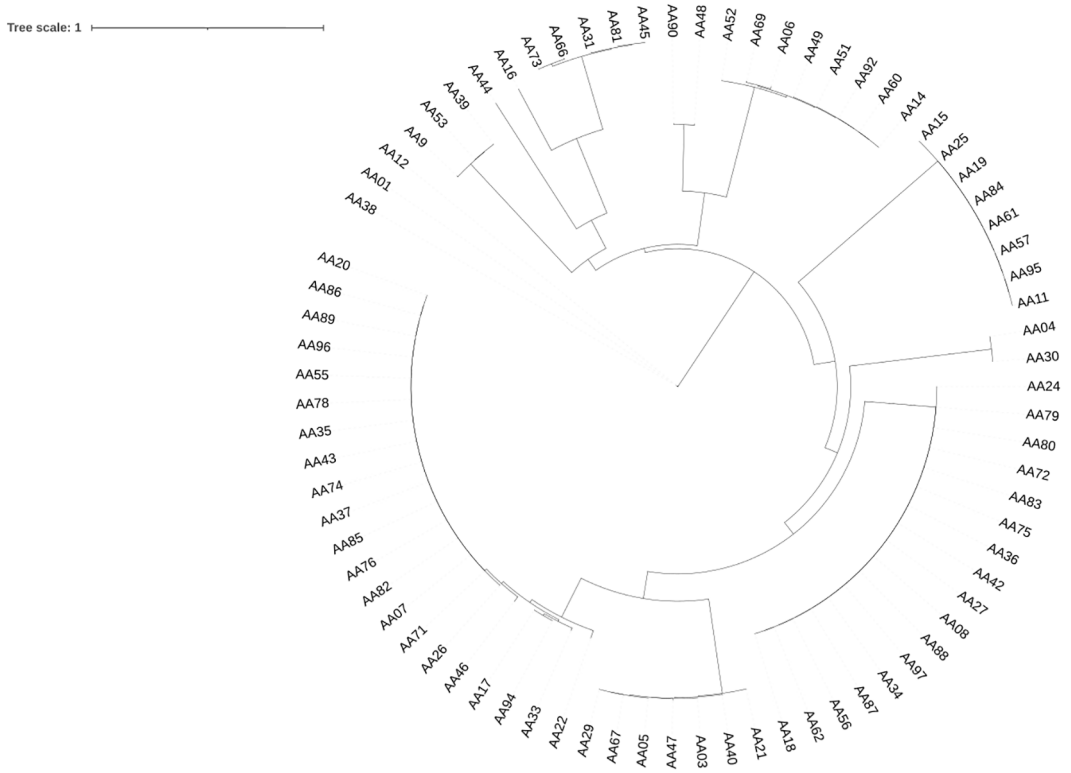

FIGURE 4
Phylogenetic Tree of *P. aeruginosa*-associated prophages. The phylogeny tree was constructed using the neighbor-joining method with the MAFFT program based on major capsid protein (MCP) sequences. Only prophage genomes containing MCP sequences were included in the analysis, while prophages without MCPs were excluded. The schematic representation of the tree was visualized using the iTOL v6 software (Letunic and Bork, 2021).

The strains belonging to the different STs were more diverse in their prophage arrangement. Although the remaining strains harbored at least one intact prophage, the distribution of these prophages was irregular and lacked a clear association.

Most common anti-phage defense systems identified in analyzed genomes

a. Defense against restriction-modification systems

In this study, 28 out of 97 prophages were found to encode DNA methyltransferases. Prophages use DNA methyltransferases to methylate their DNA to evade the host cell's restriction-modification system, regulate viral gene expression, and facilitate DNA packaging into the preformed capsids (Burke et al., 2021; Loenen and Raleigh, 2014). Additionally, restriction alleviation proteins were found in 20 prophage genomes; these proteins are known to protect against the host cell's restriction-modification systems (Supplementary Table 8) (Loenent and Murray1, 1986; Toothmant, 1981).

b. Toxin/antitoxin systems

Toxin-antitoxin (TA) modules play important roles in plasmid and prophage stability and are also key factors in bacterial physiology (Harms et al., 2018). A proposed system protects bacteria from phages, alongside CRISPR and restriction-modification systems. In this context, it is not surprising that prophages carry antitoxins to counteract bacterial defense mechanisms, or even toxins alone, to compete against external phages preying on their host (Leroux and Laub, 2022). In this study where the proposed system was detailed, prophages were found to encode TA modules belonging to the type II systems. The type II toxin YafO was found in 16 prophage genomes (Zhang et al., 2009). Additionally, the type II TA system putative toxin HigB2 was found in ten prophages. In bacteria, toxin HigB2 has been shown to reduce the expression of virulence-associated traits such as the production of pyochelin and pyocyanin, biofilm formation, and swarming motility. Thus, this system affects the pathogenicity of the strain in a manner not previously demonstrated for TA systems (Table 2; Supplementary Table 8) (Wood and Wood, 2016).

DNA scission proteins

Prophages encode junction-resolving enzymes, such as Holliday junction resolvases. Specifically, prophages encode RusA-like Holliday junction resolvase, Lar-like restriction alleviation protein, and restriction alleviation Ral (Supplementary Table 8). These enzymes have been described as being involved in the degradation of the host's DNA, self-DNA maturation, and cleavage prior to packaging (Wyatt and West, 2014).

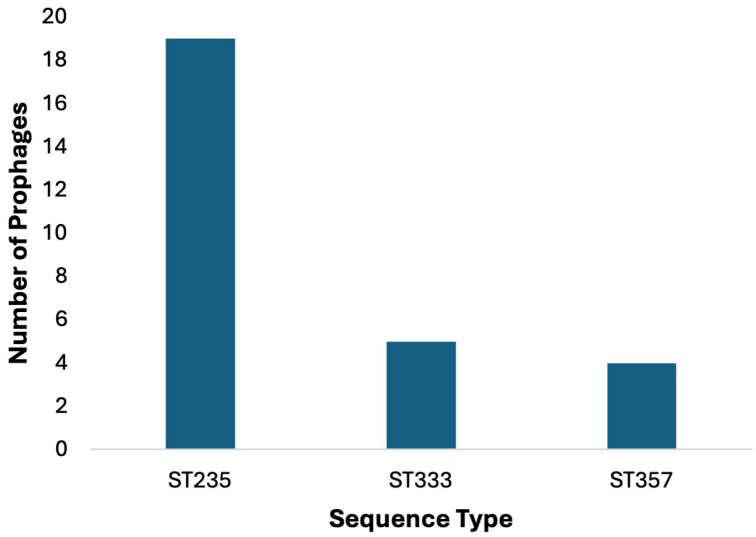

FIGURE 5
Prophage counts in most common sequence types (STs). Prophages were predominantly identified in the 44 P. *aeruginosa* strains belonging to ST235 (n=19), followed by ST233 (n = 5) and ST357 (n = 4).

Discussion

This study encompassed the search and analysis of prophages within a set of 44 multidrug-resistant (MDR) *P. aeruginosa* clinical strains isolated from different hospitals across different regions of Saudi Arabia (Doumith et al., 2022). Our findings demonstrate that these prophages are present in the majority of strains (Supplementary Tables 1 and 9). Many of the prophages were found in more than one strain, following a similar ST pattern. In only 6.8% of the strains (n = 3), no intact prophages as predicted by the PHASTER tool were identified, showing that prophage harboring is a very frequent trait among circulating *P. aeruginosa* strains in Saudi Arabia.

Prophages have been linked to bacterial diversification and evolution, exerting a strong selection pressure on bacterial fitness and virulence (Brüssow et al., 2004; Canchaya et al., 2004; Casjens, 2003; Desiere et al., 2001). A limited number of studies have characterized the prevalence of prophages in bacterial species and evaluated their role in virulence in the Arab region, specifically in clinical strains from Saudi Arabia. In this study, we report the analysis of prophage prevalence in clinical MDR *P. aeruginosa* and discuss their possible contribution to the evolution of the pathogenicity of *P. aeruginosa*.

We found that the 44 P. *aeruginosa* strains harbored a total of 270 prophages following genomic analysis. A significant number of these prophages (n = 97) were classified as intact prophages, while detective prophages (96 incomplete and 77 questionable) were also detected in large numbers. The subset of 97 intact prophages were classified into distinct taxonomic groups (Figure 3). The defective prophages were attributed to strong stress selection, which resulted in mutations or gene loss that inactivated the prophages (Bobay et al., 2014). Genomic diversification was observed among the sequences, revealing novel genera and species among the prophages. Using the TaxMYPHAGE tool, genomic comparisons indicated that 33.33% of the prophages within *P. aeruginosa* genomes were assigned to known genera (Figure 3), while 55% were classified as novel genera. This highlights the discovery of new phage groups and emphasizes the need for additional research to better understand phage diversity within clinically isolated *P. aeruginosa* strains. Interestingly, prophage genomes AA29, AA52, and AA62 were classified under the *Lambdavirus* genus, however, when compared against the NCBI database, they unexpectedly showed similarities to *Pseudomonas* associated phages. This could be attributed due to two key reasons; (i) complex evolutionary and taxonomic relationships, such as horizontal gene transfer (Hulin et al., 2023); (ii) mis-annotation due to sequence similarities, which may also explain the inclusion of Lambdaviruses among Pseudomonas phages as classification tools rely heavily on conserved genomic regions. Moreover, as genomic technologies advance even more rapidly, that there will be more discoveries in the near future. These findings suggest exercising caution when classifying phages, as reliance on specific conserved regions may lead to inaccuracies in taxonomic assignments. Overall, our findings reveal a significant degree of genomic diversity within the prophages within the clinically isolated *P. aeruginosa* strains.

The correlation between bacterial genome sizes and their GC content was studied by Chen et al. (2016). Applying their findings to prophages, shorter prophage genomes might have higher GC content due to selective pressures favoring energy-efficient nucleotide usage and the retention of stable, essential genes. However, it is important to note that this is a hypothesis derived from related studies and this relationship is influenced by various factors, including the specific bacterial host, environmental conditions, and evolutionary pressures.

Some genes expressed from prophage regions can alter the properties of the host, ranging from increased protection against further phage infection to increased virulence (Casjens, 2003). High-risk STs, such as ST235, were identified as carrying various prophages. ST235 is known for its ability to acquire mobile genetic elements, its

10.3389/fcimb.2025.1563781

TABLE 2 Viral defense and regulatory proteins identified in 13 prophages common across all 44 P. *aeruginosa* genomes analyzed in this study.

Prophage	Viral Defense proteins				Regulatory Proteins	
	Glycosyltransferases and Acetylases	Defense Against Restriction-Modification Systems	TA systems	DNA Scission Proteins	Latency-Promoting Repressors	Other Proteins
AA18	ND	ND	Putative toxin HigB2	ND	ND	HTH-type transcriptional regulator PrtR
AA23	ND	ND	ND	ND	ND	ND
AA27	ND	ND	Putative toxin HigB2	ND	ND	HTH-type transcriptional regulator PrtR
AA34	ND	ND	Putative toxin HigB2	ND	ND	HTH-type transcriptional regulator PrtR
AA36	ND	ND	Putative toxin HigB2	ND	ND	HTH-type transcriptional regulator PrtR
AA42	ND	ND	Putative toxin HigB2	ND	ND	HTH-type transcriptional regulator PrtR
AA56	ND	ND	ND	ND	ND	ND
AA62	ND	ND	Putative toxin HigB2	ND	ND	HTH-type transcriptional regulator PrtR
AA75	ND	ND	Putative toxin HigB2	ND	ND	HTH-type transcriptional regulator PrtR
AA77	ND	ND	ND	ND	ND	ND
AA80	ND	ND	ND	ND	ND	HTH-type transcriptional regulator PrtR
AA83	ND	ND	Putative toxin HigB2	ND	ND	HTH-type transcriptional regulator PrtR
AA88	ND	ND	Putative toxin HigB2	ND	ND	HTH-type transcriptional regulator PrtR

*ND refers to No Data; no available information for the given parameter.

elevated antimicrobial resistance rates, and its global distribution (Kabic et al., 2023; Treepong et al., 2018). In particular, ST235, the most prevalent ST among MDR *P. aeruginosa* clinical isolates (Table 1). has been shown to lack a functional CRISPR-Cas system, thus explaining its ability to acquire exogenous genetic elements, such as genomic matter from bacteriophage.

The prevalence of the putative toxin HigB2 was highlighted, as a part of a TA system in prophage genomes, which is known to stabilize the prophage within the bacterial cell. Under stressful conditions, the activation of HigB2 might initiate entering a state of dormancy, allowing bacterial cells to withstand adverse environments and delay prophages from entering the lytic cycle. The dormant state may contribute to the persistence of bacteria even in the presence of antibiotics (Leroux and Laub, 2022; Yang and Walsh, 2017). Collectively, these findings highlight the functional versatility of prophage-encoded toxins like HigB2, underscoring their roles in bacterial survival and adaptation in challenging environments.

The prophage-encoded HTH-type transcriptional regulator PrtR acts as a key modulator in controlling phage life cycle transitions, responding to host stress, and potentially influencing host virulence. Its regulatory function ensures that the prophage remains latent under stable conditions and activates lytic genes when the host environment becomes unfavorable, enhancing both phage survival and bacterial adaptability (Dodd et al., 2005; Oppenheim et al., 2005). In the presence of DNA damage, such as treatment with mitomycin C, the activation of RecA causes the PrtR repressor to self-cleave, which together with PrtN, regulates the production of pyocins (Matsui et al., 1993; Penterman et al., 2014; Walker, 1984; Wu and Jin, 2005). This highlights the importance of prophage-borne counter-defense mechanisms, which not only protect the prophage against the bacterial host's immune system, but also protect the host from infection by other phages, enabling survival and transmission to bacterial progeny.

Prophages can be induced from their host and can contribute to phage therapy. Although prophages incorporate their genomes into the host and integrate within the host genome, they can also serve as effective candidates for phage therapy. Genetic engineering of prophages, such as the removal of the integrase protein, and genomes are cleared of virulence genes, resistance related genes, and generally undesirable genes can make engineered prophages safe for use it patients. In 2019, a patient with a disseminated multi-drug-resistant *Mycobacterium abscessus* was treated with a cocktail of

mutant phages engineered to remove lysogeny associated genes (Dedrick et al., 2019). This case highlighted the feasibility of phage engineering for complex bacterial infections. Another form of phage engineering involves extracting specific lytic proteins, such as lysins and holin, and using them for therapeutic purposes instead of whole viral particles. Their effect of these phage derived enzymes on MDR *P. aeruginosa* has been investigated *in vitro* and reported in the literature (Cui et al., 2023). Building on the prophages identified in this study, these approaches could be adapted in the future to design tailored therapies for *Pseudomonas*-related infections.

On the other hand, the presence of prophages can have an impact on antibiotic and phage therapies. Certain antibiotics can induce prophages within bacterial genomes, leading to the release of phage particles and potential horizontal gene transfer. A study demonstrated that common oral medications, including antibiotics, can lead to prophage induction in gut bacterial isolates, suggesting that antibiotic therapy might inadvertently activate prophages, influencing bacterial behavior and resistance patterns (Sutcliffe et al., 2021). Additionally, Prophages can confer resistance to superinfection by other phages through mechanisms such as superinfection exclusion and the CRISPR-Cas system. This resistance poses challenges to phage therapy, as therapeutic phages may be rendered ineffective against lysogenic bacteria (Bondy-Denomy et al., 2016).

One limitation of our study is that some of the *P. aeruginosa* isolates were sequenced using short-read bridge amplification technology (Illumina, Oxford Genomics Centre, Oxford, UK), generating 150 bp fragments. After assembly, these sequences resulted in 206 to 3,252 contigs per genome (an average of 1,602 contigs per genome). The more fragmented the genomes are, the more difficult it is to identify intact prophages, meaning that some prophages would have not been identified based on the tools used as they would have been split across several contigs. To circumvent this issue, a combination of both short- and long-read sequencing could be performed to obtain high-quality, complete bacterial genomes. This study focused its analysis on intact prophages only. Overall, our results suggest a significant contribution of prophages to the evolution and adaptation of *P. aeruginosa* clinical strains.

In conclusion, this study demonstrates the pivotal role of prophages in shaping the genomic landscape and adaptive capabilities of MDR *P. aeruginosa* clinical strains. These findings not only advance our understanding of phage-bacteria interactions but also open new avenues for therapeutic applications and treatment of MDR infections. Future research should focus on integrating long-read sequencing technologies with functional studies to enhance the therapeutic potential of prophages. This will help refine prophage classification, uncover novel targets, and develop customized interventions against *P. aeruginosa* and other multidrug-resistant pathogens.

Data availability statement

The original contributions presented in the study are included in the article/Supplementary Material. Further inquiries can be directed to the corresponding author.

Author contributions

AhA: Conceptualization, Data curation, Formal Analysis, Funding acquisition, Investigation, Methodology, Resources, Software, Supervision, Validation, Visualization, Writing – original draft, Writing – review & editing. AAA: Data curation, Formal Analysis, Software, Writing – review & editing. MI: Methodology, Validation, Writing – review & editing. SA: Validation, Visualization, Writing – review & editing. AmA: Data curation, Validation, Writing – review & editing. HA: Data curation, Validation, Writing – review & editing. MB: Validation, Writing – review & editing.

Funding

The author(s) declare that financial support was received for the research and/or publication of this article. The authors declare that financial support was received from KAIMRC for the research, authorship and/or publication of this article under the projects NRC22R-354-08.

Acknowledgments

The authors are grateful for the support from the management and staff of King Abdullah International Medical Research Center (KAIMRC).

Conflict of interest

The authors declare that the research was conducted in the absence of any commercial or financial relationships that could be construed as a potential conflict of interest.

Generative AI statement

The author(s) declare that no Generative AI was used in the creation of this manuscript.

Publisher's note

Supplementary material

The Supplementary Material for this article can be found online at: https://www.frontiersin.org/articles/10.3389/fcimb.2025.1563781/full#supplementary-material

References

Ackermann, H. W. (2007). 5500 Phages examined in the electron microscope. *Arch. Virol.* 152, 227–243. doi: 10.1007/s00705-006-0849-1

Adriaenssens, E. M., and Rodney Brister, J. (2017). How to name and classify your phage: An informal guide. *Viruses* 9 (4), 1–9. doi: 10.3390/v9040070

Alcock, B. P., Raphenya, A. R., Lau, T. T. Y., Tsang, K. K., Bouchard, M., Edalatmand, A., et al. (2020). CARD 2020: Antibiotic resistome surveillance with the comprehensive antibiotic resistance database. *Nucleic Acids Res.* 48, D517–D525. doi: 10.1093/nar/gkz935

Ambroa, A., Blasco, L., López, M., Pacios, O., Bleriot, I., Fernández-García, L., et al. (2022). Genomic analysis of molecular bacterial mechanisms of resistance to phage infection. *Front. Microbiol.* 12. doi: 10.3389/fmicb.2021.784949

Baliga, P., Shekar, M., and Kallappa, G. S. (2021). Genome-wide identification and analysis of chromosomally integrated putative prophages associated with clinical klebsiella pneumoniae strains. *Curr. Microbiol.* 78, 2015–2024. doi: 10.1007/s00284-021-02472-2

Bobay, L. M., Touchon, M., and Rocha, E. P. C. (2014). Pervasive domestication of defective prophages by bacteria. *Proc. Natl. Acad. Sci. United. States America* 111, 12127–12132. doi: 10.1073/pnas.1405336111

Bondy-Denomy, J., Pawluk, A., Maxwell, K. L., and Davidson, A. R. (2013). Bacteriophage genes that inactivate the CRISPR/Cas bacterial immune system. *Nature* 493, 429–432. doi: 10.1038/nature11723

Bondy-Denomy, J., Qian, J., Westra, E. R., Buckling, A., Guttman, D. S., Davidson, A. R., et al. (2016). Prophages mediate defense against phage infection through diverse mechanisms. *ISME J.* 10 (12), 2854–2866. doi: 10.1038/ismej.2016.79

Brüssow, H., Canchaya, C., and Hardt, W.-D. (2004). Phages and the evolution of bacterial pathogens: from genomic rearrangements to lysogenic conversion. *Microbiol. Mol. Biol. Rev.* 68, 560–602. doi: 10.1128/mmbr.68.3.560-602.2004

Burke, E. J., Rodda, S. S., Lund, S. R., Sun, Z., Zeroka, M. R., O'Toole, K. H., et al. (2021). Phage-encoded ten-eleven translocation dioxygenase (TET) is active in C5-cytosine hypermodification in DNA. *PNAS* 118, 2026742118. doi: 10.1073/pnas.2026742118/-/DCSupplemental

Canchaya, C., Fournous, G., and Brüssow, H. (2004). The impact of prophages on bacterial chromosomes. *Mol. Microbiol.* 53, 9–18. doi: 10.1111/j.1365-2958.2004.04113.x

Canchaya, C., Proux, C., Fournous, G., Bruttin, A., and Brüssow, H. (2003). Prophage genomics. *Microbiol. Mol. Biol. Rev.* 67, 473–473. doi: 10.1128/mmbr.67.3.473.2003

Casjens, S. (2003). Prophages and bacterial genomics: What have we learned so far? *Mol. Microbiol.* 49, 277–300. doi: 10.1046/j.1365-2958.2003.03580.x

Chen, W. H., Van Noort, V., Lluch-Senar, M., Hennrich, M. L., Wodke, J. A. H., Yus, E., et al. (2016). Integration of multi-omics data of a genome-reduced bacterium: Prevalence of post-transcriptional regulation and its correlation with protein abundances. *Nucleic Acids Res.* 44 (3), 1192–1202. doi: 10.1093/nar/gkw004

Cieślik, M., Bagińska, N., Jończyk-Matysiak, E., Węgrzyn, A., Węgrzyn, G., and Górski, A. (2021). Temperate bacteriophages—the powerful indirect modulators of eukaryotic cells and immune functions. *Viruses* 13 (6), 1013. doi: 10.3390/v13061013

Cohen, D., Melamed, S., Millman, A., Shulman, G., Oppenheimer-Shaanan, Y., Kacen, A., et al. (2019). Cyclic GMP–AMP signalling protects bacteria against viral infection. *Nature* 574, 691–695. doi: 10.1038/s41586-019-1605-5

Colomer-Lluch, M., Imamovic, L., Jofre, J., and Muniesa, M. (2011). Bacteriophages carrying antibiotic resistance genes in fecal waste from cattle, pigs, and poultry. *Antimicrob. Agents Chemother.* 55, 4908–4911. doi: 10.1128/AAC.00535-11

Costa, A. R., Monteiro, R., and Azeredo, J. (2018). Genomic analysis of Acinetobacter baumannii prophages reveals remarkable diversity and suggests profound impact on bacterial virulence and fitness. *Sci. Rep.* 8 (1), 15346. doi: 10.1038/s41598-018-33800-5

Cui, J., Shi, X., Wang, X., Sun, H., Yan, Y., Zhao, F., et al. (2023). Characterization of a lytic Pseudomonas aeruginosa phage vB_PaeP_ASP23 and functional analysis of its lysin LysASP and holin HolASP. *Front. Microbiol.* 14. doi: 10.3389/fmicb.2023.1093668

DATAtab: DATAtab Team (2025). DATAtab: online Statistics Calculator (Graz, Austria: DATAtab e.U). Available at: https://datatab.net.

Dedrick, R. M., Guerrero-Bustamante, C. A., Garlena, R. A., Russell, D. A., Ford, K., Harris, K., et al. (2019). Engineered bacteriophages for treatment of a patient with a disseminated drug-resistant Mycobacterium abscessus. *Nat. Med.* 25, 730–733. doi: 10.1038/s41591-019-0437-z

Desiere, F., McShan, W. M., Van Sinderen, D., Ferretti, J. J., and Brüssow, H. (2001). Comparative genomics reveals close genetic relationships between phages from dairy bacteria and pathogenic streptococci: Evolutionary implications for prophage-host interactions. *Virology* 288, 325–341. doi: 10.1006/viro.2001.1085

Diggle, S. P., and Whiteley, M. (2020). Microbe profile: Pseudomonas aeruginosa: Opportunistic pathogen and lab rat. *Microbiol. (United Kingdom).* 166, 30–33. doi: 10.1099/mic.0.000860

Dion, M. B., Oechslin, F., and Moineau, S. (2020). Phage diversity, genomics and phylogeny. *Nat. Rev. Microbiol.* 18, 125–138. doi: 10.1038/s41579-019-0311-5

Dodd, I. B., Shearwin, K. E., and Egan, J. B. (2005). Revisited gene regulation in bacteriophage λ. *Curr. Opin. Genet. Dev.* 15, 145–152. doi: 10.1016/j.gde.2005.02.001

Doumith, M., Alhassinah, S., Alswaji, A., Alzayer, M., Alrashidi, E., Okdah, L., et al. (2022). Genomic characterization of carbapenem-non-susceptible pseudomonas aeruginosa clinical isolates from Saudi Arabia revealed a global dissemination of GES-5-producing ST235 and VIM-2-producing ST233 sub-lineages. *Front. Microbiol.* 12. doi: 10.3389/fmicb.2021.765113

Duncan-Lowey, B., Tal, N., Johnson, A. G., Rawson, S., Mayer, M. L., Doron, S., et al. (2023). Cryo-EM structure of the RADAR supramolecular anti-phage defense complex. *Cell* 186, 987–998.e15. doi: 10.1016/j.cell.2023.01.012

Fortier, L. C., and Sekulovic, O. (2013). Importance of prophages to evolution and virulence of bacterial pathogens. *Virulence* 4, 354–365. doi: 10.4161/viru.24498

Gandon, S. (2016). Why be temperate: lessons from bacteriophage λ. *Trends Microbiol.* 24, 356–365. doi: 10.1016/j.tim.2016.02.008

Garb, J., Lopatina, A., Bernheim, A., Zaremba, M., Siksnys, V., Melamed, S., et al. (2022). Multiple phage resistance systems inhibit infection via SIR2-dependent NAD + depletion. *Nat. Microbiol.* 7 (11), 1849–1856. doi: 10.1101/2021.12.14.472415

Göker, M., García-Blázquez, G., Voglmayr, H., Tellería, M. T., and Martín, M. P. (2009). Molecular taxonomy of phytopathogenic fungi: A case study in peronospora. *PloS One* 4 (7), e6319. doi: 10.1371/journal.pone.0006319

González de Aledo, M., Blasco, L., Lopez, M., Ortiz-Cartagena, C., Bleriot, I., Pacios, O., et al. (2023). Prophage identification and molecular analysis in the genomes of Pseudomonas aeruginosa strains isolated from critical care patients. *MSphere* 8 (4), e0012823. doi: 10.1128/msphere.00128-23

Gordon, M. A., Canals, R., Hammarlöf, D. L., Makumi, A., Aertsen, A., Feasey, N. A., et al. (2017). Characterization of the prophage repertoire of african salmonella typhimurium ST313 reveals high levels of spontaneous induction of novel phage BTP1. *Front. Microbiol.* 8. doi: 10.3389/fmicb.2017.00235

Harms, A., Brodersen, D. E., Mitarai, N., and Gerdes, K. (2018). Toxins, targets, and triggers: an overview of toxin-antitoxin biology. *Mol. Cell* 70, 768–784. doi: 10.1016/j.molcel.2018.01.003

Hatfull, G. F., and Hendrix, R. W. (2011). Bacteriophages and their genomes. *Curr. Opin. Virol.* 1, 298–303. doi: 10.1016/j.coviro.2011.06.009

Hay, I. D., and Lithgow, T. (2019). Filamentous phages: masters of a microbial sharing economy. *EMBO Rep.* 20 (6), e47427. doi: 10.15252/embr.201847427

Hayashi, T., Baba, T., Matsumoto, H., and Terawaki, Y. (1990). Phage-conversion of cytotoxin production in Pseudomonas aerug'inosa. *Mol. Microbiol.* 4 (10), 1703–1709. doi: 10.1111/j.1365-2958.1990.tb00547.x

Heaton, B. E., Herrou, J., Blackwell, A. E., Wysocki, V. H., and Crosson, S. (2012). Molecular structure and function of the novel BrnT/BrnA toxin-antitoxin system of Brucella abortus. *J. Biol. Chem.* 287, 12098–12110. doi: 10.1074/jbc.M111.332163

Hulin, M. T., Rabiey, M., Zeng, Z., Vadillo Dieguez, A., Bellamy, S., Swift, P., et al. (2023). Genomic and functional analysis of phage-mediated horizontal gene transfer in pseudomonas syringae on the plant surface. *New Phytol.* 237 (3), 959–973. doi: 10.1111/nph.18573

Kabic, J., Fortunato, G., Vaz-Moreira, I., Kekic, D., Jovicevic, M., Pesovic, J., et al. (2023). Dissemination of metallo-β-lactamase-producing pseudomonas aeruginosa in Serbian hospital settings: expansion of ST235 and ST654 clones. *Int. J. Mol. Sci.* 24 (2), 1519. doi: 10.3390/ijms24021519

Kelley, L. A., Mezulis, S., Yates, C. M., Wass, M. N., and Sternberg, M. J. E. (2015). The Phyre2 web portal for protein modeling, prediction and analysis. *Nat. Protoc.* 10 (6), 845–858. doi: 10.1038/nprot.2015.053

Klockgether, J., Cramer, N., Wiehlmann, L., Davenport, C. F., and Tümmler, B. (2011). Pseudomonas aeruginosa genomic structure and diversity. *Front. Microbiol.* 2. doi: 10.3389/fmicb.2011.00150

Knezevic, P., Voet, M., and Lavigne, R. (2015). Prevalence of Pf1-like (pro)phage genetic elements among Pseudomonas aeruginosa isolates. *Virology* 483, 64–71. doi: 10.1016/j.virol.2015.04.008

Kondo, K., Kawano, M., and Sugai, M. (2021). Distribution of antimicrobial resistance and virulence genes within the prophage-associated regions in nosocomial pathogens. *MSphere* 6 (4), e0045221. doi: 10.1128/msphere.00452-21

Kuzio, J., and Kropinski, A. M. (1983). O-Antigen Conversion in Pseudomonas aeruginosa PAO1 by Bacteriophage D3. *J. Bacteriol.* 155 (1), 203–212. doi: 10.1128/jb.155.1.203-212.1983

Labrie, S. J., Samson, J. E., and Moineau, S. (2010). Bacteriophage resistance mechanisms. *Nat. Rev. Microbiol.* 8, 317–327). doi: 10.1038/nrmicro2315

Lefort, V., Desper, R., and Gascuel, O. (2015). FastME 2.0: A comprehensive, accurate, and fast distance-based phylogeny inference program. *Mol. Biol. Evol.* 32 (10), 2798–2800. doi: 10.1093/molbev/msv150

Leroux, M., and Laub, M. T. (2022). Toxin-antitoxin systems as phage defense elements. *Annu. Rev. Microbiol.* 76, 21–43. doi: 10.1146/annurev-micro-020722-013730

Leroux, M., and Laub, M. T. (2025). Toxin-antitoxin systems as phage defense elements. *Annu. Rev. Microbiol.* 51, 56. doi: 10.1146/annurev-micro-020722

Letunic, I., and Bork, P. (2021). Interactive tree of life (iTOL) v5: An online tool for phylogenetic tree display and annotation. *Nucleic Acids Res.* 49, W293–W296. doi: 10.1093/nar/gkab301

Li, G., Lu, S., Shen, M., Le, S., Shen, W., Tan, Y., et al. (2017). Characterization and interstrain transfer of prophage pp3 of Pseudomonas aeruginosa. *PloS One* 12 (3), e0174429. doi: 10.1371/journal.pone.0174429

Little, J. W. (2005). Lysogeny, Prophage Induction, and Lysogenic Conversion. *Phages* 37–54. doi: 10.1128/9781555816506.ch3

Liu, B., Zheng, D., Jin, Q., Chen, L., and Yang, J. (2019). VFDB 2019: A comparative pathogenomic platform with an interactive web interface. *Nucleic Acids Res.* 47, D687–D692. doi: 10.1093/nar/gky1080

Loenen, W. A. M., and Raleigh, E. A. (2014). The other face of restriction: Modification-dependent enzymes. *Nucleic Acids Res.* 42, 56–69. doi: 10.1093/nar/gkt747

Loenent, W. A. M., and Murray1, N. E. (1986). Modification enhancement by the restriction alleviation protein (Ral) of bacteriophage lambda. *J Mol Biol.* 190 (1), 11–22. doi: 10.1016/0022-2836(86)90071-9

Ma, D., Gu, H., Shi, Y., Huang, H., Sun, D., and Hu, Y. (2021). Edwardsiella piscicida yefM-yoeB: A type II toxin-antitoxin system that is related to antibiotic resistance, biofilm formation, serum survival, and host infection. *Front. Microbiol.* 12. doi: 10.3389/fmicb.2021.646299

Matsui, H., Sano, Y., Ishihara, H., and Shinomiya, T. (1993). Regulation of pyocin genes in pseudomonas aeruginosa by positive (prtN) and negative (prtR) regulatory genes. *J. Bacteriol.* 175 (5), 1257–1263. doi: 10.1128/jb.175.5.1257-1263.1993

Meier-Kolthoff, J. P., Auch, A. F., Klenk, H.-P., and Oker, M. G. (2013). Genome sequence-based species delimitation with confidence intervals and improved distance functions. *BMC Bioinf.* 14, 60. doi: 10.1186/1471-2105-14-60

Meier-Kolthoff, J. P., and Göker, M. (2017). VICTOR: genome-based phylogeny and classification of prokaryotic viruses. *Bioinf. (Oxford England).* 33, 3396–3404. doi: 10.1093/bioinformatics/btx440

Millard, A., Denise, R., Lestido, M., Thomas, M., Turner, D., Turner, D., et al. (2024). taxmyPHAGE: Automated taxonomy of dsDNA phage genomes at the genus and species level. *PHAGE* 6 (1), 5–11. doi: 10.1101/2024.08.09.606593

Monday, S. R., and Schiller, N. L. (1996). Alginate synthesis in pseudomonas aeruginosa: the role of algL (Alginate lyase) and algX. *J. Bacteriol.* 178 (3), 625–632. doi: 10.1128/jb.178.3.625-632.1996

Oppenheim, A. B., Kobiler, O., Stavans, J., Court, D. L., and Adhya, S. (2005). Switches in bacteriophage lambda development. *Annu. Rev. Genet.* 39, 409–429. doi: 10.1146/annurev.genet.39.073003.113656

Pawluk, A., Davidson, A. R., and Maxwell, K. L. (2018). Anti-CRISPR: Discovery, mechanism and function. *Nat. Rev. Microbiol.* 16, 12–17. doi: 10.1038/nrmicro.2017.120

Pelegrin, A. C., Palmieri, M., Mirande, C., Oliver, A., Moons, P., Goossens, H., et al. (2021). Pseudomonas aeruginosa: A clinical and genomics update. *FEMS Microbiol. Rev.* 45 (6), fuab026. doi: 10.1093/femsre/fuab026

Penadés, J. R., Chen, J., Quiles-Puchalt, N., Carpena, N., and Novick, R. P. (2015). Bacteriophage-mediated spread of bacterial virulence genes. *Curr. Opin. Microbiol.* 23, 171–178. doi: 10.1016/j.mib.2014.11.019

Penterman, J., Singh, P. K., and Walker, G. C. (2014). Biological cost of pyocin production during the SOS response in Pseudomonas aeruginosa. *J. Bacteriol.* 196, 3351–3359. doi: 10.1128/JB.01889-14

Pirnay, J. P., Bilocq, F., Pot, B., Cornelis, P., Zizi, M., Van Eldere, J., et al. (2009). Pseudomonas aeruginosa population structure revisited. *PloS One* 4 (11), e7740. doi: 10.1371/journal.pone.0007740

Platt, M. D., Schurr, M. J., Sauer, K., Vazquez, G., Kukavica-Ibrulj, I., Potvin, E., et al. (2008). Proteomic, microarray, and signature-tagged mutagenesis analyses of anaerobic Pseudomonas aeruginosa at pH 6.5, likely representing chronic, late-stage cystic fibrosis airway conditions. *J. Bacteriol.* 190, 2739–2758. doi: 10.1128/JB.01683-07

Rice, L. B. (2008). Federal funding for the study of antimicrobial resistance in nosocomial pathogens: No ESKAPE. *J. Infect. Dis.* 197, 1079–1081. doi: 10.1086/533452

Rice, S. A., Tan, C. H., Mikkelsen, P. J., Kung, V., Woo, J., Tay, M., et al. (2009). The biofilm life cycle and virulence of Pseudomonas aeruginosa are dependent on a filamentous prophage. *ISME. J.* 3, 271–282. doi: 10.1038/ismej.2008.109

Shah, M., Taylor, V. L., Bona, D., Tsao, Y., Stanley, S. Y., Pimentel-Elardo, S. M., et al. (2021). A phage-encoded anti-activator inhibits quorum sensing in Pseudomonas aeruginosa. *Mol. Cell* 81, 571–583.e6. doi: 10.1016/j.molcel.2020.12.011

Shen, J., Zhou, J., Xu, Y., and Xiu, Z. (2020). Prophages contribute to genome plasticity of Klebsiella pneumoniae and may involve the chromosomal integration of ARGs in CG258. *Genomics* 112, 998–1010. doi: 10.1016/j.ygeno.2019.06.016

Silby, M. W., Winstanley, C., Godfrey, S. A. C., Levy, S. B., and Jackson, R. W. (2011). Pseudomonas genomes: Diverse and adaptable. *FEMS Microbiol. Rev.* 35, 652–680. doi: 10.1111/j.1574-6976.2011.00269.x

Sutcliffe, S. G., Shamash, M., Hynes, A. P., and Maurice, C. F. (2021). Common oral medications lead to prophage induction in bacterial isolates from the human gut. *Viruses* 13 (3), 455. doi: 10.3390/v13030455

Tal, N., Morehouse, B. R., Millman, A., Stokar-Avihail, A., Avraham, C., Fedorenko, T., et al. (2021). Cyclic CMP and cyclic UMP mediate bacterial immunity against phages. *Cell* 184, 5728–5739.e16. doi: 10.1016/j.cell.2021.09.031

Tal, N., and Sorek, R. (2022). SnapShot: bacterial immunity. *Cell* 185, 578–578.e1. doi: 10.1016/j.cell.2021.12.029

Tariq, M. A., Everest, F. L. C., Cowley, L. A., Wright, R., Holt, G. S., Ingram, H., et al. (2019). Temperate bacteriophages from chronic pseudomonas aeruginosa lung infections show disease-specific changes in host range and modulate antimicrobial susceptibility. *MSystems* 4 (4), e00191–18. doi: 10.1128/msystems.00191-18

Terzian, P., Olo Ndela, E., Galiez, C., Lossouarn, J., Pérez Bucio, R. E., Mom, R., et al. (2021). PHROG: Families of prokaryotic virus proteins clustered using remote homology. *NAR. Genomics Bioinf.* 3 (3), lqab067. doi: 10.1093/nargab/lqab067

Toothmant, P. (1981). Restriction alleviaion by bacteriophages lambda and lambda reverse. *J. Virol.* 38 (2), 621–631. doi: 10.1128/JVI.38.2.621-631.1981

Treepong, P., Kos, V. N., Guyeux, C., Blanc, D. S., Bertrand, X., Valot, B., et al. (2018). Global emergence of the widespread Pseudomonas aeruginosa ST235 clone. *Clin. Microbiol. Infect.* 24, 258–266. doi: 10.1016/j.cmi.2017.06.018

Walker, G. C. (1984). Mutagenesis and inducible responses to deoxyribonucleic acid damage in escherichia coli. *Microbiol. Rev.* 48 (1), 60–93. doi: 10.1128/mr.48.1.60-93.1984

Wang, X., Kim, Y., Ma, Q., Hong, S. H., Pokusaeva, K., Sturino, J. M., et al. (2010). Cryptic prophages help bacteria cope with adverse environments. *Nat. Commun.* 1 (9), 147. doi: 10.1038/ncomms1146

Williams, S. R., Gebhart, D., Martin, D. W., and Scholl, D. (2008). Retargeting R-type pyocins to generate novel bactericidal protein complexes. *Appl. Environ. Microbiol.* 74, 3868–3876. doi: 10.1128/AEM.00141-08

Wood, T. L., and Wood, T. K. (2016). The HigB/HigA toxin/antitoxin system of Pseudomonas aeruginosa influences the virulence factors pyochelin, pyocyanin, and biofilm formation. *MicrobiologyOpen* 5, 499–511. doi: 10.1002/mbo3.346

Wu, W., and Jin, S. (2005). PtrB of Pseudomonas aeruginosa suppresses the type III secretion system under the stress of DNA damage. *J. Bacteriol.* 187, 6058–6068. doi: 10.1128/JB.187.17.6058-6068.2005

Wyatt, H. D. M., and West, S. C. (2014). Holliday junction resolvases. *Cold Spring Harbor Perspect. Biol.* 6 (9), a023192. doi: 10.1101/cshperspect.a023192

Yang, Q. E., and Walsh, T. R. (2017). Toxin-antitoxin systems and their role in disseminating and maintaining antimicrobial resistance. *FEMS Microbiol. Rev.* 41, 343–353. doi: 10.1093/femsre/fux006

Yu, G., Smith, D. K., Zhu, H., Guan, Y., and Lam, T. T. Y. (2017). Ggtree: an r package for visualization and annotation of phylogenetic trees with their covariates and other associated data. *Methods Ecol. Evol.* 8 (1), 28–36. doi: 10.1111/2041-210X.12628

Zhang, Y., Yamaguchi, Y., and Inouye, M. (2009). Characterization of YafO, an Escherichia coli toxin. *J. Biol. Chem.* 284, 25522–25531. doi: 10.1074/jbc.M109.036624

Zimmermann, L., Stephens, A., Nam, S. Z., Rau, D., Kübler, J., Lozajic, M., et al. (2018). A completely reimplemented MPI bioinformatics toolkit with a new HHpred server at its core. *J. Mol. Biol.* 430 (15), 2237–2243. doi: 10.1016/j.jmb.2017.12.007

frontiers | Frontiers in Cellular and Infection Microbiology

TYPE Original Research
PUBLISHED 23 May 2025
DOI 10.3389/fcimb.2025.1597009

OPEN ACCESS

EDITED BY
Mercedes Gonzalez Moreno,
Leibniz Institute for Natural Product Research and Infection Biology, Hans Knoll Institute, Germany

REVIEWED BY
Yunxue Guo,
Chinese Academy of Sciences (CAS), China
Robert Ramirez-Garcia,
Imperial College London, United Kingdom

*CORRESPONDENCE
Imke H.E. Korf
imke.korf@item.fraunhofer.de
Dieter Jahn
d.jahn@tu-bs.de

†These authors have contributed equally to this work and share last authorship

RECEIVED 20 March 2025
ACCEPTED 14 April 2025
PUBLISHED 23 May 2025
CORRECTED 20 August 2025

CITATION
Rieper F, Wittmann J, Bunk B, Spröer C, Häfner M, Willy C, Müsken M, Ziehr H, Korf IHE and Jahn D (2025) Systematic bacteriophage selection for the lysis of multiple *Pseudomonas aeruginosa* strains. *Front. Cell. Infect. Microbiol.* 15:1597009. doi: 10.3389/fcimb.2025.1597009

Systematic bacteriophage selection for the lysis of multiple *Pseudomonas aeruginosa* strains

Finja Rieper[1,2], Johannes Wittmann[3], Boyke Bunk[3], Cathrin Spröer[3], Melanie Häfner[4], Christian Willy[4], Mathias Müsken[5], Holger Ziehr[1], Imke H.E. Korf[1*†] and Dieter Jahn[2,6*†]

[1]Pharmaceutical Biotechnology, Fraunhofer Institute for Toxicology and Experimental Medicine (ITEM), Braunschweig, Germany, [2]Institute of Microbiology, Braunschweig University of Technology, Braunschweig, Germany, [3]Leibniz Institute DSMZ-German Collection of Microorganisms and Cell Cultures GmbH (DSMZ), Braunschweig, Germany, [4]Department Trauma & Orthopedic Surgery, Septic & Reconstructive Surgery, Research and Treatment Center Septic Defect Wounds, Federal Armed Forces of Germany, Military Academic Hospital Berlin, Berlin, Germany, [5]Central Facility for Microscopy, Helmholtz Centre for Infection Research (HZI), Braunschweig, Germany, [6]Institute of Microbiology, Braunschweig Center of Systems Biology (BRICS), Braunschweig, Germany

Pseudomonas aeruginosa is an opportunistic pathogen causing severe infections of the lung, burn wounds and eyes. Due to its intrinsic high antibiotic resistance the bacterium is difficult to eradicate. A promising therapeutic option is the use of *P. aeruginosa*-specific bacteriophages. Thus, the implementation of a phage therapy requires their selection, production and systematic administration using multiple strains of the bacterial target. Here, we used 25 phages and tested their susceptibility on 141 different *P. aeruginosa* strains isolated from patients with different types of infection. Comparative host spectrum analyses were carried out using double agar overlay plaque assay (DPA) and planktonic killing assay (PKA), which resulted in 70% of the cases in the same host range. All phages were assigned to known phage genera, but some of the phages are new species. Isolated members of the genera *Pakpunavirus*, *Pbunavirus* (myoviruses), *Pawinskivirus*, *Elvirus* (myoviruses, jumbo phages), *Litunavirus* and *Bruynoghevirus* (podoviruses) demonstrated great therapeutic potential due to strong lysis behavior on diverse strains. Seven phages were excluded for therapeutic purposes due to genetic determinants that confer lysogenicity. Due to automation with lower time expenditure in execution and analysis, PKA has the higher potential for implementation in diagnostics. Finally, different combinations of phages were tested *in silico* with various *P. aeruginosa* strains. Highly efficient phage combinations eradicating multiple *P. aeruginosa* strains were found. Thus, a solid basis for the development of a broad host range phage therapy was laid.

KEYWORDS

bacteriophages, *Pseudomonas aeruginosa*, phage susceptibility testing, antibiotic resistance, phage selection

1 Introduction

P. aeruginosa is a Gram-negative rod-shaped bacterium that is ubiquitous found in the environment. But, it also causes infectious diseases that often lead to long and expensive antibiotic treatments due to a large number of intrinsic antibiotic resistance and virulence factors (Aloush et al., 2006; Azam and Khan, 2019; Horcajada et al., 2019; Hilliam et al., 2020; Nazarov, 2022; Qin et al., 2022). In some cases, none of the eight antibiotic classes, including the reserve antibiotic class of carbapenems, commonly employed for *P. aeruginosa* infection treatment are effective anymore (Bassetti et al., 2018; Miller and Arias, 2024). For this reason *P. aeruginosa* is classified as high-risk pathogen on the World Health Organization's global priority list for antibiotic-resistant bacteria (https://www.who.int/publications/i/item/9789240093461, accessed on 19 Nov 2024 (Miller and Arias, 2024; World Health Organization, 2024). Common sites of infection with *P. aeruginosa* in the human body are the respiratory tract, urinary tract, burn wounds, or the eyes (Poggio et al., 1989; Schein et al., 1989; Cheng et al., 1999; Serra et al., 2015; Prevaldi et al., 2016; La Rosa-Carrillo et al., 2022). Particularly in patients with predispositions like cystic fibrosis, bronchiectasis, chronic obstructive pulmonary disease (COPD), vascular diseases, diabetes, or immunocompromised patients there is a high risk of infection with *P. aeruginosa* (Prevaldi et al., 2016; La Rosa-Carrillo et al., 2022). Additionally, infections in difficult to reach sites in the body i. e. (eye background, sputum of cystic fibrosis lung) in combination with an intensive biofilm formation lead to poor pharmacokinetic distribution of applied antibiotics.

Consequently, other forms of bactericidal treatments are urgently required. One long-time known alternative and supplement to antibiotics is the use of bacteriophages (phages), viruses that infect bacteria. Phages show different pharmacokinetics and pharmacodynamics compared to classical drugs, as they multiply and self-regulate at the site of infection (Payne et al., 2000; Danis-Wlodarczyk et al., 2021b).

Around 10^{31} virus particles are estimated to exist on earth (Mushegian, 2020). But only a small part of these viruses, 2,818 genera, 84 subgenera and 11,273 species, have been classified by the International Committee for Taxonomy of Viruses (ICTV) in 2023 (International Committee of Taxonomy of Viruses, 2023). Of the sequences that can be unambiguously assigned to *P. aeruginosa* phages so far, about 2,148 nucleotide sequences, with 275 reference sequences and 55 different already classified genera have been deposited in the NCBI virus data base (https://www.ncbi.nlm.nih.gov/labs/virus/vssi/#/ accessed on 25 Oct 2024 (Hatcher et al., 2017; Alipour-Khezri et al., 2024). Due to the ubiquitous nature of *P. aeruginosa*, corresponding phages are found in soil, aquatic habitats, sewage, but also in humans and animals (Garbe et al., 2011; Amgarten et al., 2017; Shi et al., 2020; Aghaee et al., 2021; Alkalay-Oren et al., 2022; Hashemi Shahraki et al., 2023). Most *P. aeruginosa* phages described so far, including jumbo phages, belong to the *Caudoviricetes* (dsDNA genome) (Lecoutere et al., 2009; Yuan and Gao, 2017). A small part belongs to the *Inoviridae* (ssDNA), *Fiersviridae* (ssRNA) or *Cystoviridae* (dsRNA) (Sepúlveda-Robles et al., 2012; Pires et al., 2015; NCBI Virus, 2023). Shortly after the discovery of the phages by Frederick Twort and Félix Hubert d´Hérelle in the beginning of the last century, the latter developed the first phage therapeutic approaches together with the Georgian microbiologist Georgi Eliava. He founded the Bacteriological Institute Tiflis, later on renamed to the George Eliava Research Institute of Bacteriophage (Eliava Institute), today one of the leading institutions for phage therapy, even though most Western countries lost interest in phage therapy research during the time of the discovery and development of antibiotics. One major target of their research was the treatment of cystic fibrosis patients with *P. aeruginosa* infections (Parfitt, 2005; Chanishvili et al., 2022). Today, *Pseudomonas* phages have already shown their therapeutic potential against *P. aeruginosa* in several *in vitro*, *in vivo* and compassionate case studies on acute and respiratory infections, bacteremia, and wound infections (Debarbieux et al., 2010; Waters et al., 2017; Arumugam et al., 2022; Silva et al., 2022; Onallah et al., 2023; Rappo et al., 2023; Alipour-Khezri et al., 2024). The phages used therapeutically belong to twelve different phage genera - *Pakpunavirus*, *Pbunavirus*, *Phikzvirus* and *Nankokuvirus* (morphotype myovirus); *Litunavirus*, *Bruynoghevirus*, *Paundecimvirus* and *Phikmvvirus* (morphotype podovirus); *Septimatrevirus* and *Nipunavirus* (morphotype siphovirus) and *Perrunavirus* and *Cystovirus* (morphotype enveloped, spherical or icosahedral virion) (Rose et al., 2014; Ferry et al., 2021; Mabrouk et al., 2022; Silva et al., 2022; Alipour-Khezri et al., 2024; Pirnay et al., 2024; Pye et al., 2024). In general, prior to the treatments, phages were checked for an obligatory lytic lifecycle and the absence of virulence factors, toxins or antibiotic resistance genes in their genomes (Alipour-Khezri et al., 2024; Pirnay et al., 2024). Two generally different strategies exist for the application of phage therapy for the treatment of *P. aeruginosa* infections. Firstly, the use of a pre-composed phage cocktail such as practiced in the PhagoBurn project (Jault et al., 2019), composed of 12 phages directed against *Pseudomonas* infections of burn wounds, the various cocktails from the Eliava Institute in Georgia (Chanishvili, 2012) and from BiomX Gaithersburg, MD, USA (Rappo et al., 2023). In most cases their composition is not publicly available. The commercial cocktail of BiomX BX004-A in combination with antibiotics provided good tolerability and a bacterial reduction of 1.42 log in a clinical phase 1b/2a study of cystic fibrosis patients (Rappo et al., 2023). Secondly, a magistral preparation, as used in Belgium, Israel or Germany as part of the PhagoFlow project (Onallah et al., 2023; Pirnay and Verbeken, 2023; Willy et al., 2023), enables a customized selection of phages for each patient, often employed in combination with antibiotics (Onallah et al., 2023; Pirnay and Verbeken, 2023). Clinical improvement was reported for 77.2% of 100 cases of *P. aeruginosa* infections. In 61.3% of the cases a complete eradication of the targeted bacteria was found (Onallah et al., 2023; Pirnay et al., 2024).

A crucial factor during the establishment of phage therapeutic approaches is the quantitative determination of the efficiency phage activity using a phage susceptibility test (PST). Classically, a double agar overlay plaque assay (DPA) is performed that visualizes phage infection as plaques (Kropinski et al., 2009). Variations of DPA include the use of only one phage concentration or different dilutions applied as spots or discs with phages (RPST) (Skusa et al., 2023). Alternatively, phage lysis behavior can also be studied in liquids using a planktonic killing assay (PKA). To date, no standard conditions, cut-offs and breakpoints for bacterial lysis in the PST have been defined to determine the efficacy of phage lysis, which would contribute to comparability between laboratories (Parmar et al., 2023; Yerushalmy et al., 2023). It is already known from previous studies that the DPA and PKA methods lead to different results. One advantage of PKA is that the phages can be analyzed not only individually but also in combinations, which allows the identification of synergistic and antagonistic effects (Haines et al., 2021; Steffan et al., 2022).

Nevertheless, a systematic collection of *P. aeruginosa* phages tested in various combination on a broad spectrum of *P. aeruginosa* strain isolated from different types of infection is missing to generate generally applicable knowledge for *P. aeruginosa* phage therapies. This is necessary to select safe and broad host spectrum phages for a clinical magistral application to individually treat as many patients as possible. Thus, in this project, 25 phages and 141 P. *aeruginosa* strains were isolated, characterized, sequenced and their interaction investigated. In the context of phage susceptibility, DPA was compared with serial dilutions as spots and PKA on a large phage-host panel to reveal the advantages and disadvantages of each of the method.

2 Materials and methods

2.1 Bacterial strains and growth conditions

P. aeruginosa strains BWKH001–133 were isolated by the military hospital in Berlin and Hamburg (Germany) between 2015 and 2018. A description of the corresponding infection type (wounds, skin, repository tract, urinary tract, rectal, tissue) is given in Supplementary Data Sheet 1. Additionally, *P. aeruginosa* MH16, MH19, MH27, MH38 and RN21 were isolated from the urinary tract (Tielen et al., 2011, 2014). Five *P. aeruginosa* strains from patients with cystic fibrosis, five strains from patients with chronic obstructive pulmonary disease (COPD56-COPD129) and 14 strains of bronchiectasis (Bron08-Bron76) patients were provided by B. Tümmler (Medical School Hannover MHH, Germany) (Hamed et al., 2023). The model strains PAO1 (DSM 19880) and PA14 (DSM 19882) were obtained from the German Collection of Microorganisms and Cell Cultures (DSMZ Braunschweig, Germany) (Rahme et al., 1995; Stover et al., 2000; Mathee, 2018). All *P. aeruginosa* strains were cultivated aerobically in LB veggie medium (10 g/L veggie peptone, 5 g/L veggie yeast extract, 10 g/L NaCl (all Merck, Darmstadt, Germany)) at 37°C. For growth on agar plates 1.5 g/L agar (Merck, Darmstadt, Germany) was added.

2.2 Antibiograms of the *P. aeruginosa* strains

Bacterial strains were tested for antibiotic susceptibility using the disc diffusion method. Discs according to EUCAST concentrations were ordered by Mast Diagnostica GmbH, Reinfeld/Germany (Supplementary Data Sheet 2). Briefly, freshly streaked bacteria from cryo culture (LB veggie agar, 37°C, 18 h) were suspended in 10 mL 0.85% NaCl (Merck, Darmstadt, Germany) solution to an OD_{600nm} of 0.25. A cotton swab was dipped once into the inoculum, squeezed, and streaked in three directions on Mueller Hinton agar plates (25 mL/dish, 38 g/L, Roth, Karlsruhe, Germany). Afterwards six antibiotic discs were placed per plate with a dispenser (Mast Diagnostica GmbH, Reinfeld, Germany). After an overnight growth (35°C, 17h ± 1h) the zone of inhibition was measured and compared to the EUCAST thresholds (European Committee on Antimicrobial Susceptibility Testing, 2022).

2.3 Phage isolation, purification, and propagation

For isolation of *P. aeruginosa* phages, enrichments from different environments in Germany, including clinical sewage, washing machines and garden compost were performed between 2007 and 2022 and detected by DPA as described by Kropinski et al. with minor changes (Kropinski et al., 2009). A list of the phages and their characteristic is given in Supplementary Data Sheet 3. Agar concentration in top agars for host range analyses was 0.5% (Sigma Aldrich, Darmstadt, Germany), while different top agar concentrations (0.3 to 0.7%) were applied for visualization of the individual phages (Supplementary Data Sheet 3). Clonal purification was performed by in least three consecutive rounds of single plaque picking and streaking out on double ager overlay plates. Plaque sizes were determined via ruler measurement. In general, phage lysates were prepared either in liquid form by infecting logarithmically growing *P. aeruginosa* cultures with phages at a multiplicity of infection (MOI) between 0.01 to 0.5 followed by an incubation at 37°C and 140 rpm until complete lysis or for 22 hours. Alternatively, top agar of double agar overlay plates were incubated with phages until semiconfluent lysis occurred, subsequently covered with SM buffer, and finally scraped off after incubation. After centrifugation (10,967 x g, 4°C, 10 min), the phage-containing supernatant was filtered through 0.2 µm syringe filters (cellulose acetate, Sartorius, Germany), quantified using DPA and stored at 4°C.

2.4 DNA isolation and determination of DNA concentration

For DNA isolation the "Phage DNA Isolation Kit" (Norgen, Thorold, Canada) was used following the manufacturer's protocol

10.3389/fcimb.2025.1597009

and DNA was stored at 4°C. The concentration was determined using the Qubit® dsDNA broad range and 1x dsDNA high-sensitive assay kit (Thermo Fisher Scientific, Waltham, USA) following the manufacturer's instructions.

2.5 Library preparation and whole genome sequencing

The protocols for library preparation and whole genome sequencing for PacBio RSII and Illumina were described before (Korf et al., 2019). Other long read sequencing of phage genomes was performed with Nanopore technology using the protocol, "Ligation sequencing gDNA - SQK-LSK109 version: GDE_9063_v109_revAP_25May2022" (ONT, Oxford, United Kingdom), flongles version 9.4.1 with default parameters and basecaller Guppy version 7.1.4 with high-accuracy model.

2.6 Genome assembly, annotation and comparison

Either SPAdes version 3.12.0 (PacBio and Illumina) or flye version 2.9.3-b1794 (ONT and Illumina) was used for genome assembly, before long reads were trimmed with porechop version 0.2.4 (threshold of 10). Short reads were mapped using BWA short reads version 0.7.17.5 with default parameters and polished using polypolish version 0.5.0 (default parameters). All genomes, including those already published, were annotated using pharokka version 1.7.1 and compared with clinker version v0.0.28. Phylogenomic tree was performed with VICTOR (Meier-Kolthoff and Göker, 2017), visualized with iTOL (Letunic and Bork, 2024) and annotation was generated with table2itol (https://github.com/mgoeker/table2itol).

2.7 Morphological analysis via transmission electron microscopy

For TEM analysis, phages were prepared for analysis as previously described (Korf et al., 2019). Briefly, thin carbon support films were prepared by evaporating a carbon thread onto a freshly cleaved mica surface. Small pieces of mica were then cut, and phages were negatively stained with 2% (w/v) aqueous uranyl acetate, pH 5.0. The samples were examined at an acceleration voltage of 80 kV/120 kV in a Zeiss EM 910 or Zeiss Libra120 Plus transmission electron microscope (Carl Zeiss, Oberkochen, Germany). The dimensions of heads and tails was determined for 3–10 different phage particles using ITEM software (Olympus Soft Imaging Solutions, Münster, Germany). The head dimension was estimated on the basis of head length x head width. The phenotypic classification was done using the morphological criteria of Ackermann (Ackermann and Eisenstark, 1974; Ackermann, 2011).

2.8 Host range analysis by DPA (double agar overlay plaque assay)

The phage host range was determined by spotting serial dilutions (adjusted to 1E9 PFU/ml) on double agar plates containing 100 µL of a logarithmic culture of the potential host. After incubation for 18h ± 2h at 37°C, the plates were examined for lysis. The host was categorized as sensitive if individual plaques could be detected (lysis), or as insensitive if either no visible plaques (no lysis) or reduced growth was observed.

2.9 Host range analysis by PKA (planktonic killing assay)

A PKA was performed to analyze the host range of the phages in liquid bacterial culture. A culture was inoculated with an overnight culture to an OD_{600nm} of 0.05, allowed to grow above an OD_{600nm} of 0.1 and finally adjusted to an OD_{600nm} of 0.1. 200 µL adjusted culture were infected with 10 µL phage (2E8 PFU/mL) to reach an approximate MOI of 0.1. The optical density was measured in SpectraMax 250 (MWG-Biotech, Ebersberg, Germany) at 600 nm every 15 min for 24 h. The 96 well plate was mixed for 3 s before measurement. The host was classified as sensitive when the normalized area under curve (AUC_{norm}) was < 0.8 (lysis) and insensitive when AUC_{norm} was ≥ 0.8 (no lysis).

$$AUC_{norm} = \frac{[AUC]_{0h}^{24h} \textit{with phage}}{[AUC]_{0h}^{24h} \textit{without phage}}$$

For all combinations that were classified as lytic, the time point of lysis was calculated. This value was set as the first time point, where AUC_{norm} was below 0.8.

2.10 Host range comparison of DPA and PKA

To compare DPA and PKA, corresponding results of their host spectra were merged in each possible combination. Resulting matches or deviations were grouped as follows: group 1 was "DPA and PKA tests resulted in no phage lysis", group 2 was "DPA resulted reduced bacterial growth and PKA with no lysis", group 3 was "DPA with lysis and PKA without lysis", group 4 was "DPA with no lysis and PKA with lysis", group 5 was "DPA with reduced growth and PKA with lysis", and group 6 was "DPA and PKA with lysis". The rows and columns of the heatmap were clustered using the distinct method in R software with resulting categories.

2.11 Determining the optimal phage combination

Optimal phage combinations based on host ranges identified by DPA and PKA were determined by Phage Cocktail Optimizer by Stephen T. Abedon (https://www.phage-therapy.org/calculators/

cocktail_optimizer.html, accessed on 5 Jul 2024). "Lysis" determined as described above was rated as "positive" phage-host interaction.

2.12 MOI dependent planktonic killing assay and virulence index

The original bacterial host on which the phage was isolated was tested with different MOIs to determine the lysis behavior. The culture was inoculated from an overnight culture with OD_{600nm} of 0.05 and grown to an OD_{600nm} of 0.1. Serial dilutions of the culture at the time of infection were plated to determine the colony forming units (CFU) of the host *P. aeruginosa*. The phage was adjusted to 2E9 PFU/mL and serial diluted to 2E5 PFU/mL with LB veggie medium. 200 µL culture were infected with 10 µL phage dilutions in triplicates (final MOI between 1 to 0.0001). Optical density was measured using a SpectraMax 250 (MWG-Biotech, Ebersberg, Germany) every 15 min for 24 h. After incubation the triplicates were pooled and centrifuged (16,200 x g, 2 min, at room temperature) (Fresco 21, Thermo Scientific, Waltham, US). The phage titer t_{24h} was determined by DPA from corresponding supernatants. Local virulence index (vi) was assessed as previously described (Storms et al., 2020). The beginning of the stationary phase was defined as the first local maximum with a threshold value of 5:

$$v_i = 1 - \frac{[AUC]_{0h}^{stationary\ phase}\ with\ phage}{[AUC]_{0h}^{stationary\ phase}\ without\ phage}$$

The global virulence index (vp) was calculated as the quotient of the area under the virulence curve (A_p) divided by the theoretical maximum area under the virulence curve (A_{max}) (Storms et al., 2020):

$$v_p = \frac{A_p}{A_{max}}$$

2.13 Ranking score

For the final ranking phages received score for the categories DPA, PKA, virulence index (vp) and safety according to Supplementary Data Sheet 4.

3 Result

3.1 Isolation and initial characterization of 25 *P. aeruginosa* phages

In order to systematically test multiple *P. aeruginosa* strains isolated from highly different infections corresponding phages were selected as a first step. For this purpose, phages were isolated from wastewater (partly with clinical proximity), garden compost and washing machines between 2004 and 2022 from locations in northern Germany. After isolation and propagation, phages were systematically characterized for their head, tail, plaque size, halo formation, plaque appearance, genome size, number of genes, GC content, virulence index and lysis behavior as shown in Figures 1, 2 and Supplementary Data Sheet 1 (complete dataset).

3.2 Phage morphology

Using transmission electron microscopy (TEM), the 25 phages were classified as twelve myoviruses including three jumbo phages, four siphoviruses and nine podoviruses (Figure 1). All phages had a symmetrical hexagonal head and were categorized in A1 (myoviruses), B1 (siphoviruses) and C1 (podoviruses) according to Ackermann and Eisenstark, 1974. Prolonged heads were not observed. When analyzing phage dimensions, the myovirus morphotype showed the greatest diversity (myoviruses: mean head height 93 ± 29 nm; mean head width 87 ± 25 nm; mean tail length 151 ± 26 nm, podoviruses: 67 ± 8 nm, 65 ± 6 nm; 16 ± 8 nm and siphoviruses 62 ± 4 nm, 59 ± 3 nm; 192 ± 5 nm (Figures 2A, B). The phages HHBS36_1 (*Pawinskivirus*), HHBS8_1 and HHBS47_1 (both *Elviruses*) are representatives of the jumbo phages with head heights ranging from 139 to 147 nm. This means that they are not only larger in terms of their genome (see Chapter 3.5.1), but also in terms of their head and tail.

3.3 Plaque morphology and halo formation of the isolated phages

The diversity of phages can also be illustrated by their plaque morphology (Figure 2C, Supplementary Figure 1). DPA was performed with different concentrations of top agar (Supplementary Data Sheet 3). Plaque size ranged between 0.1 mm at 0.3% top agar concentration for HHBS8_1 (*Elvirus)* to 3.5 mm at 0.7% top agar concentration for JG004 (*Pakpunavirus)*. Most myoviruses formed clear plaques, whereas the plaques of podoviruses and siphoviruses tended to be turbid. All temperate phages (Supplementary Data Sheet 3) produced turbid plaques. Halo structures could be found through all morphotypes. However, it should be noted that only 16% of all phages studied produced halos.

3.4 Lysis behavior of isolated phages

The actual virulence and efficacy of lysis were assessed in 96-well format using different MOIs and calculating the virulence index (vp) to compare the phages for later therapeutic potential (Figure 2D). The host bacteria used were the same as those used for the isolation. A high virulence index is characterized by rapid and complete lysis. Some phages of the morphotype myovirus (vp mean 0.58 ± 0.31) and podovirus (vp mean 0.57 ± 0.28) lysed in a short period and had a high virulence index of e. g. 0.95 - JG004 (*Pakpunavirus*) or 0.88 - HHBS9_2 (*Litunavirus*). On the other hand, there were also phages

10.3389/fcimb.2025.1597009

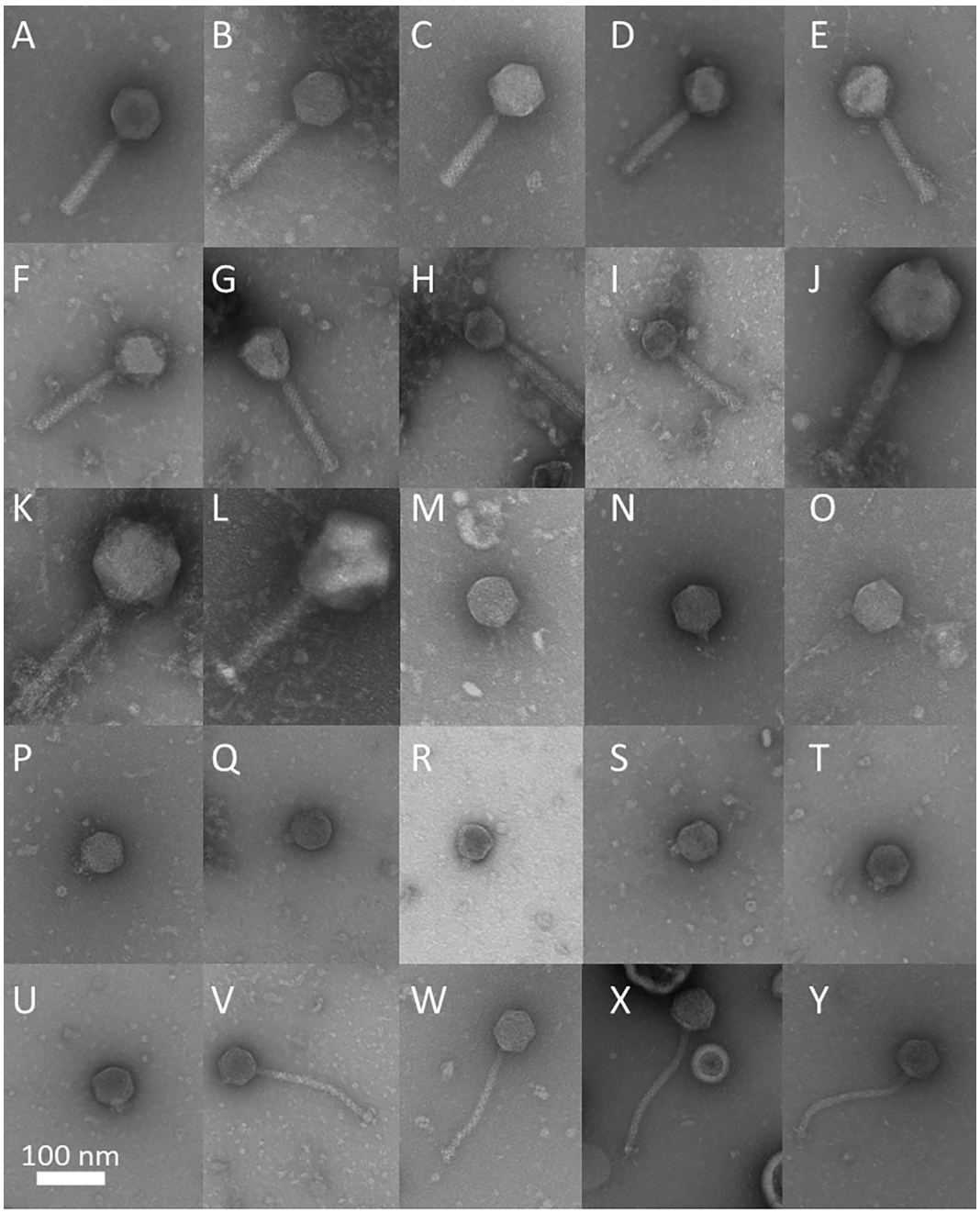

FIGURE 1
Electron micrographs of isolated phages with the morphotype myovirus [JG004 **(A)**, HHBS9_1 **(B)**, HHB18_1 **(C)**, PTLAW1 **(D)**, HHBS12_2 **(E)**, HHBS42_2 **(F)**, HHBS51_1 **(G)**, Komp_PAO1_1 **(H)**, BIBS67 **(I)**, HHBS47_1 **(J)**, HHBS8_1 **(K)**, HHBS36_1 **(L)**], and morphotype podovirus [BWKH3_L8_1 **(M)**, BWKH3_R8_1A **(N)**, HHBS9_2 **(O)**, HHBS10_2 **(P)**, HHBS55_2 **(Q)**, HHBS14_1 **(R)**, Flu_PA14_3 **(S)**, Flu_PA14_4 **(T)**, Komp_PA14_gP **(U)**] and morphotype siphovirus (HHBS29_1 **(V)**, 22043_B8_1 **(W)**, Tom33 **(X)**, Komp_PA14_H **(Y)**. Bar represents 100 nm.

from the same morphotype that had a very low virulence index of 0.23 - BIBS67 (*Phitrevirus*) or 0.09 – Flu_PA14_4 (*unclassified phage*). For HHBS29_1 (*Septimatrevirus* – morphotype siphovirus) lysis was only observed at high MOI (1 and 0.1) so the virulence index was correspondingly low (vp 0.04). Two myoviruses JG004 and HHBS9_1 (both *Pakpunavirus*) underwent a second lysis after regrowth (Supplementary Figure 2A).

3.5 Genome of the isolated phages

3.5.1 General genetic properties

Phage sequencing was performed using PacBio or ONT (long reads) and Illumina (short reads) technologies for taxonomic classification and to exclude unwanted genes. Phage genome size ranged from 30,180 bp (BIBS67 - *Phitrevirus*) to 302,046 bp

10.3389/fcimb.2025.1597009

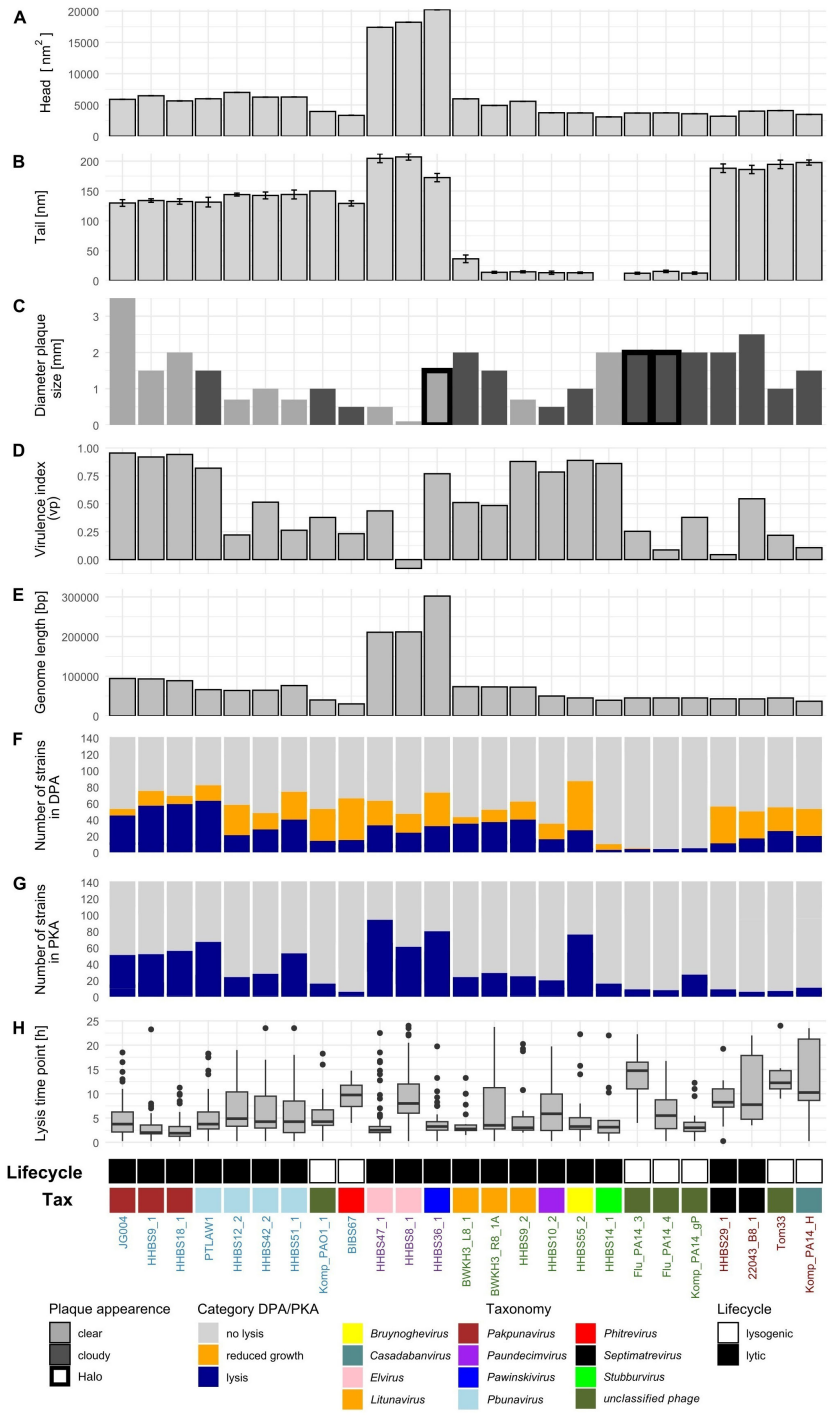

FIGURE 2
The diversity of the phages was assessed based on ten parameters. For all parameters phages are grouped based on morphotype (colored names at the bottom: myo- (blue) – jumbo phages (violet), podo- (green) or siphovirus (brown)) and taxonomy. Lysogenic phages are indicated in white, strictly lytic phages in black. Head size (head length x head width), tail length, plaque appearance, genome size, as well as virulence index (vp) are shown as barplots **(A-E)**. Distribution of lysis behavior in DPA and PKA resulting in either no lysis, reduced growth or lysis are displayed in **(F, G)**. Boxplots represent the time of lysis in PKA (first time normalized AUC was < 0.8) for all strains **(H)**.

(HHBS36_1 – *Pawinskivirus*) (Figure 2E). Phages of the jumbo phage genera *Elvirus* and *Pawinskivirus* reached the upper limit in both physical and genome size (mean 246,208 bp). Other myoviruses also tended to have slightly larger genomes (mean 68,619 bp) than podoviruses (56,496 bp) and siphoviruses (41,912 bp). The GC content was between 44% and 64%, while all temperate phages had higher GC content (mean 61%) then lytic phages (mean 52%).

3.5.2 Phylogenetic tree of the isolated phages

The diversity of *P. aeruginosa* phages can also be demonstrated by examining their genome. At the time of the study, 18,673 reference genomes were deposited in the NCBI Virus Database (https://www.ncbi.nlm.nih.gov/labs/virus/vssi/#/ accessed on April 2nd, 2025). If all phage genomes whose host does not contain the search terms "*Pseudomonas aeruginosa*", "*Pseudomonas*" or "*Pseudomonas* sp." were removed, 275 reference genomes remained. At least one genome from each *P. aeruginosa* phage genus (complete reference sequence deposited in NCBI Virus Database) was selected and the relationships were presented in a phylogenetic tree (Figure 3). The distribution of morphotypes is very diverse, as it is spread across different clusters. While *Pakpunavirus* and *Pbunavius* are clearly separated, the jumbo phages all cluster together and have a relatively low GC content. Members of *Bruynoghevirus*, *Paundecimvirus* and *Litunavirus* share only individual genes with transcriptional regulatory or metabolic function. This makes them more closely related to each other than to *Stubburvirus* (e.g. HHBS14_1) or unclassified podoviruses (e.g. Flu_PA14_3). The unclassified phages including Tom33 form a very distinct cluster, most of which perform a lysogenic cycle and have a relative high GC content (Carballo-Ontiveros et al., 2020). But even within a genus, the phages were quite different, as only a nucleotide identity of 70% (coverage * identity) is required (Turner et al., 2021). Twelve out of 55 P. *aeruginosa* phage genera were covered by the phage panel characterized in this study. Some genera have already been described frequently and have many reference species. For example, 38 reference species are known for *Pakpunavirus*, 37 for *Pbunavirus*, 13 for *Litunavirus* and 20 for *Septimatrevirus*, while only one reference phage exists for relatively new species such as *Elvirus* and *Pawinskivirus*.

However, despite the high sequence identity, the genome of phage species within these common genera sometimes differs considerably. The phages within *Litunavirus* and *Pakpunavirus* are more conserved than *Pbunavirus*, *Bruynoghevirus* and *Septimatrevirus*. In all genera, highly conserved genes (core genome) belong to proteins related to phage head and packaging, DNA, RNA and nucleotide metabolism (Supplementary Figures 3-8). When all phages are aligned with dnaapler at the same starting point (*terL*), the greatest variability is seen in proteins of the tail structures, such as the tail fiber protein, and at the end of the genome, where many small, hypothetical proteins are located. It is noteworthy that HHBS51_1 exhibits an insertion of 10 kb, which is not observed in other *Pbunavirus*. The insertion includes an endolysin, DNA primase and many small proteins of unknown function, but no genes that cause a lysogenic life cycle (Supplementary Figure 3).

3.6 Isolation and antibiotic sensitivity of 141 *P. aeruginosa* strains

Most *P. aeruginosa* isolates were isolated in the military hospitals in Berlin and Hamburg as well as at the Medical School in Hannover (MHH) in Germany from various types of infection, resulting in great diversity in terms of isolation time, geographical origin and indication (Supplementary Data Sheet 1). A detailed characterization of these strains will be subject of a different investigation. The susceptibility of *P. aeruginosa* isolates to different antibiotics (Supplementary Figure 9) was tested to compare susceptibility to antibiotics with susceptibility to phages. Twelve antibiotics including ceftazidime*, ceftazidime/avibactam, ceftolozane/tazobactam, cefiderocol (cephalosporins), piperacillin*, piperacillin/tazobactam (penicillins), imipenem*, meropenem* (carbapenems), azetreonam (monobactam), and ciprofloxacin* (fluoroquinolone), and some other antibiotics like amikacin and tobramycin (aminoglycosides) which are used as standard or reserved therapy for *P. aeruginosa* infections were chosen. All lead substances of antibiotic classes (underlined) were included (Supplementary Data Sheet 2). According to Robert-Koch-Institute in Germany, a distinction was made between 3 MRGN being resistant to three and 4 MRGN being resistant to four antibiotic classes (Kommission für Krankenhaushygiene und Infektionsprävention, 2019). Based on the antibiogram, 39% 3 MRGN (55/141 strains) and 61% 4 MRGN (86/141 strains) were identified (meropenem used as lead substance). Many wound isolates were only susceptible to cefiderocol, a last resort antibiotic. However, *P. aeruginosa* strains BWKH001, BWKH038 (both wound isolates) and Bron11 (respiratory tract) were even resistant to cefiderocol.

3.7 Host range of the phages tested with the 141 *P. aeruginosa* strains

A classical host range analysis (DPA) was performed with the diverse phage panel (Figures 2F, 4). *Pbunavirus* and *Pakpunavirus* had a broad host range (15 – 45%) and clustered close together although they are not genetically related (Figure 3). PTLAW1 (*Pakpunavirus*) had the highest coverage with 45% (63/141 strains). HHBS36_1 (*Pawinskivirus)*, HHBS47_1 and HHBS8_1 (both *Elviruses)* had a medium coverage of 21% (mean 30/142 strains), but phage-host interactions were often categorized as reduced growth, in 22% of interactions. Among the myoviruses, BIBS67, a temperate *Phitrevirus*, had a narrow host spectrum with a coverage of 11% (15/141 strains). In comparison to *Pakpunavirus*, the *Litunavirus* (podoviruses) grouped together more strongly and lysed other strains (see Figures 4, 5). Twelve out of 33 wound and seven out of 24 urinary tract isolates were covered by *Litunavirus* with at least one phage. Strikingly, the *Bruynoghevirus* HHBS55_2 showed reduced growth for a particularly large number of strains 43% (60/141 strains), whereas plaques were only determined for 19% of the strains (27/141 strains). In contrast, HHBS14_1 (*Stubburvirus*) was very specific and covered 2% of the tested strains (3/141 strains). Similarly, Flu_PA14_3, Flu_PA14_4 and Komp_PA14_H (*unclassified phage*) covered 3 - 4% of the strains. The two *Septimatrevirus* (siphoviruses) were quite different from each other. HHBS29_1 showed lytic behavior on 8% of the strains (11/141 strains), some of which were cystic fibrosis isolates, and 22043_B8_1 lysed 12% of the strains (17/141 strains) (see Figures 4, 5). Both phages tend to have many phage-host interactions that we classified as reduced growth. No plaques were detected in about 9% of the strains (13/141 strains) from different

10.3389/fcimb.2025.1597009

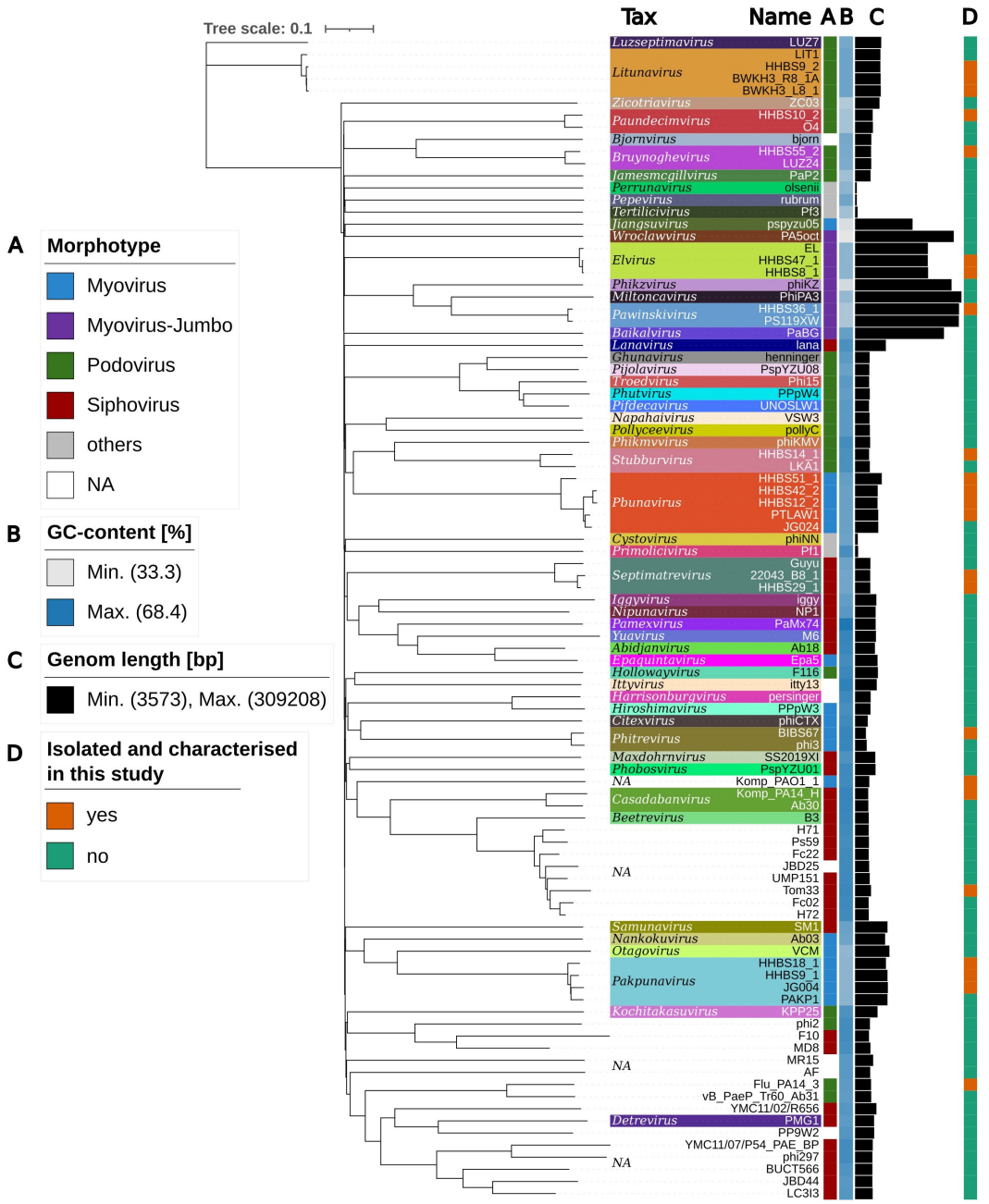

FIGURE 3
Phylogenomic tree of *P. aeruginosa* phages created with VICTOR and visualized with iTOL. At least one phage was selected from each *P. aeruginosa* phage genus uniquely colored (Tax). Morphotype and GC-content of phage are shown as color bars **(A, B)**. Genome size is displayed as bar chart **(C)**. All phages isolated and characterized in this study are labeled in orange **(D)**.

sampled sites. 10% (14/141 strains) of *P. aeruginosa* strains were only covered by one phage, showing visible plaques. On the other hand, there were also 10% (14/141 strains) of *P. aeruginosa* strains that could be covered by ten or more of the phages tested. Interestingly, the susceptibility of the *P. aeruginosa* strains against phages tended to correlate positively with the susceptibility of antibiotics (Supplementary Figure 10). Lytic behavior of phages could not be shown for *P. aeruginosa* strains BWKH17 (wound), BWKH23 (respiratory tract), BWKH24 (skin), BWKH35 (wound), BWKH68 (urinary tract), BWKH96 (rectal swab) or BWKH115 (rectal swab) with any method. All of them are highly resistant to antibiotics.

3.8 Comparison of the PKA and DPA methods

However, it is not yet clear which is the best *in vitro* method for determining the phage susceptibility that best predicts *in vivo*

10.3389/fcimb.2025.1597009

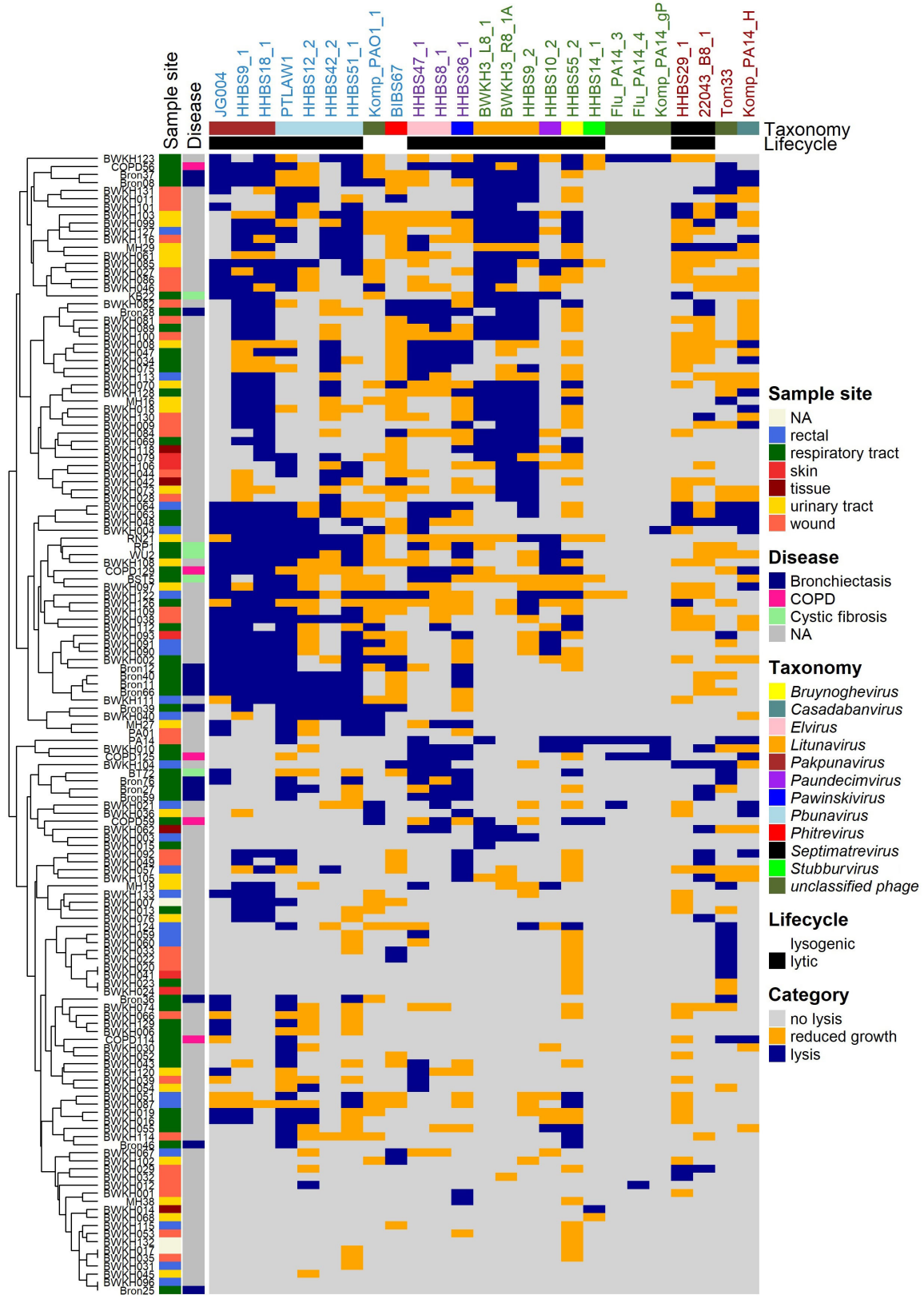

FIGURE 4
Host range analysis by DPA (top agar 0.5%) of 25 phages. Interaction is classified into "no lysis" (grey), "reduced growth" (orange) and "lysis" (blue). The used phages are colored based on their morphotype (colored names at the top: myo- (blue) – jumbo phages (violet), podo- (green) or siphovirus (brown)), taxonomic classification and lifestyle. Analyses was performed using 142 clinical isolates of *P. aeruginosa* sampled from different habitats and patients with different diseases (colored left). Clustering of rows is performed by distinct method of ComplexHeatmap package in R.

10.3389/fcimb.2025.1597009

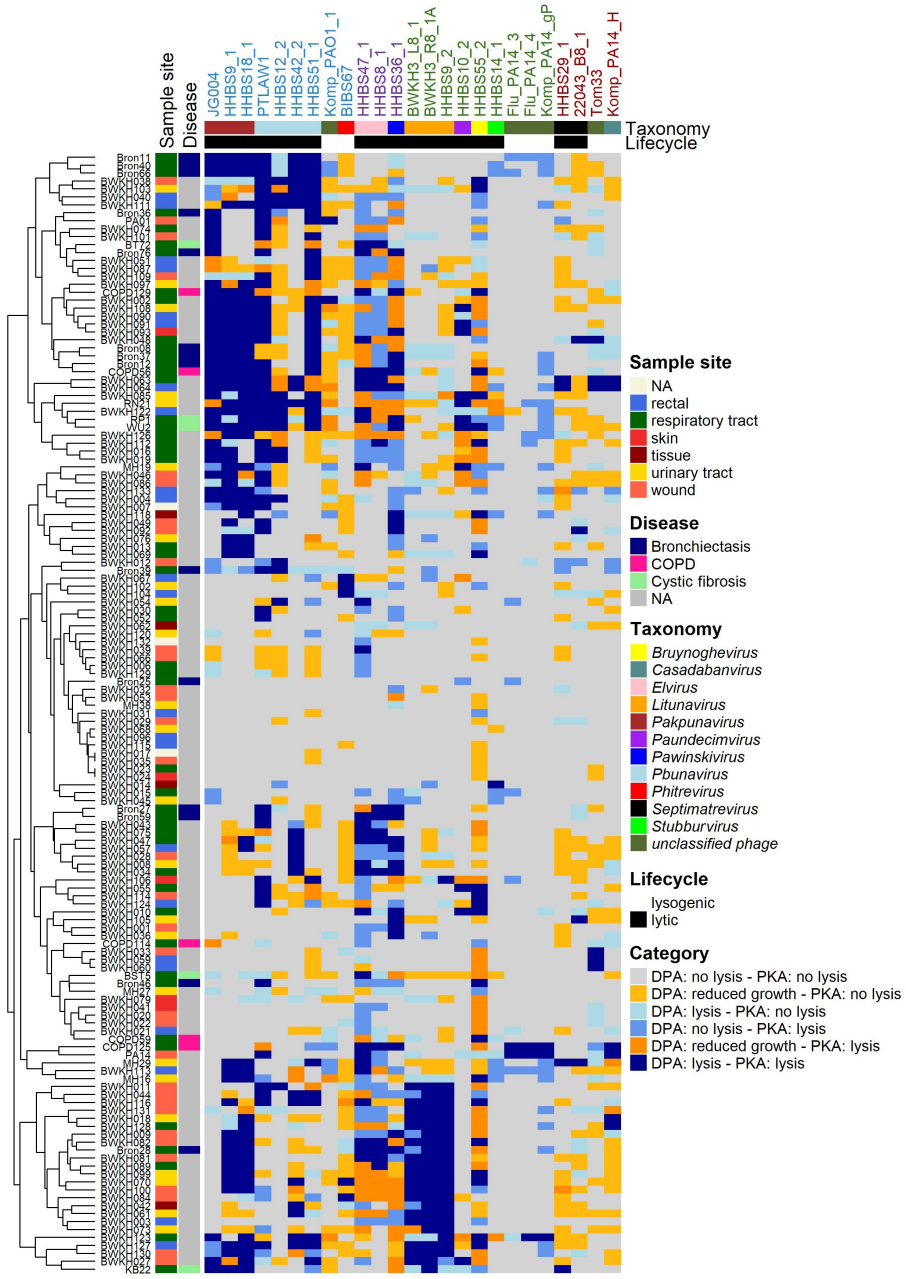

FIGURE 5
Comparison of host spectra determined by DPA and PKA respectively. Phages are colored based on their morphotype (colored names at the top: myo- (blue) – jumbo phages (violet), podo- (green) or siphovirus (brown)), genus and lifecycle (top) and the *P. aeruginosa* strains are shown with the sample site (left). DPA was performed using 0.5% top agar concentration and serial dilutions of phage lysates and classified as "no lysis", "reduced growth" and "lysis". PKA was performed in LB veggie medium at MOI 0.1. The growth curves of PKA are integrated for 24h and normalized against the control without phage. Normalized AUC ≥ 0.8 is classified as "no lysis" and normalized AUC < 0.8 as "lysis". Both results are combined with the expressions DPA: lysis - PKA lysis in dark blue, DPA: reduced growth - PKA lysis in dark orange; DPA: no lysis - PKA lysis in mid blue; DPA: lysis - PKA no lysis in light orange; DPA: reduced growth - PKA no lysis in light blue and DPA: no lysis - PKA no lysis in grey. Heatmap is clustered with average methods of ComplexHeatmap (R) in rows and columns.

efficacy. Therefore, we determined the host range using both PKA and DPA method and systematically compared the results in order to contrast the advantages, disadvantages and limitations of both methods. The comparison of both methods revealed a correlation of 70%, of which 13% is attributable to a lytic interaction (dark green) and 57% to a non-lytic interaction (light green) (Supplementary Figure 11A). A high correlation of lytic and non-lytic interaction can be observed particularly in the genera *Pbunavirus*, *Pakpunavirus* and *Litunavirus* (Supplementary Figure 11B). At the same time, the PKA method tended to identify more lytic phage-host interactions for these genera than DPA. In 17% of the cases there were ambiguous results, which can be further distinguished. There are 5% of the cases in the category "DPA: reduced growth - PKA: lysis" (dark orange), in which the host range

of phages was underestimated using the DPA method. Many of these cases were related to jumbo phages. This is due to the fact that members of *Elvirus*, *Pawinskivirus* and *Bruynoghevirus* in particular formed invisible, too tiny or not clearly defined individual plaques with 0.5% top agar. When the lysis behavior is tested with PKA, these phages sometimes achieve even better coverage (43 to 67%) than the other myoviruses (Figure 2G). On the other hand, 13% of the cases were classified as "DPA: reduced growth – PKA: no lysis" (light orange). In particular, phages with the morphotype siphovirus accounted for more than 21% in this category, which means that they were probably overestimated by the DPA. If the plaques were cloudy in DPA, often no lysis was observed in the PKA (Figure 5). No correlation was found in 6% of the cases with expression "DPA: no lysis - PKA: lysis" and 6% of the cases with the expression "DPA: lysis - PKA: no lysis". The second case was particularly prevalent in *Litunavirus* and phages with the morphotype siphovirus (Figure 5). Since both methods lead to different results and this can have an influence on the selection of phages, both methods must be taken into account for the PST.

This study also investigated whether there are infection-specific phages by analyzing the host spectrum with regard to the isolation type of the hosts. Figure 6 represents the percentage coverage of the lysed strains depending on the type of infection of strains shown for DPA and PKA. A specificity of certain phages toward *P. aeruginosa* from specific habitats or diseases could not be determined in this study. The only finding was that *Litunavirus* lysed fewer strains from the respiratory tract than myoviruses.

3.9 Final ranking of phages suitable for a phage therapy

Two aspects need to be distinguished for a ranking of the phage concerning their application in a phage therapy. Which phages are suitable for (individual) therapy and which phages have favorable properties for production. Both aspects should be considered for the selection to ensure an efficient and safe treatment as well as successful production. Here we provide a ranking (Figure 7) with multiple factors like safety, host range determined by DPA and PKA and virulence index (vp) included.

We suggest that phages with a broad (*Pakpunavirus*) or narrow (*Stubburvirus*) host spectrum should be assessed equally for therapy if they are effective on a patient isolate. Even more important are the safety aspects. In order to exclude risk factors for the patients, the genomes of the phages were examined. 18/25 phages were strictly lytic, do not encode any virulence factors or antibiotic resistance genes (analyzed with Virulence factor database (VFDB) (Liu et al., 2022) and AMRfinderPlus (Feldgarden et al., 2021) (Altschul et al., 1997; Feldgarden et al., 2021) and could be used for therapy purposes (Figure 7). All lysogenic phages (*unclassified phages, Casadabanvirus* and *Phitrevirus*) with integrase, transposase, excisionase or other DNA transposition proteins were excluded (Figure 7B) for therapeutic use.

Looking at our ranking, PTLAW1 (*Pbunavirus*) ranked the highest with ten final points. Other phages like HHBS18_1, JG004 and HHBS9_1 (*Pakpunavirus* with morphotype myovirus) received 9 points. They lysed their production host efficiently and fast (Figure 2H). HHBS55_2 (*Bruynoghevirus*) and HHBS36_1 (*Pawinskivirus*) were also promising candidates (9 points) because of their great host range in PKA. HHBS47_1 should be preferred (8 points) over HHBS8_1 (both *Elvirus*) (6 points) because of a higher virulence index. Various phages with the podovirus morphotype ranked in the midfield, including the promising phage HHBS9_2 (*Litunavirus*) (7 points). On average, siphoviruses ended up at the bottom of the ranking. The biggest influence was their low virulence index (vp). This made HHBS29_1 (*Septimatrevirus*) difficult to produce in liquid (Figure 7, Supplementary Data Sheet 3, Supplementary Figure 2A)).

3.10 Theoretical combination of phages for phage therapy

The effectiveness of phage therapy depends not only on the selection of individual phages but also on a combination of phages. Thus, the theoretical coverage of multiple phage applications was analyzed *in silico* using the Phage Cocktail Optimizer (Abedon, 2020) to identify the phage combination that maximizes coverage. Only safe phages that could be used for treatment were included in this calculation. The maximum coverage of 92% of all strains with at least one phage per bacterium was achieved with six phages, based on the PKA results. For the DPA results, the maximum coverage is 86% with a total of twelve phages combined (Table 1). The greatest theoretical coverage was always achieved when phages of different genera were combined. If three phages were theoretically combined in a cocktail, this would result in a coverage of over 74% (DPA) or 86% (PKA) (Table 1). Many possible combinations contain PTLAW1 (*Pbunavirus*) and HHBS47_1 (*Elvirus*) or HHBS55_2 (*Bruynoghevirus*).

4 Discussion

Our data highlights the diversity of *P. aeruginosa* phages. We were able to isolate 25 phages, 18 of which pursue a strictly lytic lifecycle (all isolated from wastewater samples), while only temperate phages could be extracted from the environmental samples (garden compost, tomato, washing machine). New phages should therefore be sequenced at an early stage of the work to determine the life cycle and avoid labor-intensive experiments. All lytic phages could be assigned to previously published genera, but many phages represent a potential new species (Supplementary Data Sheet 3). Some temperate phages, on the other hand, were assigned to following new genera: first new genus include Flu_PA14_3, Flu_PA14_4, Komp_PA14_gP, second new genus Komp_PAO1_1 and third genus Tom33.

Our study revealed a high diversity in particular among in the morphotype myoviruses of our *P. aeruginosa* phage panel. Although they all have a hexagonal head and tail, they differ considerably at the genome level. Therefore, it is more contemporary to compare phages within their genus and not

10.3389/fcimb.2025.1597009

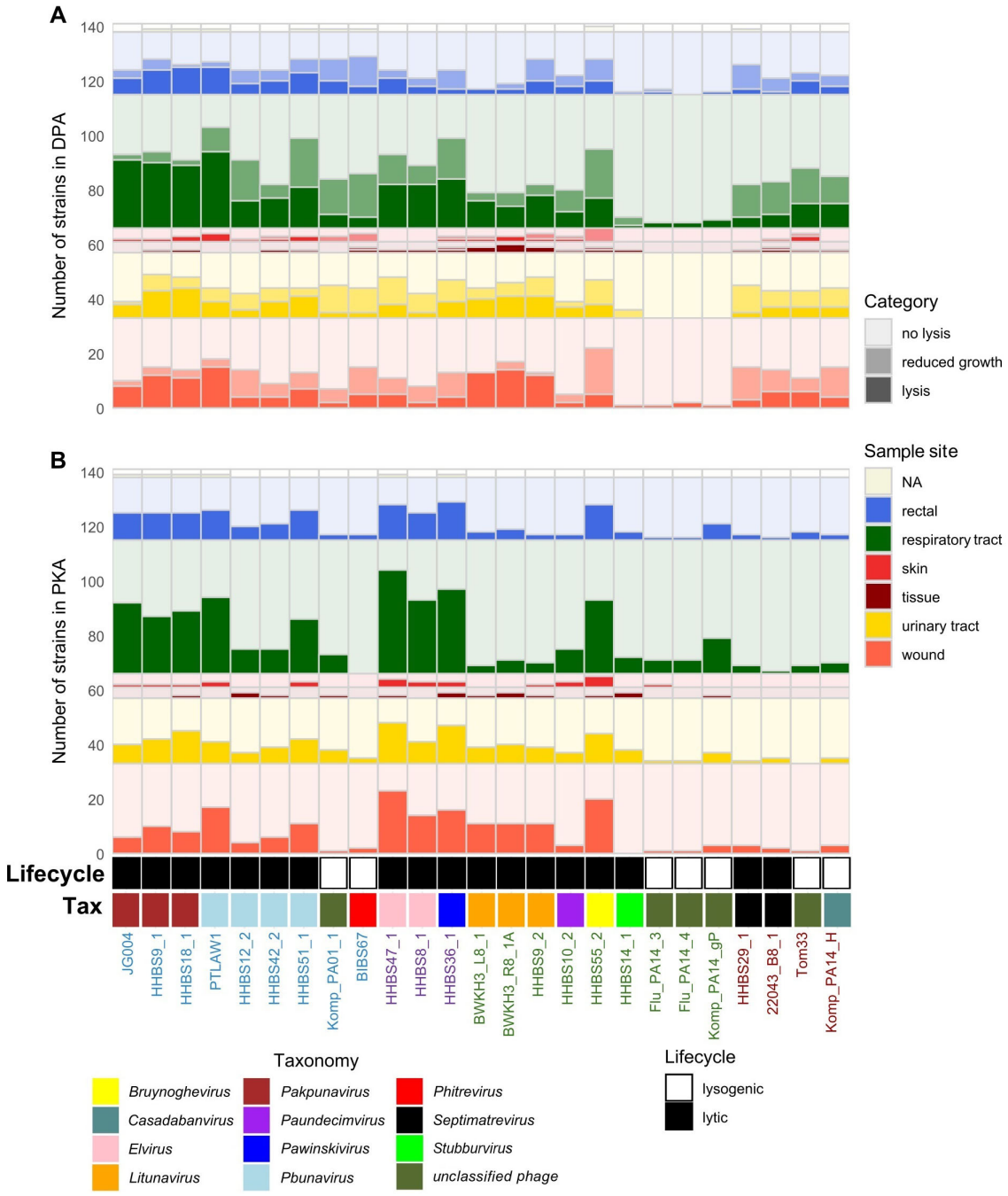

FIGURE 6
Percentage of lysed clinical *P. aeruginosa* strains depending on the phage and the PST. The phage-host interaction is shown with increasing intensity: DPA assay in three categories (no lysis, reduced growth, lysis) **(A)** and PKA assay in two categories (lysis: normalized AUC < 0.8 and no lysis: normalized AUC ≥ 0.8) **(B)**. Both plots are grouped based on morphotype (colored names at the bottom: myo- (blue) – jumbo phages (violet), podo- (green) or siphovirus (brown)), genus and lifecycle of the phage. The habitats from which *P. aeruginosa* was sampled are light grey = not available, blue = rectal, dark green = respiratory tract, red = skin, brown = tissue, yellow = urinary tract and orange = wound.

their morphotypes (Turner et al., 2021). There are many variations within a phage genus, including insertions, deletions, and mutations within genes. Mutations within the tail proteins are primarily responsible for adsorption to the host (Gaborieau et al., 2024) and the resulting variability of host specificity.

Virus- and plaque morphologies are often used as a basic characterization as they are easy to compare and allow phage identification. The formation of large, clear plaques should be favored over cloudy plaques, as this often represents temperate phages. Small plaques are problematic as well, as they can be difficult to detect. However, phages should only be excluded after sequencing, as morphological characteristics only provide an initial indication of which phages have therapeutic potential. By determining the virulence index (vp), phages can be qualitatively compared for the

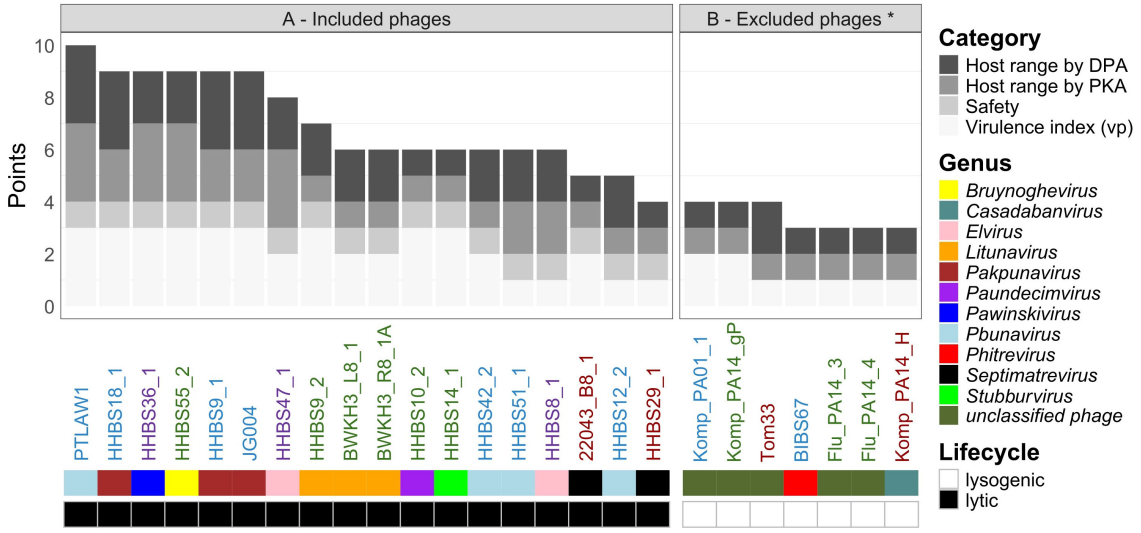

FIGURE 7
The ranking of phages regarding therapeutic potential and production is visualized by several categories in descending order and subdivided according to safety aspects. Both plots are shown with the morphotype (colored names: myo- (blue) – jumbo phages (violet), podo- (green) or siphovirus (brown)), genus and lifecycle of the phage. **(A)** shows all phages without safety concerns and **(B)** shows all phages with safety concerns due to a lysogenic life cycle *. In both diagrams, the distribution of points is determined as described in Supplementary Data Sheet 4. In detail, the points for DPA are as follows: 3 points for ≥ 42 lysed strains, 2 points for 21–42 lysed strains and 1 point for < 21 lysed strains. Classification of host range determined by PKA is: 3 points for ≥ 63 lysed strains, 2 points for 31–63 lysed strains and 1 point for < 31 lysed strains. Strictly lytic phages without toxins, antibiotic resistance genes or genes that induce a lysogenic cycle receive 1 point, otherwise 0 point*. Virulence index (vp) is classified like 3 points: vp ≥ 0.6, 2 points: vp 0.3-0.6 and 1 point: vp < 0.3. In addition, the phages are colored based on their genera, morphotype and lifecycle.

first time (Storms et al., 2020). For this purpose, MOI-dependent lysis curves were recorded, the AUC was normalized against an uninfected control, and these local virulence indices (vi) are integrated a second time against the log MOI to obtain the virulence index (vp). A comparison of vp of different phages presents some difficulties, as almost all parameters must be identical for vp to be successfully calculated. Normally, only one parameter like growth medium or temperature may be changed in order to achieve optimal comparability. Nevertheless in our data, two parameters (phage and host) were adapted. Our aim was to determine which phage with its host is best suited for production. It has been shown that the production of *Pakpunavirus*, even at low MOIs, results in a significantly greater bacterial reduction than *Litunavirus* (Supplementary Data Sheet 3). Some of the phages (HHBS8_1 and HHBS47_1 (*Elvirus*)) lyse only after the onset of the steady-state phase, so that the vp is very small due to the official calculation that includes the time of the steady-state phase of the control. Therefore, for the determination of susceptibility in PKA, we calculated the AUC over 24 h rather than up to the steady-state phase to compensate for the different growth behavior of the strains. We consider that Peters et al, 2023 had similar difficulties in calculating the vp according to the original definition by Storms et al, 2020 and therefore set the cut-off to 8 hours and thus included early regrowth of the bacteria in the virulence index. Normally, phages with a high vp value should be favored. Nevertheless, we would like to raise the question of whether late-lysing phages with different lysis kinetics are even advantageous in combination with other early-lysing phages.

The phages can be differentiated according to their host spectrum. Using our broad phage and host panel, we compared 3525 phage-host interactions with DPA and PKA. We found that the comparability of the two methods strongly depends on the phage genus analyzed (Supplementary Figure 11). In particular, members of *Pbunavirus*, *Pakpunavirus* and *Litunavirus* can be compared very well (comparability of the methods on average > 76%), as they form very large plaques. The method DPA has some limitations if the plaque morphology is not unambiguous in the case of small or cloudy plaques. For example, the formation of small plaques of jumbo phages, which lead to the lytic interaction being undetected, could be avoided by decreasing the top agar concentration (Serwer et al., 2007; Yuan and Gao, 2017). However, other problems can then arise, such as the overgrowth of plaques with very mucous clinical isolates, and the plaques sometimes only grow very slowly (HHBS8_1 at 0.3% in Supplementary Figure 1) (Staudinger et al., 2014). Low adsorption rates favor the formation of small plaques not only in jumbo phages (Abedon and Culler, 2007). In contrast to the assumption that phages that do not lyse a liquid culture fail to form plaques as published by Haines et al., 2021, our results demonstrate that this behavior is exhibited by siphoviruses in particular. In addition, we were able to show that the plaque morphology of phages with regard to turbidity is dependent on the strain, especially in case of temperate phages. However, the boundaries between clear and cloudy plaques are difficult to distinguish by eye. HHBS55_2 (*Bruynoghevirus*), BWKH3_L8_1 and BWKH3_R8_1A (both *Litunavirus*), which are lytic phages, form cloudy plaques in their original strains (Figure 2C) and in some cases also on other strains (Figure 4, data not shown).

Considering all these arguments we propose to use PKA as the standard method for PST. It offers several advantages: an already successfully implemented automation, easy performance in replicates

TABLE 1 Coverage of a theoretical phage combination determined with Phage Cocktail Optimizer (Abedon, 2020) depending on the method and the depth of the cocktail (only safe phages used).

Method	DPA				PKA								
Number of phages in cocktail	2	3	4	12	2	3			4			5	6
Theoretical number of lysed strains	91	104	109	121	113	121			126			129	130
Theoretical percentage of lysed strains	65%	74%	77%	86%	80%	86%			89%			91%	92%
Phage1	HHBS18_1	HHBS47_1	HHBS47_1	**HHBS47_1**	HHBS47_1	HHBS47_1	HHBS47_1	HHBS47_1	HHBS47_1	HHBS47_1	HHBS47_1	HHBS47_1	HHBS47_1
Phage2	PTLAW1	PTLAW1	HHBS36_1	**HHBS8_1**	HHBS55_2	PTLAW1	HHBS36_1	JG004	HHBS36_1	HHBS36_1	JG004	HHBS36_1	HHBS36_1
Phage3		HHBS9_2	PTLAW1	**HHBS9_1**		HHBS55_2	HHBS55_2	HHBS55_2	PTLAW1	HHBS51_1	HHBS36_1	HHBS12_2	HHBS12_2
Phage4			HHBS9_2	**JG004**					HHBS55_2	HHBS55_2	HHBS55_2	HHBS51_1	HHBS51_1
Phage5				**HHBS36_1**								HHBS55_2	HHBS55_2
Phage6				**HHBS12_2**									HHBS10_2
Phage7				**HHBS29_1**									
Phage8				**HHBS14_1**									
Phage9				**BWKH3_L8_1**									
Phage10				HHBS55_2 or PTLAW1									
Phage11				HHBS9_2 or BWKH3_R8_1A									
Phage12				PTLAW1 or HHBS51_1									

*8 combinations of phages possible, only one combination shown. Core backbone of all 8 cocktail combination is displayed in **bold**.

10.3389/fcimb.2025.1597009

and with different MOIs, and quantitative measurements in a high throughput screening format. For most phage-host interactions, PKA is faster, it can detect possible lytic behavior after only a few hours. In addition, several phages can be tested simultaneously or in a combination of phages with antibiotics. However, it should be noted that the lysis behavior can also be caused by toxins, endolysins, tailocins etc. when using crude lysates and therefore purified lysates should be preferred and the results should be validated with those of the DPA (Kim et al., 2020). In the future it may also be possible to predict phage-host interaction *in silico*, as this has already been done for selected bacteria such as *Staphylococcus aureus* (Moller et al., 2021), *Escherichia coli* (Gaborieau et al., 2024) and *Klebsiella pneumoniae* (Boeckaerts et al., 2024). The prediction tools that are currently available, such as HostPhinder, DeepHost, do not yet differentiate between phage-host interaction in *P. aeruginosa* at the strain level (Villarroel et al., 2016; Ruohan et al., 2022). But regardless of whether DPA and PKA are used as PST, the more important comparison is with the *in vivo* data, so that we can understand which assay better mimics the situation in the patient. So far there is still little data available. In many studies, it would be helpful for the comparison of *P. aeruginosa* phages if both the phage name and the corresponding genus is mentioned.

There is a tendency for phage susceptibility in the classical host spectrum to correlate negatively with antibiotic resistance (Supplementary Figure 10). Despite repeated efforts, we were unable to find a matching phage for every clinical *P. aeruginosa* isolate with twelve of 37 known *P. aeruginosa* phage genera. Especially the wound isolates were less covered with the phage panel. To verify possible explanations like anti-phage defense mechanism of the bacteria, interacting prophages or missing receptors, the strains need to be sequenced (Makarova et al., 2020; Markwitz et al, 2022; Georjon and Bernheim, 2023). Since there are limitations regarding the selected phages and antibiotics, further experiments, including *in vitro* studies, need to be performed to verify the correlation.

Our ranking suggests that *Pakpunavirus*, *Pbunavirus*, *Pawinskivirus* and *Elvirus* (myoviruses) as well as *Litunavirus* and *Bruynoghevirus* (podoviruses) have great potential for an application in phage therapy because they lyse many strains and are easy to produce (Figure 7). In previous studies, these phage genera have often been used *in vitro* and *in vivo* in animals and humans against *P. aeruginosa* infections (Silva et al., 2022). In particular, various *Pbunavirus* such as Pa193, Pa204, Pb10, which are > 95% identical (coverage x identity) to PTLAW1, have already demonstrated their high potential for phage therapy against *P. aeruginosa* as single phages (Supplementary Figure 3) (Forti et al., 2018; Aslam et al., 2019; Alkalay-Oren et al., 2022; Shafigh Kheljan et al., 2023). These phages have also been used in phage cocktails. A metagenomic analysis in 2017 identified eight different phage genera in Pyo Bacteriophage™ (Georgia) against *P. aeruginosa*, which have many similarities with our phages (*Pakpunavirus, Pbunavirus, Phikzvirus, Nankokuvirus, Phikmvvirus* (myoviruses) and *Bruynoghevirus, Litunavirus, unclassified phage* (podoviruses)) (McCallin et al., 2018). For other phage cocktails, such as PP1131 (PhagoBurn) or BX004-A™ (BiomX, Israel), compositions have not yet been reported (Jault et al., 2019; Rappo et al., 2023). However, the use of different genera increases the likelihood that many strains/isolates can be treated (Figure 5). Not only do the host ranges of the individual phages often add up, there is also the chance of phage-phage synergy (PPS) (Schmerer et al., 2014). Whether synergistic or antagonistic effects exist for the best predicted cocktails with the specific phages would require further *in vitro* or biofilm analysis. In order to increase the overall coverage, phages with a narrow host range should also be included. Only a few siphoviruses have been used for therapy so far (Silva et al., 2022). We assume that this is due to their narrow host range (Figures 2F, G), and also due to the fact that the probability of finding lytic phages with the morphotype siphovirus is much lower, as the majority of *P. aeruginosa* prophages belong to the morphotype siphovirus (Johnson et al., 2022). However, this does not mean that no lytic siphoviruses are found (see 22043_B8_1 and HHBS29_1 (*Septimatrevirus*)).

In addition to safety and the suitable host spectrum, there are other factors that should be included in a ranking. Depending on the indication, efficacy against biofilms could also play a role in the selection. Among others the stability of the phages, which is often tested at different pH values and temperatures. Stability of the phages should be ensured regarding the various therapeutic indications (bladder, lungs, etc.). In addition, phages must be sequenced to exclude possible induced prophages from the host, as *P. aeruginosa* usually has more than one prophage (Johnson et al., 2022). Furthermore, combinations with other phages or antibiotics should be considered for therapy (Nikolic et al., 2022). Phage-antibiotic-antagonism (Gu Liu et al., 2020; Danis-Wlodarczyk et al., 2021a) and phage-phage antagonism should be avoided (Schmerer et al., 2014). At the same time, it should be tested whether phages of the same genus should be used together, as they probably have similar receptors (Pleteneva et al., 2008). In the best case the phages would be selected and combined in a way that it would make it difficult for the bacteria to adapt via the receptor or defense systems.

5 Conclusion

25 *P. aeruginosa* phages were characterized and compared showning a great diversity within all morphotypes. A combination of six phages could theoretically lyse 92% of clinical *P. aeruginosa* strains. Further, we showed that especially *Pakpunavirus*, *Pbunavirus, Pawinskivirus, Elvirus* (all myoviruses), *Litunavirus* and *Bruynoghevirus* (all podoviruses) showed the greatest potential in the proposed ranking and should be employed with priority, as they have already been used for phage therapy. Siphoviruses were less suitable. Phages with a lysogenic cycle also have less potential due to their narrow host range and efficiency (low vp value), as well as safety concerns regarding phage therapy.

We also compared the classic DPA (0.5% top agar) with the liquid PKA (MOI 0.1). Both methods are easy to perform but offer different limitations depending on the phage. Host analysis using DPA did not detect phages that form very small plaques, while PKA could not clearly state whether lysis by some siphoviruses and temperate phages was caused by phage activity. Overall, we suggest that PKA is the better method for phage susceptibly prediction because it is usually faster and less prone to individual interpretation. However, both methods should also be compared with *in vivo* data from patients in the future.

Data availability statement

The datasets presented in this study can be found in online repositories. The names of the repository/repositories and accession number(s) can be found in the article/Supplementary Material.

Author contributions

FR: Conceptualization, Data curation, Formal Analysis, Investigation, Validation, Visualization, Writing – original draft, Writing – review & editing. JW: Data curation, Investigation, Writing – review & editing. BB: Investigation, Writing – review & editing. CS: Investigation, Writing – review & editing. MH: Resources, Writing – review & editing. CW: Resources, Writing – review & editing. MM: Investigation, Writing – review & editing. HZ: Funding acquisition, Supervision, Writing – review & editing. IK: Conceptualization, Data curation, Funding acquisition, Investigation, Project administration, Supervision, Validation, Writing – original draft, Writing – review & editing. DJ: Conceptualization, Funding acquisition, Supervision, Writing – original draft, Writing – review & editing.

Funding

The author(s) declare that financial support was received for the research and/or publication of this article. This work received funding from "Gemeinsamer Bundesausschuss, Innovationsausschuss, Germany" under the grant "PTmHBP", 01VSF18049 (to IK between 2019 and 2021, to MH between 2019 and 2024).

Acknowledgments

Authors thank Laura Wicke for isolating the phage PTLAW1, Ella Siegel for helping with the PKA - host spectrum and Stephanie Peter and Simone Schrader for generating phage libraries. Special thanks also go to Ina Brentop for EM sample preparation.

Conflict of interest

Author BB, CS alnd JW was employed by Leibniz Institute DSMZ, which is an independent, non-profit research infrastructure.

The remaining authors declare that the research was conducted in the absence of any commercial or financial relationships that could be construed as a potential conflict of interest.

Generative AI statement

The author(s) declare that Generative AI was used in the creation of this manuscript. Deepl and ChatGPT were used to revise the text.

Correction note

A correction has been made to this article. Details can be found at: 10.3389/fcimb.2025.1650832.

Publisher's note

All claims expressed in this article are solely those of the authors and do not necessarily represent those of their affiliated organizations, or those of the publisher, the editors and the reviewers. Any product that may be evaluated in this article, or claim that may be made by its manufacturer, is not guaranteed or endorsed by the publisher.

Supplementary material

The Supplementary Material for this article can be found online at: https://www.frontiersin.org/articles/10.3389/fcimb.2025.1597009/full#supplementary-material

References

Abedon, S. T. (2020). *Phage Cocktail Optimizer*. https://www.phage-therapy.org/calculators/cocktail_optimizer.html (Accessed July 5, 2024).

Abedon, S. T., and Culler, R. R. (2007). Bacteriophage evolution given spatial constraint. *J. Theor. Biol.* 248, 111–119. doi: 10.1016/j.jtbi.2007.02.014

Ackermann, H. W. (2011). Bacteriophage taxonomy. *Microbiol. Aust.* 32, 90–94. doi: 10.1071/MA11090

Ackermann, H. W., and Eisenstark, A. (1974). The present state of phage taxonomy. *Intervirology* 3, 201–219. doi: 10.1159/000149758

Aghaee, B. L., Mirzaei, M. K., Alikhani, M. Y., and Mojtahedi, A. (2021). Sewage and sewage-contaminated environments are the most prominent sources to isolate phages against Pseudomonas aeruginosa. *BMC Microbiol.* 21, 132. doi: 10.1186/s12866-021-02197-z

Alipour-Khezri, E., Skurnik, M., and Zarrini, G. (2024). Pseudomonas aeruginosa bacteriophages and their clinical applications. *Viruses* 16, 1051. doi: 10.3390/v16071051

Alkalay-Oren, S., Yerushalmy, O., Adler, K., Khalifa, L., Gelman, D., Coppenhagen-Glazer, S., et al. (2022). Complete genome sequence of Pseudomonas aeruginosa bacteriophage PASA16, used in multiple phage therapy treatments globally. *Microbiol. Resour Announc* 11, e0009222. doi: 10.1128/mra.00092-22

Aloush, V., Navon-Venezia, S., Seigman-Igra, Y., Cabili, S., and Carmeli, Y. (2006). Multidrug-resistant Pseudomonas aeruginosa: risk factors and clinical impact. *Antimicrob. Agents Chemother.* 50, 43–48. doi: 10.1128/aac.50.1.43-48.2006

Altschul, S. F., Madden, T. L., Schäffer, A. A., Zhang, J., Zhang, Z., Miller, W., et al. (1997). Gapped BLAST and PSI-BLAST: a new generation of protein database search programs. *Nucleic Acids Res.* 25, 3389–3402. doi: 10.1093/nar/25.17.3389

Amgarten, D., Martins, L. F., Lombardi, K. C., Antunes, L. P., de Souza, A. P. S., Nicastro, G. G., et al. (2017). Three novel Pseudomonas phages isolated from composting provide insights into the evolution and diversity of tailed phages. *BMC Genomics* 18, 346. doi: 10.1186/s12864-017-3729-z

Arumugam, S. N., Manohar, P., Sukumaran, S., Sadagopan, S., Loh, B., Leptihn, S., et al. (2022). Antibacterial efficacy of lytic phages against multidrug-resistant Pseudomonas aeruginosa infections in bacteraemia mice models. *BMC Microbiol.* 22, 187. doi: 10.1186/s12866-022-02603-0

Aslam, S., Courtwright, A. M., Koval, C., Lehman, S. M., Morales, S., Furr, C.-L. L., et al. (2019). Early clinical experience of bacteriophage therapy in 3 lung transplant recipients. *Am. J. Transplant.* 19, 2631–2639. doi: 10.1111/ajt.15503

Azam, M. W., and Khan, A. U. (2019). Updates on the pathogenicity status of Pseudomonas aeruginosa. *Drug Discovery Today* 24, 350–359. doi: 10.1016/j.drudis.2018.07.003

Bassetti, M., Vena, A., Croxatto, A., Righi, E., and Guery, B. (2018). How to manage Pseudomonas aeruginosa infections. *Drugs Context* 7, 212527. doi: 10.7573/dic.212527

Boeckaerts, D., Stock, M., Ferriol-González, C., Oteo-Iglesias, J., Sanjuán, R., Domingo-Calap, P., et al. (2024). Prediction of Klebsiella phage-host specificity at the strain level. *Nat. Commun.* 15, 4355. doi: 10.1038/s41467-024-48675-6

Carballo-Ontiveros, M. A., Cazares, A., Vinuesa, P., Kameyama, L., and Guarneros, G. (2020). The Concerted Action of Two B3-Like Prophage Genes Excludes Superinfecting Bacteriophages by Blocking DNA Entry into Pseudomonas aeruginosa. *J. Virol.* 94, e00953-20. doi: 10.1128/jvi.00953-20

Chanishvili, N. (2012). Phage therapy–history from Twort and d'Herelle through Soviet experience to current approaches. *Adv. Virus Res.* 83, 3–40. doi: 10.1016/B978-0-12-394438-2.00001-3

Chanishvili, N., Myelnikov, D., and Blauvelt, T. K. (2022). Professor Giorgi eliava and the eliava institute of bacteriophage. *PHAGE* 3, 71–80. doi: 10.1089/phage.2022.0016

Cheng, K. H., Leung, S. L., Hoekman, H. W., Beekhuis, W. H., Mulder, P. G., Geerards, A. J., et al. (1999). Incidence of contact-lens-associated microbial keratitis and its related morbidity. *Lancet* 354, 181–185. doi: 10.1016/S0140-6736(98)09385-4

Danis-Wlodarczyk, K., Cai, A., Chen, A., Gittrich, M. R., Sullivan, M. B., Wozniak, D. J., et al. (2021a). Friends or foes? Rapid determination of dissimilar colistin and ciprofloxacin antagonism of Pseudomonas aeruginosa phages. *Pharmaceuticals* 14, 1162. doi: 10.3390/ph14111162

Danis-Wlodarczyk, K., Dąbrowska, K., and Abedon, S. T. (2021b). Phage therapy: the pharmacology of antibacterial viruses. *Curr. Issues Mol. Biol.* 40, 81–164. doi: 10.21775/cimb.040.081

Debarbieux, L., Leduc, D., Maura, D., Morello, E., Criscuolo, A., Grossi, O., et al. (2010). Bacteriophages can treat and prevent Pseudomonas aeruginosa lung infections. *J. Infect. Dis.* 201, 1096–1104. doi: 10.1086/651135

European Committee on Antimicrobial Susceptibility Testing (2022). *Breakpoint tables for interpretation of MICs and zone diameters: Version 12.0.* Available online at: http://www.eucast.org (Accessed July 10, 2023).

Feldgarden, M., Brover, V., Gonzalez-Escalona, N., Frye, J. G., Haendiges, J., Haft, D. H., et al. (2021). AMRFinderPlus and the Reference Gene Catalog facilitate examination of the genomic links among antimicrobial resistance, stress response, and virulence. *Sci. Rep.* 11, 12728. doi: 10.1038/s41598-021-91456-0

Ferry, T., Kolenda, C., Batailler, C., Gaillard, R., Gustave, C.-A., Lustig, S., et al. (2021). Case report: arthroscopic "Debridement antibiotics and implant retention" With local injection of personalized phage therapy to salvage a relapsing Pseudomonas aeruginosa prosthetic knee infection. *Front. Med.* 8. doi: 10.3389/fmed.2021.569159

Forti, F., Roach, D. R., Cafora, M., Pasini, M. E., Horner, D. S., Fiscarelli, E. V., et al. (2018). Design of a broad-range bacteriophage cocktail that reduces Pseudomonas aeruginosa biofilms and treats acute infections in two animal models. *Antimicrob. Agents Chemother.* 62, e02573-17. doi: 10.1128/aac.02573-17

Gaborieau, B., Vaysset, H., Tesson, F., Charachon, I., Dib, N., Bernier, J., et al. (2024). Prediction of strain level phage-host interactions across the Escherichia genus using only genomic information. *Nat. Microbiol.* 9, 2847–2861. doi: 10.1038/s41564-024-01832-5

Garbe, J., Bunk, B., Rohde, M., and Schobert, M. (2011). Sequencing and characterization of Pseudomonas aeruginosa phage JG004. *BMC Microbiol.* 11, 102. doi: 10.1186/1471-2180-11-102

Georjon, H., and Bernheim, A. (2023). The highly diverse antiphage defence systems of bacteria. *Nat. Rev. Microbiol.* 21, 686–700. doi: 10.1038/s41579-023-00934-x

Gu Liu, C., Green, S. I., Min, L., Clark, J. R., Salazar, K. C., Terwilliger, A. L., et al. (2020). Phage-antibiotic synergy is driven by a unique combination of antibacterial mechanism of action and stoichiometry. *mBio* 11, e01462-20. doi: 10.1128/mBio.01462-20

Haines, M. E. K., Hodges, F. E., Nale, J. Y., Mahony, J., van Sinderen, D., Kaczorowska, J., et al. (2021). Analysis of selection methods to develop novel phage therapy cocktails against antimicrobial resistant clinical isolates of bacteria. *Front. Microbiol.* 12. doi: 10.3389/fmicb.2021.613529

Hamed, M. M., Abdelsamie, A. S., Rox, K., Schütz, C., Kany, A. M., Röhrig, T., et al. (2023). Towards translation of PqsR inverse agonists: from *in vitro* efficacy optimization to *in vivo* proof-of-principle. *Advanced Sci.* 10, e2204443. doi: 10.1002/advs.202204443

Hashemi Shahraki, A., Vahed, M., Masood, S., and Mirsaeidi, M. (2023). Complete genome sequence of Pseudomonas aeruginosa phage UF_RH6, isolated from human lung. *Microbiol. Resour Announc* 12, e0020623. doi: 10.1128/mra.00206-23

Hatcher, E. L., Zhdanov, S. A., Bao, Y., Blinkova, O., Nawrocki, E. P., Ostapchuck, Y., et al. (2017). Virus Variation Resource - improved response to emergent viral outbreaks. *Nucleic Acids Res.* 45, D482–D490. doi: 10.1093/nar/gkw1065

Hilliam, Y., Kaye, S., and Winstanley, C. (2020). *Pseudomonas aeruginosa* and microbial keratitis. *J. Med. Microbiol.* 69, 3–13. doi: 10.1099/jmm.0.001110

Horcajada, J. P., Montero, M., Oliver, A., Sorlí, L., Luque, S., Gómez-Zorrilla, S., et al. (2019). Epidemiology and treatment of multidrug-resistant and extensively drug-resistant Pseudomonas aeruginosa infections. *Clin. Microbiol. Rev.* 32, e00031-19. doi: 10.1128/CMR.00031-19

International Committee of Taxonomy of Viruses (2023). *International Committee of Taxonomy of Viruses: Current Taxonomy Release*. Available online at: https://ictv.global/taxonomy (Accessed June 22, 2023).

Jault, P., Leclerc, T., Jennes, S., Pirnay, J. P., Que, Y.-A., Resch, G., et al. (2019). Efficacy and tolerability of a cocktail of bacteriophages to treat burn wounds infected by Pseudomonas aeruginosa (PhagoBurn): a randomised, controlled, double-blind phase 1/2 trial. *Lancet Infect. Dis.* 19, 35–45. doi: 10.1016/S1473-3099(18)30482-1

Johnson, G., Banerjee, S., and Putonti, C. (2022). Diversity of Pseudomonas aeruginosa temperate phages. *mSphere* 7, e0101521. doi: 10.1128/msphere.01015-21

Kim, S., Lee, D.-W., Jin, J.-S., and Kim, J. (2020). Antimicrobial activity of LysSS, a novel phage endolysin, against Acinetobacter baumannii and Pseudomonas aeruginosa. *J. Glob Antimicrob. Resist.* 22, 32–39. doi: 10.1016/j.jgar.2020.01.005

Korf, I. H. E., Meier-Kolthoff, J. P., Adriaenssens, E. M., Kropinski, A. M., Nimtz, M., Rohde, M., et al. (2019). Still Something to Discover: Novel Insights into Escherichia coli Phage Diversity and Taxonomy. *Viruses* 11, 454. doi: 10.3390/v11050454

KRINKO (2019). Ergänzung zur Empfehlung der KRINKO „Hygienemaßnahmen bei Infektionen oder Besiedlung mit multiresistenten gramnegativen Stäbchen" (2012) im Zusammenhang mit der von EUCAST neu definierten Kategorie „I" bei der Antibiotikaresistenzbestimmung: Konsequenzen für die Definition von MRGN. *Epid Bull* 9, 82–83. doi: 10.25646/5916

Kropinski, A. M., Mazzocco, A., Waddell, T. E., Lingohr, E., and Johnson, R. P. (2009). Enumeration of bacteriophages by double agar overlay plaque assay. *Methods Mol. Biol.* 501, 69–76. doi: 10.1007/978-1-60327-164-6_7

La Rosa-Carrillo, D., Suárez-Cuartín, G., Golpe, R., Máiz Carro, L., and Martinez-Garcia, M. A. (2022). Inhaled colistimethate sodium in the management of patients with bronchiectasis infected by Pseudomonas aeruginosa: A narrative review of current evidence. *Infect. Drug Resist.* 15, 7271–7292. doi: 10.2147/IDR.S318173

Lecoutere, E., Ceyssens, P.-J., Miroshnikov, K. A., Mesyanzhinov, V. V., Krylov, V. N., Noben, J.-P., et al. (2009). Identification and comparative analysis of the structural proteomes of phiKZ and EL, two giant Pseudomonas aeruginosa bacteriophages. *Proteomics* 9, 3215–3219. doi: 10.1002/pmic.200800727

Letunic, I., and Bork, P. (2024). Interactive Tree of Life (iTOL) v6: recent updates to the phylogenetic tree display and annotation tool. *Nucleic Acids Res.* 52 (W1), W78–W82. doi: 10.1093/nar/gkae268

Liu, B., Zheng, D., Zhou, S., Chen, L., and Yang, J. (2022). VFDB 2022: a general classification scheme for bacterial virulence factors. *Nucleic Acids Res.* 50, D912–D917. doi: 10.1093/nar/gkab1107

Mabrouk, S. S., Abdellatif, G. R., Abu Zaid, A. S., Aziz, R. K., and Aboshanab, K. M. (2022). *In Vitro* and Pre-Clinical Evaluation of Locally Isolated Phages, vB_Pae_SMP1 and vB_Pae_SMP5, Formulated as Hydrogels against Carbapenem-Resistant Pseudomonas aeruginosa. *Viruses* 14, 2760. doi: 10.3390/v14122760

Makarova, K. S., Wolf, Y. I., Iranzo, J., Shmakov, S. A., Alkhnbashi, O. S., Brouns, S. J. J., et al. (2020). Evolutionary classification of CRISPR-Cas systems: a burst of class 2 and derived variants. *Nat. Rev. Microbiol.* 18, 67–83. doi: 10.1038/s41579-019-0299-x

Markwitz, P., Lood, C., Olszak, T., van Noort, V., Lavigne, R., and Drulis-Kawa, Z. (2021). Genome-driven elucidation of phage-host interplay and impact of phage resistance evolution on bacterial fitness. *ISME J.* 16, 533–542. doi: 10.1038/s41396-021-01096-5

Mathee, K. (2018). Forensic investigation into the origin of Pseudomonas aeruginosa PA14 - old but not lost. *J. Med. Microbiol.* 67, 1019–1021. doi: 10.1099/jmm.0.000778

McCallin, S., Sarker, S. A., Sultana, S., Oechslin, F., and Brüssow, H. (2018). Metagenome analysis of Russian and Georgian Pyophage cocktails and a placebo-controlled safety trial of single phage versus phage cocktail in healthy Staphylococcus aureus carriers. *Environ. Microbiol.* 20, 3278–3293. doi: 10.1111/1462-2920.14310

Meier-Kolthoff, J. P., and Göker, M. (2017). VICTOR: genome-based phylogeny and classification of prokaryotic viruses. *Bioinformatics* 33, 3396–3404. doi: 10.1093/bioinformatics/btx440

Miller, W. R., and Arias, C. A. (2024). ESKAPE pathogens: antimicrobial resistance, epidemiology, clinical impact and therapeutics. *Nat. Rev. Microbiol.* 22, 598–616. doi: 10.1038/s41579-024-01054-w

Moller, A. G., Winston, K., Ji, S., Wang, J., Hargita Davis, M. N., Solís-Lemus, C. R., et al. (2021). Genes influencing phage host range in Staphylococcus aureus on a species-wide scale. *mSphere* 6, e01263-20. doi: 10.1128/msphere.01263-20

Mushegian, A. R. (2020). Are there 1031 virus particles on earth, or more, or fewer? *J. Bacteriol* 202, e00052-20. doi: 10.1128/jb.00052-20

Nazarov, P. A. (2022). MDR pumps as crossroads of resistance: antibiotics and bacteriophages. *Antibiotics* 11, 734. doi: 10.3390/antibiotics11060734

NCBI Virus (2023). (Accessed June 29, 2023).

Nikolic, I., Vukovic, D., Gavric, D., Cvetanovic, J., Aleksic Sabo, V., Gostimirovic, S., et al. (2022). An optimized checkerboard method for phage-antibiotic synergy detection. *Viruses* 14, 1542. doi: 10.3390/v14071542

Onallah, H., Hazan, R., Nir-Paz, R., Brownstein, M. J., Fackler, J. R., Horne, B., et al. (2023). Refractory Pseudomonas aeruginosa infections treated with phage PASA16: A compassionate use case series. *Med* 4, 600–611.e4. doi: 10.1016/j.medj.2023.07.002

Parfitt, T. (2005). Georgia: an unlikely stronghold for bacteriophage therapy. *Lancet* 365, 2166–2167. doi: 10.1016/S0140-6736(05)66759-1

Parmar, K., Komarow, L., Ellison, D. W., Filippov, A. A., Nikolich, M. P., Fackler, J. R., et al. (2023). Interlaboratory comparison of Pseudomonas aeruginosa phage susceptibility testing. *J. Clin. Microbiol.* 61, e0061423. doi: 10.1128/jcm.00614-23

Payne, R. J., Phil, D., and Jansen, V. A. (2000). Phage therapy: the peculiar kinetics of self-replicating pharmaceuticals. *Clin. Pharmacol. Ther.* 68, 225–230. doi: 10.1067/mcp.2000.109520

Peters, D. L., Davis, C. M., Harris, G., Zhou, H., Rather, P. N., Hrapovic, S., et al. (2023). Characterization of virulent T4-like Acinetobacter baumannii bacteriophages DLP1 and DLP2. *Viruses* 15. doi: 10.3390/v15030739

Pires, D. P., Vilas Boas, D., Sillankorva, S., and Azeredo, J. (2015). Phage therapy: a step forward in the treatment of pseudomonas aeruginosa infections. *J. Virol.* 89, 7449–7456. doi: 10.1128/JVI.00385-15

Pirnay, J.-P., Djebara, S., Steurs, G., Griselain, J., Cochez, C., Soir, S., et al. (2024). Personalized bacteriophage therapy outcomes for 100 consecutive cases: a multicentre, multinational, retrospective observational study. *Nat. Microbiol.* 9, 1434–1453. doi: 10.1038/s41564-024-01705-x

Pirnay, J.-P., and Verbeken, G. (2023). Magistral phage preparations: is this the model for everyone? *Clin. Infect. Dis.* 77, S360–S369. doi: 10.1093/cid/ciad481

Pleteneva, E. A., Shaburova, O. V., Sykilinda, N. N., Miroshnikov, K. A., Kadykov, V. A., Krylov, S. V., et al. (2008). Study of the diversity in a group of phages of Pseudomonas aeruginosa species PB1 (*Myoviridae*) and their behavior in adsorbtion-resistant bacterial mutants. *Russ J Genet.* 44, 150–158. doi: 10.1134/S1022795408020051

Poggio, E. C., Glynn, R. J., Schein, O. D., Seddon, J. M., Shannon, M. J., Scardino, V. A., et al. (1989). The incidence of ulcerative keratitis among users of daily-wear and extended-wear soft contact lenses. *N Engl. J. Med.* 321, 779–783. doi: 10.1056/NEJM198909213211202

Prevaldi, C., Paolillo, C., Locatelli, C., Ricci, G., Catena, F., Ansaloni, L., et al. (2016). Management of traumatic wounds in the Emergency Department: position paper from the Academy of Emergency Medicine and Care (AcEMC) and the World Society of Emergency Surgery (WSES). *World J. Emerg. Surg.* 11, 30. doi: 10.1186/s13017-016-0084-3

Pye, H. V., Krishnamurthi, R., Cook, R., and Adriaenssens, E. M. (2024). Phage diversity in one health. *Essays Biochem.* 68, 607–619. doi: 10.1042/EBC20240012

Qin, S., Xiao, W., Zhou, C., Pu, Q., Deng, X., Lan, L., et al. (2022). Pseudomonas aeruginosa: pathogenesis, virulence factors, antibiotic resistance, interaction with host, technology advances and emerging therapeutics. *Signal Transduct Target Ther.* 7, 199. doi: 10.1038/s41392-022-01056-1

Rahme, L. G., Stevens, E. J., Wolfort, S. F., Shao, J., Tompkins, R. G., and Ausubel, F. M. (1995). Common virulence factors for bacterial pathogenicity in plants and animals. *Science* 268, 1899–1902. doi: 10.1126/science.7604262

Rappo, U., Cohen, A., Kario, E., Gold, J., Nevenzal, H. T., Levy-Saar, I., et al. (2023). 2891. Nebulized phage therapy for patients with cystic fibrosis with chronic Pseudomonas aeruginosa pulmonary infection: A phase 1b/2a randomized, double-blind, placebo-controlled, multicenter study. *Open Forum Infect. Dis.* 10, ofad500.2474. doi: 10.1093/ofid/ofad500.2474

Rose, T., Verbeken, G., Vos, D., Merabishvili, M., Vaneechoutte, M., Lavigne, R., et al. (2014). Experimental phage therapy of burn wound infection: difficult first steps. *Int. J. Burns Trauma* 4, 66–73.

Ruohan, W., Xianglilan, Z., Jianping, W., and Shuai Cheng, L. I. (2022). DeepHost: phage host prediction with convolutional neural network. *Brief Bioinform.* 23, bbab385. doi: 10.1093/bib/bbab385

Schein, O. D., Glynn, R. J., Poggio, E. C., Seddon, J. M., and Kenyon, K. R. (1989). The relative risk of ulcerative keratitis among users of daily-wear and extended-wear soft contact lenses. A case-control study. Microbial Keratitis Study Group. *N Engl. J. Med.* 321, 773–778. doi: 10.1056/NEJM198909213211201

Schmerer, M., Molineux, I. J., and Bull, J. J. (2014). Synergy as a rationale for phage therapy using phage cocktails. *PeerJ* 2, e590. doi: 10.7717/peerj.590

Sepúlveda-Robles, O., Kameyama, L., and Guarneros, G. (2012). High diversity and novel species of Pseudomonas aeruginosa bacteriophages. *Appl. Environ. Microbiol.* 78, 4510–4515. doi: 10.1128/AEM.00065-12

Serra, R., Grande, R., Butrico, L., Rossi, A., Settimio, U. F., Caroleo, B., et al. (2015). Chronic wound infections: the role of Pseudomonas aeruginosa and Staphylococcus aureus. *Expert Rev. Anti Infect. Ther.* 13, 605–613. doi: 10.1586/14787210.2015.1023291

Serwer, P., Hayes, S. J., Thomas, J. A., and Hardies, S. C. (2007). Propagating the missing bacteriophages: a large bacteriophage in a new class. *Virol. J.* 4, 21. doi: 10.1186/1743-422X-4-21

Shafigh Kheljan, F., Sheikhzadeh Hesari, F., Aminifazl, M. S., Skurnik, M., Gholadze, S., and Zarrini, G. (2023). Design of phage-cocktail-containing hydrogel for the treatment of Pseudomonas aeruginosa-infected wounds. *Viruses* 15, 803. doi: 10.3390/v15030803

Shi, X., Zhao, F., Sun, H., Yu, X., Zhang, C., Liu, W., et al. (2020). Characterization and Complete Genome Analysis of Pseudomonas aeruginosa Bacteriophage vB_PaeP_LP14 Belonging to Genus Litunavirus. *Curr. Microbiol.* 77, 2465–2474. doi: 10.1007/s00284-020-02011-5

Silva, C., Sá, S., Guedes, C., Oliveira, C., Lima, C., Oliveira, M., et al. (2022). The history and applications of phage therapy in Pseudomonas aeruginosa. *Microbiol. Res.* 13, 14–37. doi: 10.3390/microbiolres13010002

Skusa, R., Kohlen, J., Podbielski, A., and Warnke, P. (2023). Introducing "Rapid phage susceptibility testing" (RPST): an accelerated lytic phage activity test for routine diagnostic laboratories within eight hours. *Diagn. Microbiol. Infect. Dis.* 107, 116054. doi: 10.1016/j.diagmicrobio.2023.116054

Staudinger, B. J., Muller, J. F., Halldórsson, S., Boles, B., Angermeyer, A., Nguyen, D., et al. (2014). Conditions associated with the cystic fibrosis defect promote chronic Pseudomonas aeruginosa infection. *Am. J. Respir. Crit. Care Med.* 189, 812–824. doi: 10.1164/rccm.201312-2142OC

Steffan, S. M., Shakeri, G., Kehrenberg, C., Peh, E., Rohde, M., Plötz, M., et al. (2022). Campylobacter bacteriophage cocktail design based on an advanced selection scheme. *Antibiotics* 11, 228. doi: 10.3390/antibiotics11020228

Storms, Z. J., Teel, M. R., Mercurio, K., and Sauvageau, D. (2020). The virulence index: A metric for quantitative analysis of phage virulence. *PHAGE* 1, 27–36. doi: 10.1089/phage.2019.0001

Stover, C. K., Pham, X. Q., Erwin, A. L., Mizoguchi, S. D., Warrener, P., Hickey, M. J., et al. (2000). Complete genome sequence of Pseudomonas aeruginosa PAO1, an opportunistic pathogen. *Nature* 406, 959–964. doi: 10.1038/35023079

Tielen, P., Narten, M., Rosin, N., Biegler, I., Haddad, I., Hogardt, M., et al. (2011). Genotypic and phenotypic characterization of Pseudomonas aeruginosa isolates from urinary tract infections. *Int. J. Med. Microbiol.* 301, 282–292. doi: 10.1016/j.ijmm.2010.10.005

Tielen, P., Wibberg, D., Blom, J., Rosin, N., Meyer, A.-K., Bunk, B., et al. (2014). Genome sequence of the small-colony variant Pseudomonas aeruginosa MH27, isolated from a chronic urethral catheter infection. *Genome Announc* 2, e01174-13. doi: 10.1128/genomeA.01174-13

Turner, D., Kropinski, A. M., and Adriaenssens, E. M. (2021). A roadmap for genome-based phage taxonomy. *Viruses* 13, 506. doi: 10.3390/v13030506

Villarroel, J., Kleinheinz, K. A., Jurtz, V. I., Zschach, H., Lund, O., Nielsen, M., et al. (2016). HostPhinder: A phage host prediction tool. *Viruses* 8, 116. doi: 10.3390/v8050116

Waters, E. M., Neill, D. R., Kaman, B., Sahota, J. S., Clokie, M. R. J., Winstanley, C., et al. (2017). Phage therapy is highly effective against chronic lung infections with Pseudomonas aeruginosa. *Thorax* 72, 666–667. doi: 10.1136/thoraxjnl-2016-209265

Willy, C., Bugert, J. J., Classen, A. Y., Deng, L., Düchting, A., Gross, J., et al. (2023). Phage therapy in Germany-update 2023. *Viruses* 15, 588. doi: 10.3390/v15020588

World Health Organization (2024). *World Health Organization: Bacterial Priority Pathogens List 2024 Bacterial Pathogens of Public Health Importance, to Guide Research, Development, and Strategies to Prevent and Control Antimicrobial Resistance* (Geneva: World Health Organization).

Yerushalmy, O., Braunstein, R., Alkalay-Oren, S., Rimon, A., Coppenhagn-Glazer, S., Onallah, H., et al. (2023). Towards standardization of phage susceptibility testing: the Israeli phage therapy center "Clinical phage microbiology"-A pipeline proposal. *Clin. Infect. Dis.* 77, S337–S351. doi: 10.1093/cid/ciad514

Yuan, Y., and Gao, M. (2017). Jumbo bacteriophages: an overview. *Front. Microbiol.* 8. doi: 10.3389/fmicb.2017.00403

frontiers | Frontiers in Cellular and Infection Microbiology

TYPE Correction
PUBLISHED 20 August 2025
DOI 10.3389/fcimb.2025.1650832

OPEN ACCESS

APPROVED BY
Frontiers Editorial Office,
Frontiers Media SA, Switzerland

*CORRESPONDENCE
Imke H.E. Korf
imke.korf@item.fraunhofer.de
Dieter Jahn
d.jahn@tu-bs.de

†These authors have contributed equally to this work and share last authorship

RECEIVED 20 June 2025
ACCEPTED 11 July 2025
PUBLISHED 20 August 2025

CITATION
Rieper F, Wittmann J, Bunk B, Spröer C, Häfner M, Willy C, Müsken M, Ziehr H, Korf IHE and Jahn D (2025) Correction: Systematic bacteriophage selection for the lysis of multiple *Pseudomonas aeruginosa* strains. *Front. Cell. Infect. Microbiol.* 15:1650832. doi: 10.3389/fcimb.2025.1650832

Correction: Systematic bacteriophage selection for the lysis of multiple *Pseudomonas aeruginosa* strains

Finja Rieper[1,2], Johannes Wittmann[3], Boyke Bunk[3], Cathrin Spröer[3], Melanie Häfner[4], Christian Willy[4], Mathias Müsken[5], Holger Ziehr[1], Imke H.E. Korf[1*†] and Dieter Jahn[2,6*†]

[1]Pharmaceutical Biotechnology, Fraunhofer Institute for Toxicology and Experimental Medicine (ITEM), Braunschweig, Germany, [2]Institute of Microbiology, Braunschweig University of Technology, Braunschweig, Germany, [3]Leibniz Institute DSMZ-German Collection of Microorganisms and Cell Cultures GmbH (DSMZ), Braunschweig, Germany, [4]Department Trauma & Orthopedic Surgery, Septic & Reconstructive Surgery, Research and Treatment Center Septic Defect Wounds, Federal Armed Forces of Germany, Military Academic Hospital Berlin, Berlin, Germany, [5]Central Facility for Microscopy, Helmholtz Centre for Infection Research (HZI), Braunschweig, Germany, [6]Institute of Microbiology, Braunschweig Center of Systems Biology (BRICS), Braunschweig, Germany

KEYWORDS

bacteriophages, *Pseudomonas aeruginosa*, phage susceptibility testing, antibiotic resistance, phage selection

A Correction on

Systematic bacteriophage selection for the lysis of multiple Pseudomonas aeruginosa strains

By Rieper F, Wittmann J, Bunk B, Spröer C, Häfner M, Willy C, Müsken M, Ziehr H, Korf IHE and Jahn D (2025) *Front. Cell. Infect. Microbiol.* 15:1597009. doi: 10.3389/fcimb.2025.1597009

The **Conflict of interest statement** was erroneously given as "Author XY was employed by Leibniz Institute DSMZ, which is an independent, non-profit research infrastructure.

All authors declare that the research was conducted in the absence of any commercial or financial relationships that could be construed as a potential conflict of interest."

The correct **Conflict of interest statement** is "Author BB, CS alnd JW was employed by Leibniz Institute DSMZ, which is an independent, non-profit research infrastructure.

The remaining authors declare that the research was conducted in the absence of any commercial or financial relationships that could be construed as a potential conflict of interest."

The original version of this article has been updated.

In the published article, there was a mistake in the numbers of isolated phages. The number of myoviruses was given as "13" and the number of podoviruses as "eight".

A correction has been made to the section 3.2 Phage morphology, Line 284:285:

"Using transmission electron microscopy (TEM), the 25 phages were classified as twelve myoviruses including three jumbo phages, four siphoviruses and nine podoviruses (Figure 1)".

The original version of this article has been updated.

Conflict of interest

Author BB, CS alnd JW was employed by Leibniz Institute DSMZ, which is an independent, non-profit research infrastructure.

The remaining authors declare that the research was conducted in the absence of any commercial or financial relationships that could be construed as a potential conflict of interest.

Publisher's note

frontiers | Frontiers in Cellular and Infection Microbiology

TYPE Perspective
PUBLISHED 27 May 2025
DOI 10.3389/fcimb.2025.1611857

OPEN ACCESS

EDITED BY
Mercedes Gonzalez Moreno,
Leibniz Institute for Natural Product Research and Infection Biology, Hans Knoll Institute, Germany

REVIEWED BY
Robert Ramirez-Garcia,
Imperial College London, United Kingdom

*CORRESPONDENCE
Steffanie A. Strathdee
sstrathdee@health.ucsd.edu

RECEIVED 14 April 2025
ACCEPTED 30 April 2025
PUBLISHED 27 May 2025

CITATION
Doud MB, Robertson JM and Strathdee SA (2025) Optimizing phage therapy with artificial intelligence: a perspective. *Front. Cell. Infect. Microbiol.* 15:1611857. doi: 10.3389/fcimb.2025.1611857

Optimizing phage therapy with artificial intelligence: a perspective

Michael B. Doud[1], Jacob M. Robertson[2] and Steffanie A. Strathdee[1*]

[1]Division of Infectious Diseases and Global Public Health, Department of Medicine, University of California, San Diego, San Diego, CA, United States, [2]Department of Ecology, Behavior & Evolution, School of Biological Sciences, University of California, San Diego, La Jolla, CA, United States

Phage therapy is emerging as a promising strategy against the growing threat of antimicrobial resistance, yet phage and bacteria are incredibly diverse and idiosyncratic in their interactions with one another. Clinical applications of phage therapy often rely on a process of manually screening collections of naturally occurring phages for activity against a specific clinical isolate of bacteria, a labor-intensive task that is not guaranteed to yield a phage with optimal activity against a particular isolate. Herein, we review recent advances in artificial intelligence (AI) approaches that are advancing the study of phage-host interactions in ways that might enable the design of more effective phage therapeutics. In light of concurrent advances in synthetic biology enabling rapid genetic manipulation of phages, we envision how these AI-derived insights could inform the genetic optimization of the next generation of synthetic phages.

KEYWORDS

phage therapy, artificial intelligence, phage specificity, gene discovery, phage engineering, machine learning, synthetic biology

Introduction

The nascent fields of phage therapy, synthetic biology and artificial intelligence (AI) are coalescing at a time in history when antimicrobial resistance (AMR) is increasingly an urgent global health threat (Strathdee et al., 2023). Recent estimates indicate that over the next twenty-five years, 39 million people will die from a multi-drug resistant bacterial infection (Naghavi et al., 2024). Bacteriophage (phage) therapy is emerging as a promising tactic to confront this crisis. Despite the fact that phage were discovered over one hundred years ago and played prominent roles in launching the fields of molecular biology and genetic engineering, clinical applications of phage to treat acute bacterial infections were largely limited to parts of the former Soviet Union and Poland until the past decade, when a series of high-profile case reports ushered in a new era of phage therapy in the West (Strathdee et al., 2023).

In his 2020 commentary published in *Frontiers in Microbiology*, Belgian phage researcher Jean-Paul Pirnay re-imagined phage therapy in the year 2035 (Pirnay, 2020). His vision leverages advances in synthetic biology whereby phage could be generated *de novo* based on genetic sequences of bacterial host isolates without the need to ship bacterial cultures to laboratories for phage matching. In cases where bacterial isolates could not be obtained from patients (e.g., due to antibiotic suppressive therapy), he posited that AI algorithms could be applied to metagenomic data to predict the most likely bacterial sequence to facilitate phage matching. Further, he envisioned a global phage governance platform that would create an efficient, standardized, sustainable and ethical phage supply chain.

How close are we to achieving these realities? In this perspective, we review available literature on emerging advances in AI and synthetic biology that could be used to understand and engineer host specificity and other phage functions, considering the entire phage life cycle (i.e., binding and entry, replication, and lysis). We also consider how AI could be used to mine large datasets for accessory gene discovery and phage genome annotation. Finally, given the need to take phage therapy to scale, we discuss future avenues for research that could further advance the field.

Understanding phage-host specificity determinants using AI

Identifying infectious phage strains for a given host is essential for phage therapy. However, it is logistically challenging to screen a panel of phage on each clinical isolate, especially when time is of the essence in the treatment of patients with multi-drug resistant bacterial infections. With rapid and inexpensive sequencing increasingly available, matching a potential phage to a target host based on bacterial whole genome or metagenomic data has the potential to accelerate these earliest stages of preparing a therapeutic phage. Recently, several groups have made promising use of AI to achieve strain-level prediction of phage infection from host genome sequences (Boeckaerts et al., 2024; Gaborieau et al., 2024).

Strain-level prediction of infectious phages for a given host genome has been reported for *Klebsiella* spp. (Boeckaerts et al., 2024) and *Escherichia* spp (Gaborieau et al., 2024), whereby shared aspects of these studies reflect the current state of the art. In both cases, machine learning algorithms were constructed using genotypic information as features and large phenotypic datasets (i.e., phage-bacteria infection networks, or PBINs) as outcomes in training data. Both studies made use of pre-existing tools to construct relevant features from genotypic information [e.g., Kaptive (Lam et al., 2022), ECtyper (Bessonov et al., 2021)]. The features predictive of infection were the attachment factors that phages of these genera tend to utilize: surface polysaccharide traits such as capsular K-serotype, lipopolysaccharide (LPS) outer core variations, or O-antigen serotypes. Impressively, both studies encompass genus-level diversity, yet can predict strain-level phage-host specificity.

Interestingly, outer membrane proteins are also frequent attachment factors for phages of *Escherichia* and other spp (Nobrega et al., 2018), yet they were not significantly associated with infection in the dataset analyzed by Gaborieau et al. (2024). Strain-specific amino-acid variation in phage receptor proteins has been shown to modulate phage infectivity (Suga et al., 2021), suggesting that future work may be necessary to develop AI-guided phage matching algorithms for outer membrane protein-targeting phages. One potential way to approach this problem is to use protein structural modeling to predict infection based on interactions between phage receptor variants and phage receptor-binding proteins (RBPs). However, this approach has not yet been evaluated to our knowledge and may be susceptible to false-positive results that accurately predict receptor-RBP binding for phage-host pairs that, for other reasons, do not result in productive phage infection. For instance, in an *in vitro* receptor binding experiment, the phage T4 RBP bound to 85% of the 72 strains in an *E. coli* reference collection, yet T4 phage only formed plaques on 11% of the collection (Farquharson et al., 2021). This indicates that, although receptor-RBD binding may be necessary for infection, it is not sufficient, suggesting that deeper understanding of phage-host interactions downstream from phage attachment may need to be incorporated to improve the accuracy of predictive algorithms.

Even with these recent advances in matching potential phages to target hosts, major gaps remain for strain-level matching in the context of phage therapy. The current AI models for phage matching from host genome sequences are highly specific to host genus, and no classifiers of this type are yet available for highly prevalent ESKAPE pathogens like *Staphylococcus aureus* or *Pseudomonas aeruginosa*. *S. aureus* exhibits surface polysaccharide diversity, with phage predominantly targeting wall teichoic acid (Krusche et al., 2025), so a machine learning approach using teichoic acid variations as features, analogous to using capsular types for *Klebsiella* (Boeckaerts et al., 2024), might be a promising approach. However, for *P. aeruginosa*, phage interactions may involve a larger diversity of receptor types, with resistance mutations in flagella, type IV pili, and LPS evolving against a single phage strain (Kortright et al., 2022). Moreover, some strains of *P. aeruginosa* harbor extensive defense systems (Costa et al., 2024), suggesting these may play a greater role in predicting phage effectiveness from host genomes than that observed in *E. coli* or *Klebsiella*. The degree to which the presence of defense systems is predictive of infection by *Pseudomonas* phages is an area of ongoing work (Müller et al., 2024). With these differences in mind, a holistic approach evaluating the importance of different *P. aeruginosa* genomic features across many phage host pairs (akin to what was undertaken for *E. coli* (Gaborieau et al., 2024) may be required to build a reliable model for this species. Nonetheless, there appears to be great potential for researchers to extend recent examples by leveraging AI to achieve effective strain-level phage matching models in other pathogenic bacteria (Figure 1).

Since the above models for phage selection are largely based on host-phage genotype matching, these models would likely struggle to predict the effects of novel resistance mutations outside the training data. Training data are often comprised of a variety of

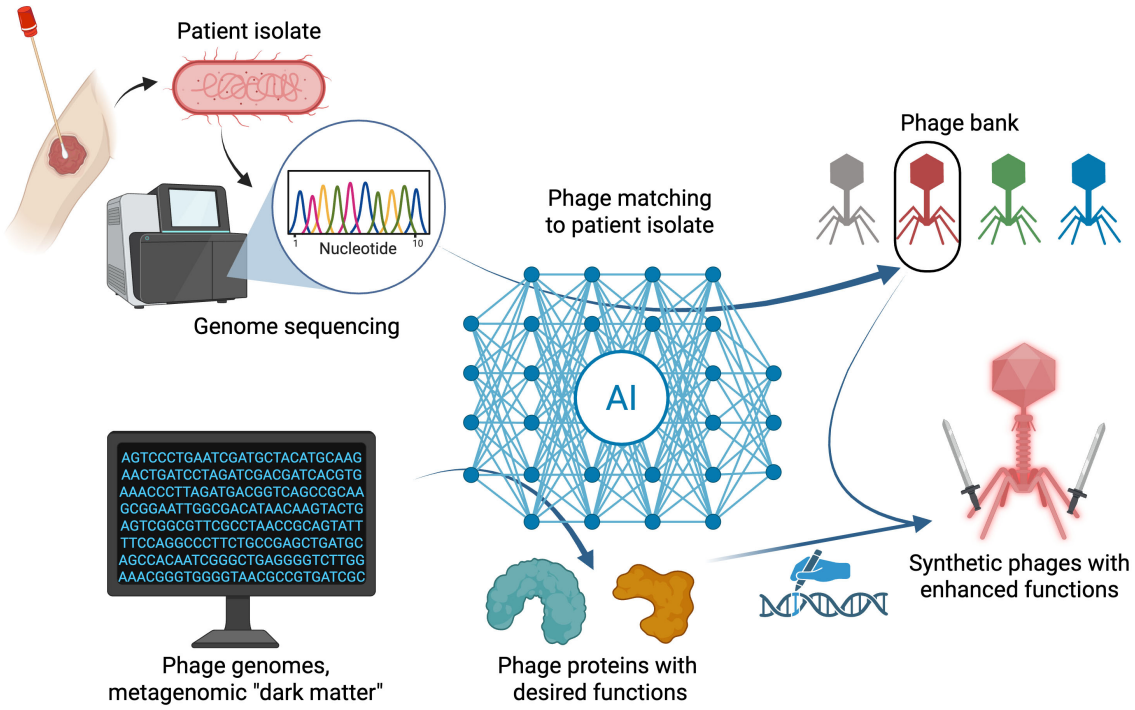

FIGURE 1
Overview of recent advances and future vision for AI methods to optimize phage therapy. Top: Phage matching based on genetic features in phage and bacterial genome sequences using AI-based algorithms can help identify candidate phages within phage banks for a provided patient isolate bacterium. Bottom: AI algorithms can predict functional phage genes from large sequence databases. Desired phage functions can be genetically grafted onto synthetic phages and evaluated for enhanced phage activity. Created in BioRender.

strains of bacteria and phages representing a coarse sampling of genetic variation, but fine genetic variation (such as point mutations) arising during phage-bacteria coevolution can modulate infection outcome. Bacterial evolution of resistance to phage is frequently observed in clinical phage therapy settings (Schooley et al., 2017; Pirnay et al., 2024) and in the laboratory (Luria and Delbrück, 1943; Meyer et al., 2012). Experimental coevolution of bacteria and phages has revealed not only phages' ability to evolve counter-resistance, but the potential for long-term evolutionary and ecological conflict between phage and bacteria (Borin et al., 2021, 2023; Shaer Tamar and Kishony, 2022; Chen et al., 2024). By experimentally identifying how to position phage with an early evolutionary advantage in the microbial arms race, coevolutionary phage training has the potential to improve the effectiveness of phage therapy (Borin et al., 2021). Recent advances have used machine learning (e.g., L1-penalized logistic regression) to predict the outcome of fine genetic variation in mutation profiles within coevolutionary PBINs assembled through experimental coevolution (Shaer Tamar and Kishony, 2022; Lucia-Sanz et al., 2024). A future challenge will be to combine insights gained through these analyses of fine-scaled genetic variation in laboratory coevolution with predictive models trained on more coarse genetic variation at the strain level observed across natural isolates. Furthermore, while most of the effort in this space has focused on understanding phage-bacteria interactions at the attachment step, which appears to provide the strongest predictive power for infectivity (Boeckaerts et al., 2024; Gaborieau et al., 2024), future work should identify how phage-bacteria interactions downstream of attachment modulate phage activity in ways that could improve efficacy of phage therapy.

Recent AI advances in the discovery of phage genes with specific functions

There has been an explosion in the number and variety of phage sequences available in public databases in recent years. This has been fueled by both the increase in the number of sequencing studies (often metagenome sequencing) as well as AI-driven improvements in identifying phage sequences in the "dark matter" of metagenome data (Hatfull, 2015). The applications of AI in discriminating phage from non-phage sequences in metagenomic datasets have been extensively reviewed (Nami et al., 2021; Flamholz et al., 2024). There is a wide collection of AI-driven tools for identifying phage genetic sequences (McNair et al., 2012; Auslander et al., 2020; Wu et al., 2021; Johansen et al., 2022; Shang et al., 2023) and classifying phage virion proteins (Thung et al., 2021; Ahmad et al., 2022; Fang et al., 2022). These tools are accelerating the annotation of predicted phage sequences,

allowing for a greater diversity of phage sequences to be used for comparative studies.

Ultimately, phage therapy requires cultivated phages, but the discovery of novel functional phage genes in sequence databases can be leveraged to program naturally occurring phages with specific biological functions. A key impediment to harnessing the huge and growing amount of phage sequencing data is that the number of potential genes of interest is vast, making it experimentally intractable to functionally screen sequences for biological function. Several recent studies (Concha-Eloko et al., 2024; Zhang et al., 2024; Yirmiya et al., 2025) exemplify recent advances in leveraging AI to sift through large sequencing datasets to predict putative phage genes with specific functions, triaging labor-intensive experimental validation for predicted candidate genes. Once validated, these novel gene sequences can be tested for their ability enhance the efficacy of engineered therapeutic phages (Figure 1).

Anti-phage defense systems are diverse and heterogeneously distributed throughout bacteria (Doron et al., 2018; Bernheim and Sorek, 2020; Georjon and Bernheim, 2023), and there is a growing collection of phage genes that have been identified as counter-defenses against these bacterial immune systems (Vassallo et al., 2022; Mayo-Muñoz et al., 2024; Murtazalieva et al., 2024; Yirmiya et al., 2024). It is likely that many phage counter-defenses are yet to be discovered. Yirmiya et al. (Yirmiya et al., 2025) used protein structure and interaction prediction using AlphaFold2-Multimer (Evans et al., 2022) to screen approximately two million phage genomes containing over 30 million phage genes, and identify phage proteins predicted to fold and interact with pre-chosen bacterial phage defense proteins. By carefully and iteratively designing a computational workflow, they were able to attain a ~50% success rate in identifying experimentally validated novel phage inhibitors of several well-characterized bacterial defense systems. Although there are limitations to this approach – including the need to select appropriate protein-binding partners such as a bacterial defense system of interest *a priori*, and a substantial false-positive rate – this approach more generally establishes a paradigm that leverages AI to predict novel phage genes that interact with specific proteins of interest. As additional bacterial anti-phage defense systems are functionally and structurally characterized, this approach will likely uncover additional novel phage counter-defense genes that may find utility in synthetic phages armed to match the capabilities of the target bacteria they are deployed against.

Bacterial capsules and biofilms are virulence factors that pose challenges in the treatment of bacterial infections (Chang et al., 2022). Some phages rely upon recognition and digestion of polysaccharide components in bacterial capsules and biofilms as their first step in the infection process (Knecht et al., 2020). The use of phage as a strategy for overcoming biofilms in difficult-to-treat infections has long been proposed and is recognized to require very specific interactions between phage and host (Hughes et al., 1998; Mayorga-Ramos et al., 2024). Some phage genes necessary for biofilm and capsule degradation have been identified as depolymerases that can attach to the distal tips of phage tails where they simultaneously act as enzymes that degrade polysaccharide components and as specific receptor-binding proteins for which presence of the cognate capsule is required for infection (Dunstan et al., 2021). Mirroring the genetic and antigenic diversity of capsular polysaccharide serotypes in pathogenic bacteria (Shu et al., 2009), phage depolymerase sequences are also quite diverse in amino-acid sequences (Knecht et al., 2020) and this high degree of sequence variability complicates the process of identifying novel depolymerases in sequence databases. To overcome these difficulties, Concha-Eloko et al. (2024) demonstrate how a protein language model fine-tuned for depolymerases and trained on carefully curated data has advanced the annotation of depolymerase genes and their respective enzymatic domains, beyond currently available computational tools. The improved AI-guided annotation of depolymerase genes enables further study of the use of diverse depolymerase genes in recombinant phages to reprogram specificity and enzymatic capabilities for targeted therapeutic applications against specific capsule types.

Phage lysins are enzymes that degrade peptidoglycans, playing an essential role in the phage life cycle by promoting host cell lysis and cell death. There has long been interest in developing recombinant lysins as treatments for bacterial infections since they can also lyse the cell from the outside (Fischetti, 2018). A recent Phase 3 clinical trial of a lysin targeting *Staphylococcus aureus* added to standard of care antibiotics was ended for futility after an interim efficacy analysis (ClinicalTrials.gov ID NCT04160468). However, there is potential to advance their use, using engineered lysins selected from combinatorial libraries recombining portions of known lysin sequences (Gerstmans et al., 2020), with the potential to develop novel synthetic lysins with fine-tuned specificity and activity. Further advances in lysin engineering – whether for use as therapeutic protein products or as genetic cargo in engineered therapeutic phages – has been limited by the lack of computational methods to comprehensively screen metagenomic or uncharacterized phage genome sequence data to identify new lysin genes. Recent work by Zhang et al. provides a machine learning based software package that identifies putative lysin genes from assembled contigs (Zhang et al., 2024). Among 17 predicted novel lysin sequences selected for experimental validation, seven exhibited appropriate activity. Similar to the approach used by Yirmiya et al. (2025), there is a substantial false positive rate requiring rigorous experimental validation of AI-produced screening candidates, however, these are substantial advances in that they allow researchers to triage valuable time and resources validating candidate genes selected from otherwise intractably large datasets.

A key theme emerging from each of these studies is that an enormous amount of careful human planning, intuition of biological plausibility, and iterative human-driven improvement to AI algorithms is necessary to realize the potential of these approaches. By facilitating a computational screening process for specific biological functions, these emerging AI models are enabling

researchers to exploit vast troves of data to discover a diversity of new phage genes that can antagonize bacterial defense systems, degrade biofilm and lyse infected cells, each of which may be useful in the future design of therapeutic phages with desired functions.

Future outlook: AI-guided development of synthetic phages as enhanced therapeutics

The AI-driven advances described above are beginning to generate tools that can predict which naturally occurring phages are most likely to infect a target bacterium. A deeper level of understanding of which genetic determinants drive these predictions, and the underlying mechanisms behind productive infection, are beginning to emerge to enable phage specificity programming (Dunne et al., 2021). Synthetic biology methods are already available to modify many phage genomes (Jaschke et al., 2012; Ando et al., 2015; Kilcher et al., 2018; Pires et al., 2021; Adler et al., 2022; Assad-Garcia et al., 2022; Kamata et al., 2024) and have begun to be applied to study granular determinants of phage specificity through high-throughput mutational studies of phage receptor binding proteins (Dunne et al., 2019; Yehl et al., 2019; Andrews and Fields, 2021; Huss et al., 2021, 2023). Huss et al. have recently developed a method of analyzing deep mutational scanning data of a phage receptor binding protein to develop a motif-searching algorithm that identifies novel phage receptor-binding sequences from metagenomic data (Huss et al., 2024). Collections of new receptor-binding protein sequences from these and other studies can be used as the substrate for future AI-guided protein design, leveraging generative models of protein sequences (Hsu et al., 2024). In a manner analogous to using protein language models to accelerate directed evolution of antibody sequences targeting specific antigens (Hie et al., 2023), phage receptor-binding protein engineering may also be amenable to machine-learning-guided directed evolution to modulate receptor specificity. While such fine-tuning of phage receptor binding through protein design has the potential to generate phages with defined bacterial receptor targets, it is important to note that binding affinity alone is not always sufficient to confer productive infection (Farquharson et al., 2021), and more work is needed to understand the mechanisms of infection immediately downstream of receptor binding, which are incompletely understood for even some of the most heavily studied model phages (Hu et al., 2015; Ge and Wang, 2024). More broadly, generative models of entire genomes, including phage genomes, have recently been described (Nguyen et al., 2024; Shao and Yan, 2024), and although these models are in their infancy and do not yet produce biologically functional whole genomes, they are already able to recapitulate coarse genomic architectures similar to natural phage genomes and can even produce gene sequences for functionally active multicomponent systems (Nguyen et al., 2024).

The recent AI-guided advances outlined above identifying novel phage lysins, depolymerases, and counter-defenses to bacterial immune systems similarly lay the groundwork for incorporating these functions into designed, synthetic phages (Lenneman et al., 2021) or other therapeutics, expanding the armamentarium of engineered phages that can deliver heterologous effector proteins (Du et al., 2023; Gencay et al., 2023) or augment natural phage function in other ways favorable for therapy. Phages engineered to avoid lysogeny have already been used clinically (Dedrick et al., 2019). Future work will be necessary to identify whether the rational design of synthetic phages with other various functions can increase treatment efficacy. Additionally, the bioethical and environmental implications of treating patients with genetically engineered phages requires continued careful contemplation from a One Health perspective, since engineered phages have the potential to impact human-, animal-, and environment-associated microbial communities (Hernando-Amado et al., 2019; Nair and Khairnar, 2019; Banerjee and van der Heijden, 2023). Although the dream of instant AI-designed therapeutic phage synthesis for a provided target bacterium is unlikely to be achieved in the next 10 years (Pirnay, 2020), advances in AI are both accelerating the identification of naturally occurring phages for therapy, as well as enabling the distillation of useful knowledge from otherwise untenably large sequencing databases abundant with uncharacterized phage genes that could find utility in synthetic phages. In the meantime, coordinated efforts are needed to make the growing number of phage libraries across the world compatible with one another, and accessible for compassionate use cases, clinical trials, and translational research experiments.

Data availability statement

The original contributions presented in the study are included in the article/supplementary material. Further inquiries can be directed to the corresponding author.

Author contributions

MD: Conceptualization, Writing – original draft, Writing – review & editing. JR: Writing – original draft, Writing – review & editing. SS: Conceptualization, Writing – original draft, Writing – review & editing.

Funding

The author(s) declare that financial support was received for the research and/or publication of this article. MD was supported by the National Institute of Allergy and Infectious Diseases (NIAID) T32AI007036. JR was supported by Howard Hughes Medical

Institute Emerging Pathogens Initiative grant 7012574. SAS acknowledges support from the Mallory Smith Legacy Fund and the Herbert W. Hoover Foundation.

Acknowledgments

We are grateful to members of the Meyer laboratory for fruitful discussions and to Dr. Jean-Paul Pirnay for inspiration.

Conflict of interest

The authors declare that the research was conducted in the absence of any commercial or financial relationships that could be construed as a potential conflict of interest.

Generative AI statement

The author(s) declare that no Generative AI was used in the creation of this manuscript.

Publisher's note

References

Adler, B. A., Hessler, T., Cress, B. F., Lahiri, A., Mutalik, V. K., Barrangou, R., et al. (2022). Broad-spectrum CRISPR-Cas13a enables efficient phage genome editing. *Nat. Microbiol.* 7, 1967–1979. doi: 10.1038/s41564-022-01258-x

Ahmad, S., Charoenkwan, P., Quinn, J. M. W., Moni, M. A., Hasan, M. M., Lio', P., et al. (2022). SCORPION is a stacking-based ensemble learning framework for accurate prediction of phage virion proteins. *Sci. Rep.* 12, 4106. doi: 10.1038/s41598-022-08173-5

Ando, H., Lemire, S., Pires, D. P., and Lu, T. K. (2015). Engineering modular viral scaffolds for targeted bacterial population editing. *Cell Syst.* 1, 187–196. doi: 10.1016/j.cels.2015.08.013

Andrews, B., and Fields, S. (2021). Balance between promiscuity and specificity in phage λ host range. *ISME J.* 15, 2195–2205. doi: 10.1038/s41396-021-00912-2

Assad-Garcia, N., D'Souza, R., Buzzeo, R., Tripathi, A., Oldfield, L. M., Vashee, S., et al. (2022). Cross-genus "Boot-up" of synthetic bacteriophage in *staphylococcus aureus* by using a new and efficient DNA transformation method. *Appl. Environ. Microbiol.* 88, e0148621. doi: 10.1128/AEM.01486-21

Auslander, N., Gussow, A. B., Benler, S., Wolf, Y. I., and Koonin, E. V. (2020). Seeker: alignment-free identification of bacteriophage genomes by deep learning. *Nucleic Acids Res.* 48, e121. doi: 10.1093/nar/gkaa856

Banerjee, S., and van der Heijden, M. G. A. (2023). Soil microbiomes and one health. *Nat. Rev. Microbiol.* 21, 6–20. doi: 10.1038/s41579-022-00779-w

Bernheim, A., and Sorek, R. (2020). The pan-immune system of bacteria: antiviral defence as a community resource. *Nat. Rev. Microbiol.* 18, 113–119. doi: 10.1038/s41579-019-0278-2

Bessonov, K., Laing, C., Robertson, J., Yong, I., Ziebell, K., Gannon, V. P. J., et al. (2021). ECTyper: in silico Escherichia coli serotype and species prediction from raw and assembled whole-genome sequence data. *Microb. Genomics* 7, 728. doi: 10.1099/mgen.0.000728

Boeckaerts, D., Stock, M., Ferriol-González, C., Oteo-Iglesias, J., Sanjuán, R., Domingo-Calap, P., et al. (2024). Prediction of Klebsiella phage-host specificity at the strain level. *Nat. Commun.* 15, 4355. doi: 10.1038/s41467-024-48675-6

Borin, J. M., Avrani, S., Barrick, J. E., Petrie, K. L., and Meyer, J. R. (2021). Coevolutionary phage training leads to greater bacterial suppression and delays the evolution of phage resistance. *Proc. Natl. Acad. Sci.* 118, e2104592118. doi: 10.1073/pnas.2104592118

Borin, J. M., Lee, J. J., Lucia-Sanz, A., Gerbino, K. R., Weitz, J. S., and Meyer, J. R. (2023). Rapid bacteria-phage coevolution drives the emergence of multiscale networks. *Science* 382, 674–678. doi: 10.1126/science.adi5536

Chang, C., Yu, X., Guo, W., Guo, C., Guo, X., Li, Q., et al. (2022). Bacteriophage-mediated control of biofilm: A promising new dawn for the future. *Front. Microbiol.* 13. doi: 10.3389/fmicb.2022.825828

Chen, L., Zhao, X., Wongso, S., Lin, Z., and Wang, S. (2024). Trade-offs between receptor modification and fitness drive host-bacteriophage co-evolution leading to phage extinction or co-existence. *ISME J.* 18, wrae214. doi: 10.1093/ismejo/wrae214

Concha-Eloko, R., Stock, M., Baets, B. D., Briers, Y., Sanjuán, R., Domingo-Calap, P., et al. (2024). DepoScope: Accurate phage depolymerase annotation and domain delineation using large language models. *PloS Comput. Biol.* 20, e1011831. doi: 10.1371/journal.pcbi.1011831

Costa, A. R., van den Berg, D. F., Esser, J. Q., Muralidharan, A., van den Bossche, H., Bonilla, B. E., et al. (2024). Accumulation of defense systems in phage-resistant strains of Pseudomonas aeruginosa. *Sci. Adv.* 10, eadj0341. doi: 10.1126/sciadv.adj0341

Dedrick, R. M., Guerrero-Bustamante, C. A., Garlena, R. A., Russell, D. A., Ford, K., Harris, K., et al. (2019). Engineered bacteriophages for treatment of a patient with a disseminated drug-resistant Mycobacterium abscessus. *Nat. Med.* 25, 730–733. doi: 10.1038/s41591-019-0437-z

Doron, S., Melamed, S., Ofir, G., Leavitt, A., Lopatina, A., Keren, M., et al. (2018). Systematic discovery of anti-phage defense systems in the microbial pan-genome. *Science* 359, eaar4120. doi: 10.1126/science.aar4120

Du, J., Meile, S., Baggenstos, J., Jäggi, T., Piffaretti, P., Hunold, L., et al. (2023). Enhancing bacteriophage therapeutics through in *situ* production and release of heterologous antimicrobial effectors. *Nat. Commun.* 14, 4337. doi: 10.1038/s41467-023-39612-0

Dunne, M., Prokhorov, N. S., Loessner, M. J., and Leiman, P. G. (2021). Reprogramming bacteriophage host range: design principles and strategies for engineering receptor binding proteins. *Curr. Opin. Biotechnol.* 68, 272–281. doi: 10.1016/j.copbio.2021.02.006

Dunne, M., Rupf, B., Tala, M., Qabrati, X., Ernst, P., Shen, Y., et al. (2019). Reprogramming bacteriophage host range through structure-guided design of chimeric receptor binding proteins. *Cell Rep.* 29, 1336–1350.e4. doi: 10.1016/j.celrep.2019.09.062

Dunstan, R. A., Bamert, R. S., Belousoff, M. J., Short, F. L., Barlow, C. K., Pickard, D. J., et al. (2021). Mechanistic Insights into the Capsule-Targeting Depolymerase from a Klebsiella pneumoniae Bacteriophage. *Microbiol. Spectr.* 9. doi: 10.1128/spectrum.01023-21

Evans, R., O'Neill, M., Pritzel, A., Antropova, N., Senior, A., Green, T., et al. (2022). Protein complex prediction with AlphaFold-Multimer 463034. doi: 10.1101/2021.10.04.463034

Fang, Z., Feng, T., Zhou, H., and Chen, M. (2022). DeePVP: Identification and classification of phage virion proteins using deep learning. *GigaScience* 11, giac076. doi: 10.1093/gigascience/giac076

Farquharson, E. L., Lightbown, A., Pulkkinen, E., Russell, T., Werner, B., and Nugen, S. R. (2021). Evaluating phage tail fiber receptor-binding proteins using a luminescent flow-through 96-well plate assay. *Front. Microbiol.* 12. doi: 10.3389/fmicb.2021.741304

Fischetti, V. A. (2018). Development of phage lysins as novel therapeutics: A historical perspective. *Viruses* 10, 310. doi: 10.3390/v10060310

Flamholz, Z. N., Li, C., and Kelly, L. (2024). Improving viral annotation with artificial intelligence. *mBio* 15, e03206–e03223. doi: 10.1128/mbio.03206-23

Gaborieau, B., Vaysset, H., Tesson, F., Charachon, I., Dib, N., Bernier, J., et al. (2024). Prediction of strain level phage–host interactions across the Escherichia genus using only genomic information. *Nat. Microbiol.* 9, 2847–2861. doi: 10.1038/s41564-024-01832-5

Ge, X., and Wang, J. (2024). Structural mechanism of bacteriophage lambda tail's interaction with the bacterial receptor. *Nat. Commun.* 15, 4185. doi: 10.1038/s41467-024-48686-3

Gencay, Y. E., Jasinskytė, D., Robert, C., Semsey, S., Martínez, V., Petersen, A. Ø, et al. (2023). Engineered phage with antibacterial CRISPR–Cas selectively reduce E. coli burden in mice. *Nat. Biotechnol.* 42, 265–274. doi: 10.1038/s41587-023-01759-y

Georjon, H., and Bernheim, A. (2023). The highly diverse antiphage defence systems of bacteria. *Nat. Rev. Microbiol.* 21, 686–700. doi: 10.1038/s41579-023-00934-x

Gerstmans, H., Grimon, D., Gutiérrez, D., Lood, C., Rodríguez, A., van Noort, V., et al. (2020). A VersaTile-driven platform for rapid hit-to-lead development of engineered lysins. *Sci. Adv.* 6, eaaz1136. doi: 10.1126/sciadv.aaz1136

Hatfull, G. F. (2015). Dark matter of the biosphere: the amazing world of bacteriophage diversity. *J. Virol.* 89, 8107–8110. doi: 10.1128/JVI.01340-15

Hernando-Amado, S., Coque, T. M., Baquero, F., and Martínez, J. L. (2019). Defining and combating antibiotic resistance from One Health and Global Health perspectives. *Nat. Microbiol.* 4, 1432–1442. doi: 10.1038/s41564-019-0503-9

Hie, B. L., Shanker, V. R., Xu, D., Bruun, T. U. J., Weidenbacher, P. A., Tang, S., et al. (2023). Efficient evolution of human antibodies from general protein language models. *Nat. Biotechnol.* 42, 275–283. doi: 10.1038/s41587-023-01763-2

Hsu, C., Fannjiang, C., and Listgarten, J. (2024). Generative models for protein structures and sequences. *Nat. Biotechnol.* 42, 196–199. doi: 10.1038/s41587-023-02115-w

Hu, B., Margolin, W., Molineux, I. J., and Liu, J. (2015). Structural remodeling of bacteriophage T4 and host membranes during infection initiation. *Proc. Natl. Acad. Sci. U. S. A.* 112, E4919–E4928. doi: 10.1073/pnas.1501064112

Hughes, K. A., Sutherland, I. W., and Jones, M. V. (1998). Biofilm susceptibility to bacteriophage attack: the role of phage-borne polysaccharide depolymerase. *Microbiol. Read. Engl.* 144, 3039–3047. doi: 10.1099/00221287-144-11-3039

Huss, P., Chen, J., and Raman, S. (2023). High-throughput approaches to understand and engineer bacteriophages. *Trends Biochem. Sci.* 48, 187–197. doi: 10.1016/j.tibs.2022.08.012

Huss, P., Kieft, K., Meger, A., Nishikawa, K., Anantharaman, K., and Raman, S. (2024). Engineering bacteriophages through deep mining of metagenomic motifs 527309. doi: 10.1101/2023.02.07.527309

Huss, P., Meger, A., Leander, M., Nishikawa, K., and Raman, S. (2021). Mapping the functional landscape of the receptor binding domain of T7 bacteriophage by deep mutational scanning. *eLife* 10, e63775. doi: 10.7554/eLife.63775

Jaschke, P. R., Lieberman, E. K., Rodriguez, J., Sierra, A., and Endy, D. (2012). A fully decompressed synthetic bacteriophage øX174 genome assembled and archived in yeast. *Virology* 434, 278–284. doi: 10.1016/j.virol.2012.09.020

Johansen, J., Plichta, D. R., Nissen, J. N., Jespersen, M. L., Shah, S. A., Deng, L., et al. (2022). Genome binning of viral entities from bulk metagenomics data. *Nat. Commun.* 13, 965. doi: 10.1038/s41467-022-28581-5

Kamata, K., Birkholz, N., Ceelen, M., Fagerlund, R. D., Jackson, S. A., and Fineran, P. C. (2024). Repurposing an endogenous CRISPR-cas system to generate and study subtle mutations in bacteriophages. *CRISPR J.* 7 (6), 343-354. doi: 10.1089/crispr.2024.0047

Kilcher, S., Studer, P., Muessner, C., Klumpp, J., and Loessner, M. J. (2018). Cross-genus rebooting of custom-made, synthetic bacteriophage genomes in L-form bacteria. *Proc. Natl. Acad. Sci. U. S. A.* 115, 567–572. doi: 10.1073/pnas.1714658115

Knecht, L. E., Veljkovic, M., and Fieseler, L. (2020). Diversity and function of phage encoded depolymerases. *Front. Microbiol.* 10. doi: 10.3389/fmicb.2019.02949

Kortright, K. E., Chan, B. K., Evans, B. R., and Turner, P. E. (2022). Arms race and fluctuating selection dynamics in Pseudomonas aeruginosa bacteria coevolving with phage OMKO1. *J. Evol. Biol.* 35, 1475–1487. doi: 10.1111/jeb.14095

Krusche, J., Beck, C., Lehmann, E., Gerlach, D., Daiber, E., Mayer, C., et al. (2025). Characterization and host range prediction of *Staphylococcus aureus* phages through receptor-binding protein analysis. *Cell Rep.* 44, 115369. doi: 10.1016/j.celrep.2025.115369

Lam, M. M. C., Wick, R. R., Judd, L. M., Holt, K. E., and Wyres, K. L. (2022). Kaptive 2.0: updated capsule and lipopolysaccharide locus typing for the Klebsiella pneumoniae species complex. *Microb. Genomics* 8, 800. doi: 10.1099/mgen.0.000800

Lenneman, B. R., Fernbach, J., Loessner, M. J., Lu, T. K., and Kilcher, S. (2021). Enhancing phage therapy through synthetic biology and genome engineering. *Curr. Opin. Biotechnol.* 68, 151–159. doi: 10.1016/j.copbio.2020.11.003

Lucia-Sanz, A., Peng, S., Leung, C. Y. J., Gupta, A., Meyer, J. R., and Weitz, J. S. (2024). Inferring strain-level mutational drivers of phage-bacteria interaction phenotypes arising during coevolutionary dynamics. *Virus Evol.* 10, veae104. doi: 10.1093/ve/veae104

Luria, S. E., and Delbrück, M. (1943). Mutations of bacteria from virus sensitivity to virus resistance. *Genetics* 28, 491–511. doi: 10.1093/genetics/28.6.491

Mayo-Muñoz, D., Pinilla-Redondo, R., Camara-Wilpert, S., Birkholz, N., and Fineran, P. C. (2024). Inhibitors of bacterial immune systems: discovery, mechanisms and applications. *Nat. Rev. Genet.* 25, 237–254. doi: 10.1038/s41576-023-00676-9

Mayorga-Ramos, A., Carrera-Pacheco, S. E., Barba-Ostria, C., and Guamán, L. P. (2024). Bacteriophage-mediated approaches for biofilm control. *Front. Cell. Infect. Microbiol.* 14. doi: 10.3389/fcimb.2024.1428637

McNair, K., Bailey, B. A., and Edwards, R. A. (2012). PHACTS, a computational approach to classifying the lifestyle of phages. *Bioinform. Oxf. Engl.* 28, 614–618. doi: 10.1093/bioinformatics/bts014

Meyer, J. R., Dobias, D. T., Weitz, J. S., Barrick, J. E., Quick, R. T., and Lenski, R. E. (2012). Repeatability and contingency in the evolution of a key innovation in phage lambda. *Science* 335, 428–432. doi: 10.1126/science.1214449

Müller, D. M., Pourtois, J. D., Kim, M. K., Targ, B., Burgener, E. B., Milla, C., et al. (2024). Bacterial Receptors but Not Anti-Phage Defence Mechanisms Determine Host Range for a Pair of Pseudomonas aeruginosa Lytic Phages 591980. doi: 10.1101/2024.04.30.591980

Murtazalieva, K., Mu, A., Petrovskaya, A., and Finn, R. D. (2024). The growing repertoire of phage anti-defence systems. *Trends Microbiol.* 32 (12), 1212-1228. doi: 10.1016/j.tim.2024.05.005

Naghavi, M., Vollset, S. E., Ikuta, K. S., Swetschinski, L. R., Gray, A. P., Wool, E. E., et al. (2024). Global burden of bacterial antimicrobial resistance 1990–2021: a systematic analysis with forecasts to 2050. *Lancet* 404, 1199–1226. doi: 10.1016/S0140-6736(24)01867-1

Nair, A., and Khairnar, K. (2019). Genetically engineered phages for therapeutics: proceed with caution. *Nat. Med.* 25, 1028–1028. doi: 10.1038/s41591-019-0506-3

Nami, Y., Imeni, N., and Panahi, B. (2021). Application of machine learning in bacteriophage research. *BMC Microbiol.* 21, 193. doi: 10.1186/s12866-021-02256-5

Nguyen, E., Poli, M., Durrant, M. G., Kang, B., Katrekar, D., Li, D. B., et al. (2024). Sequence modeling and design from molecular to genome scale with Evo. *Science* 386, eado9336. doi: 10.1126/science.ado9336

Nobrega, F. L., Vlot, M., de Jonge, P. A., Dreesens, L. L., Beaumont, H. J. E., Lavigne, R., et al. (2018). Targeting mechanisms of tailed bacteriophages. *Nat. Rev. Microbiol.* 16, 760–773. doi: 10.1038/s41579-018-0070-8

Pires, D. P., Monteiro, R., Mil-Homens, D., Fialho, A., Lu, T. K., and Azeredo, J. (2021). Designing P. aeruginosa synthetic phages with reduced genomes. *Sci. Rep.* 11, 2164. doi: 10.1038/s41598-021-81580-2

Pirnay, J.-P. (2020). Phage therapy in the year 2035. *Front. Microbiol.* 11. doi: 10.3389/fmicb.2020.01171

Pirnay, J.-P., Djebara, S., Steurs, G., Griselain, J., Cochez, C., De Soir, S., et al. (2024). Personalized bacteriophage therapy outcomes for 100 consecutive cases: a multicentre, multinational, retrospective observational study. *Nat. Microbiol.* 9, 1434–1453. doi: 10.1038/s41564-024-01705-x

Schooley, R. T., Biswas, B., Gill, J. J., Hernandez-Morales, A., Lancaster, J., Lessor, L., et al. (2017). Development and use of personalized bacteriophage-based therapeutic cocktails to treat a patient with a disseminated resistant acinetobacter baumannii infection. *Antimicrob. Agents Chemother.* 61, e00954–e00917. doi: 10.1128/AAC.00954-17

Shaer Tamar, E., and Kishony, R. (2022). Multistep diversification in spatiotemporal bacterial-phage coevolution. *Nat. Commun.* 13, 7971. doi: 10.1038/s41467-022-35351-w

Shang, J., Tang, X., and Sun, Y. (2023). PhaTYP: predicting the lifestyle for bacteriophages using BERT. *Brief. Bioinform.* 24, bbac487. doi: 10.1093/bib/bbac487

Shao, B., and Yan, J. (2024). A long-context language model for deciphering and generating bacteriophage genomes. *Nat. Commun.* 15, 9392. doi: 10.1038/s41467-024-53759-4

Shu, H.-Y., Fung, C.-P., Liu, Y.-M., Wu, K.-M., Chen, Y.-T., Li, L.-H., et al. (2009). Genetic diversity of capsular polysaccharide biosynthesis in Klebsiella pneumoniae clinical isolates. *Microbiol. Read. Engl.* 155, 4170–4183. doi: 10.1099/mic.0.029017-0

Strathdee, S. A., Hatfull, G. F., Mutalik, V. K., and Schooley, R. T. (2023). Phage therapy: From biological mechanisms to future directions. *Cell* 186, 17–31. doi: 10.1016/j.cell.2022.11.017

Suga, A., Kawaguchi, M., Yonesaki, T., and Otsuka, Y. (2021). Manipulating interactions between T4 phage long tail fibers and escherichia coli receptors. *Appl. Environ. Microbiol.* 87, e00423–e00421. doi: 10.1128/AEM.00423-21

Thung, T. Y., White, M. E., Dai, W., Wilksch, J. J., Bamert, R. S., Rocker, A., et al. (2021). Component parts of bacteriophage virions accurately defined by a machine-learning approach built on evolutionary features. *mSystems* 6. doi: 10.1128/msystems.00242-21

Vassallo, C. N., Doering, C. R., Littlehale, M. L., Teodoro, G. I. C., and Laub, M. T. (2022). A functional selection reveals previously undetected anti-phage defence systems in the E. coli pangenome. *Nat. Microbiol.* 7, 1568–1579. doi: 10.1038/s41564-022-01219-4

Wu, S., Fang, Z., Tan, J., Li, M., Wang, C., Guo, Q., et al. (2021). DeePhage: distinguishing virulent and temperate phage-derived sequences in metavirome data with a deep learning approach. *GigaScience* 10, giab056. doi: 10.1093/gigascience/giab056

Yehl, K., Lemire, S., Yang, A. C., Ando, H., Mimee, M., Torres, M. D. T., et al. (2019). Engineering phage host-range and suppressing bacterial resistance through phage tail fiber mutagenesis. *Cell* 179, 459–469.e9. doi: 10.1016/j.cell.2019.09.015

Yirmiya, E., Hobbs, S. J., Leavitt, A., Osterman, I., Avraham, C., Hochhauser, D., et al. (2025). Structure-guided discovery of viral proteins that inhibit host immunity. *Cell.* 188 (6), 1681-1692.e17. doi: 10.1016/j.cell.2024.12.035

Yirmiya, E., Leavitt, A., Lu, A., Ragucci, A. E., Avraham, C., Osterman, I., et al. (2024). Phages overcome bacterial immunity via diverse anti-defence proteins. *Nature* 625, 352–359. doi: 10.1038/s41586-023-06869-w

Zhang, Y., Li, R., Zou, G., Guo, Y., Wu, R., Zhou, Y., et al. (2024). Discovery of antimicrobial lysins from the "Dark matter" of uncharacterized phages using artificial intelligence. *Adv. Sci.* 11, 2404049. doi: 10.1002/advs.202404049

frontiers | Frontiers in Cellular and Infection Microbiology

TYPE Original Research
PUBLISHED 25 June 2025
DOI 10.3389/fcimb.2025.1561443

OPEN ACCESS

EDITED BY
Derry Keith Mercer,
INCATE, Switzerland

REVIEWED BY
Huong Minh Nguyen,
Jichi Medical University, Japan
Panos G. Kalatzis,
University of Copenhagen, Denmark

*CORRESPONDENCE
Robert Ramirez-Garcia
r.ramirez-garcia@imperial.ac.uk
Alfonso Jaramillo
alfonso.jaramillo@csic.es

RECEIVED 15 January 2025
ACCEPTED 14 May 2025
PUBLISHED 25 June 2025

CITATION
Ramirez-Garcia R, Sagona AP, Barr JJ and Jaramillo A (2025) High-yield bioproduction of virus-free virus-like P4-EKORhE multi-lysin transducing particles as an antimicrobial gene therapeutic. *Front. Cell. Infect. Microbiol.* 15:1561443. doi: 10.3389/fcimb.2025.1561443

High-yield bioproduction of virus-free virus-like P4-EKORhE multi-lysin transducing particles as an antimicrobial gene therapeutic

Robert Ramirez-Garcia[1,2,3,4,5]*, Antonia P. Sagona[1], Jeremy J. Barr[2] and Alfonso Jaramillo[6]*

[1]School of Life Sciences, Faculty of Science, Engineering and Medicine, The University of Warwick, Coventry, United Kingdom, [2]School of Biological Sciences, Faculty of Sciences, Monash University, Melbourne, VIC, Australia, [3]Department of Computing, Faculty of Engineering, Imperial College London, London, United Kingdom, [4]Translation & Innovation Hub (I-HUB), Imperial College London, London, United Kingdom, [5]ACGTx, London, United Kingdom, [6]Institute for Integrative Systems Biology (I2SysBio), CSIC-Universitat de València, Paterna, Spain

A description of the construction of the bioengineered P4-EKORhE and a comprehensive method for producing very high yields (up to 10^{12} particles per millilitre) enable the use of virus-like particles to transduce genetically encoded antimicrobials through a combination of synthetic biology and optimised upstream and downstream processing. The final product, a gene-delivered antimicrobial in the form of the multi-lysin cassette, is fully functional before and after packaging within P4-EKORhE particles. The antimicrobial activity of the multi-lysin cassette, characterised by its lysis proteins, was tested *in vivo* in both pure bacterial *Escherichia coli* cultures and a model of phage infection in co-culture with A549 immortalised human epithelial tissue cells. This work exemplifies several bioproduction methods and demonstrates how the virology of the P4 and P2 phages can be harnessed to establish a bioprocess for producing transducing particles at very high yields, avoiding contamination by the natural virus while maintaining the antimicrobial effectiveness of the final product.

KEYWORDS

high-yield bioproduction, bioprocess engineering, virus-like particles, transducing particles, antimicrobials, gene therapeutics, A549-model of infection, P4-EKORhE

1 Introduction

Harnessing the natural mechanisms that phages use to repurpose their host bacteria's metabolism to produce viral structural material and package viral DNA for self-replication and propagation is how transducing particles are produced. The most characteristic protein-made parts of phages are the capsid, which packages and protects the genetic

material; a tail, which allows the genetic material to be ejected upon infection; and the tail fibres, which enable specific interaction with a particular bacterial host (Mourosi et al., 2022). For a general schematic of these basic structures, see Figure 1. These protein structures allow the phage to store, protect, and, upon infection, release the genetic material within the target bacteria. If these protein components can be produced while blocking the virus's ability to package its own viral DNA, it is possible to produce a transducing particle that contains and delivers a heterologous genetic payload to a target bacterial host. This is particularly straightforward when using phages whose "cos site" has been identified, such as the λ or P2/P4 phages.

1.1 Virus-free virus-like particle production based on conditionally propagating P4 phage

As described extensively in the literature (Goldstein et al., 1974; Gibbs et al., 1973; Six and Klug, 1973; Six, 1975), phage P4 is a helper-dependent phage that uses the late gene products of temperate phage P2 to encapsulate its own P4 double-stranded DNA. The P4 capsid is approximately one-third the volume of the P2 capsid (Inman et al., 1971) and harbours a genome also one-third its size (i.e. 11.624 versus 33.574 kb, respectively). As aforementioned, the P4 phage overexpresses the P2 prophage late genes (Six and Klug, 1973) without the P2 prophage being excised or replicated (Six and Lindqvist, 1971). Another characteristic of P4 is that, when a P2 prophage is not present in the host bacterial cell, P4 can still be maintained as a plasmid (Lindqvist and Six, 1971), which allows P4 to hijack a subsequent infection by a virulent P2 phage. Therefore, the viral cycle of phage P4 is a unique phenomenon in which one phage parasitises another to perpetuate itself, repurposing the gene products of the helper phage. While phage P2 constructs an icosahedral capsid (head) with T = 7 symmetry using the *gpN* capsid protein, the *gpO* scaffolding protein, and the *gpQ* portal protein, the presence of P4 drives these structural proteins into a smaller capsid with T = 4 symmetry. The regulation of this size transformation is facilitated by the P4-encoded protein *Sid*, which creates an external scaffold around the compact P4 procapsids (Dearborn et al., 2012). This capsid reduction restricts P2's larger genome from propagating while favouring the packaging of the smaller P4 genome. The P4 phage viral cycle is described in the literature (Lindqvist et al., 1993). This interplay lets P4 exploit P2 resources while preserving its unique life cycle traits. Since P4 can be maintained as a plasmid and depends on P2 for conditional propagation (i.e. using P2's late structural proteins for packaging and storage), it is feasible to use this phenomenon to produce transducing particles via P4's conditionally propagating capability. Moreover, a minimal essential region of P4 has been described (Lin, 1984; Ghisotti et al., 1990). One can thus engineer a "conditionally propagating transducing particle" with a P4-minimal construct, here referred to as "P4-min", measuring 7.190 kb and allowing the expression of the necessary gene products for fully functional P4 plus an additional capacity for a heterologous genetic sequence payload of up to 4.434 kb. This capacity parallels the full-size 11.624 kb of P4. A P4-min-based system can host a genetic device encoding antimicrobial-like molecules. This work illustrates a system that includes *the multi-lysin cassette*, a kanamycin-resistant marker, and a co-located P4 cos site spanning 4.151 kb. In this context, P4-min functions as a transducing particle capable of propagation only in the presence of P2. It thus reaches yields that are typical of natural phages ($\geq 10^8$ cfu/mL). Here, a transducing particle is defined as a viral particle that carries a plasmid encoding heterologous or synthetic genetic

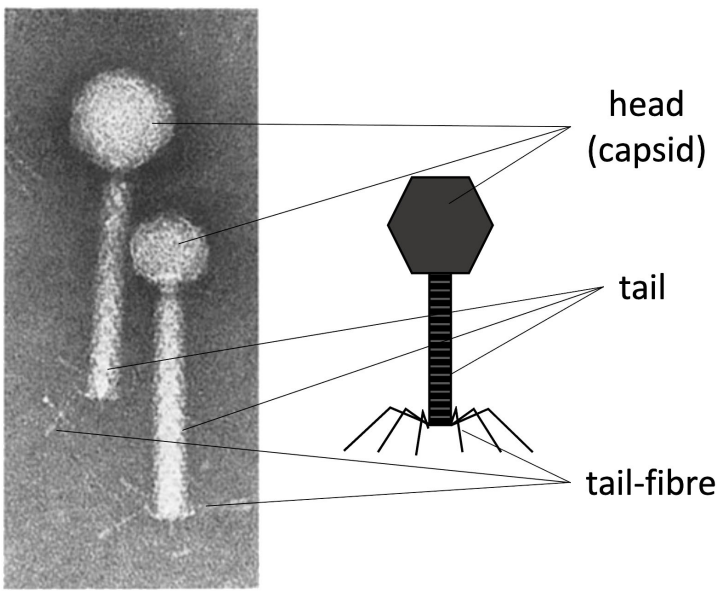

FIGURE 1
The characteristic protein structures in phages. *Left:* An electron microscope image of phage P2 (with a larger head) and P4 (with a smaller head). *Right:* A schematic labelling of the main protein structures in tailed phages. The capsid (head), the tail, and the tail fibres. The right side of the image was made by the author. Left side of the Figure was adapted with permission from (Goldstein et al., 1974), licensed under [6037081204133], [SPRINGER-NATURE].

material, along with a "cos site" acting as a "packaging signal", instead of the phage's own genome. Figure 2 summarises how the P2/P4 phages can generate transducing particles.

The main disadvantage of using helper P2 phages for transducing particle production is the contamination of the lysate with wild-type phages, which are self-replicating and highly propagative. Such contamination can arise from non-adsorbed helper phage and the packaging of competing viral genomes. Because the virus's DNA and the proteins needed for virion assembly are produced in the host cell, both the cosmid and the viral genome compete for packaging, yielding a mixture of transducing particles (plasmid/cosmid) and viruses (viral genome). Figures 2A, B show these scenarios. Using helper P2 prophages (i.e. lysogens) to produce transducing particles presents another drawback: the spontaneous induction of lysogenic cells into a lytic cycle occurs at a low frequency (Bertani, 1951). Temperate strains can be activated chemically (Endo et al., 1963) or by UV light (Baluch and Sussman, 1978; Berenstein, 1986), but each activator is phage-specific. For example, UV light can induce λ lysogens, but not P2 lysogens. In this regard, the epsilon (ε) gene product from natural P4 phage activates temperate P2 prophages (Liu et al., 1997). P2 (Lindqvist et al., 1993) "late genes" contribute to the production of the aforementioned phage structural proteins such as the capsid, the tail, and tail fibres (Figure 1) for its complete constitution as a virus (Kahn et al., 1991). In this light, transactivation of P2 late gene expression by P4 requires the P4 delta (δ) gene product and works even without P2 DNA replication (Halling and Calendar, 1990), benefiting P4 viral genome packaging over competing P2. Hence, P2 lysogenic strains can help produce phage-based transducing particles because inducers have been identified, and cosmid packaging can outcompete native viral genomes. Furthermore, temperate lysates become virus-free (Figure 2C) by *knocking out* the cos site of the temperate strain's genome, ensuring that only foreign cosmids (with the intact cos site) get packaged. In this work, the P4-EKORhE, a virus-free virus-like transducing particle production system based on P4's ability to hijack the P2 prophage's late structural proteins, is shown to deliver a multi-lysin cassette as a gene-delivered antimicrobial.

1.2 Phage lysins as a gene-delivered antimicrobial

The multi-lysin cassette is a combination of genetically encoded lysins designed for delivery via transducing particles. Phage lysins and lysis accessory proteins (e.g. holins and spanins) are natural effectors that disrupt bacterial membranes or cell walls to release phage progeny. Because these proteins typically target bacterial membranes and cell walls, they resemble membrane-disrupting antibiotics by compromising bacterial viability (Monnard and Walde, 2015). Phage satellite P4 host range is restricted to Enterobacteriaceae (Gjorgjevikj et al., 2025). In this sense, *Escherichia coli* K12 is used as a target because of its low biosecurity risk and its role as a model for more pathogenic strains, including *E. coli* K1, which can cross the blood–brain barrier in neonatal meningitis and is a known uropathogen (Møller-Olsen et al., 2018). Combining multiple lysins and lysis accessory proteins can strengthen antimicrobial effects, as seen previously with extracellular lysins (Budič et al., 2011). Here, however, the lysins are genetically encoded and expressed intracellularly in the target bacterium. Both MS2 gpL and PhiX174 gpE single-gene lysis proteins and the λ lysis system (LysS, LysR, and

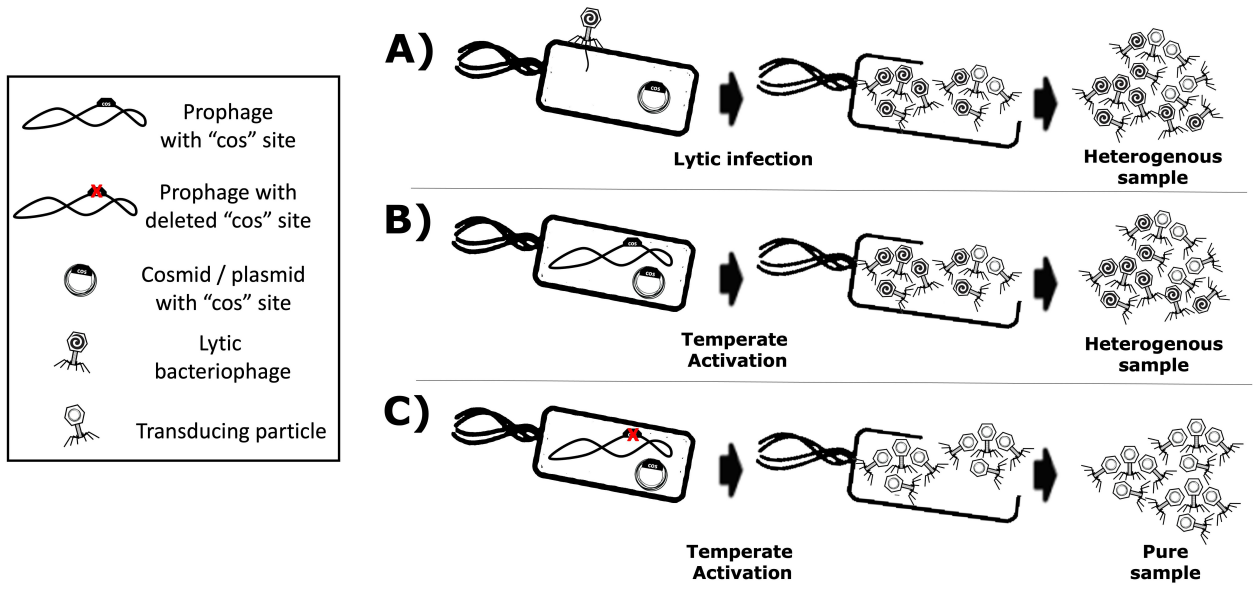

FIGURE 2
Production of transducing particles using lytic or temperate phages that use a cos site for packaging. Transducing particles are phage-based particles harbouring cosmids instead of phage genomes, which have been selected and maintained within host-producing strains. **(A)** Lytic phage production yields a mixture of phages and transducing particles. **(B)** Temperate phages with functional cos site also yield a mixture of phages and transducing particles. **(C)** A temperate phage with a *knocked-out* cos site yields a "virus-free" pure sample of transducing particles.

Rz) are used within a single cassette (Supplementary Section SS4.5). Figures 3 and 4 illustrate how these components function synergistically. In this work, a rhamnose-inducible, controllable, and conditionally propagating phage, the P4-EKORhE (Figure 5), is utilised to encode within its genetic cargo capacity, which is only limited by the *headful* size of its original genome, the multi-lysin cassette, as a means to test the use of a gene-delivered antimicrobial. Using a high-yield bioproduction protocol (Figure 6) of transducing particles encoding the multi-lysin cassette, these particles are then characterised for its effectiveness as an antimicrobial (Figure 4), using both pure bacterial cell cultures (Figure 7C) and a human model of phage infection in co-culture with A459 immortalised human epithelial cells (Figures 7D, E) used to corroborate the effectiveness of gene-delivered antimicrobials using P4-EKORhE in a more challenging biological environment. In this light, one of the novelties of the proposed approach is applying the concept of searching synergies among different lysins and lysis accessory proteins that act as they are meant to act: intracellularly, taking advantage of transduction as a gene delivery vehicle for the intracellular expression of effector proteins (i.e. the lysins and lysis accessory proteins, showcased in this work). Supplementary Figure S12 shows the first version of a functional cosmid, encoding the multi-lysin cassette, with a strong anhydrous tetracycline (aTc)-inducible promoter. Figure 3 shows a conceptual scheme of how the P4-EKORhE multi-lysins are employed as an antimicrobial therapeutic.

2 Results

2.1 The multi-lysin cassette

Figure 4 demonstrates the effectiveness of each lysin and its combined bactericidal activity. PhiX174 gpE is the strongest contributor to multi-lysin synergy. Figure 4 shows that the activation of lysis results in an antimicrobial effect, as observed over a 5-hour period. This (together with results demonstrated in Figures 5, 7) suggests that the multi-lysin cassette is a strong alternative to natural phages.

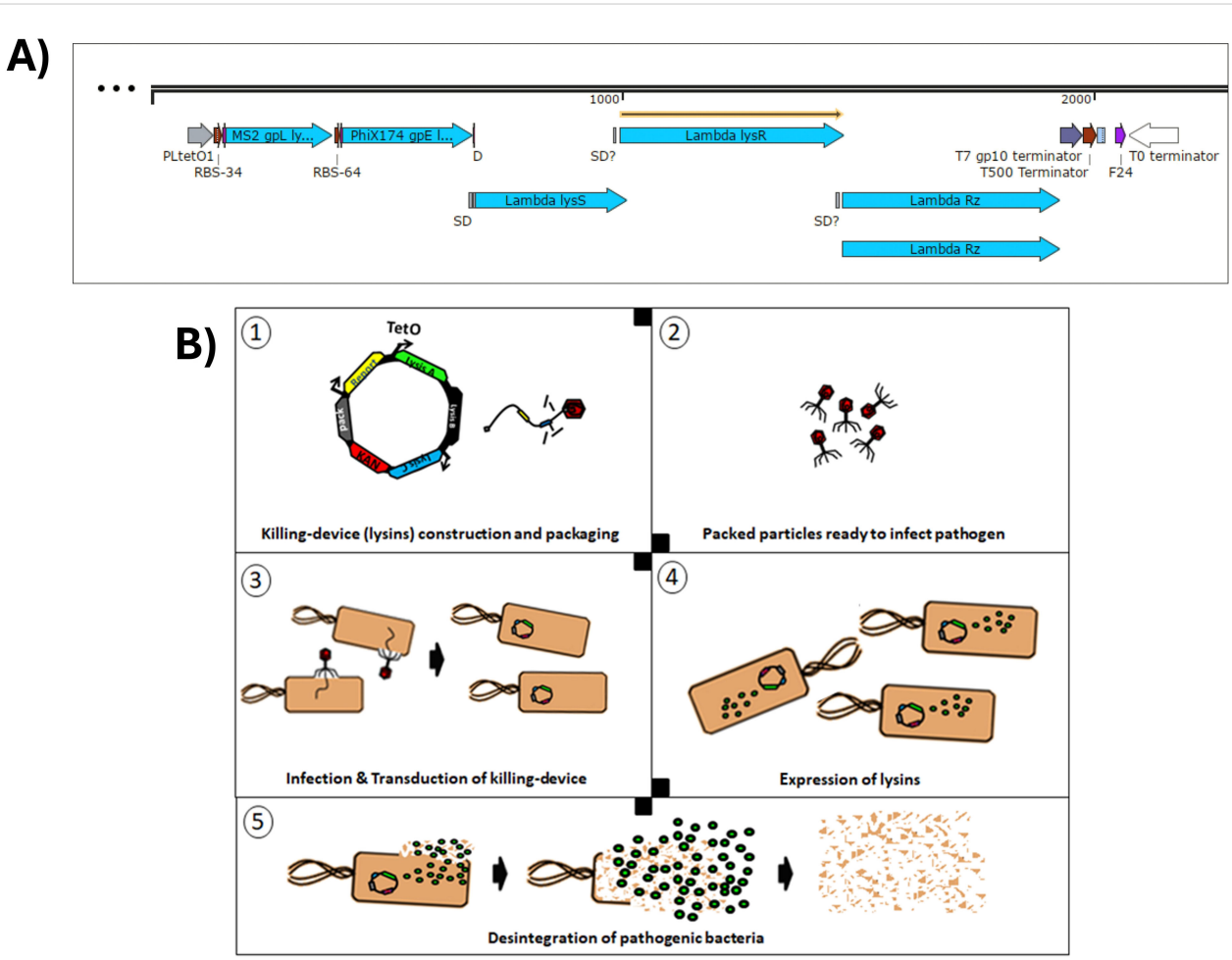

FIGURE 3
Conceptual scheme of the P4-EKORhE multi-lysin antimicrobial. **(A)** The multi-lysin cassette harbouring all lysins and lysis accessory proteins. The different encoded lysis and lysis accessory proteins used to construct the multi-lysin cassette. A study of the functionality of these circuits is presented in Figure 4. The "SD" and "SD?" labels contained within the construct are predicted "Shine–Dalgarno" sequences that correspond to the multi-cistronic nature of the λ phage lysis operon n (*lysS*, *lysR*, and *Rz*) and the likely presence of unidentified *cryptic promoters*. **(B)** Conceptual scheme of the P4-EKORhE multi-lysins as a genetically encoded antimicrobial therapeutic.

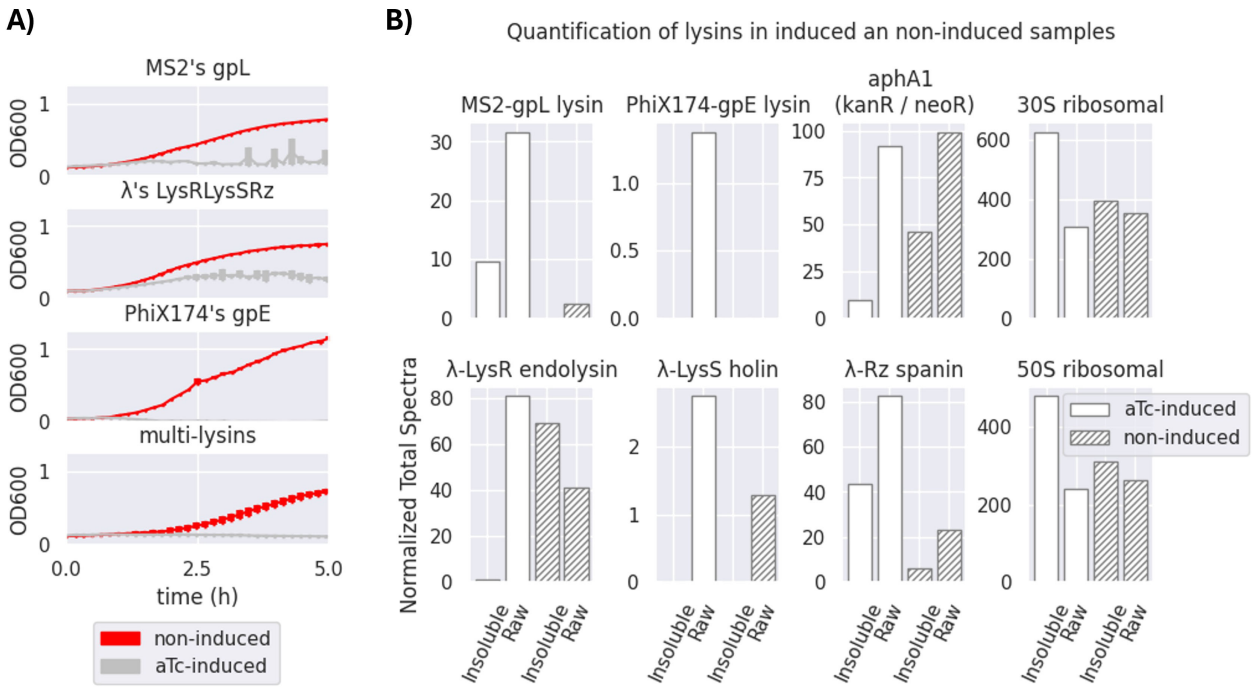

FIGURE 4
Effectiveness of a transformed multi-lysin cassette. **(A)** Optical density (OD_{600}) measurements of bacterial survival profiles in pure bacterial cell cultures of *Escherichia coli* DH5α Z1 showing the antimicrobial effect of the multi-lysin cassette (the bottom-most plot) and each of its contributors (MS2's gpL, λ's lysis cassette, and PhiX174's gpE; the top-three-to-bottom plots). The red lines represent the bacterial cells harbouring the multi-lysin cassette that have not been induced with anhydrous tetracycline (aTc). The silver lines represent bacterial cells harbouring the lysin cassette that have been induced with anhydrous tetracycline at the start of the culture. * A second replica is available in Supplementary Figure S1 of Supplementary Section SS2 for Replicas. The thickness of each line represents variability among the "n" samples using the standard deviation, where n = 3. **(B)** Normalised Total Spectra (NTS) obtained from a mass spectrometry (MS) analysis of four different samples (two induced and two non-induced, raw and insoluble phases) of bacteria containing the multi-lysin cassette. The Normalised Total Spectra include data that compute the peptides found with over 95% probability that belong to each of the lysin sequences studied. aTc-induced: The protein extract comes from bacteria for which cosmids containing the multi-lysin cassette have been activated by adding aTc (anhydrous tetracycline) to the culture media. Non-induced: The protein extract comes from bacteria for which cosmids containing the multi-lysin cassette have not been externally induced with aTc. Insoluble fraction: Protein fraction extracted from the pellet of the lysed cells. Raw fraction: Protein fraction extracted from samples containing both the supernatant and the pellet of lysed cells. For more details, see Supplementary Section SS3.

The controllable expression of the multi-lysin cassette relies on the tightly conditional expression of lysins upon the addition of aTc, which hampers the structure of the tetR repressor. In this regard, there is an ample variety of promoters available that are of diverse strengths in *E. coli* (Meyer et al., 2019). In this work, a strong aTc-repressible promoter (Debowski et al., 2013), for the tight and strong induction of the multi-lysin cassette, and a weaker, rhamnose-inducible promoter (Wegerer et al., 2008; Kelly et al., 2018), to control P4-EKORhE transducing particle production, were used. The weak rhamnose-inducible promoter has a low expression profile even during induction, compared with tetO1, which helps express ε at very small levels and mitigates the potential leakage by weakness rather than tightness (a particularity of the tetO1 promoter that was decisive for its use in lysin expression).

In Supplementary Figure S7, the function of the tetO1 promoter in conjunction with the tetR repressor is exemplified (Debowski et al., 2013). The rhamnose-inducible promoter, instead, works by a different mechanism related to glucose availability (Kelly et al., 2018). The "tetO1 promoter" (Debowski et al., 2013) is only repressed if utilised in "Z1 cells" containing the "tetR repressor". The Z1 cells used in this work were *E. coli* strains, such as DH5α Z1 or Marionette Z1. When the tetO1 promoter is present in bacterial cells not containing the Z1 cassette (e.g. the BW25113 cells), the promoter is not repressible; therefore, constitutive gene expression of the coding sequences downstream of the tetO1 promoter occurs. Since genetically encoded antimicrobials are to be delivered via bacteriophage-like transducing particles, it is important that during the production of transducing particles and the packaging of genetically encoded antimicrobials, a strong enough promoter be used (e.g. the tetO1 when used in Z1 cells). As shown in Supplementary Figure S7, the tetO1 promoter would repress the encoded genetic circuit in "production cells" harbouring the tetR repressor, which is what can be observed in non-induced samples in Figure 4. Conclusively, these can be safely used to produce high titres of transducing particles ready to package cosmids (i.e. plasmids with a packaging signal) containing an aTc-inducible lysin cassette without the risk of activating it, as is also demonstrated in Figure 5D.

Given that the multi-lysin cassette is delivered via P4-EKORhE transducing particles, a sufficiently strong promoter is essential during the production and packaging of this genetically encoded antimicrobial (e.g. the tetO1/aTc-inducible promoter used in Z1 cells). The tetO1/aTc-inducible promoter (PLtetO1 in Figure 3A) represses the encoded genetic circuit in "production cells" harbouring the tetR repressor. These cells can safely produce high titres of transducing particles ready to package P4-EKORhE cosmids encoding the multi-lysin cassette without the risk of premature activation. Supplementary Figure S12 shows the first functional version of the multi-lysin cassette under the tetO1 promoter, also used in the high-yield P4-EKORhE that appears in Figure 5. The multi-lysin cassette in this work combines three lysis systems from the PhiX174, MS2, and λ phages (Garrett and Young, 1982; Didovyk et al., 2017; Young et al., 1979; Hutchison and Sinsheimer, 1966; Atkins et al., 1979) (Supplementary Section SS4.5), expressed under a single promoter and sized appropriately for packaging in P4-EKORhE.

As seen in Figure 4, all three systems of lysins (MS2, λ, and PhiX174) seem to contribute noticeably to the multi-lysin cassette, with PhiX174 gpE being the most outstanding contributor. Proteomics analysis of lysins/lysis accessory proteins in induced and non-induced samples of the multi-lysin cassette is shown in Figure 4B. Four samples were analysed: two induced with aTc (both soluble and insoluble fractions, as well as insoluble-only fractions) and two non-induced samples (labelled as non-induced in the figure) also for both raw and insoluble fractions. Figure 4 shows the Normalised Total Spectra (NTS) of peptides corresponding to the lysins and lysis accessory proteins targeted in this work, with kanamycin-resistant aphA1, 30S, and 50S ribosomal proteins acting as positive controls for cosmid-borne and genome-borne expression. Supplementary Section SS3 further details peptide coverage for these MS samples (Supplementary Figures S5, S6). Figure 4 confirms the presence of cryptic promoters and Shine–Dalgarno (SD) sequences in the λ-lysis cassette (Figure 3A; Supplementary Figure S8). Peptides from λ-lysis cassette were detected in both induced and non-induced samples, with an important increase observed upon activation with aTc.

2.2 Construction of the P4-EKORhE

The virus-free, virus-like, conditionally propagating P4-EKORhE (a latinised transcription for P4-εKO-Rhε), which literally stands for "P4 epsilon (ε) knock-out rhamnose-inducible epsilon (ε)", is a bioengineered rhamnose-inducible P4-based system for the high-yield bioproduction of transducing particles presenting itself as a genome-minimised P4 (P4-min) phage with its *ε* gene *knocked out*, and a degenerate, codon-optimised *ε* expressed elsewhere under the control of a rhamnose-inducible promoter (Figure 5), which is in this work used to harbour the multi-lysin cassette (Supplementary Figure S12).

During construction, P4-min (from P4p05 to P4s04, Figure 5A or Supplementary Section SS8) was PCR-amplified and cloned together with the multi-lysin cassette to confer a selection marker (kanamycin resistance). Following successful selection with kanamycin, the genome-minimised P4 (P4min) was further amplified by PCR to produce a *knock-out* in the native *ε* gene coding sequence and to insert a codon-optimised *ε* that cannot recombine with the native gene. The whole *ε* gene, the target for the *knock-out*, was not fully removed; instead, a minimal deletion was introduced to avoid the potential disruption of P4 functionality. Ultimately, a final mutant was obtained with a stably *knocked-out ε* gene, and a construct was inserted containing a degenerate version of the *ε* gene downstream of the cos site (located away from the original position of the *ε* gene) under a rhamnose-inducible promoter. Therefore, P4-EKORhE differs from a natural P4 phage because it is a cosmid that 1) remains genome-minimised, 2) carries a selection marker, and 3) incorporates two *ε* gene sequences (with the native epsilon being non-functional and the inserted version fully functional), thereby preventing recombination. Figure 5 displays the final construct of P4-EKORhE harbouring the multi-lysin cassette. The P4-EKORhE genetic sequence was confirmed by analysing trace sequences from the assembled P4-EKORhE (Figures 5A, B), and the full sequence of the "stabilised form" of P4-EKORhE was obtained via whole-plasmid sequencing (Figure 5B); both sequences appear in Supplementary Sections SS8.5 and SS8.6. Figure 5C illustrates a scheme that shows how the controllable, gene-minimised P4-EKORhE produces transducing particles. The figure demonstrates that the system activates upon induction because P4-EKORhE encodes a synthetic *ε* coding sequence downstream of the rhamnose-inducible promoter.

2.3 High-yield bioproduction of transducing particles with P4-EKORhE

The use of the P4-EKORhE system for transducing particle production benefits from the controllable feature of its rhamnose-inducible synthetic *ε* cassette. However, optimising the bacterial cell culture conditions upstream, together with downstream processing that preserves particle integrity and maximises yield, remains essential. Figure 6 highlights the improvement obtained when the literature standard PEG8000 phage purification is replaced with an ultrafiltration protocol (Bonilla et al., 2016), and the culture medium is switched from Luria–Bertrani (LB) to Terrific Broth (TB). The non-propagating nature of transducing particles when used on target strains requires high concentrations sufficient to observe a bacterial count decrease on the optical density measurements (Figure 7) that usually start at the range of $10^{7-}10^{8}$ bacterial cells per millilitre when the optical densities are still close to zero. The controllability of P4-EKORhE enables the implementation of a specialised bioprocess in which continuously enriched phage lysates in a fed-batch fashion can be supplemented with growing cultures in parallel, successive batches of fresh Δcos-P2-c5545 Z1 cells harbouring P4-EKORhE (as shown in steps 5 and 6 in Figure 8). The process shown in Figure 6 yields at least 10^{9}

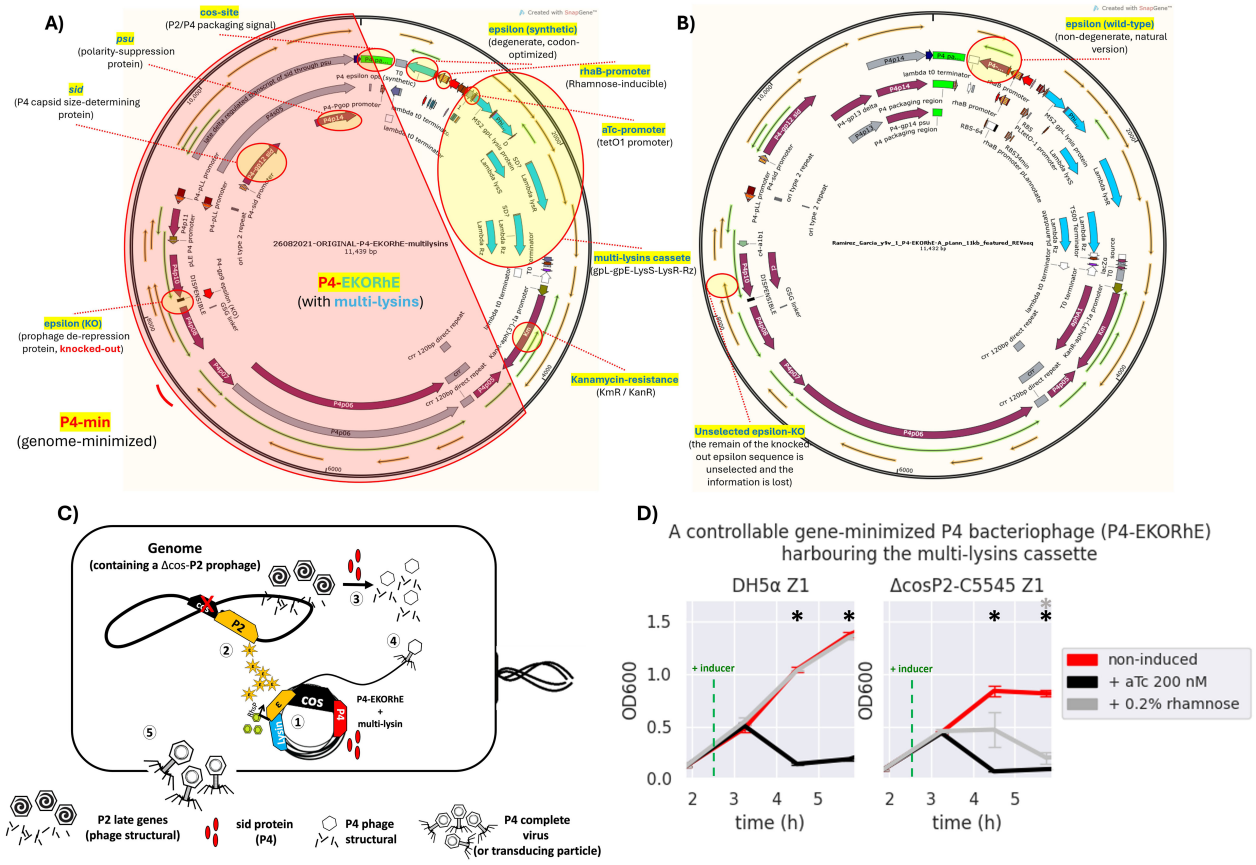

FIGURE 5
The bioengineered P4-EKORhE harbouring the multi-lysin cassette. **(A)** A kanamycin-selectable cosmid of 11,439 bp containing a genome-minimised P4 phage (P4-min, highlighted in red) that has a knocked-out version of the epsilon (*ε*) gene; an alternative functional synthetic, codon-optimised, and degenerate version of the *ε* gene; and the multi-lysin cassette harbouring the three systems of lysis from MS2, PhiX174, and *λ* phages. **(B)** The same cosmid after a few passages loses the dysfunctional *knocked-out wild-type* version of the *ε* gene, while the synthetic degenerate version gets restored to the sequence observed in the wild-type *ε* protein commonly seen in the natural P4 phage [see red circles for "unselected epsilon-KO" and "epsilon (wild-type)"]. The stable version of the P4-EKORhE is now 11,432 bp. Fully featured sequences of panels A and B can be found in Supplementary Sections SS8.5 and SS8.6, respectively. **(C)** A conditionally propagating and rhamnose-inducible P4 phage as a transducing particle. (1) The P4-EKORhE is replicated as a cosmid harbouring the multi-lysin cassette and expresses the *Sid* protein upon activation. (2) A Δcos version of the P2 prophage is inhibited by the activity of P4 but activates its late genes, with the delta (*δ*) gene product, which are the necessary structural proteins for P2. Additionally, the rhamnose-inducible *ε* gene product activates the self-replication of the Δcos version of the P2 prophage. (3) The *Sid* protein from P4 converts P2 heads into smaller P4 heads, thus further compromising P2 propagation. (4) P4 structural proteins package the P4 cosmid harbouring the multi-lysin cassette (i.e. or any other engineered circuit) or any other accessory cosmid. **(D)** Dynamics of the activation of the P4-EKORhE multi-lysin cosmids with inducer, aTc or rhamnose, in strains of *Escherichia coli*, transformed on *E. coli* DH5*α* Z1, or the engineered lysogen Δcos:TriR-P2-c5545 Z1. The sample size (n) used is n = 3; *p-value < 0.05, measured at the data points used after the addition of the inducer, using a standard t-test using SciPy libraries (see General Methods SS6.1).

infectious particles per drop of 10 µL used for the spot assay (Supplementary Figure S4), which translates to a lysate titre of approximately 10^{12} pfu/mL (i.e. a transduction capacity of 10^{12} cfu/mL), according to the formula below:

$$titer = dilution_{lysate} \cdot count_{plaques} \cdot volume^{-1}_{sample}$$

$$= pfu \cdot mL^{-1} \quad or \quad cfu \cdot mL^{-1}$$

Therefore, Figure 6 shows how the P4-EKORhE system can be optimised to yield 10^{12} cfu/mL of transducing particles by performing up to four enrichment cycles, utilising a nutrient-rich TB and the ultrafiltration protocol as a physical means of separation and concentration (Figure 8) of a high-yield virus-free lysate of transducing particles without P2 phage contamination (Supplementary Figures S3, S4).

2.4 Transduction of the multi-lysin cassette with P4-EKORhE

In Figure 7A, the antimicrobial potential of the multi-lysin cassette delivered by P4-EKORhE particles is demonstrated. The optical densities (OD_{600}) of a transduced bacterial culture were measured over 5 hours and compared with natural phages T4 and K1F using the same target bacteria (Figures 7B, C).

Figure 7 shows that P4-EKORhE multi-lysin particles exert an antimicrobial activity proportional to the multiplicity of infection

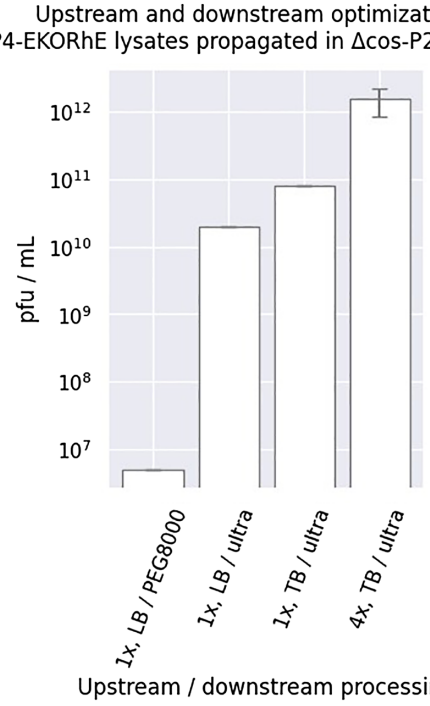

FIGURE 6
Upstream and downstream optimisation of P4-EKORhE. Different yields were obtained when using P4EKORhE according to the upstream and downstream optimisation. In regard to upstream optimisation, lysates were produced using either one or four enrichment cycles (i.e. 1× or 4×) using Luria–Bertrani (LB) or Terrific Broth (TB) broth. In regard to downstream optimisation, lysates were concentrated using either 10% PEG8000 or molecular weight cut-off ultrafiltration. The plaque-forming units are taken from the plates shown in Supplementary Figure S4. The sample size (n) used is n = 1, except for "4×, TB/ultra", which has n = 3.

(MOI). In particular, effective activity was observed at an MOI of 10. In the positive control, where the tetR repressor was inactivated with 200 nM aTc, the antimicrobial response was distinctive compared to the negative control, in which active tetR repressor significantly inhibited lysin expression. The target strain's response matched or exceeded that of the positive control over the 5-hour measurement period.

2.5 The P4-EKORhE on A549 tissue cultures as a model of phage infection

Experiments measuring optical cell densities in pure bacterial cultures were used as an initial assessment of transducing particle effectiveness, alongside natural phages. However, to develop a potential antimicrobial therapeutic, it is valuable to replicate experimental conditions similar to real scenarios. Therefore, an infection model was employed that uses A549 human lung epithelial immortalised cells to further assess the capacity of P4-EKORhE encoding the multi-lysin cassette to function as an antimicrobial in a more complex environment.

In Figure 7D, the ratio of bacteria to nuclei is demonstrated from images taken in two experiments: one where 100 µL of an SM2 buffer solution containing P4-EKORhE transducing particles harbouring the multi-lysin cassette was supplemented after 1 hour of bacterial incubation on the A549 cell layer and another where 100 µL of blank SM2 buffer was added instead. The figure reveals that the differences in bacterial count after 1 hour of bacterial growth, followed by 2 hours post-treatment with P4-EKORhE, indicate the system's ability to deliver the multi-lysin cassette in a complex environment. Figure 7D shows a remarkable difference in average bacterial counts between samples treated with P4-EKORhE particles in SM2 buffer (target samples) and those treated with SM2 buffer only (negative control). However, the significance analysis for a sample size (n) of n = 6 yields only p = 0.31, suggesting the need for further optimisation or larger sample sizes to substantiate the observed differences. The images in Figure 7E further illustrate this remarkable difference in averages, and additional images used for bacteria/cell nuclei counts are available in Supplementary Figure S13 for target samples and Supplementary Figure S14 for negative controls.

In the context of evaluating the multi-lysin cassette as a gene-delivered antimicrobial, these results demonstrate the potential of P4-EKORhE as a high-yield transducing particle bioproduction system capable of delivering a genetically encoded antimicrobial (the multi-lysin cassette) in a human cell culture infection model, thereby corroborating the results obtained from pure bacterial cultures.

3 Discussion

3.1 Effectiveness of the multi-lysin cassette

In regard to the effectiveness of the multi-lysin cassette, Figure 4 suggests that the activation of lysis leads to an antimicrobial effect that is shown over the period of 5 hours, which suggests this device as a powerful alternative to natural phages because of the observed decrease in bacterial cell optical densities.

The results demonstrated in Figure 4 indicate that the λ-lysis cassette and MS2 gpL have moderate but detectable activities even before induction, likely due to the accumulation of gene products (LysS holin/antiholin, Rz and Rz1 spanins, and the LysR endolysin) over time. Both MS2 gpL and PhiX174 gpE appear only in aTc-induced samples, consistent with the absence of cryptic promoters or SD sequences upstream of their respective coding sequences (Supplementary Figure S8). The constitutive expression of LysS and LysR proteins, as well as Rz, can be explained by the presence of a cryptic promoter upstream of the potential SD-like sequence "GGAAGGAG" at the −3 position of PhiX174 gpE, or from upstream cryptic promoters in the sequences *lysS* and *Rz* (found exclusively in non-induced samples) (Supplementary Section SS8). Figure 4B confirms cryptic promoters and SD sequences, evidencing their presence when the cosmid is not activated with aTc. However, due to the minimal contribution of these cryptic

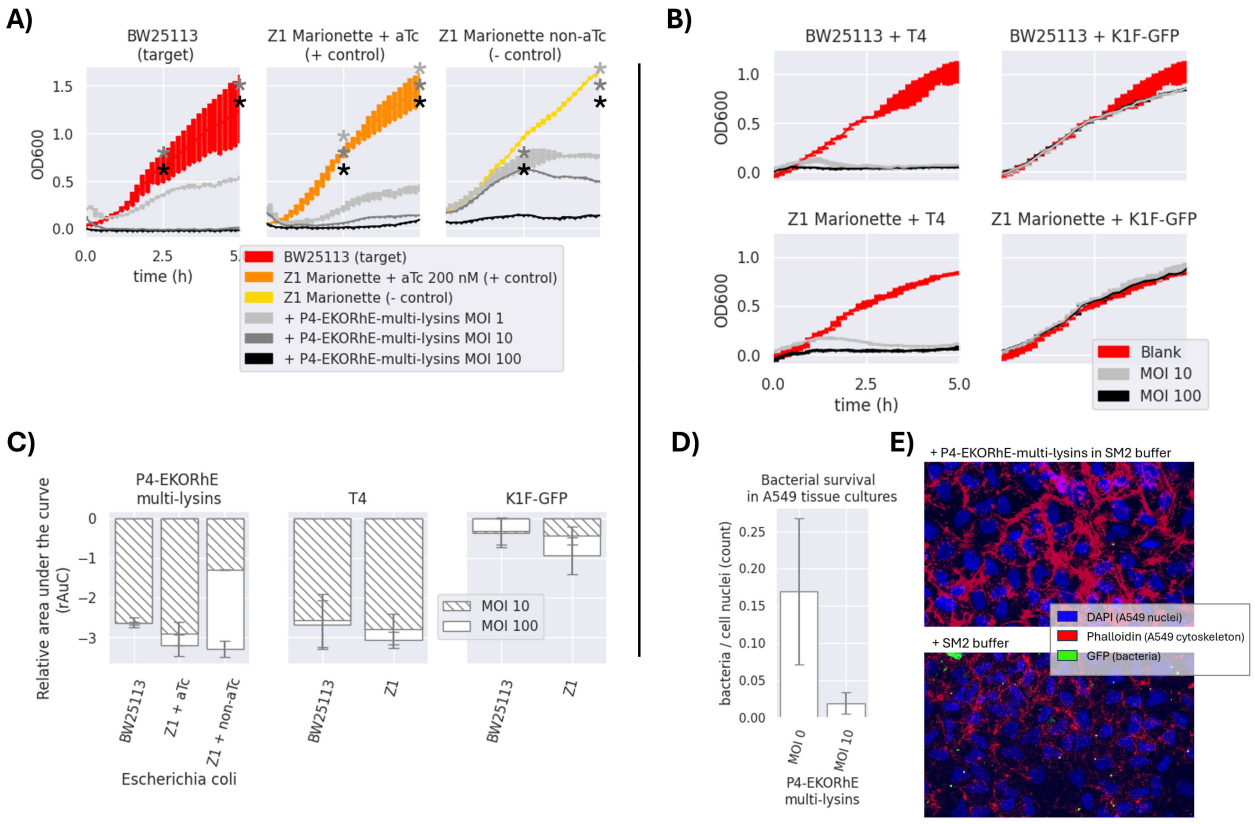

FIGURE 7
(A) Antimicrobial activity of P4-EKORhE multi-lysins. Optical density measurements of the target and control *Escherichia coli* strains, i.e. BW25113 and Z1 Marionette, respectively, when exposed to P4-EKORhE multi-lysin particles at different multiplicities of infection (MOIs). No selection antibiotics were used for the realisation of these experiments. **(B)** Antimicrobial activity of natural enterobacteriophages to their respective hosts. Antimicrobial activity of enterobacteriophages to their respective target and control *E. coli* strains, i.e. BW25113 and Z1 Marionette, when exposed to natural enterobacteriophages containing a replicative virus at different MOIs. For a replica of the same set of experiments, see Supplementary Figure S2 in Supplementary Section SS2 for Replicas. The thickness of each line represents variability among the "n" samples using the standard deviation, where n = 3. **(C)** Relative area under the curve of P4-EKORhE multi-lysins, T4, and K1F-GFP at MOIs of 10 and 100 on *E. coli* strains BW25113 (target) and Z1 Marionette (+/– control). rAuC(MOI = 0) = 0 ± 1. The sample size (n) is n = 2 from the results obtained in the two different replicas in Figure 7 and Supplementary Figure S2, which contains n = 3 for each measure of time (total n = 6). The rAuC has been integrated from 0 to 5 hours in all cases. **(D)** The differences in bacterial count following treatment with P4-EKORhE harbouring the multi-lysin cassette on A549 cell tissue at an MOI of 10 versus with a blank solution (MOI = 0) of SM2 buffer, following an immunohistochemistry fluorescence image analysis. **(E)** Immunohistochemistry fluorescence image analysis on a sample infected with GFP-fluorescent bacteria treated with P4-EKORhE harbouring the multi-lysin cassette versus the blank solution of SM2 buffer. The sample size (n) used is n = 7 for the control, while n = 6 for the target. The p-value for the difference between the two samples is p = 0.31. The images used to count for the results shown in panel D can be found in Supplementary Section SS5 for immunohistochemistry imaging. * means p-value < 0.05.

elements (especially for PhiX174 gpE), they do not impede the system's use for transducing particle production, as shown in Figure 5C. In contrast, MS2 gpL and PhiX174 gpE are only present in aTc-induced samples, supporting their reliance on induction.

The hypothesised mechanism for the synergistic lysis dynamics of the multi-lysin cassette is as follows (refer to Supplementary Section SS4.5 for a comprehensive discussion): 1) λ's LysS (UniProt Consortium, 2024d) accumulates in the cytoplasm and, upon reaching critical concentration, forms pores in the cytoplasmic side of the bacterial membrane (White et al., 2010). 2) This pore formation facilitates the intrusion of λ LysR endolysin (White et al., 2011; UniProt Consortium, 2024c), along with single-gene lysins MS2's gpL (UniProt Consortium, 2024b) and PhiX174's gpE (UniProt Consortium, 2024a), which disrupt the membrane (Bernhardt et al., 2002; Orta et al., 2023). 3) λ's Rz (UniProt Consortium, 2024e) and Rz1 (UniProt Consortium, 2024f) then deliver the final blow after the membrane is disrupted (Zhang and Young, 1999; Berry et al., 2012). This lysis is observed in non-aTc-induced (non-induced) samples (from cryptic promoter/SD sequences allowing λ-lysis cassette expression), suggesting an automatic activation of lysis when the accumulation of gene products occurs. The results confirm that the activation of the multi-lysin cassette with aTc corresponds to the presence of lysins, lysis accessory proteins, and antimicrobial activity as shown in Figure 4.

Regarding the effectiveness of using lysins, this work demonstrates that the multi-lysin cassette—encoding a combination of lysins and lysis accessory proteins (such as holins and spanins)—constructs a genetically encoded antimicrobial with synergistic effects by activating multiple lysis mechanisms. The results obtained suggest that the incorporation

of additional kill switches, such as nuclease elements (e.g. CRISPR-Cas9) (Singh et al., 2017) or alternative growth inhibitors that target divergent bacterial survival pathways, could further enhance the cassette's potency.

3.2 High-yield bioproduction with P4-EKORhE

The assessment of the capacity of P4-EKORhE for the production of transducing particles, shown in Figure 5D, depicts the dynamics of P4-EKORhE carrying the multi-lysin cassette. The data show that this production system represses phage production when rhamnose is absent (while maintaining 50 µg/mL kanamycin in the culture) and activates fully when 0.2% (w/v) rhamnose is added. This work highlights the characteristic feature of P4-EKORhE for controllable propagation (Figures 5, 6, 8), which is a milestone for bioproduction because 1) it enables the delay in the activation of phage bioproduction during the exponential phase to maximise bacterial cell densities and thus phage yields and 2) it forcefully activates phage bioproduction through ϵ inducible heterologous expression. As expected, the P4-EKORhE propagates only in Δcos:TriR-P2-c5545 Z1 cells since no ε gene activation was observed in DH5α Z1 cells upon rhamnose treatment. Instead, P4-EKORhE remains repressed in the absence of rhamnose and becomes fully inducible when 0.2% (w/v) rhamnose is added. Moreover, a notable drop in OD_{600} was observed upon the addition of aTc to the production culture due to the controlled activation of the multi-lysin cassette. Figure 5D demonstrates that although repression of P4-EKORhE is not absolute, it sustains a stable culture suitable for high-yield bioproduction. This stability allows for the maintenance of P4-EKORhE, alongside other cosmids, within a production strain, such as Δcos:TriR-P2-c5545 Z1, using a transformation protocol and to store the strain in glycerol stocks at −80°C for later expansion. The frozen strain can then be used as a master seed for future culture expansion and further induced with 0.2% (w/v) rhamnose to produce a new batch of P4-EKORhE transducing particles. In this way, the repressible capability of P4-EKORhE allows for an easier and more reproducible production of P4-based transducing particles. Conclusively, the bioengineered P4-EKORhE, a minimised, controllable, and conditionally propagating phage that employs temperate P2 phages with *knocked-out* cos sites, produces virus-free P4-like transducing particles at remarkably high yields (ranging from 10^6 to 10^{10} pfu/mL) while eliminating infectious wild-type P2 or P4 phages. The ε gene was used as a transactivator to exploit natural P4 phage proteins that activate temperate P2 phages, thereby enabling the reproducible and controllable production of transducing particles. The further downstream processing optimisations (using nutrient-rich TB and an optimised hybrid fed-batch process) achieve yields greater than 10^{12} pfu/mL, demonstrating that the P4-EKORhE system provides an optimal procedure for the high-yield production of transducing particles.

3.3 Transduction of the multi-lysin cassette with P4-EKORhE

Figures 7A–C confirm the initial characterisation of the multi-lysin cassette in Figure 4. Notably, increasing the MOI from 10 to 100 for natural phages did not produce an appreciably different result, even though an MOI of 10 produces transient growth at approximately 1 hour post-infection, while P4EKORhE delays growth until after 2.5 hours, as reflected in the relative area under the curve (rAuC). Moreover, at an MOI of 100, the antimicrobial activity in negative control strains of *E. coli* Marionette, where the tetR repressor remains active in the absence of aTc, suggests an additional mechanism involved in the lysis that goes beyond the expression of lysins.

To facilitate discussion, Figure 7C uses the rAuC for the growth curves in Figures 7A, B to compare antimicrobial effectiveness among samples and MOIs for both P4-EKORhE and T4/K1F-GFP phages. These results show that infecting *E. coli* BW25114 with T4 produces a response similar to that observed with controllable P4-EKORhE. Of note, K1F phages specialise in infecting encapsulated strains of *E. coli* (Møller-Olsen et al., 2018), so their effectiveness against normal strains such as BW25113 is expected to be compromised, as shown by the figure and corresponding rAuC values.

Regarding the effect of MOI on the bacteriostatic activity of P4-EKORhE encoding the multi-lysin cassette, Figure 7A and literature (Abedon, 1994) indicate that at high MOIs (100), "lysis-from-without" may contribute to the observed results, although the multi-lysin cassette plays the primary role at lower MOIs (10). This effect becomes apparent in the negative control results at MOIs of 100 without aTc. Figure 7C shows that the differences in rAuC values for MOIs of 10 versus MOIs of 100 with P4-EKORhE do not scale equally between BW25113 and the Z1 controls, suggesting that "lysis-from-without" does not fully account for the differences. However, the non-induced Z1 strains display a notable increase in antimicrobial effectiveness only at an MOI of 100, which may result from "lysis-from-without" if the tetR repressor remains fully functional in the absence of aTc. An alternative, although less likely, would be the effect of tetR repressor depletion. At high MOIs (e.g. 100), a single bacterial cell may be transduced multiple times, exhausting its tetR repressors and leading to leaky gene expression of the multi-lysin cassette. This phenomenon could contribute to the bacteriostatic effect observed at high MOI but is not apparent at lower MOIs of 10 (compare the rAuC and the bacteriostatic times for the "Z1 + aTc" versus the "Z1 non-aTc", when using the P4-EKORhE, in the rAuC plot in Figure 7C).

Whether high MOIs cause effects via "lysis-from-without" or by tetR repressor depletion remains speculative. Further experiments, for example, using P4-EKORhE carrying blank genetic sequences, could clarify this contribution. Based on these data, it is possible to conclude that the substantial differences between aTc-induced and non-induced Z1 cells cannot be solely attributed to the multi-lysin cassette, as antimicrobial effectiveness (albeit milder) at low MOIs

(10) is still observed, which is less pronounced than in the "Z1 Marionette + aTc" positive control.

If "lysis-from-without" occurred at lower MOIs, the 2.5-hour lysis delay in the negative control (Figure 7A) would not be observed. In both replicas (Figure 7A and Supplementary Figure S2) for non-activated Z1 cells infected with P4-EKORhE, a mild antimicrobial activity at an MOI of 100 (indicated by a bump in growth at 2.5 hours starting at time = 0), which suggests that the effect in the negative controls at high MOIs likely results from "lysis-from-without" or tetR repressor depletion, was observed.

These data underscore the potential of P4-EKORhE particles as an antimicrobial alternative to natural phages. Figures 7B, C show that BW25113 and Z1 Marionette, when infected with T4 phage, fail to grow during the 5-hour measurement period, similar to transduction with P4-EKORhE. These results support the feasibility of using transducing particles as an alternative to natural phages, with the advantage of full control over lysis mechanisms and without relying on viral replication in target bacteria.

The transduction of the multi-lysin cassette via P4-EKORhE produces an antimicrobial effect that is not compromised but rather enhanced compared to the results obtained in transformed bacterial cell cultures. The results obtained from pure bacterial cultures closely resemble those found with natural phages such as T4, highlighting the clinical potential of both P4-EKORhE and the multi-lysin cassette. Moreover, these data indicate that antibiotic marker selection (used to maintain the transduced cosmids within bacterial hosts) does not impair performance at MOIs of 10 or 100, suggesting that antibiotic co-delivery is unnecessary for achieving similar or superior bacteriostatic effects compared to systems where kanamycin (50 µg/mL) is added before aTc activation. An improved antimicrobial effect can be attributed to multiple transducing particles that likely transduce cosmids multiple times during the initial hours of infection. Additionally, at high MOIs (100), the phenomenon of "lysis-from-without" may enhance the effect, as indicated by comparisons between positive and negative control outcomes with P4-EKORhE. The use of P4-EKORhE harbouring the multi-lysin cassette in A549 cell cultures contaminated with *E. coli* shows (despite a p-value of 0.31) a notable reduction in average bacterial counts that correlates with results from pure bacterial cell cultures. The findings invite further experiments at higher MOIs, with additional replicas and testing on different cell lines, where a clearer difference between treated and untreated samples may be observed, especially considering that P4-EKORhE does not propagate in target host bacteria.

Ultimately, these data demonstrate that encoding the multi-lysin cassette in a cosmid packaged within a P4-EKORhE system produces a non-replicative, yet conditionally propagable, finely tunable antimicrobial agent as effective as natural phages. Therefore, this work provides a comprehensive proof-of-concept gene therapeutic where a phage-based transducing particle with a genetically encoded antimicrobial offers an alternative to natural phages using P4-EKORhE as gene delivery vehicle to produce high yields of transducing particles for delivering the multi-lysin cassette into target bacteria—both in pure bacterial cultures and in co-cultured using A549 human epithelial cell cultures infected with *E. coli*. This approach opens the door to novel and effective antimicrobial therapeutics targeting a range of pathogenic bacterial strains.

4 Materials and methods

4.1 General materials

All chemicals were purchased from Sigma-Aldrich (now Merck, Kenilworth, NJ, USA) or Thermo Fisher Scientific (Waltham, MA, USA) unless stated otherwise. Primers and gene fragments were commercially synthesised by Integrated DNA Technologies (IDT; Coralville, IA, USA) or GENEWIZ (South Plainfield, NJ, USA). The stock and working concentrations of antibiotics used in this work are stated in Supplementary Table S1. All strains used throughout this work are stated in Supplementary Table S3. For the construction of genetic devices (Supplementary Section SS4 and SS8), Q5 High-Fidelity Polymerase, Phusion High-Fidelity DNA Polymerase, and NEBuilder HiFi DNA Assembly Master Mix were purchased from New England Biolabs (NEB; Ipswich, MA, USA) and used according to protocol. All enzymes were stored at −20°C and used with the buffers provided according to the manufacturer's instructions.

4.2 Mass spectrometry and proteomics

In order to ascertain that bacterial cells are eliminated upon the activation of the multi-lysin cassette when using aTc, it is useful to identify these lysins on via Western blotting only when the circuits are activated in order to relate the correspondence between gene expression and a decrease in the optical cell densities, as shown in Figure 4. However, because the encoded lysins included in the multi-lysin cassette are many (i.e. up to six different coding sequences, Supplementary Figure S12), when constructing the system, it was unfeasible to include *Histidine-tags*, which would otherwise facilitate its purification and identification because having repetitive DNA sequences within the cassette would generate genetic stability problems in the cosmids encoding repetitive sequences, which would lead to the impossibility of gene synthesis using a commercial supplier. Therefore, in order to demonstrate the presence of the lysins, upon activation with aTc, and to relate its expression to its antimicrobial effect, an sodium dodecyl sulfate polyacrylamide gel electrophoresis (SDS-PAGE) gel for expression verification (Protocol SS6.12), and later extraction for mass spectrometry (MS) analysis, was employed after the protein extraction of experimental samples (Protocol SS6.11). However, because bacterial cells would be disrupted upon the activation of the lysin cassette, an SDS–PAGE gel did not yield bands sharp enough to be distinguished by raw inspection (i.e. to distinguish them among the

remaining proteins in the lysate). Instead, a lower fraction band of the SDS–PAGE gel was used for protein extraction and MS, confirming the presence of the lysins and lysis accessory proteins showcased in this work (Figure 4). To prepare samples for MS (Supplementary Section SS3), induced and non-induced protein lysates from a culture of Marionette Z1 bacterial cells containing a P4-EKORhE cosmid, i.e. in Figure 5, which harbours the aTc-inducible multi-lysin cassette showcased in this work, was processed and purified using a standard protein extraction protocol (see Protocol SS6.11). Two types of lysates were produced, one coming from the pellet, or insoluble phase (i.e. as lysins are expected to act within cell walls and membranes), and another that was considered a "raw lysate", i.e. containing both soluble and insoluble phases of the lysate. Four different samples of pure bacterial cell cultures (*E. coli* Z1 cells) transformed with the multi-lysin cassette cosmid were grown in a 1-mL Eppendorf tube at 37°C under shaking conditions until reaching the exponential growth phase (approximately 0.4–0.5 OD_{600}). Subsequently, two of the samples were aTc-induced with 200 nM (Zhang and Poh, 2018) of anhydrous tetracycline and grown for a further 2 hours to allow for the lysis of the bacterial cell culture. The bacterial cell cultures were treated with Lysis buffer (50 mM Tris-HCl, 150 mM NaCl, 1% Triton X-100, and 5 mM EDTA) and sonicated to make sure both induced and non-induced samples were treated equally and also so that non-induced samples were indeed lysed (see Protocol SS6.11 for more details).

4.3 Preparation of optical density measurements

In order to ascertain the antimicrobial effectiveness of the P4-EKORhE transducing particles encoding the multi-lysin cassette (Figures 7A, B), replicas of 96-well plates were utilised. For each well on a 96-well plate (Cellstar Multiwell Plates, Sigma-Aldrich), 100 µL of bacterial culture of *E. coli* at an OD_{600} = 0.1 was dissolved in doubly concentrated LB media and half diluted with an additional 100 µL of either an SM2 buffer solution supplemented with P4-EKORhE multi-lysin transducing particles or T4 or T7 phages (at MOIs of 10 or 100) or with an SM2 buffer only solution for blanks (i.e. for MOI = 0). The plates were measured using a plate reader to measure optical densities at approximately 600 nm to determine bacterial cell densities over time. When the bacterial cells being tested were the Z1 cells, and there was the intention to activate the multi-lysin cassette upon infection with P4-EKORhE, anhydrous tetracycline was added at a concentration of 200 nM (Zhang and Poh, 2018). For the transformed multi-lysin cassette experiments (Figures 4, 5D), the same methodology was employed, but without doubling LB medium concentration and without adding any SM2 buffer solutions, kanamycin (50 µg/mL) was used instead to recover the cells after cosmid transformation and selection before activation. Before activation, cosmid-harbouring cells were resuspended in LB media, the multi-lysin cassette was activated using anhydrous tetracycline (aTc, 200 nM) (Zhang and Poh, 2018), and L-rhamnose was added at a concentration of 0.2% (w/v) (Wegerer et al., 2008).

4.4 Relative area under the curve as antimicrobial effectiveness

For a more accurate comparison between the antimicrobial effect of the P4-EKORhE transducing particles harbouring the multi-lysin cassette with the antimicrobial effect of natural phages T4 and K1F-GFP, the rAuC values from the OD_{600} plots over the time span of 0 to 5 hours were extracted for all plots. The rAuC was plotted using the area under the curve (AuC) obtained using the scripted def AuC(x, y): function shown below of the non-induced or non-transduced (i.e. MOI = 0) sample and using it to subtract the mean values of the induced samples and the standard deviation normalised (by dividing its values) from the blank experiments with non-transduced or non-infected bacterial cells. It is understood that rAuC(MOI = 0) = 0 ± 1, i.e. for MOI = 0, the rAuC = 0 with an absolute standard deviation of 1. Therefore, MOIs of zero were not included in the rAuC plots, as these are a relative measure. For the integration of each of the curves from the corresponding plots used to obtain the values of AuC, which can later be used to compute the rAuC as aforementioned, the trapezoid rule was used to interpolate the area under the curve using the equation encoded in the following script:

```
0  def  AuC(x, y):
1    sum = 0
2    for i in range (1, len(x))
3      h = x[i] − x[i − 1]
4      sum+ = h⋆(y[i − 1] + y[i])/2
5    return sum
```

where x is the time and y is the point value of OD_{600} over time, which form the basis of the total sum of the area under the curve against the x-axis from x = 0 (i.e. time = 0) until the final value of x.

4.5 Preparation of animal tissue cultures for transduction

In regard to the mammalian cell culture for the transduction of co-cultured target bacteria, cell lawns of A549 cells (A549—ATCC CCL-185) were cultivated. The A549 cells were cultured using a base medium F12/K (Gibco, Grand Island, NY, USA/Invitrogen, Carlsbad, CA, USA) with 10% foetal bovine serum (FBS) added to the base medium with a standard amount of penicillin/streptomycin (P/S), incubated at 37°C with 5% CO_2. The A549 cells were seeded in T25 flasks until they were transferred to 6-well plates (Cellstar Multiwell Plates, Sigma-Aldrich). When the growing A549 cells were transferred to the 6-well plates, using 2 mL of media per well, these were grown on top of microscopy coverslip slides that have been deposited on each of the 6-well plates so as to be able to remove the coverslip slides for later preparation,

following an immunohistochemistry protocol, for fluorescence imaging using DAPI, phalloidin, and a green fluorescent protein (GFP) enhancer to count bacterial cells (i.e. transformed with a GFP plasmid) alongside cell nuclei (stained with DAPI) surrounded by the cell cytoskeleton (stained with phalloidin). Once the 6-well plate with the lawn of A549 cells was grown to approximately 90% confluency, the media were changed with 2 mL Leibovitz CO_2-supplemented media (L-15 Medium, Sigma-Aldrich) with 10% FBS only, without antibiotics, before adding bacteria to the media. Following it, 100 µL of bacteria at an OD_{600} of 0.1 was added to the media, grown, and incubated at 37°C for 1 hour. After that, either 100 µL of a particular SM2 buffer solution supplemented with P4-EKORhE transducing particles harbouring the *multi*-lysin cassette at an MOI of 10 or 100 µL of a blank solution of SM2 buffer (i.e. for MOI = 0) was added to each well. Further incubation for 1 hour was applied before removing the media and starting the following immunohistochemistry protocol. For the immunohistochemistry protocol, which was adapted from the literature (Møller-Olsen et al., 2018), the liquid phase of the cell cultures grown in the 6-well plate was removed by aspiration. The 6-well plate was placed under the fume hood, and cells were fixed by adding 500 µL of a solution of 4% paraformaldehyde (PFA) before placing the plate on ice for 15 minutes. The liquid was again removed from the plate, and its wells were washed three times with phosphate-buffered saline (PBS) for 5 minutes each time. The cells were then permeabilised with 500 µL of ice-cold PEM/0.05% saponin [PEM Buffer: 0.1 M PIPES/1,4-piperazinediethanesulfonic acid, piperazine-1,4-bis(2-ethanesulfonic acid), piperazine-*N*,*N*′-bis (2-ethanesulfonic acid), 5 mM EGTA, and 2 mM magnesium chloride], brought to pH 6.8 using a NaOH solution, and later aspirated and washed three times with PBS for 5 minutes. The remaining cells on each well were aspirated before being incubated for 15 minutes, at room temperature, with 500 µL of a 50-mM solution of ammonium chloride. The wells containing the coverslip slides with the cells were then aspirated and washed once for 5 minutes with PBS/0.05% saponin. Subsequently, 40 µL of a mixture that contains 300 µL of 0.05% saponin, 7.5 µL of phalloidin, and 1.5 µL of a GFP enhancer was added to each of the six wells of the plate and incubated for 45 minutes in the dark. The wells were then washed twice for 5 minutes with PBS/0.05% saponin and once with PBS. After aspiration, a drip of Fluoroshield (Fluoroshield™ with DAPI, Sigma-Aldrich) was added to each coverslip glass slide in each well of the 6-well plate. The coverslips were then delicately rinsed with water before being put on microscope slides. The microscope slides with the coverslips were then allowed to dry in the dark, and after sealing with CoverGrip (CoverGrip™, Biotium, Fremont, CA, USA) sealant, they were finally stored at 4°C until microscopy imaging. For the microscopy (ZEISS Celldiscoverer 7—Automated Live Cell Imaging, Oberkochen, Germany), images were taken at random, and images where more than 60 nuclei per image could be counted were taken to ensure the homogeneity of the samples from which imaging was performed. After obtaining the images, bacteria were counted in each image with respect to the number of nuclei (blue nuclei stained with DAPI), together with bacteria expressing GFP (green dots stained with GFP enhancer).

4.6 Upstream optimisation and downstream processing with P4-EKORhE

For the production of P4-EKORhE-based transducing particles harbouring the multi-lysin cassette, several protocols were tested, which have led to different results. The outputs of such protocols are shown in Supplementary Figure S3.

The proposed protocol was established for producing transducing particles by growing an overnight (O/N) culture of *E. coli* Δcos:TriR-P2-c5545, which was pre-transformed with a P4-EKORhE multi-lysin cosmid in culture media of LB with 50 µg/mL kanamycin (to select for the selection marker in the P4-EKORhE) and 10 µg/mL trimethoprim (to select for the Δcos:TriR cassette in the c5545 strain harbouring the P2 prophage) at 37°C. Then, 10% (v/v) of the O/N culture was combined with LB media using 50 µg/mL kanamycin and 10 µg/mL trimethoprim. The culture was shaken for 3–4 hours at 150 rpm and 37°C and grown until the exponential phase (OD_{600} to 0.2–0.5). During the exponential phase, the epsilon (ε) gene encoded within the P4-EKORhE cosmid was activated by adding 0.2% (w/v) rhamnose to the media and further incubated at 150 rpm and 37°C for 3 hours until lysis was observed. The debris from the lysate was pelleted at 4,000 *g* for 30 minutes. The lysate was then filter-sterilised, with the option to store the filter-sterilised lysates at 4°C if desired.

After the lysate was obtained, a PEG8000 concentration protocol (Protocol SS7.2) or an ultrafiltration protocol (Bonilla et al., 2016) was applied in order to purify and concentrate the lysate samples with the conditionally propagating transducing particles. When using the PEG8000 protocol, the yields would not improve over 10^6 transducing particles per millilitre (Supplementary Figure S3, measured as pfu/mL). An alternative strategy using ultrafiltration is shown to improve the yields to up to 10^{10} particles per millilitre (as can be seen in the replica "P4-EKORhE, ×1 LB broth + ultrafiltration" shown in Supplementary Figure S3).

Fortunately, even higher yields of P4-EKORhE transducing particles were obtained when using TB as culturing media and using a four-step enrichment technique, followed by ultrafiltration (as depicted in Figure 8), with observed yields of up to 10^{12} particles per millilitre, as it is seen in the three replicas on the top row of the spot assay shown in Figure 6.

The protocol, using the showcased enrichment technique, is characteristic of P4-EKORhE because of its capacity to be repressed and activated (i.e. a controllable P4-EKORhE system). This characteristic allows for the multiplication of the Δcos:TriR-P2-c5545 Marionette Z1 *E. coli* lysogenic bacteria in a *fed-batch* fashion while maintaining a "dormant cosmid" before its activation with 0.2% (w/v) rhamnose. A high concentration of producing bacteria harbouring the P4-EKORhE is thus possible, and the later activation of the P4-EKORhE renders the highest yields obtained throughout this work. In this procedure, an O/N culture of Δcos:TriR-P2-c5545 *E. coli* lysogens, previously transformed with the P4-EKORhE cosmid, was grown in LB medium using 50 µg/mL kanamycin (to select for the selection marker in the P4-EKORhE) and 10 µg/mL trimethoprim (to select for the Δcos:TriR cassette in the c5545 strain harbouring the P2 prophage). Subsequently, 10% (v/v) of the

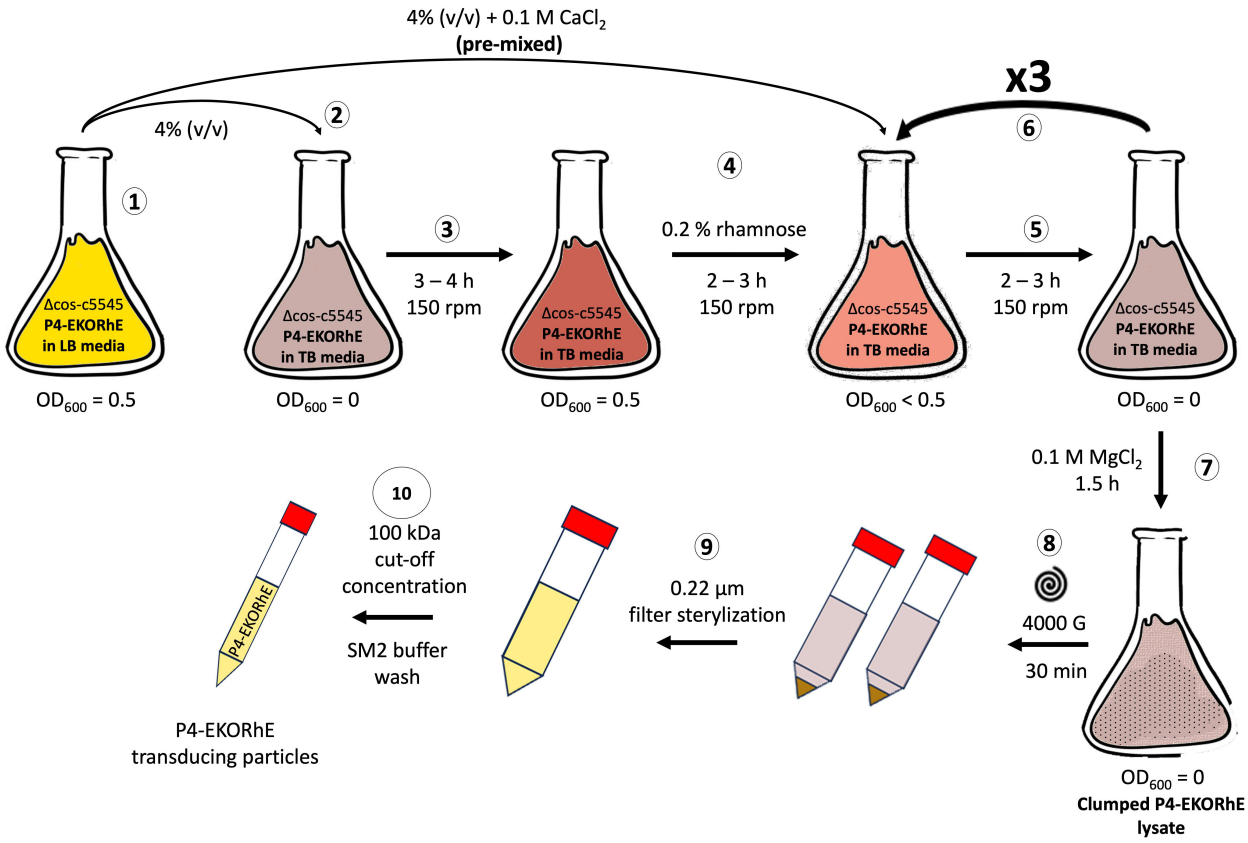

FIGURE 8
High yield P4-EKORhE-based transducing particle production protocol. Steps (1) to (10): (1) A flask containing a Δcos:TriR-P2-c5545 Z1 culture maintaining the P4-EKORhE cosmid is grown in Luria–Bertrani (LB) media until reaching exponential phase (i.e. OD_{600} = 0.5). (2) A 4% (v/v) sample of the exponentially growing LB culture is transferred into a flask containing Terrific Broth (TB) media. (3) The TB culture is grown to an exponential phase. (4) The TB culture is supplemented with 0.2% (w/v) rhamnose for the activation of the P2 prophage to enable the production of P4 particles, and a pre-mixed solution of exponentially growing cells with $CaCl_2$ is prepared to reach a concentration of 0.1 M. (5) The TB culture is grown for 2–3 hours to accumulate lysed cells containing a proportion transducing particles. (6) The TB culture is re-supplemented at a 4% (v/v) with the initial exponentially growing LB culture of Δcos:TriR-P2-c5545 Z1 and re-balanced to maintain 0.1 M $CaCl_2$ and 0.2% (w/v) rhamnose for as many cycles as necessary (i.e. from 5 to 6). (7) The TB culture is supplemented with 0.1 M $MgCl_2$ and further grown for 1.5 hours or until clumps are observed. (8) The clumped lysate is pelleted at 4,000 *g* for 30 minutes to separate cell debris. (9) The supernatant is filter-sterilised. (10) The lysate is concentrated using a 100-kDa molecular weight cut-off ultrafiltration column and replaced with SM2 buffer to obtain a cleaned-up final lysate of P4-EKORhE transducing particles.

aforementioned overnight culture was combined with fresh LB media (with kanamycin and trimethoprim) and shaken for 2 hours at 150 rpm and 37°C until the culture was recalled at the exponential growth phase (OD_{600} = 0.5). Concurrently, another 4% (v/v) portion of the overnight culture was pre-mixed with the necessary amount of $CaCl_2$ to make a final solution of 0.1 M in a flask containing a volume of TB media, including kanamycin and trimethoprim at the aforementioned concentrations, and shaken for 3–4 hours at 150 rpm and 37°C, reaching the exponential growth phase. Pre-mixture of cells with $CaCl_2$ is essential to avoid the precipitation of phosphate salts in the TB broth used for the culture. After reaching the exponential growth phase, 0.2% (w/v) rhamnose was added to the TB culture to induce the production of the ε gene to activate the Δcos:TriR-P2 prophage. After 2 hours of lysis in the TB culture, a 4% (v/v) sample of bacteria from the LB culture was introduced into the lysing TB-grown culture, again pre-mixing it with the necessary amount of $CaCl_2$ to maintain a final solution of 0.1 M in the growing TB culture and compensating the rhamnose to maintain the 0.2% (w/v) proportion. Nevertheless, concurrently, a new exponentially growing LB culture was prepared by adding 10% (v/v) of the overnight culture, which was shaken in parallel for a further 2 hours at 150 rpm and 37°C until it reached the "recall stage" at the exponential growth phase. This growing LB culture was also introduced into the ongoing lysis process of the TB culture, after 2 hours, and pre-mixed with the necessary amount of $CaCl_2$ to make a final solution of 0.1 M while maintaining the proportion to a final 0.2% (w/v) rhamnose. This re-lysing procedure can be repeated as many times as necessary (e.g. 0 to 3 times), ideally up to three additional times, to maximise the yield of transducing particles obtained. The lysis procedure was finished by adding 0.1 M $MgCl_2$, and the culture was shaken at 37°C for a further 1.5 hours until visible clumps were observed. Afterwards, the debris from the lysate was pelleted at 4,000 *g* for 30 minutes, followed by filter sterilisation of the lysate using 0.22-µm sterile syringe filters. After filtration, the lysate can be paused and stored at 4°C if desired until further use. The lysate can then be ultrafiltrated using the Amicon

100-kDa cut-off columns by centrifuging at 3,000 *g*. The recovered, non-eluted residue contains the highly concentrated P4-EKORhE-based transducing particles. Before titration, the lysate was pre-treated with DNAseI from NEB using 10 µL lysate + 10 µL DNAseI buffer + 10 µL DNAseI + 79 µL of water and incubated for 1 hour. Because P4 phages were conditionally propagated, lysates were titrated using a spot assay (Supplementary Section SS7.4.1) on lawned plates of Δcos:TriR-P2-c5545 Marionette Z1 *E. coli* lysogenic bacteria with 5 mM Ca^{++}.

Data availability statement

The raw data supporting the conclusions of this article will be made available by the authors upon reasonable request.

Ethics statement

Ethical approval was not required for the studies on humans in accordance with the local legislation and institutional requirements because only commercially available established cell lines were used. Ethical approval was not required for the studies on animals in accordance with the local legislation and institutional requirements because only commercially available established cell lines were used.

Author contributions

RR: Conceptualization, Data curation, Formal analysis, Funding acquisition, Investigation, Methodology, Project administration, Resources, Software, Supervision, Validation, Visualization, Writing – original draft, Writing – review & editing. AS: Funding acquisition, Project administration, Resources, Supervision, Validation, Writing – original draft. JB: Funding acquisition, Project administration, Resources, Supervision, Validation, Writing – review & editing, Writing – original draft. AJ: Funding acquisition, Project administration, Resources, Supervision, Validation, Writing – review & editing, Writing – original draft.

Funding

The author(s) declare that financial support was received for the research and/or publication of this article. RR-G was funded with a Joint PhD scholarship award from the Monash-Warwick Alliance and received additional funds from the Monash-Warwick Alliance, the School of Life Sciences at the University of Warwick, the School of Biological Sciences at Monash University, and the Warwick Quantitative Biomedical Program (WQBP). AJ acknowledges funding from the Biotechnology and Biological Sciences Research Council [grant BB/P020615/1 (EVO-ENGINE), BB/M017982/1 (Warwick Integrative Synthetic Biology Centre, WISB)].

Acknowledgments

RR-G is grateful to Gianni Dehò and Federica Briani, from Università degli Studi di Milano, for kindly and promptly providing a comprehensive collection of P4 and P2 phage strains and host cells essential to completing this work. RR-G also acknowledges the Monash-Warwick Alliance's financial sponsorship and support throughout the joint doctoral program. RR-G thanks Sahan B.W. Liyanagedera for his help in the laboratory and for scientific discussion, Satya Prakash for his help with difficult cloning, Gurneet Dhanoa and Josh Williams for their help with immunohistochemistry and fluorescence microscopy, and Cleidi Zampronio for her support with mass spectrometry and the analysis of protein sequences. RR-G thanks A.P.S., J.J.B., and his PhD viva jury, composed of Paul Jaschke and Danish Malik, for their valuable comments on his doctoral thesis that have been directly and indirectly implemented in this manuscript. sAJM.1505 was a gift from Christopher Voigt (Addgene #108253).

Conflict of interest

RR-G is the founder of ACGTx formerly Genova Tx.

The remaining authors declare that the research was conducted in the absence of any commercial or financial relationships that could be construed as a potential conflict of interest.

The author(s) declared that they were an editorial board member of Frontiers, at the time of submission. This had no impact on the peer review process and the final decision.

Generative AI statement

The author(s) declare that no Generative AI was used in the creation of this manuscript.

Publisher's note

Supplementary material

The Supplementary Material for this article can be found online at: https://www.frontiersin.org/articles/10.3389/fcimb.2025.1561443/full#supplementary-material

References

Abedon, S. T. (1994). "Lysis and the interaction between free phages and infected cells," in *The Molecular Biology of Bacteriophage T4*. Ed. J. D. Karam (ASM Press, Washington, DC), 397–405.

Atkins, J. F., Steitz, J. A., Anderson, C. W., and Model, P. (1979). Binding of mammalian ribosomes to MS2 phage RNA reveals an overlapping gene encoding a lysis function. *Cell* 18, 247–256. doi: 10.1016/0092-8674(79)90044-8

Baluch, J., and Sussman, R. (1978). Correlation between UV dose requirement for lambda bacteriophage induction and lambda repressor concentration. *J. Virol.* 26, 595–602. doi: 10.1128/jvi.26.3.595-602.1978

Berenstein, D. (1986). Prophage induction by ultraviolet light in acinetobacter calcoaceticus. *J. Gen. Microbiol.* 132, 2633–2636. doi: 10.1099/00221287-132-9-2633

Bernhardt, T. G., Roof, W. D., and Young, R. (2002). The Escherichia coli FKBP-type PPIase SlyD is required for the stabilization of the E lysis protein of bacteriophage PhiX174. *Mol. Microbiol.* 45, 99–108. doi: 10.1046/j.1365-2958.2002.02984.x

Berry, J., Rajaure, M., Pang, T., and Young, R. (2012). The spanin complex is essential for lambda lysis. *J. Bacteriology* 194, 5667–5674. doi: 10.1128/JB.01245

Bertani, G. (1951). Studies on lysogenesis. i. the mode of phage liberation by lysogenic Escherichia coli. *J. Bacteriology* 62, 293–300. doi: 10.1128/jb.62.3.293-300.1951

Bonilla, N., Rojas, M. I., Cruz, G. N. F., Hung, S.-H., Rohwer, F., and Barr, J. J. (2016). Phage on tap-a quick and efficient protocol for the preparation of bacteriophage laboratory stocks. *PeerJ* 4, e2261. doi: 10.7717/peerj.2261

Budič, M., Rijavec, M., Petkovšek,, and Žgur Bertok, D. (2011). Escherichia coli bacteriocins: antimicrobial efficacy and prevalence among isolates from patients with bacteraemia. *PloS One* 6, 1–7. doi: 10.1371/journal.pone.0028769

Dearborn, A., Laurinmaki, P., Chandramouli, P., Rodenburg, C., Wang, S., Butcher, S., et al. (2012). Structure and size determination of bacteriophage P2 and P4 procapsids: Function of size responsiveness mutations. *J. Struct. Biol.* 178, 215–224. doi: 10.1016/j.jsb.2012.04.002

Debowski, A., Verbrugghe, P., Sehnal, M., Marshall, B., and Benghezal, M. (2013). Development of a tetracycline-inducible gene expression system for the study of helicobacter pylori pathogenesis. *Appl. Environ. Microbiol.* 79, 7351–7359. doi: 10.1128/AEM.02701-13

Didovyk, A., Tonooka, T., Tsimring, L., and Hasty, J. (2017). Rapid and scalable preparation of bacterial lysates for cell-free gene expression. *ACS Synth Biol.* 6, 2198–2208. doi: 10.1021/acssynbio.7b00253

Endo, H., Ishizawa, M., and Kamiya, T. (1963). Induction of bacteriophage formation in lysogenic bacteria by a potent carcinogen, 4-nitroquinoline l-oxide, and its derivatives. *J. Bacteriology* 85, 593–600. doi: 10.1038/198195a0

Garrett, J. M., and Young, R. (1982). Lethal action of bacteriophage lambda S gene. *J. Virol.* 44, 886–892. doi: 10.1128/jvi.44.3.886-892.1982

Ghisotti, D., Finkel, S., Halling, C., Dehò, G., Sironi, G., and Calendar, R. (1990). Nonessential region of bacteriophage P4: DNA sequence, transcription, gene products, and functions. *J. Virol.* 64, pp.24–pp.36. doi: 10.1128/jvi.64.1.24-36.1990

Gibbs, W., Goldstein, R. N., Wiener, R., Lindqvist, B., and Calendar, R. (1973). Satellite bacteriophage P4: characterization of mutants in two essential genes. *Virology* 53, 24–39. doi: 10.1016/0042-6822(73)90462-5

Gjorgjevikj, D., Kumar, N., Wang, B., Hilal, T., Said, N., Loll, B., et al. (2025). The psu protein of phage satellite p4 inhibits transcription termination factor by forced hyper-oligomerization. *Nat. Commun.* 16, 550. doi: 10.1038/s41467-025-02123-8

Goldstein, R., Lengyel, J., Pruss, G., Barrett, K., Calendar, R., and Six, E. (1974). "Head size determination and the morphogenesis of satellite phage P4. In Current Topics in Microbiology and Immunology/Ergebnisse der Mikrobiologie und Immunitätsforschung," in *Current Topics in Microbiology and Immunology/ Ergebnisse der Mikrobiologie und Immunitätsforschung*, vol. 68. (Springer, Berlin, Heidelberg). doi: 10.1007/978-3-642-66044-33

Halling, C., and Calendar, R. (1990). Bacteriophage P2 ogr and P4 delta genes act independently and are essential for P4 multiplication. *J. Bacteriology* 172, 3549–3558. doi: 10.1128/jb.172.7.3549-3558.1990

Hutchison, C. A., and Sinsheimer, R. L. (1966). The process of infection with bacteriophage PhiX174: X. mutations in a phi-X lysis gene. *J. Mol. Biol.* 18, 429–447. doi: 10.1016/S0022-2836(66)80035-9

Inman, R., Schnös, M., Simon, L., Six, E., and Walker, D. Jr (1971). Some morphological properties of P4 bacteriophage and P4 DNA. *Virology* 68, 59–75. doi: 10.1016/0042-6822(71)90153-X

Kahn, M. L., Ziermann, R., Dehó, G., Ow, D. W., Sunshine, M. G., and Calendar, R. (1991). Bacteriophage P2 and P4. *Methods Enzymology* 204, 264–280. doi: 10.1016/0076-6879(91)04013-E

Kelly, C., Taylor, G., Hitchcock, A., Torres-Mendez, A., and Heap, J. (2018). A rhamnose-inducible system for precise and temporal control of gene expression in cyanobacteria. *ACS SynBio* 7, 1056–1066. doi: 10.1021/acssynbio.7b00435

Lin, C. (1984). Nucleotide sequence of the essential region of bacteriophage P4 get access arrow. *Nucleic Acids Res.* 12, 8667–8684. doi: 10.1093/nar/12.22.8667

Lindqvist, B., Dehò, G., and Calendar, R. (1993). Mechanisms of genome propagation and helper exploitation by satellite phage P4. *Microbiological Rev.* 57, 683–702. doi: 10.1128/mr.57.3.683-702.19

Lindqvist, B., and Six, E. (1971). Replication of bacteriophage P4 DNA in a nonlysogenic host. *Virology* 43, 1–7. doi: 10.1016/0042-6822(71)90218-2

Liu, T., Renberg, S., and Haggård-Ljungquist, E. (1997). Derepression of prophage P2 by satellite phage P4: cloning of the P4 epsilon gene and identification of its product. *J. Virol.* 71, 4502–4508. doi: 10.1128/jvi.71.6.4502-4508.1997

Meyer, A., Segall-Shapiro, T., Glassey, E., Zhang, J., and Voigt, C. (2019). Escherichia coli "marionette" strains with 12 highly optimized small-molecule sensors. *Nat. Chem. Biol.* 15, 196–204. doi: 10.1038/s41589-018-0168-3

Møller-Olsen, C., Ho, S. F. S., Shukla, R. D., Feher, T., and Sagona, A. P. (2018). Engineered K1F bacteriophages kill intracellular Escherichia coli K1 in human epithelial cells. *Sci Rep.* 8, 17559. doi: 10.1038/s41598-018-35859-6

Monnard, P., and Walde, P. (2015). Current ideas about prebiological compartmentalization. *Life (Basel).* 5, 1239–1263. doi: 10.3390/life5021239

Mourosi, J. T., Awe, A., Guo, W., Batra, H., Ganesh, H., Wu, X., et al. (2022). Understanding bacteriophage tail fiber interaction with host surface receptor: The key "blueprint" for reprogramming phage host range. *Int. J. Mol. Sci.* 23, 12146. doi: 10.3390/ijms232012146

Orta, A. K., Riera, N., Li, Y. E., Tanaka, S., Yun, H. G., La, L., et al. (2023). The mechanism of the phage-encoded protein antibiotic from X174. *Science* 381, eadg9091. doi: 10.1126/science.adg9091

Singh, V., Gohil, N., Ramírez García, R., Braddick, D., and Fofié, C. K. (2017). Recent advances in CRISPR-Cas9 genome editing technology for biological and biomedical investigations. *J. Cell Biochem.* 119, 81–94. doi: 10.1002/jcb.26165

Six, E. W. (1975). Bacteriophage P4: a satellite virus depending on a helper such as prophage P2. *Virology* 51, 327–344. doi: 10.1016/0042-6822(73)90432-7

Six, E. W., and Klug, C. A. C. (1973). The helper dependence of satellite bacteriophage P4: which gene functions of bacteriophage P2 are needed by P4? *Virology* 67, 249–263. doi: 10.1016/0042-6822(75)90422-5

Six, E. W., and Lindqvist, B. H. (1971). Multiplication of bacteriophage P4 in the absence of replication of the DNA of its helper. *Virology* 43, 8–15. doi: 10.1016/0042-6822(71)90219-4

UniProt Consortium (2024a). *Enterobacteria phage PhiX174 gpE single-gene lysis protein UniProtKB - P03639 (LYS BPPHS)*. https://www.uniprot.org/uniprotkb/P036395/entry (Accessed July 18, 2024).

UniProt Consortium (2024b). *Escherichia phage MS2 gpL single-gene lysis protein UniProtKB P03609 (LYS BPMS2)*. https://www.uniprot.org/uniprotkb/P036305/entry (Accessed July 18, 2024).

UniProt Consortium (2024c). *Lambdavirus lambda LysR endolyisin protein UniProtKB C6ZCX1 (ENLYS LAMBD)*. https://www.uniprot.org/uniprotkb/C6ZCX1/entry (Accessed July 18, 2024).

UniProt Consortium (2024d). *Lambdavirus lambda lyss holin/antiholin gene product UniProtKB - P03705 (HOLIN LAMBD)*. https://www.uniprot.org/uniprotkb/P03705/entry (Accessed July 18, 2024).

UniProt Consortium (2024e). *Lambdavirus lambda Rz spanin gene product UniProtKB - P00726 (SPAN1 LAMBD)*. https://www.uniprot.org/uniprotkb/P00726/entry (Accessed July 18, 2024).

UniProt Consortium (2024f). *Lambdavirus lambda Rz1 spanin gene product UniProtKB Q37935 (SPAN2 LAMBD)*. https://www.uniprot.org/uniprotkb/Q37935/entry (Accessed July 18, 2024).

Wegerer, A., Sun, T., and Altenbuchner, J. (2008). Optimization of an E. coli L-rhamnose-inducible expression vector: test of various genetic module combinations. *BMC Biotechnol.* 8, 1–12. doi: 10.1186/1472-6750-8-2

White, R., Chiba, S., Pang, T., Dewey, J., Savva, C., Holzenburg, A., et al. (2011). Holin triggering in real time. *Proc. Natl. Acad. Sci. United States America* 108, 798–803. doi: 10.1073/pnas.1011921108

White, R., Tran, T. A. T., Dankenbring, C. A., Deaton, J., and Young, R. (2010). The N-terminal transmembrane domain of S is required for holin but not antiholin function. *J. Bacteriology* 192, 725–733. doi: 10.1128/jb.01263-09

Young, R., Way, J., Way, S., Yin, J., and Syvanen, M. (1979). Transposition mutagenesis of bacteriophage lambda: a new gene affecting cell lysis. *J. Mol. Biol.* 132, 307–322. doi: 10.1016/0022-2836(79)90262-6

Zhang, J., and Poh, C. L. (2018). Regulating exopolysaccharide gene wcaF allows control of Escherichia coli biofilm formation. *Sci. Rep.* 8, 13127. doi: 10.1038/s41598-018-31357-w

Zhang, N., and Young, R. (1999). Complementation and characterization of the nested Rz and Rz1 reading frames in the genome of bacteriophage lambda. *Mol. Gen. Genet. (MGG)* 262, 659–667. doi: 10.1007/s004380051128

frontiers | Frontiers in Cellular and Infection Microbiology

TYPE Original Research
PUBLISHED 14 August 2025
DOI 10.3389/fcimb.2025.1643576

OPEN ACCESS

EDITED BY
Mercedes Gonzalez Moreno,
Hans Knoll Institute, Germany

REVIEWED BY
Miloud Sabri,
Istituto Agronomico Mediterraneo di Bari, Italy
Kritika Sharma,
Sanjay Gandhi Post Graduate Institute of Medical Sciences, India

*CORRESPONDENCE
Jiajun Yin
yinjiajun@dlu.edu.cn

†These authors have contributed equally to this work

RECEIVED 09 June 2025
ACCEPTED 17 July 2025
PUBLISHED 14 August 2025

CITATION
Khan MSI, Wu J, Ji S, Tan D, Sui B, Peng S, Zhan J and Yin J (2025) Expanding structural insights into DNA packaging apparatus and endolysin LysSA05 function of Epsilon15 bacteriophage. *Front. Cell. Infect. Microbiol.* 15:1643576. doi: 10.3389/fcimb.2025.1643576

Expanding structural insights into DNA packaging apparatus and endolysin LysSA05 function of Epsilon15 bacteriophage

Muhammad Saleem Iqbal Khan[1†], Ju Wu[1†], Shenlin Ji[1], Demeng Tan[2], Bingrui Sui[3], Shanshan Peng[4], Jinbiao Zhan[4] and Jiajun Yin[1*]

[1]Department of General Surgery, Affiliated Zhongshan Hospital of Dalian University, Dalian, Liaoning, China, [2]Shanghai Public Health Clinical Center, Fudan University, Shanghai, China, [3]MOE Key Laboratory of Bio-Intelligent Manufacturing, School of Bioengineering, Dalian University of Technology, Dalian, China, [4]Department of Biochemistry, The Second Affiliated Hospital, School of Medicine, Zhejiang University, Hangzhou, China

The rising prevalence of multidrug-resistant (MDR) foodborne pathogens, particularly *Salmonella* spp., necessitates alternative antimicrobial solutions. Phage therapy offers a promising solution against MDR Gram-negative infections; however, its clinical application is constrained by the presence of endotoxins, residual cellular debris, the risk of horizontal gene transfer by temperate phages, and an incomplete understanding of how phage structural integrity influences infectivity and enzyme function. In this study, we present a structural and functional analysis of temperate bacteriophage Epsilon15 (ε15), focusing on its DNA packaging and injection machinery, along with characterization of the dual-acting endolysin LysSA05. Iodixanol-purified virions suspended in phosphate-buffered saline (PBS), under conditions optimized to preserve virion stability, were analyzed using graphene oxide (GO)-supported cryo-electron microscopy. This approach resolved the full asymmetric architecture of ε15, revealing a detailed internal nucleic acid organization with at least eight concentric layers radially and approximately 28 axially compacted layers within the capsid. The DNA packaging machinery, comprising the core, portal, and hub, was resolved at high resolution, including a 42 nm-long and 18 nm-wide injection channel anchored by a dodecameric portal complex visualized at ~7 Å resolution. Concurrently, we characterized LysSA05, a dual-acting endolysin harboring a glycoside hydrolase 19 (GH19) catalytic domain accommodating peptidoglycan (PG) residues *N*-acetylmuramic acid (NAM) and *N*-acetylglucosamine (NAG) through structural docking, indicating plausible binding interactions that promote hydrolysis support vector machine (SVM), random forest (RF), discriminant analysis (DA), artificial neural network (ANN) and physicochemical scanning identified an amphipathic helix (residues 59-112) with predicted antimicrobial peptide (AMP)-like properties. Biochemical validation confirmed that LysSA05 destabilizes lipopolysaccharides

(LPS) and permeabilizes the outer membrane of Gram-negative bacteria independently of permeabilizers, with enhanced efficacy observed upon co-treatment with Ethylenediaminetetraacetic acid (EDTA) or citric acid. In summary, our findings elucidate key structural features of ε15 relevant to infection and genome delivery, while positioning LysSA05 as a promising enzybiotic candidate against MDR Gram-negative pathogens.

KEYWORDS

bacteriophage, electron microscopy, cryo-electron microscopy, endolysin, antimicrobial peptides, multidrug-resistant bacteria

1 Introduction

Members of the *Enterobacteriaceae* family, such as *Salmonella* spp. and *Escherichia coli* species, are Gram-negative pathogens responsible for a substantial burden of food-borne and gastrointestinal infections in both humans and animals (Authority et al., 2020). According to the Centers for Disease Control and Prevention (CDC), non-typhoidal *Salmonella* infections affect approximately 1.35 million individuals annually in the United States alone (Daigle, 2021). The rapid emergence and dissemination of multidrug-resistant (MDR) pathogens have intensified efforts to identify alternative antimicrobial strategies (Medalla et al., 2021; Tadesse et al., 2012).

Bacteriophages, as natural predators of bacteria, have gained renewed attention as targeted biocontrol agents, due to their specificity and lytic efficacy (Jayamanne and Foddai, 2025; Lin et al., 2018). However, their clinical use is limited by safety concerns, regulatory hurdles, and gaps in understanding phage biology and structure-function relationships. Among these, bacteriophage Epsilon15 (ε15) is a well-characterized, tailed temperate double-stranded DNA (dsDNA) phage that infects *S. enterica* serovar Anatum, a Gram-negative bacterium responsible for gastrointestinal infections in humans and animals (Kropinski et al., 2007). It exhibits host specificity via endorhamnosidase-mediated recognition of the LPS-O antigen, causing the tail hub to open and the core to exit the capsid and form a tube across the periplasmic space to introduce viral DNA into a cytoplasm of the host cell. These features make ε15 a valuable model for understanding phage-host interactions and for potential applications in food safety (Chang et al., 2010). Beyond their lytic activity, temperate phages also drive horizontal gene transfer, contributing to bacterial evolution and dissemination of antibiotic-resistance genes (Penadés et al., 2025).

Central to ε15's infection cycle is a precisely coordinated system involving an icosahedral capsid, a tail for host attachment, and a sophisticated DNA packaging motor that ensures accurate genome translocation (Chang et al., 2010). The structure of its tail DNA injection apparatus enables a better understanding of the mechanism by which bacteriophages cause genetic variation in their host. While early cryo-electron microscopy (EM) studies revealed ε15 asymmetric architecture, including a dodecameric portal complex and coaxially layered DNA was resolved at 20 Å (Jiang et al., 2006). Later, symmetry-imposed reconstructions resolved the capsid shell at near-atomic resolution and identified major capsid protein gp7 and minor capsid protein gp10 (Baker et al., 2013), while cryo-EM captured early infection stages and tail spike activity in *Salmonella* (Chang et al., 2010). According to genomic analysis, ε15 tail nucleic acid packaging/injection device is mainly composed of portal protein, corresponding to gp4, gp20, gp15 and gp17/16, respectively (Guichard et al., 2013). However, limitations in purification such as cellular debris, endotoxins and physicochemical stress, have hindered detailed analysis of infectious phage particles and constrained their potential as therapeutic agents (Reindel and Fiore, 2017; Jończyk-Matysiak et al., 2019).

Bacteriophages use precisely coordinated structures to ensure replication fidelity and to control the spatial activation of lytic enzymes such as endolysins during host infection. Endolysins are peptidoglycan (PG)-degrading enzymes that act at the end of the phage replication cycle, cleaving glycosidic bonds between *N*-acetylmuramic acid (NAM) and *N*-acetylglucosamine (NAG) (Fernandes and São-José, 2018). In Gram-negative bacteria, endolysins are typically small (~15-20 kDa) with single or dual catalytic domains, such as glycosidase, amidase, or peptidase (Nazir et al., 2023; Wang et al., 2023). Their activity is often limited by the outer membrane but can be enhanced by membrane-permeabilizing agents or fusion with antimicrobial peptide (AMP)-like domains, such as Artilysins (Islam et al., 2022). Some broad-spectrum lysins, like LysO78, Abtn-4, Ply6A3 LysAB2 and AbEndolysin, show strong activity against Gram-negative pathogens (Deng et al., 2021; Lai et al., 2011; Wu et al., 2019; Yuan et al., 2021). Most of these endolysins exhibit antimicrobial potential due to a predicted C-terminal amphipathic α-helical domain with AMP-like properties (Kim et al., 2025b; Yuan et al., 2021; Peng et al., 2017; Wu et al., 2024).

In this study, we integrate high-resolution structural biology with bioinformatic and machine learning-driven functional enzymology to advance phage-based antimicrobial strategies. By employing iodixanol gradient purification and graphene oxide

(GO)-supported vitrification, we preserved Epsilon (ε15) in a near-native, infectious state, enabling asymmetric reconstruction of the full virion at ~7 Å resolution. This reconstruction revealed detailed features of the internal nucleic acid and DNA packaging machinery, including the core, portal, and hub regions, with a portal complex exhibiting dodecameric symmetry and forming a 42 nm-long, 18 nm-wide packaging channel. Simultaneously, we identified an amphipathic helix (residues 59-112) in LysSA05, predicted via machine learning to possess AMP-like properties, and biochemically validated its ability to destabilize *Salmonella* and *E. coli* LPS. LysSA05's natural fusion of a glycoside hydrolase 19 (GH19) PG-hydrolase and outer membrane-permeabilizing AMP domain enables adjuvant-free lytic activity against MDR clinical isolates. The results indicate that ε15 is a valuable model system for understanding phage architecture and lytic enzyme function, offering a promising foundation for the development of enzybiotic-based therapeutics against Gram-negative pathogens.

2 Materials and methods

2.1 Bacterial strains, phage, and growth conditions

The bacterial strains, phage, and plasmid used in this study are listed in Supplementary Table 1. Bacteriophage ε15 was propagated using *S. enterica* serovar Anatum in 2× Yeast Extract-Tryptone (YT) broth at 37°C. Phage titers were determined using the plaque-forming unit (PFU) method and stored in phosphate-buffered saline (PBS) at 4°C for subsequent analysis. For cloning and protein expression, *E. coli* strains DH5α, BL21 (DE3), and Rosetta (DE3) were cultured in Luria Bertani (LB) medium (per liter: 10 g tryptone, 5 g yeast extract, 5 g NaCl) supplemented with kanamycin (100 μg/mL). The LysSA05 endolysin gene was cloned into the pET-28a(+) plasmid, incorporating a C-terminal 6×His-tag for affinity purification. *S. anatum* and *E. coli* C were used as model Gram-negative strains for LPS extraction and lytic activity assays. Additional MDR clinical isolates of *Salmonella* and *E. coli* were tested to evaluate the antibacterial spectrum (Supplementary Table 2). All bacterial strains were grown in LB broth or agar at 37°C with shaking at 220 rpm. Bacterial viability was assessed by colony-forming unit (CFU) per mL, enumeration under sterile conditions.

2.2 Propagation and purification of bacteriophage ε15

Bacteriophage ε15 was propagated using *S. anatum* as the host. An overnight culture of *S. anatum* was diluted 1:100 in 5 mL of 2 × YT broth and incubated at 37°C until reaching an OD_{600} of 0.4. Phage suspension (1×10^9 PFU/mL) and 20% sterile-filtered glucose were added to facilitate adsorption, followed by a 4h incubation. The culture was centrifuged at 7,155 × g for 15 min at 4°C, and the pellet was resuspended in 250 mL of 2× YT broth. Incubation continued at 37°C for 16 h until complete lysis was observed. The lysate was clarified by centrifugation at 7,155 × g for 15 min at 4°C to remove cellular debris. Phage particles were precipitated by adding polyethylene glycol (PEG) 8000 to a final concentration of 20% and NaCl to 1.5 M, followed by incubation at 4°C for 4 h. SM buffer was prepared by dissolving 11.7 g NaCl, 1.4 g $MgSO_4$, and 50 mL of 1 M Tris-HCl (pH 7.5) in 950 mL of demineralized water. For SM-gelatin buffer, 2% (w/v) gelatin was added to the SM buffer. The phage solution was kept at 4°C for subsequent analysis. Bacteriophage ε15 particles were initially concentrated by ultracentrifugation over a 12% sucrose cushion (105,000 × g, 2 h, 4°C), and the resulting pellet was resuspended in 300 μL of PBS and incubated overnight at 4°C. For further purification, samples were subjected to various density gradients, including discontinuous and continuous sucrose gradients, as well as a discontinuous iodixanol gradient (10-55%, Sigma Aldrich, D1556). The final preparation for cryo-electron microscopy (cryo-EM) was obtained using a discontinuous iodixanol gradient. Gradients were formed as described previously (Khan et al., 2021) with layers of 10%, 20%, 30%, 40%, and 55% iodixanol and centrifuged in an SW41 rotor at 175,000 × g for 4 h at 4°C. A distinct white band was collected, washed using 14 kDa MWCO (Amicon®), and resuspended in PBS. The final phage titer was 1.5×10^{10} PFU/mL, determined by standard plaque assay (Sui et al., 2025), and stored at 4°C until negative staining and cryo-EM imaging.

2.3 Negative staining and transmission electron microscopy

For morphological and purity analysis, ε15 phage particles were subjected to negative staining and observed under transmission electron microscopy (TEM). Carbon-coated copper grids were glow discharged at 15 mA for 60 s, using a PELCO easiGlow™ 91000 system (USA) to render them hydrophilic. A 3 μL aliquot of 10-fold diluted phage sample was applied to each grid and allowed to adsorb for 30 s. Excess liquid was blotted with filter paper, and the grid was stained with 2% aqueous uranyl acetate (UA) in three intervals: two brief applications of 10 s each, followed by a final application lasting 1 min. Grids were air-dried at room temperature for at least 1 min before imaging. Micrographs were acquired at magnifications of 87kx and 105kx using a FEI Tecnai Spirit 120 kV microscope at the Center for EM, Zhejiang University School of Medicine. After confirming the morphology, integrity, and purity of the sample, cryo-EM vitrification was performed.

2.4 Cryo-EM grid preparation

Cryo-EM samples were prepared using two types of grids: graphene oxide (GO; Sigma Aldrich; 763705) coated and uncoated Quantifoil R1.2/1.3 Cu 300 mesh grids. For GO coating, grids were glow discharged at 25 mA for 180 s. GO (2 mg/mL) was diluted to 0.4 mg/mL, and 2.5 μL was applied to each grid. After 180 s incubation period, excess solution was removed, and the grids were washed twice with 10 μL ultrapure water, followed by a 5 min air-drying. For both

grid types, 2.5 μL of purified ε15 phage sample were applied. Using the Vitrobot (FEI) set at 100% humidity and 22°C, grids was incubated with sample for 60 s, blotted for 6.5 s, and then rapidly plunged into liquid ethane. Cryo-EM imaging was performed using a Thermo Fisher Talos F200C microscope after confirming grid quality. The second grid type underwent direct hydrophilic treatment and sample application without GO coating.

2.5 Cryo-EM data collection and processing

High-resolution data were collected using a Thermo Fisher FEI Titan Krios cryo-EM operating at 300 kV. Microscope calibration included coma-free alignment and beam-tilt minimization. Data acquisition was conducted using SerialEM software (Schorb et al., 2019). Images were recorded in super-resolution mode on a Gatan K2 Summit direct electron detector at a nominal magnification of 22,500×, with a pixel size of 1.307 Å/pixel after binning. The total electron dose was ~50 $e^-/Å^2$, with an exposure time of 10 s and a frame rate of 4 frames per second. The defocus range was set between -2.0 μm and -3.0 μm. Drift correction was performed using MotionCor2 (Zheng et al., 2017), producing aligned and dose-weighted images for downstream analysis. Automated particle picking was conducted using Gautomatch (https://www.mrc-lmb.cam.ac.uk/kzhang/Gautomatch/). Gctf was used to estimate local defocus and correct astigmatism. Image processing, including 2D classification, 3D classification, and 3D reconstruction, was performed using RELION 2.0 (Scheres, 2016). The resulting cryo-electron density map provided structural insights into the ε15 virion.

2.6 Bioinformatics analysis

The endolysin gene *LysSA05* (locus tag: epsilon15_*gp05*, accession number: NP_848233.1) was analyzed using a comprehensive bioinformatics pipeline. Sequence identity and function were assessed via BLAST, PSI-BLAST, HMMER (Potter et al., 2018), and InterProScan (Blum et al., 2025). Domain architecture was predicted with HHpred (Söding et al., 2005), and physicochemical properties including molecular weight (MW) and isoelectric point (pI) were computed using ProtParam (Gasteiger et al., 2005). Multiple sequence alignment with homologs, including *Salmonella* phage SPN1S, was performed using Clustal Omega (Sievers and Higgins, 2018), and visualized in ESPript 3.0 (Robert and Gouet, 2014). Additional homologs identified via HMMER were aligned using MUSCLE (https://www.ebi.ac.uk/jdispatcher/msa) and used to construct a phylogenetic tree in MEGA X (Kumar et al., 2024). Secondary structure was predicted using PSIPRED (Jones, 1999) and PHD (https://npsa-prabi.ibcp.fr/cgi-bin/npsa_automat.pl?page=/NPSA/npsa_phd.html), while 3D modeling was conducted with Phyre2 (Kelley et al., 2015). The model was validated using ERRAT and PROCHECK through the SAVES server, and structural pockets were analyzed using Phyre2 "Investigator" module. Molecular docking was performed using CB-Dock2 (Liu et al., 2020), targeting PG residues NAM (SID: 24890714) and NAG (CID: 1738118). A homology model of LysSA05 was also generated using Swiss-Model. Docking simulations employed AutoDock Vina with automated cavity detection. Top-ranked poses were selected based on binding affinity (kcal/mol) and cavity volume and were visualized in 3D (within CB-Dock) and 2D formats within LigPlot+ v.2.2 (Wallace et al., 1995).

2.7 Physicochemical profiling and AMP prediction

The full-length LysSA05 protein (208 amino acids) was computationally segmented into overlapping peptides of 54 residues (pre-screening) and 20 residues (post-screening) for AMP prediction. A complementary 54-residues sliding window (three α-helical turns) was applied using HeliQuest (https://heliquest.ipmc.cnrs.fr/index.html) to assess amphipathic helicity (Gautier et al., 2008). For each segment, net charge (z), hydrophobic moment (μH), and average hydrophobicity (H) were calculated. Peptides with $z \geq 2$, $\mu H \geq 0.4$, and amphipathic features were shortlisted and ranked based on combined physicochemical scores. Helical wheel diagrams visualized residue distribution. Subsequently, 189 overlapping 20-mer peptides were submitted to the CAMP3 server (http://www.camp3.bicnirrh.res.in/) for AMP and non-AMP (NAMP) classification (Thomas et al., 2010) and peptides were evaluated using four classifiers: support vector machine (SVM), random forest (RF), discriminant analysis (DA), and artificial neural network (ANN). Prediction outputs were visualized via violin plots, boxplots, sequence position heatmaps, and Venn diagrams. Finally, the overlapping peptide in machine learning (ML) classifiers and HeliQuest were selected and these peptide underwent *de novo* 3D modeling using PEP-FOLD4 (https://bioserv.rpbs.univ-paris-diderot.fr/services/PEP-FOLD4/) under physiological conditions (pH 7.0, 150 mM ionic strength), validating the presence of membrane-active amphipathic helices (Rey et al., 2023).

2.8 Genomic DNA extraction, cloning, and expression of LysSA05 endolysin

Genomic DNA was extracted from purified ε15 phage particles using the M13 DNA Extraction Kit (Takara) and further purified by agarose gel electrophoresis and gel extraction (Omega Bio-Tek). DNA concentration and purity were assessed using a NanoDrop spectrophotometer. The *LysSA05* gene (*gp05*, 628 bp) was amplified by PCR using primers designed in SnapGene and incorporating *NcoI* and *XhoI* restriction sites: Forward: 5′-CATGCCATGGACATTAACCAGTTCCGGCGC-3′, Reverse: 5′-CCGCTCGAGTACCGCCAGCACCTTACTGGC-3′. PCR was performed using 2× Hieff Master Mix (Yeasen), and the amplicon was purified and digested with *NcoI* and *XhoI*. The PCR product was ligated into the expression vector pET-28a(+) using T4 DNA ligase, to generate the recombinant plasmid pET-28a(+)/*LysSA05*. The construct was transformed into *E. coli* DH5α via

$CaCl_2$ heat-shock transformation, and positive clones were screened by colony PCR and confirmed by Sanger sequencing. For protein expression, verified plasmids were introduced into *E. coli* BL21 (DE3) and Rosetta (DE3) strains. Cultures were grown in LB medium supplemented with kanamycin (100 µg/mL) to mid-log phase (OD_{600} = 0.4) and induced with Isopropyl β-D-1-thiogalactopyranoside (IPTG) at varying IPTG concentrations (0.1, 0.5, 1.0 mM) at either 30°C or 37°C for 5 h. Cells were harvested, lysed by sonication, and the soluble and insoluble fractions were analyzed by SDS-PAGE.

2.9 Purification, refolding, and SDS-PAGE analysis of recombinant LysSA05

Recombinant LysSA05 was predominantly expressed as insoluble inclusion bodies in both *E. coli* BL21 and Rosetta host strains. Harvested cells were lysed by sonication and centrifuged at 16,099 × g for 10 min. Inclusion bodies were washed with lysis buffer (PBS + 0.1% Triton X-100) and ddH_2O, then solubilized in Nitrilotriacetic Acid (NTA) buffer containing 8 M urea and purified via Ni^{2+}-NTA resin under denaturing conditions. The column was pre-equilibrated with binding buffer prior to sample loading. LysSA05 was eluted with a gradient of imidazole (20–250 mM) in 1× NTA buffer (8 M urea), and eluted fractions were analyzed by SDS-PAGE (12% gel) using the Laemmli protocol (sample denaturation at 95°C for 5 min in SDS loading buffer) (He, 2011). Gels were stained with Coomassie Brilliant Blue R250 for 1 h and de-stained using a methanol: acetic acid: water solution (3:1:6, v/v/v) until a clear background was achieved. A distinct ~25 kDa band corresponding to His-tagged LysSA05 was used to evaluate expression levels, solubility, and purification efficiency. Fractions containing > 90% pure LysSA05 were pooled and subjected to stepwise refolding by dialysis. The protein was first dialyzed against decreasing concentrations of urea (8 M, 4 M, 2 M, 0 M) in NTA buffer at 4°C. This was followed by sequential dialysis against: Buffer A: 20 mM Tris-Cl, 0.5 mM NaCl, 5% glycerol, 5% sucrose, 1% arginine, pH 8.0, Buffer B: 20 mM Tris-Cl, 0.5 mM NaCl, pH 8.0, Buffer C: 1× PBS supplemented with 5% glycerol, 5% sucrose, and 1% arginine, pH 7.4. Each dialysis step was carried out for 2 h at 4°C under gentle agitation. The final refolded protein was dialyzed in 1× PBS, concentrated using PEG 20,000, and filtered (0.22 µm). Protein concentration was measured using Bicinchoninic Acid (BCA) and stored at 4°C for downstream assays.

2.10 Lipopolysaccharides, silver staining, and degradation assessment

LPS was extracted from *E. coli* C and *S. anatum* using a modified hot phenol water method (Davis Jr and Goldberg, 2012). Briefly, mid-log phase cultures were harvested, washed with PBS containing 0.15 mM $CaCl_2$ and 0.5 mM $MgCl_2$, and lysed by sonication. Lysates were sequentially treated with proteinase K, DNase I, and RNase A, followed by phenol extraction at 65-70°C. LPS was precipitated with 0.5 M sodium acetate and 95% ethanol at -20°C overnight, then collected by centrifugation. Samples were extensively dialyzed against distilled water, lyophilized, and stored at 4°C. To assess the LPS degrading activity of LysSA05, 50 µL of purified LPS from *E. coli* C or *S. anatum* was incubated with recombinant LysSA05 (100 µg/mL) at 37°C for 6 h. Degradation was evaluated by SDS-PAGE followed by Ni^{2+}-enhanced silver staining and Coomassie Brilliant Blue staining for protein control. By applying this method, we could monitor the enzymatic activity of LysSA05 on LPS substrates, as degradation would result in altered banding patterns on the gel. As previously reported, silver staining has been used to visualize the LPS from Gram-negative bacteria (Tan and Grewal, 2002). No outer membrane permeabilizers were used, enabling direct assessment of LysSA05 activity on intact LPS. During silver staining, LPS was visualized using the Sangon Biotech Silver Staining Kit (C500029) according to the manufacturer's instructions. Gels were treated with solutions A-E, with protein and LPS bands appearing as dark signals. The reaction was stopped with solution E, and gels were rinsed with ddH_2O. LPS purity was confirmed by comparing silver-stained and Coomassie-stained SDS-PAGE gels.

2.11 Assessment of LysSA05 lytic activity

The dual lytic activity of LysSA05 was assessed *in vitro* against *S. anatum* and *E. coli* C to evaluate its ability to degrade both LPS and PG. Bacterial cultures were grown overnight in LB broth at 37°C, harvested at OD_{600} = 0.4, washed with PBS (pH 7.4), and resuspended to a final concentration of 10^8 CFU/mL. Purified LysSA05 (100 µg/mL) was added to 800 µL of bacterial suspension and incubated at 37°C for 5 h. Negative controls received an equal volume of PBS without enzyme. To investigate the impact of outer membrane permeabilizers (OMPs), additional treatments were performed with LysSA05 in the presence of Ethylenediaminetetraacetic acid (EDTA) or citric acid (0-0.5 mM) for 1 min at 37°C. Antibacterial activity was quantified by CFU enumeration, and results were expressed as reductions in viable bacterial counts. All experiments were conducted in triplicate to ensure reproducibility.

2.12 Antibacterial spectrum of different food-borne isolates

After confirming the lytic activity of endolysin LysSA05, its antibacterial efficacy was further evaluated against MDR clinical isolates of *Salmonella* and *E. coli* (Supplementary Table S2). The susceptibility of these resistant isoltes to LysSA05 (100 µg/mL) was analyzed using a CFU/mL plating assay. Prior to treatment, the clinical isolates were cultured in LB medium to an optical density (OD_{600}) of 0.4 and incubated at 37°C for 1 h. Following endolysin treatment, bacterial viability was assessed by CFU/mL enumeration. All experiments were conducted in triplicate to ensure accuracy and reproducibility.

2.13 Statistical analysis

Statistical analyses and graph generation were conducted using GraphPad Prism software (GraphPad Prism 9.2, La Jolla, CA). Data are presented as the mean ± standard deviation (SD). Statistical significance was assessed using one-way ANOVA followed by Turkey's multiple comparison test to compare stability and infectivity of the phages in the presence of the various buffers and gradient techniques. A P-value < 0.05 was considered statistically significant; $^{*}P \leq 0.05$; $^{**}P \leq 0.01$; $^{***}P \leq 0.001$; and $^{****}P \leq 0.0001$.

3 Results

3.1 Assessing stability and morphological integrity of ε15

Optimized purification and preparation protocols preserved ε15 virion integrity and infectivity, enabling high-resolution structural and functional analysis. Structural resilience of ε15 varied significantly across tested buffers, with SM buffer (Figure 1B) providing superior preservation of intact capsid-tail complexes and minimal debris compared to Tris and PBS. Tris buffer resulted in extensive particle breakage, detached tails, and high background debris (Figure 1A), while PBS produced heterogeneous populations with partial capsid collapse, moderate tail loss, and aggregation (Figure 1D). The addition of gelatin to SM buffer further enhanced structural integrity, yielding monodisperse, intact virions with virtually no fragments (Figure 1C). However, despite its visual advantages, SM + gelatin did not improve infectivity, with PFU titers comparable to those of PBS and SM, and it posed challenges for cryo-EM grid preparation due to potential imaging artifacts (Supplementary Figure 1A). Therefore, PBS was selected for downstream assays, as it balances between particle stability and infectivity, despite showing slightly reduced morphological preservation.

The choice of purification method profoundly influenced ε15 virion integrity and cryo-EM sample quality. Negative-stain EM revealed that ultracentrifugation and discontinuous sucrose cushions caused extensive particle aggregation, fragmentation, and capsid disruption (Figures 1E, G). Continuous sucrose gradients modestly improved particle preservation, with a higher number of intact virions, though structural damage remained common (Figure 1F). In contrast, iodixanol gradients yielded the highest-quality preparations, with the highest number of virions retaining intact capsid-tail complexes and densely packed genomes (Figure 1H). These preparations also exhibited superior infectivity, significantly outperforming other methods ($P < 0.0001$), while no notable differences were observed among sucrose-based or ultracentrifugation preparations (Supplementary Figure 1B). The buoyant density of ε15 differed across all gradient media, as shown in Supplementary Figures 1C–E.

Cryo-EM grid assessments confirmed that iodixanol-purified ε15 samples offered optimal quality for high-resolution structural analysis (Figure 1L). Vitrification on GO-coated grids enabled uniform particle adsorption and diverse orientations, which are essential for accurate three-dimensional reconstructions. Ultracentrifugation-purified samples exhibited severe aggregation and high background noise (Figure 1I), while sucrose gradient preparations showed better dispersion but were compromised by residual debris and capsid damage (Figures 1J, K). In contrast, iodixanol-purified particles remained monodisperse, structurally intact, and were imaged against a clean background, facilitating accurate particle picking and efficient downstream processing. These results establish iodixanol purification as the optimal method for preserving ε15 integrity, offering the best balance of structural quality and functional suitability for single-particle cryo-EM studies.

3.2 Structural elucidation of the ε15 and its DNA packaging apparatus

To uncover the native architecture of ε15 and its DNA packaging machinery, high-resolution cryo-EM analysis was performed with a focus on resolving asymmetric and functionally relevant structural features. Two types of cryo-EM grids, either with or without a GO-support film, were used for vitrification. Grids lacking the support film, ε15 particles exhibited a strong preferred orientation, limiting structural information during data processing (Figure 2A). To address this, an optimized cryo-EM workflow was developed, combining iodixanol gradient purification to enhance particle integrity with GO-coated grids to reduce orientation bias and support-fragile appendages in vitreous ice. This dual strategy yielded high-quality micrographs of intact, well-dispersed ε15 virions for single-particle reconstruction (Figure 2B), enabling comprehensive structural analysis. An initial icosahedral reconstruction resolved the symmetric capsid at high resolution but, as expected, did not capture the asymmetric unique tail vertex (Figure 2C).

Asymmetric single-particle reconstruction was implemented to resolve the complete ε15 virion (Figure 2D), successfully visualizing the ~42 nm portal-tail complex anchored at a unique capsid vertex, along with distinct internal densities corresponding to the packaged genome. Cross-sectional analysis of the asymmetrical map revealed at least eight concentric DNA layers and arranged radially from the center and approximately 28 longitudinally stacked layers, underscoring the highly ordered organization of the phage genome (Figure 2E). The portal-tail machinery was clearly resolved into three modules: a central portal ring, an upper core, and a lower hub, measuring ~18 nm in width and ~42 nm in length (Figures 2F, G). Focused refinement of the central portal yielded a dodecameric architecture at ~7 Å resolution (Figure 2H), consistent with conserved portal structures in tailed phages. In contrast, the tail hub exhibited a hexameric organization, indicating structural specialization for DNA translocation.

Together, these results bridge longstanding gaps between capsid symmetry and asymmetric functional components. By overcoming sample fragility and orientation bias, the *in-situ* DNA packaging machinery and internal genome organization of ε15 were resolved in unprecedented detail. This integrated structural view reinforces ε15 as a tractable model for dissecting the molecular choreography

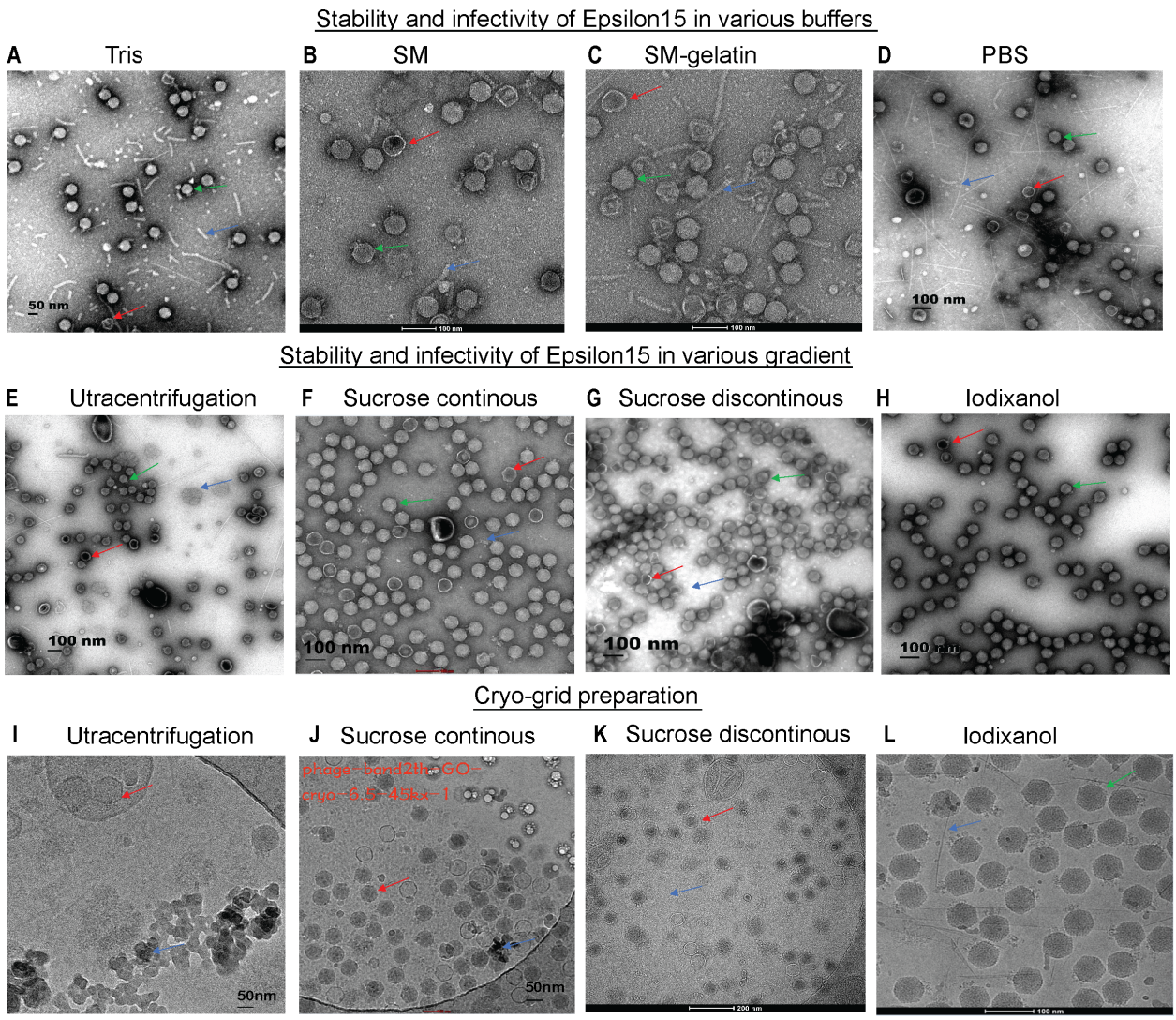

FIGURE 1
Assessment of ε15 virion stability under different purification conditions via EM/Cryo-EM grid preparation. **(A–C)** Negative-staining EM of ε15 particles purified using different buffer systems: **(A)** Tris, **(B)** SM buffer, **(C)** SM-gelatine, and **(D)** PBS. **(E–H)** Negative-staining EM of ε15 particles following density gradient centrifugation using: **(E)** ultracentrifugation, **(F)** continuous sucrose, **(G)** discontinuous sucrose, **(H)** discontinuous iodixanol gradients **(I–L)** Cryo-EM of ε15 virions vitrified on GO-coated grids following purification by: **(I)** ultracentrifugation, **(J)** continuous sucrose, **(K)** discontinuous sucrose, and **(L)** discontinuous iodixanol gradients. Red arrows indicate broken particles; green arrows denote intact virions; blue arrows highlight background debris. Scale bars are indicated 50, 100 or 200 nm in each EM panel.

of tailed phage infection and genome delivery. ε15 is a short-tailed dsDNA bacteriophage that infects *Salmonella* species. During infection, it deploys a series of enzymatic proteins to mediate host attachment, genome translocation, replication, and eventual progeny release. Among these, the endolysin encoded by gene product LysSA05 is implicated in degrading the bacterial cell wall during the final stage of the lytic cycle. Although its exact mechanism remains to be fully defined, LysSA05 may possess unique structural elements that enable it to penetrate the outer membrane of Gram-negative bacteria, a rare but valuable capability among phage-derived enzymes. Characterizing its function will advance our understanding of ε15 biology and support its development as an antimicrobial agent.

3.3 LysSA05 binding specificity toward NAM and NAG disaccharides

The *Salmonella* phage ε15 genome encodes a putative endolysin gene, *gp05* (GenBank ID: AAO06088.1), hereafter referred to as LysSA05. This gene encodes a 209-amino-acid protein with an estimated molecular weight of ~25 kDa and a theoretical pI of 9.54. ProtParam analysis yielded an instability index of 21.17 and a GRAVY score of −0.456, suggesting that LysSA05 is a stable, moderately hydrophilic protein. These properties are comparable to those of LysSE24, a dual-acting endolysin reported to be active against Gram-negative bacteria (Ding et al., 2020). BLASTP analysis revealed 94.23% sequence identity to the endolysin of

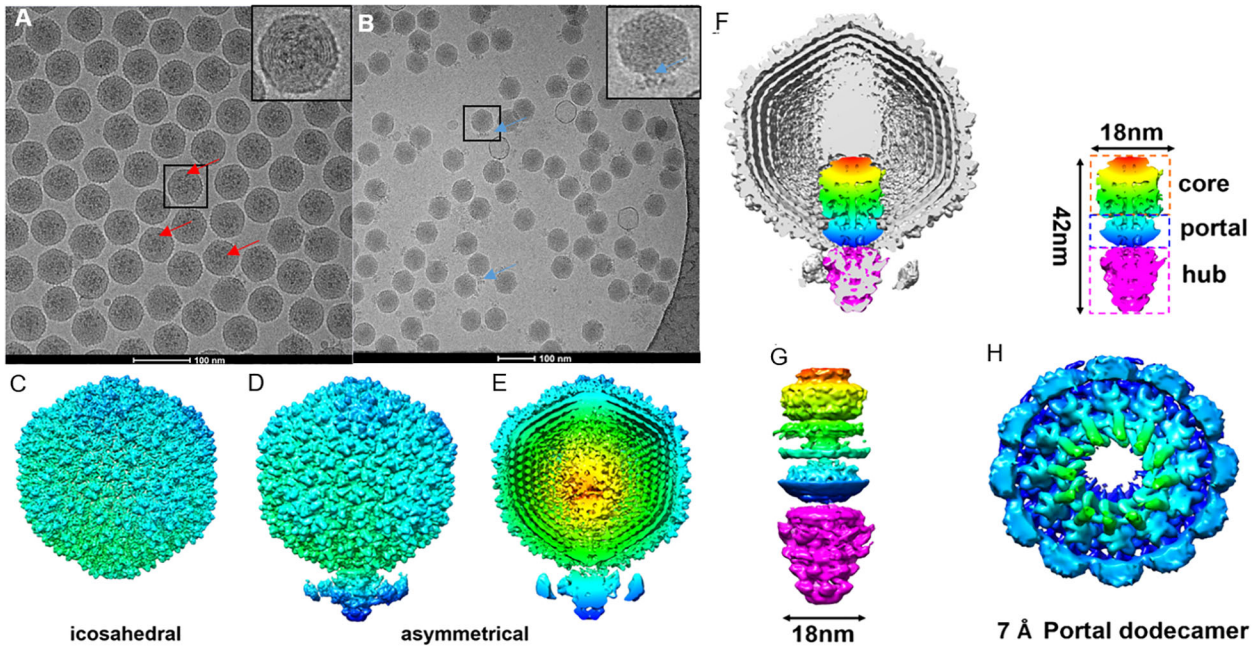

FIGURE 2
Cryo-EM grid support evaluation and asymmetric reconstruction of the genome packaging machinery in ε15. **(A)** Cryo-EM micrographs of ε15 particles vitrified on a standard holey carbon grid, exhibiting strongly preferred orientation. **(B)** Cryo-EM micrographs of ε15 prepared on a perforated grid coated with a GO, demonstrating improved particle dispersion and orientation. **(C)** Icosahedral 3D reconstruction of the capsid, revealing the symmetric protein shell architecture. **(D)** Asymmetrical reconstruction of the full virion, capturing the tail complex anchored at a unique capsid vertex. **(E)** Cross-sectional view of the asymmetric map, with radial coloring highlighting concentric layers of packaged genomic DNA. **(F)** Cutaway view of the full reconstruction, illustrating the ordered DNA arrangement and the portal-tail complex. The schematic outlines three main components: core, portal, and hub regions (~42 nm total length, ~18 nm core width). **(G)** Side view of the portal-tail complex density map, shown in both intact and exploded views corresponding to the structural elements in panel **(H)** Focused 7 Å reconstruction of the portal region, revealing a dodecameric ring composed of 12 subunits critical for DNA translocation. Red arrow: the tail of ε15 aligned with the icosahedral axis.; Blue arrow: the tail of ε15 positioned at the side of the icosahedron. Scale bar: 200 nm for panels **(A, B)**.

Salmonella phage SPN1S (Supplementary Figure 2A). Conserved domain searches and phylogenetic analysis identified a GH19 catalytic domain spanning residues 12-208 (Supplementary Figure 2C). Secondary structure prediction using PSIPRED and PHD indicated that LysSA05 is predominantly α-helical (57.89%) with notable coil regions (38.76%), including a predicted transmembrane helix between residues 39-54 (Supplementary Figure 2B). Functional annotation revealed a modular architecture comprising a peptidoglycan binding domain (PBD) and a peptidoglycan cleaving domain (PCD). HHpred analysis further classified the protein within the CAZy GH19 family (E-value = 12, probability = 83.6%), supporting its potential to hydrolyze β-1,4 glycosidic bonds between NAM and NAG within bacterial cell walls (Figure 3A). Tertiary structure modeling using Phyre2 selected the endolysin from *S. Typhimurium* phage SPN1S (PDB ID: C4OK7A) as the optimal structural template (Figure 3B). The predicted model showed a root mean square deviation (RMSD) of 0.085 relative to the template, indicating strong structural similarity (Figure 3C). Model validation by ERRAT yielded a quality score above 95%, while Ramachandran plot analysis showed 91% of residues in favored regions, collectively, supporting the reliability and accuracy of the predicted LysSA05 structure (Supplementary Figure 2D). To investigate the molecular basis of PG recognition by LysSA05 endolysin, cavity-guided blind docking was performed using CB-Dock2 with two critical PG monomers: NAM and NAG. Docking of NAM produced the top-ranked pose in the largest cavity (Vina score: -5.3 kcal/mol) (Figures 3D–G), where NAM was deeply embedded into a hydrophilic pocket lined by residues E49, R55, S50, and Q128. Multiple hydrogen bonds and hydrophobic contacts with I126 and L56 stabilized the ligand orientation within the groove. Similarly, NAG docking identified a favorable cavity (Vina score: -5.3 kcal/mol), with five hydrogen bonds formed with E49, S50, L55, L56, Q57, and E58. Additional hydrophobic interactions with N59, G123, G125, Q128, L126, and I127 contributed to ligand stabilization within a polar-hydrophobic binding pocket (Figures 3H–K). The observed binding poses and interaction geometries suggest that both NAM and NAG occupy functionally relevant substrate-binding pockets in LysSA05, mimicking native PG recognition. These insights provide a structural rationale for future mutational or inhibitor design. As with others GH19 family glycoside hydrolases, the active site is shaped to accommodate NAM-NAG disaccharides, enabling precise positioning of the scissile bond β-1,4 glycosidic for hydrolysis. The substrate is stabilized through a conserved network of hydrogen bonding and hydrophobic contacts within the catalytic groove, underscoring the structural and functional potential of LysSA05 as a PG-degrading enzyme.

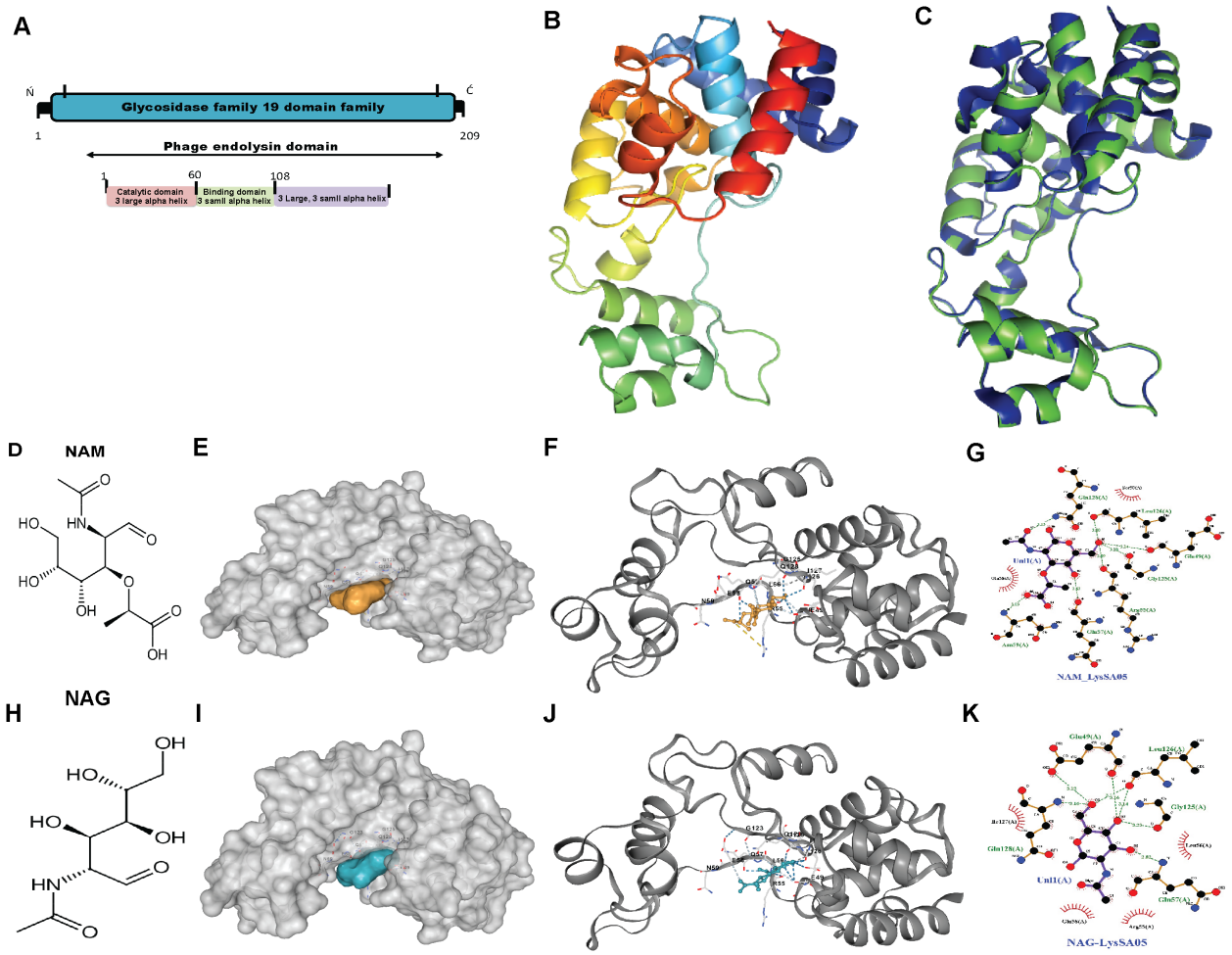

FIGURE 3
Structural features and molecular docking of LysSA05 endolysin with peptidoglycan ligands NAM and NAG. **(A)** Domain architecture of LysSA05 endolysin, highlighting the glycosidase family 19 (GH19) catalytic domain (pink) and the peptidoglycan-binding domain (green), along with predicted α-helical segments. **(B)** Ribbon diagram of the predicted 3D structure of LysSA05, showing domain organization and two prominent groove loops. **(C)** Superimposition of the predicted LysSA05 structure with a homologous template (PDB: 4OK7), shown in blue. **(D)** 2D chemical structure of NAM. **(E)** Surface representation of LysSA05 with NAM-binding cavity highlighting in yellow. **(F)** NAM docked into catalytic groove of LysSA05 (cartoon view); key interactions are shown as dashed lines. **(G)** Zoomed-in view of the NAM binding pocket, showing hydrogen bonds and hydrophobic contacts stabilizing the interaction. **(H)** 2D chemical structure of NAG. **(I)** Surface representation of LysSA05 with the NAG-binding pocket highlighted in blue. **(J)** NAG docked into LysSA05 cavity, visualizing ligand–protein interactions. **(K)** Close-up of the NAG binding site; showing hydrogen bonds are represented by green bashed lines, while red spokes denote hydrophobic interaction, with bond distance shown in angstrom Å.

3.4 Antimicrobial propensity and LysSA05 derived AMP peptides

To explore alternative therapeutics against MDR pathogens, the endolysin LysSA05 from phage ε15 was screened for membrane-active, AMP-like regions. Initial physicochemical analysis using HeliQuest on a 54-residue segment identified 155 helix positions ranked by amphipathic potential (Supplementary Table 3). Of these, 17 distinct amphipathic helices displayed pronounced AMP-like characteristics, marked by elevated hydrophobic moment (μH) and net positive charge (z), indicative of strong membrane-disruptive potential (Figure 4A). Notably, helices at positions 59 and 60 exhibited optimal μH values (≥ 0.15) and high net charge (+6), suggesting robust amphipathic properties (Figures 4B, C) and a potential role as functional AMP domains capable of destabilizing bacterial membranes. Further screening using machine learning classification of 20-residue segments across 189 peptide positions revealed varying counts of AMP-positive predictions: RF identified the most (46), followed by DA (35), ANN (34), and SVM (28). Positional mapping of these predictions revealed distinct model-specific distribution patterns. Notably, SVM exhibited a strong positional bias towards the N-terminal to mid-sequence, while other models detected AMP-like regions more broadly across the protein (Figures 4D–G). To further validate the predicted antimicrobial regions within LysSA05, the probability scores assigned by each classifier to AMP and non-AMP (NAMP) segments were analyzed. Peptides classified as AMPs consistently exhibited significantly higher probability scores than NAMPs across all models (SVM, RF, and DA), indicating high classifier confidence (Figures 4H–J). Among these, the DA model demonstrated the

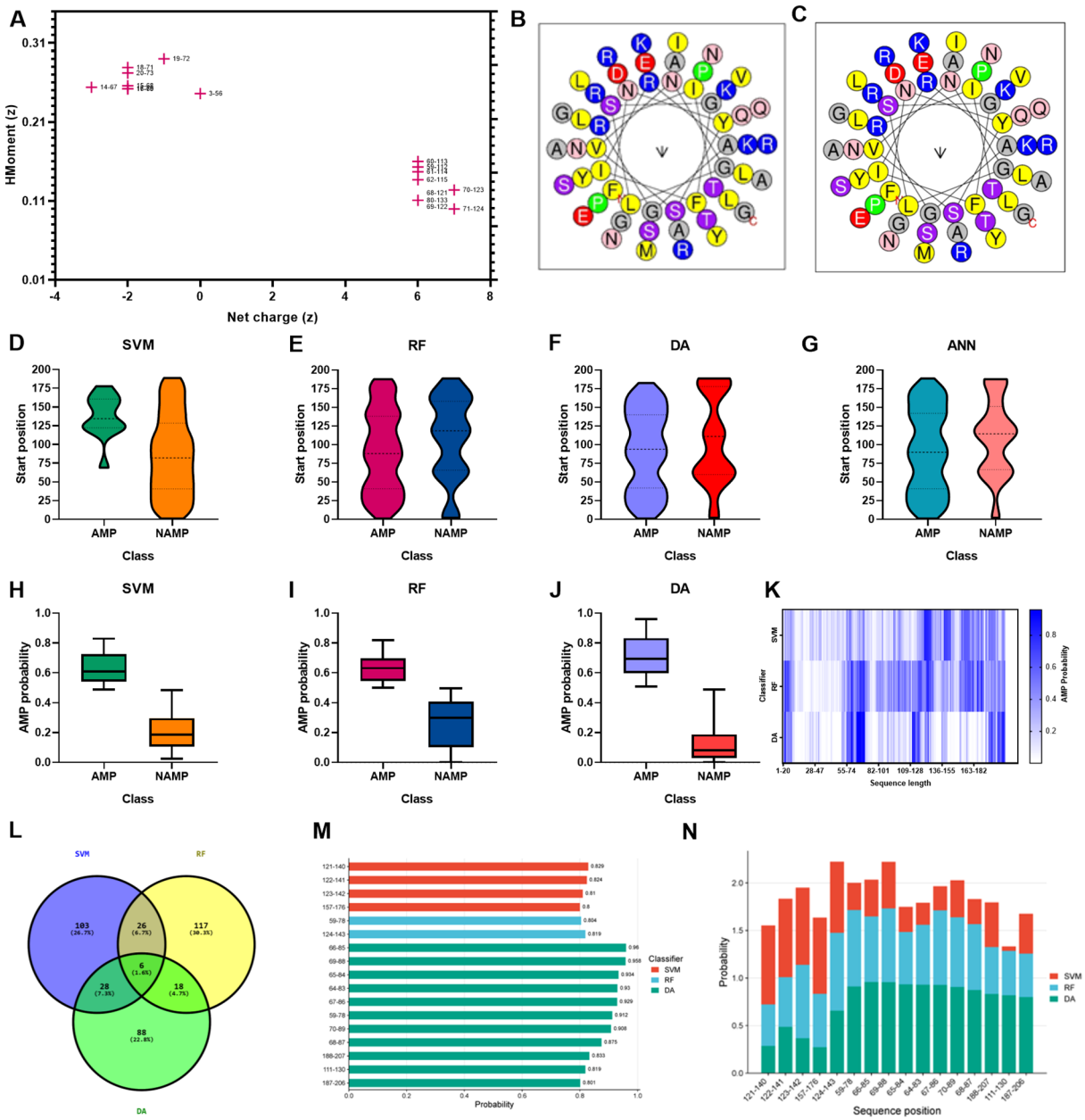

FIGURE 4
AMP prediction from LysSA05 using machine learning and physicochemical profiling. **(A)** Preliminary-HeliQuest analysis showing net charge (z) and hydrophobic moment (μH) of predicted helical segments. **(B–C)** Helical wheel projections of top two amphipathic helices, illustrating residue polarity and spatial distribution. **(D–G)** Distribution of AMP and NAMP prediction across helix position based on four machine learning classifiers: SVM, RF, DA, and ANN. **(H–J)** AMP probabilities scores for predicted segments; AMP-classified helices consistently show significantly higher probability across all the models. **(K)** Heatmap representing AMP probabilities scores across the LysSA05 sequence, highlighting regions with high AMP potential. **(L)** Venn diagram illustrating the overlap of AMP predictions among SVM, RF, and DA classifiers. **(M)** Top- ranked AMP helices predicted by SVM, RF, and DA with probability scores ≥ 0.8. **(N)** Final selection of high-confidence AMP helices in LysSA05 identified across the three classifiers (SVM, RF, DA), each with AMP probability ≥ 0.8.

strongest discriminatory power, with AMP segments clustering near probability values > 0.9, while NAMPs remained below 0.4. A heatmap analysis revealed the spatial probability distribution of AMP probability scores across the LysSA05 sequence, highlighting recurrent high-probability regions between residues 60–90 and 120-140 (Figure 4K). Notably, the top-ranked AMP segments identified by each classifier included helix 121-140 (SVM, 0.829), helix 124-143 (RF, 0.819), helix 66-85 (DA, 0.96). Although these high-scoring helices varied slightly in position across classifiers, they converged in identifying two AMP-enriched regions. Despite the strong performance of individual classifier, overlap among the top predictions was limited: only six sequences (1.6%) were shared across all three models (Figure 4L). Applying a probability threshold of ≥ 0.8, 4 helices from SVM, 2 from RF, and 11 from

DA were identified (Figure 4M). Interestingly, none of the high-confidence predictions overlapped at the same helix position across models, suggesting that each classifier captured distinct AMP-relevant features. Among these top candidates, the helices 59-78, 65-84, 67-86, and 188-207 were consistently assigned high scores by multiple models, representing promising antimicrobial targets (Figure 4N). Collectively, these findings indicate that LysSA05 harbors several AMP-like regions with distinct location-specific enrichment patterns, which may contribute to its membrane-disruptive activity and broad-spectrum antibacterial potential.

3.5 Amphipathic and structural features of top-ranked AMP-like peptides from LysSA05 endolysin

By integrating ML-based classification (Supplementary Tables 4–9, Table 1) with physicochemical screening using HeliQuest (Supplementary Table 10), four outstanding candidate peptides helix 59 (z = +2, μH = 0.29), helix 67 (z = +2, μH = 0.353), helix 68 (z = +3, μH = 0.32), and helix 69 (z = +3, μH = 0.331) were identified that exhibited both high AMP probabilities and strong amphipathic character. These candidates were selected from comprehensive segmentation of 20-residue window across 189 helical positions (Supplementary Table 11). To assess their membrane-targeting potential, helical wheel projections and 3D ribbon modeling were performed. The peptides corresponding to positions 59-78, 67-86, 68-87, and 69–88 displayed well-define amphipathic α-helical structures, characterized by a clear segregation of hydrophobic residues (F, L, I, A, G, V) on one face and positively charged residues (R, K) on the opposite hydrophilic face, a hallmark of membrane active AMPs. Helical wheel diagrams confirmed that these peptides exhibit ideal biophysical properties for membrane disruption, with hydrophobic moments ranging from 0.29 to 0.353 and net charges between +2 and +3. 3D modeling of peptide 59–78 further supported a stable α-helical conformation, consistent with its predicted role in membrane interaction (Figures 5A–D). These structural features parallel those found in previously characterized broad-spectrum phage endolysins known to possess outer membrane-permeabilizing activity. Collectively, these findings highlight the central region of LysSA05 spanning residues 59-112, as a key AMP-like domain with dual functional potential: enzymatic degradation of PG via NAM-NAG interactions, and direct disruption of the Gram-negative outer membrane through embedded amphipathic helices. This dual-action model underscores LysSA05's promise as a broad-spectrum enzybiotic candidate.

3.6 Expression optimization and purification of recombinant endolysin LysSA05

To facilitate downstream functional validation of LysSA05 as a membrane-disruptive, AMP-like endolysin, the *gp05* gene encoding LysSA05 was successfully cloned and sequence-verified (Figure 6A shows the schematic representation; Supplementary Figures 3A-C confirms successful cloning). Expression analysis revealed a ~25 kDa band consistent with the predicted molecular weight of LysSA05, with markedly stronger expression observed in *E. coli* Rosetta (DE3) induced with 1 mM IPTG at 37°C (Figures 6B–D), compared to BL21 (DE3) (Supplementary Figure 3D, E). The protein was localized exclusively in the insoluble fraction, indicating the formation of inclusion bodies under all tested conditions. Subsequent purification yielded highly enriched LysSA05 protein from Rosetta (Figure 6F), in contrast to lower yield from BL21 (Figure 6E). Final protein concentrations reached ~11 mg in Rosetta (DE3), significantly exceeding the ~2.5 mg obtained from BL21. The refolded protein with > 90% purity was stable and of sufficient quality for downstream biochemical assays. These findings confirm Rosetta as a more efficient expression host and provide a robust production system for high-purity LysSA05. This enables comprehensive investigation of its dual functional potential: enzymatic cleavage of PG and membrane-disruptive activity predicted through machine learning and structural modeling approaches.

3.7 Characterization of LysSA05 activity

The lytic activity of full-length recombinant LysSA05 was evaluated against Gram-negative strains *E. coli* C and *S. anatum*. SDS-PAGE followed by silver staining of extracted LPS matrices revealed pronounced degradation upon LysSA05 treatment, with a marked reduction in LPS band intensity in *E. coli* C compared to untreated controls (Figures 7A, B). These findings indicate that LysSA05 can directly disrupt LPS, a key structural component of Gram-negative outer membrane. Complementary CFU reduction assays further demonstrated LysSA05's intrinsic lytic activity, showing a ~2.0 $\log_{10}$ reduction in *E. coli* C and ~1.3 $\log_{10}$ in *S. anatum* after 5 h (Figure 7C). Notably, co-treatment with OMPs (EDTA and citric acid) significantly enhanced LysSA05-mediated lysis. In combination with EDTA, bacterial killing increased to ~4.5 $\log_{10}$ in *E. coli* C and ~3.4 $\log_{10}$ in *S. anatum* (Figures 7D, F), while citric acid produced comparable enhancement (Figures 7E, G). These results strongly support the presence of membrane-active elements in LysSA05, likely associated with its amphipathic α-helical regions, and highlight its capacity to overcome the intrinsic barrier imposed by Gram-negative outer membranes. Collectively, these findings support the hypothesis that full-length LysSA05 functions as a dual-acting enzybiotic, exhibiting both membrane-permeabilizing activity, experimentally confirmed through LPS degradation assays and CFU reduction assay, and PG-cleaving potential, inferred from GH19 domain modeling and ligand docking with NAM and NAG. This dual functionality underscores its promise as a therapeutic candidate against MDR Gram-negative pathogens.

3.8 Antibacterial activity of LysSA05 against MDR clinical isolates

To evaluate the broader antimicrobial potential of LysSA05, we tested the activity of full-length recombinant protein, containing

TABLE 1 Top-ranked helical segments in LysSA05 with AMP probability scores ≥ 0.8 across as predicted by three machine learning classifiers: (SVM, RF, DA, and ANN).

Position	Sequence segment	SVM	RF	DA	ANN
121-140	RGRGLIQITGLNNYRDCGNG	0.829	0.436	0.287	AMP
122-141	GRGLIQITGLNNYRDCGNGL	0.824	0.522	0.488	AMP
123-142	RGLIQITGLNNYRDCGNGLK	0.81	0.772	0.368	AMP
157-176	YAARSAAWFFATKGCMKYTG	0.8	0.561	0.274	AMP
124-143	GLIQITGLNNYRDCGNGLKV	0.746	0.819	0.658	AMP
59-78	NFNYSVNGLSGFIRAGRITP	0.285	0.804	0.912	AMP
66-85	GLSGFIRAGRITPDQANALG	0.385	0.689	0.96	AMP
69-88	GFIRAGRITPDQANALGRKT	0.488	0.775	0.958	AMP
65-84	NGLSGFIRAGRITPDQANAL	0.262	0.551	0.934	AMP
64-83	VNGLSGFIRAGRITPDQANA	0.231	0.63	0.93	NAMP
67-86	LSGFIRAGRITPDQANALGR	0.253	0.783	0.929	AMP
70-89	FIRAGRITPDQANALGRKTY	0.388	0.732	0.908	AMP
68-87	SGFIRAGRITPDQANALGRK	0.263	0.692	0.875	AMP
188-207	GQNGIDDRRARYITASKVLA	0.468	0.493	0.833	AMP
111-130	GNGPGDGWNYRGRGLIQITG	0.045	0.467	0.819	AMP
187-206	GGQNGIDDRRARYITASKVL	0.418	0.457	0.801	AMP

predicted AMP-like regions, against a panel of MDR clinical isolates of *E. coli* and *Salmonella* spp., with diverse resistance profiles (Supplementary Table 2). The CFU-based plating assays were conducted to quantify bacterial viability following treatment with LysSA05. LysSA05 exhibited broad-spectrum lytic activity against all tested *E. coli* clinical isolates, achieving reductions in viable cell counts ranging from 1.0 to 4.5 log units (Figure 8A). Similarly, all *Salmonella* isolates tested were susceptible to LysSA05, though to a lesser extent, showing reductions between 0.5 and 3.0 log units (Figure 8B). The observed variability in susceptibility likely reflects differences in outer membrane composition or LPS structure among strains, which can affect the accessibility and binding efficiency of membrane-active peptides. These findings highlight the broad-acting antibacterial potential of LysSA05, particularly its efficacy against MDR *E. coli*, and suggest that its therapeutic utility may extend beyond the classical Gram-positive targets typically associated with endolysins.

4 Discussion

Bacteriophages and their lytic enzymes have emerged as promising alternative antibacterial strategies to combat the escalating threat of antibiotic-resistant foodborne pathogens (Shah et al., 2023). However, their clinical application remains limited due to challenges such as the presence of endotoxins, residual cellular debris, and incomplete understanding of how phage structural integrity relates to infectivity and enzymatic function. Phages rely on precisely coordinated assembly of structural components such as capsid, tail fibers, DNA packaging machinery, alongside enzymatic machinery including holins, endolysins, and depolymerases to successfully infect and lyse bacterial hosts (Kim et al., 2025a; Guliy and Evstigneeva, 2025). In this study, *Salmonella* phage ε15 was employed as a model system to refine purification protocols and achieve high-resolution structural visualization. An iodixanol-based density gradient in PBS was optimized to improve phage purification while preserving structural integrity (Hirst and Hutchinson, 2025). Additionally, an enhanced cryo-EM grid preparation method using GO-support film (Fan and Sun, 2022; Chio et al., 2024) enables the capture of intact, highly purified ε15 particles with preserved infectivity and native morphology. Unlike traditional CsCl ultracentrifugation, which often compromises phage bioactivity and can lead to partial genome ejection, the iodixanol-based purification approach yielded virions that retained full genomic DNA and correctly assembled tail fibers. Importantly, the purified, intact, and infectious ε15 virions were validated through plaque assay, in contrast to many prior structural studies that did not confirm post-purification infectivity (Jiang et al., 2006; Suleman et al., 2022). This optimized method not only enabled near-native, high-resolution visualization of ε15 capsid and DNA packaging machinery but also resulted in endotoxin-free phage preparations with potential for therapeutic application. In parallel, the dual-acting endolysin LysSA05 was functionally characterized through integrative structural modelling and enzymatic assays to elucidate how phage-derived enzymes impact bacterial pathogens. Together, these analyses provide new insights into phage-host interactions at both the

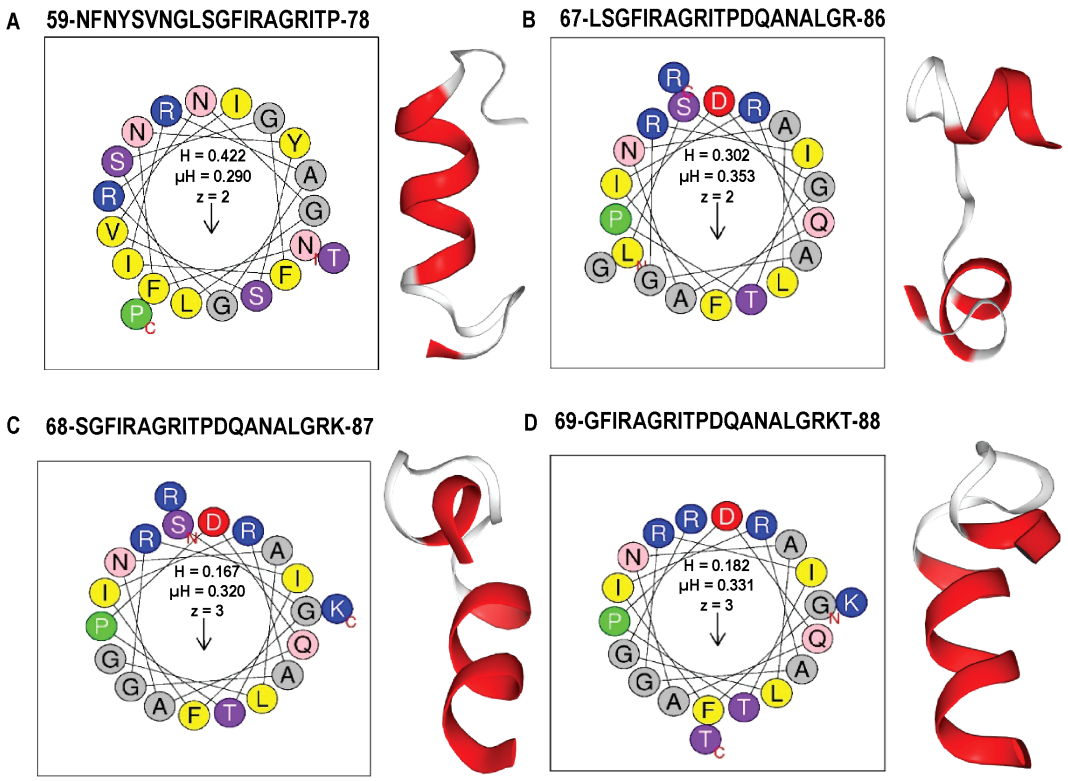

FIGURE 5
Amphipathic properties and α-helical structures of top AMP-like peptides derived from LysSA05 endolysin. **(A–D)** Helical wheel projections and physicochemical parameters for four top-ranking peptides **(A)** 59–78, **(B)** 67–86, **(C)** 68–87, and **(D)** 69–88 generated using HeliQuest. Each projection illustrates the distribution of residues around the helical axis, revealing distinct amphipathic separation: polar/charged residues (blue/purple) cluster on the solvent-exposed face, while hydrophobic residues (yellow/grey) align on the membrane-interacting face. Accompanying boxes summarize key parameters: hydrophobicity **(H)**, hydrophobic moment (μH), and net charge (z). The 3D ribbon diagram (left panels) shows predicted α-helical confirmation of each peptide, highlighting their structural potential for membrane insertion and antimicrobial activity.

structural and functional levels, supporting the advancement of phage-based therapeutics and enzybiotics targeting MDR Gram-negative pathogens.

4.1 Cryo-EM structural analysis of ε15

Cryo-EM analysis of ε15 in this study achieved substantially higher and more complete resolution than previous approaches by preserving fully intact virions. By avoiding traditional CsCl-based purification, which often compromises structural integrity, we were able to visualize the near-native icosahedral state of ε15 and reconstruct a higher-resolution density map that revealed new insights into its genome packaging architecture. In contrast, earlier reconstructions frequently suffered from partial DNA loss or excluded the asymmetric tail structure. For example, Jiang previously achieved only ~20 Å resolution for the entire ε15 virion (Jiang et al., 2006), and later improved to ~4–5 Å resolution through icosahedral averaging, which excluded the tail (Jiang et al., 2008). In this study, asymmetric reconstruction resolved the internal layers of packaged DNA, illustrating the tightly organized nature of the encapsidated genome. Detailed density analysis of the DNA translocation machinery revealed a complex comprising the portal, core, and hub regions. The portal region reached an estimated resolution of ~7 Å, enabling visualization of architectural details previously inaccessible in ε15. Notably, multiple concentric layers of DNA were clearly resolved inside the capsid, reflecting the extreme ~3,000-fold compaction required to accommodate the ~40 kb genome. This exceptionally high packing density underscores the immense internal pressure phages must withstand and offers insights into how that stored energy may be harnessed during genome ejection. These findings provide a more complete understanding of ε15 structural biology and highlight the value of improved purification and cryo-EM workflows in resolving phage architecture at near-native conditions.

The structure of bacteriophage ε15 also elucidates several key mechanistic features of infection and genome delivery. Direct visualization of the small gp10 subunits linking adjacent capsomers on the inner surface of the capsid supports the "molecular staple" hypothesis, wherein these dimers stabilize the capsid lattice under high internal pressure (Baker et al., 2013). Additionally, the portal complex located at a unique capsid vertex was conclusively shown to form a dodecameric (12-fold) ring that interfaces with a hexameric tail hub, an asymmetric interaction consistent with prior biochemical evidence (Guichard et al., 2013). This asymmetry forms a natural gating mechanism for DNA

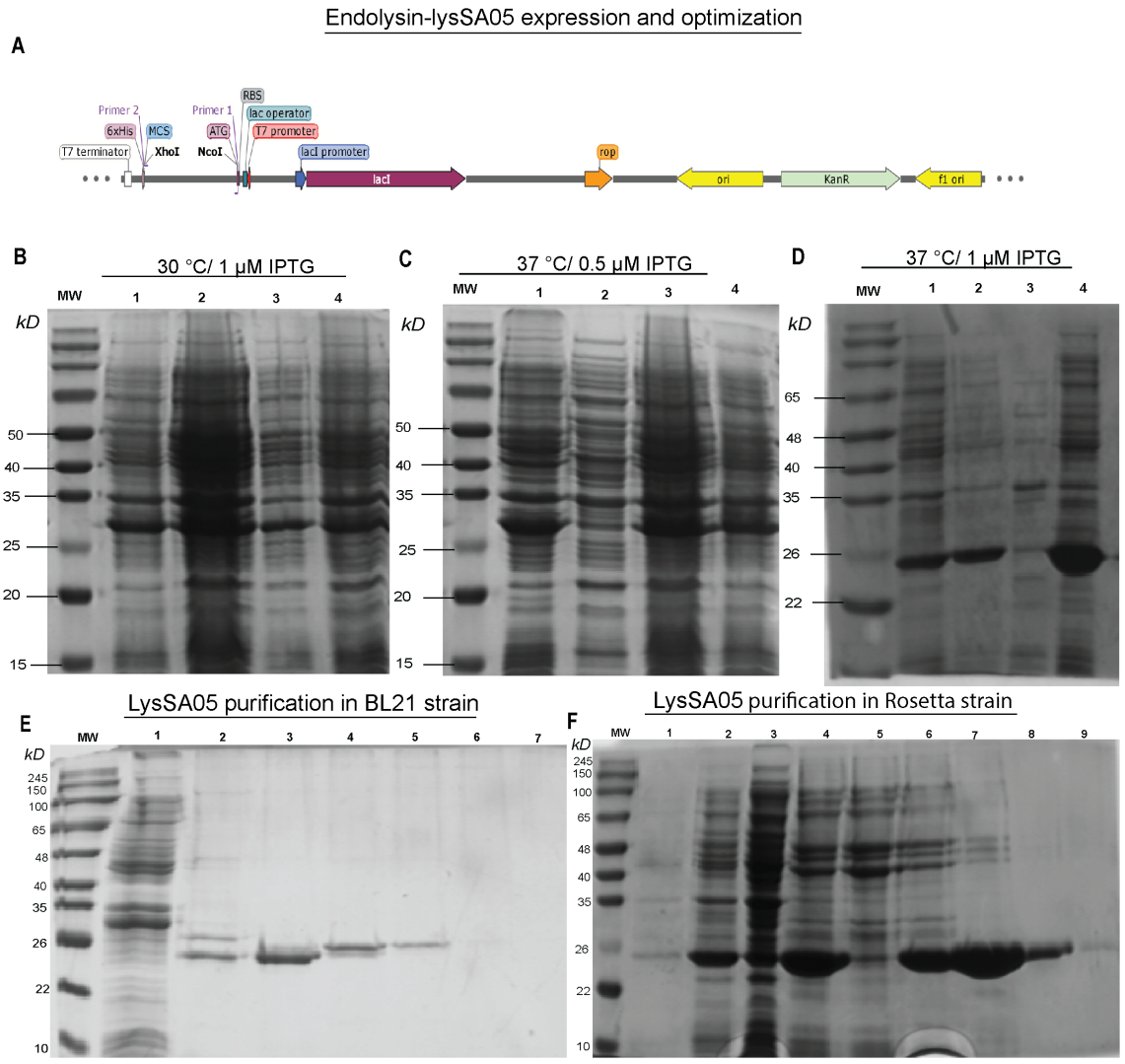

FIGURE 6
Expression optimization and purification of recombinant LysSA05. **(A)** Schematic diagram illustrating the cloning of *gp05* into the pET-28a(+) vector using *NcoI* and *XhoI* restriction sites. **(B–D)** SDS-PAGE analysis of expression optimization in *E. coli* Rosetta under varying conditions: **(B)** 30°C with 1 mM IPTG; **(C)** 37°C with 0.5 mM IPTG; **(D)** 37°C with 1 mM IPTG. A distinct ~25 kDa band corresponding to His_6-tagged LysSA05 is observed in lane 4 (Rosetta, 37°C, 1 mM IPTG), indicating optimal expression. **(E)** Purification of LysSA05 from *E. coli* BL21 showing low yield after Ni-NTA affinity chromatography across elution fractions 3-6, compared to control (lanes 1, 2). **(F)** Purification from Rosetta strain showing high expression and high >90% purity of the ~25 kDa protein across elution fractions 5-9. Lane 1: non-induced control; Lane 2: supernatant after centrifugation; Lane 3: soluble fraction post-sonication; Lane 4: total cell lysate post-sonication.

release. The portal-tail apparatus spans approximately 42 nm and functions as a conduit that holds the encapsidated genome under tension, supporting the previously proposed "primed" ejection state model (Jiang et al., 2006). Structural data from ε15 imply a spring-loaded mechanism, in which tail fiber engagement with the host cell surface triggers the opening of the portal-hub gate, leading to rapid DNA expulsion. This model aligns with *in situ* observations from cryo-electron tomography (Chang et al., 2010) and mirrors genome release strategies described in other double-stranded DNA viruses, such as herpesviruses. The precise geometry and dimensions of the ε15 DNA packaging and ejection apparatus offer quantitative parameters for modeling phage genome confinement and release dynamics. These findings not only clarify fundamental aspects of phage infection but also provide a framework for bioengineering applications involving DNA delivery systems.

These insights not only deepen our understanding of the ε15 life cycle but also carry important practical implications. The ability to visualize the complete DNA packaging and injection machinery at high resolution provides a structural blueprint for elucidating phage-host interaction mechanisms and enables structure-guided phage engineering. For example, detailed knowledge of the portal and tail structures opens avenues to modify phages for altered host specificity, enhancing their potential for therapeutic applications. Achieving even higher resolution (2–3 Å) in key regions could uncover fine structural details that govern phage infectivity, timing of lysis, and interactions with bacterial receptors. Moreover, the use

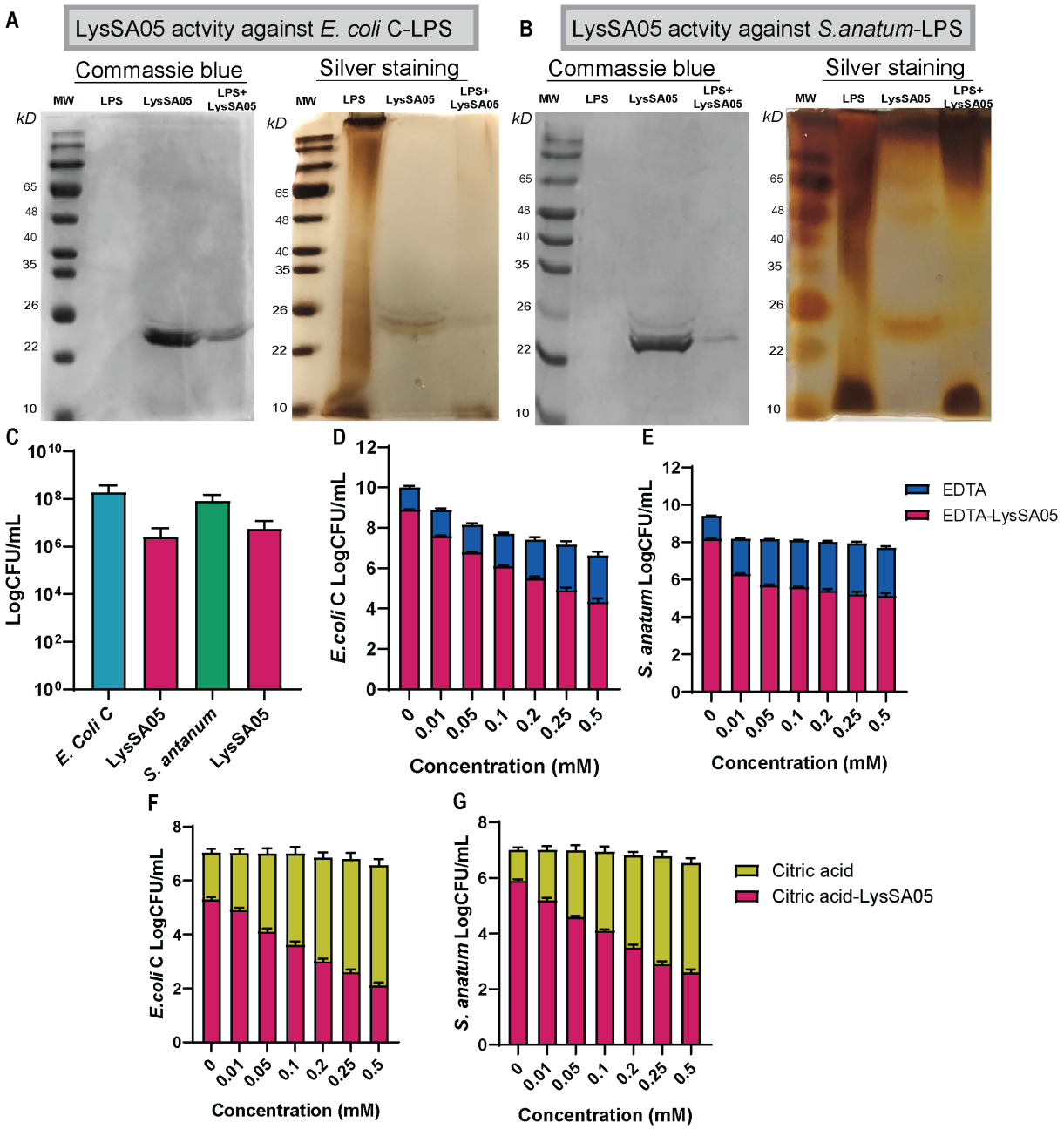

FIGURE 7
Characterization of LysSA05 LPS-degrading activity and enhancement of antibacterial activity by OMPs. **(A)** SDS-PAGE and silver staining demonstrating LPS degradation in *E. coli* C following treatment with LysSA05. **(B)** SDS-PAGE and silver staining showing LPS degradation in *S. anatum* treated with LysSA05. **(C)** CFU reduction assay indicating the direct antibacterial effect of LysSA05 against *E. coli* C and *S. anatum*, with log reductions of approximately 2.0 and 1.3, respectively, after 5 h of incubation. **(D, E)** Synergistic effect of various EDTA concentrations (mM) in combination with LysSA05 against *E. coli* C and *S. anatum*. **(F, G)** Synergistic effect of different citric acid concentrations (mM) in combination with LysSA05 against *E. coli* C and *S. anatum*.

of an endotoxin-free GO-supported cryo-EM workflow can be extended to other therapeutic phages, enabling the capture of transient intermediate states during infection, states that have previously been difficult to visualize. Future studies employing the iodixanol-based purification approach may allow real-time visualization of dynamic events such as tail tube extension during DNA injection, thereby bridging the current gap between static structural snapshots and the dynamic nature of phage infection. Such advances will not only enhance our mechanistic understanding of phage biology but also inform the rational design of next-generation phage therapeutics with improved efficacy and safety.

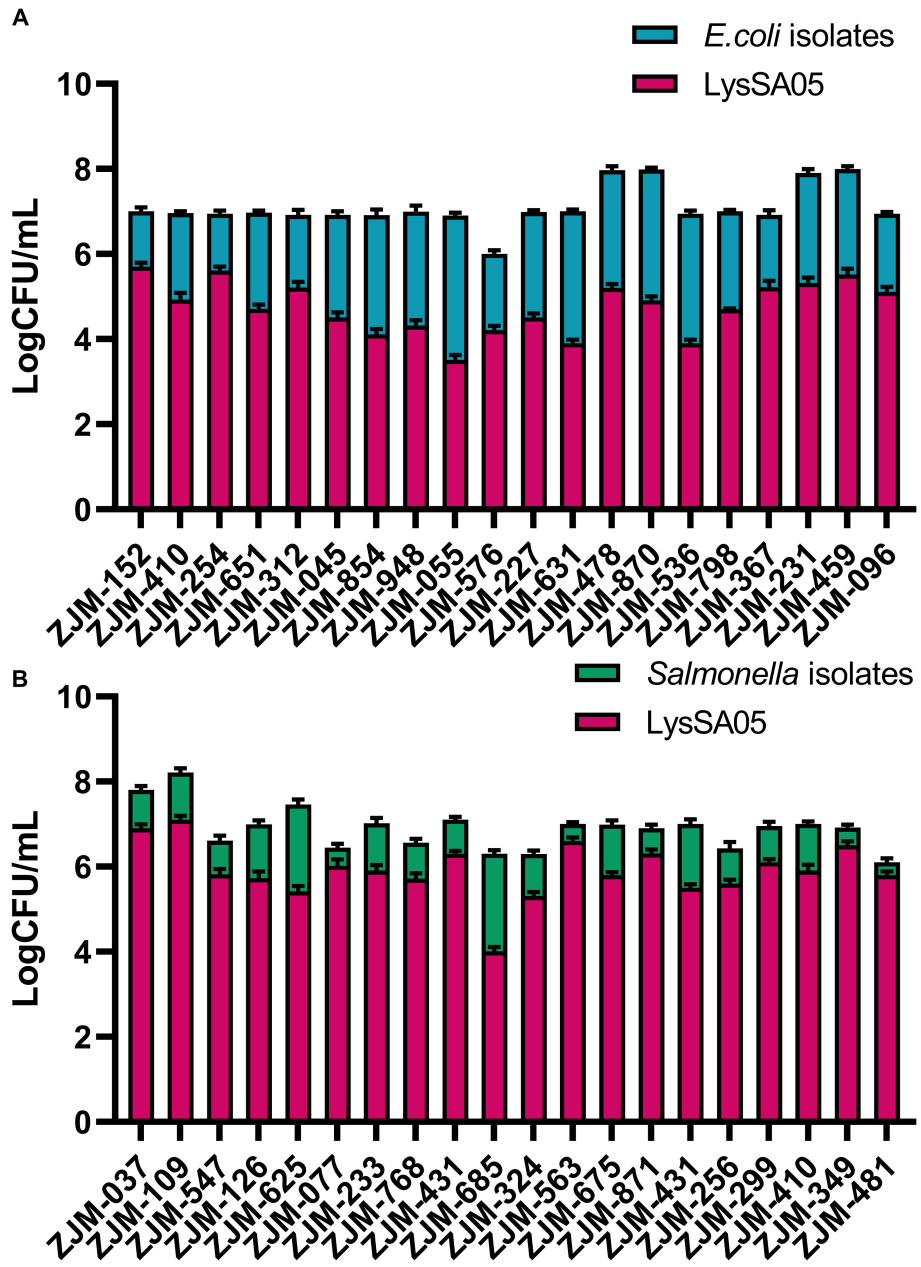

FIGURE 8
Antimicrobial activity of LysSA05 against clinical isolates of *E. coli* and *Salmonella*. **(A)**. Bactericidal effect of LysSA05 (100 µg/ml) against logarithmic-phase *E. coli* clinical isolates following 1 h incubation at 37°C. **(B)** Bactericidal effect of LysSA05 (100 µg/ml) against logarithmic-phase *Salmonella* clinical isolates under the same conditions.

4.2 LysSA05 endolysin activity against Gram-negative bacteria

The endolysin LysSA05 from ε15 highlights the potential of phage-derived enzymes as antimicrobial agents beyond their conventional role in the phage infection cycle. Typically, phage endolysins act intracellularly at the final stage of the replication cycle, cleaving the PG layer from within to facilitate the release of progeny virions (Guliy and Evstigneeva, 2025). Historically, such enzymes have been most effective against Gram-positive pathogens, whose exposed PG layers are readily accessible. In contrast, the outer membrane of Gram-negative bacteria serves as a formidable barrier, shielding the PG layer and preventing the activity of externally applied endolysins (Zampara et al., 2020). Consistent with this, the majority of endolysins derived from Gram-negative phages exhibit little to no activity unless the outer membrane is first permeabilized by OMPs (Park et al., 2014). To overcome this limitation, bioengineered chimeric endolysins, such as Artilysins and Innolysins, have been developed. These constructs combine enzymatic PG-degrading domains with OMPs, and have demonstrated broad-spectrum activity against Gram-negative

pathogens (Yang et al., 2015; Thandar et al., 2016; Murray et al., 2021).

LysSA05 is particularly significant in this context because it naturally bypasses the outer membrane barrier of Gram-negative bacteria, a key limitation for most endolysins. Docking and domain prediction analyses reveal that LysSA05 consists of a PG-cleaving glycosidase domain and a C-terminal amphipathic peptide region. Sequence homology indicates that its catalytic domain belongs to the GH19, consistent with endolysins such as LysSPN1S, PlyG, and LysCP28, which cleave PG glycan chains (Lu et al., 2023). Building upon recent advances in AMP-ESKtides databases curated from phage genomes (Wu et al., 2024), the C-terminal region of LysSA05 was identified as highly cationic and hydrophobic. This same 20-amino acid segment was predicted by multiple machine learning tools to be membrane-active and shares strong similarity with motifs found in broad-spectrum endolysins such as Abtn-4 and SPN1S, known for their activity against both Gram-positive and Gram-negative pathogens. Computational modeling suggests that upon encountering a Gram-negative bacterium, the positively charged helical tail of LysSA05 inserts into the outer membrane lipid bilayer, creating localized disruptions or pores. This perturbation of the outer membrane may enable the ~18 kDa catalytic domain to translocate, or at minimum, access, the underlying PG layer, which it can then enzymatically degrade. In essence, LysSA05 harbors its own intrinsic AMP-like module that functions similarly to an OMP. This built-in mechanism explains LysSA05's ability to exert direct lytic activity against Gram-negative bacteria without the need for external helper agents, a unique and valuable feature that distinguishes it from most known endolysins.

LysSA05 belongs to a rare class of phage-derived endolysins with intrinsic activity against Gram-negative bacteria. Notably, endolysins such as gp279 from *Pseudomonas* phage OBP and LysAB2 from an *Acinetobacter baumannii* phage harbor C-terminal amphipathic helices that allow them to breach the outer membrane, thereby conferring anti-Gram-negative activity (Cornelissen et al., 2012; Lai et al., 2011). Similarly, gp144 from *Pseudomonas aeruginosa* phage φKZ and ABgp46 from *A. baumannii* phage vb_AbaP_CEB1 have been shown to degrade the cell wall of Gram-negative bacteria and exhibit lytic activity against MDR strains (Paradis-Bleau et al., 2007; Oliveira et al., 2016). Similarly, the endolysin ABgp46 demonstrates broad-spectrum activity against Gram-negative bacteria, including MDR *A. baumannii* (Oliveira et al., 2016). Strikingly, LysSA05 demonstrated potent intrinsic lytic activity against Gram-negative bacteria without the need for external membrane-disrupting agents. Purified LPS degradation assays and antibacterial activity measurements confirmed that this ε15-derived endolysin possesses dual functionality: it not only degrades PG through its GH19 catalytic domain but also contains an amphipathic α-helical region at the C-terminus that facilitates outer membrane permeabilization. This dual action enables LysSA05 to overcome the outer membrane barrier, a major obstacle for most native endolysins targeting Gram-negative pathogens. The findings presented here align with previous reports of broad-spectrum or engineered endolysins, such as PlyF307, which also exhibit potent activity against MDR Gram-negative bacteria (Lood et al., 2015). However, the ability of LysSA05 to naturally bypass the outer membrane without auxiliary agents is uncommon and underscores its potential as a highly effective therapeutic enzybiotic.

The dual functional profile of LysSA05 holds considerable promise for combating antibiotic-resistant Gram-negative infections. As a purified endolysin enzyme with both PG-cleaving and membrane-disruptive activities, LysSA05 could potentially be employed as a stand-alone antibacterial agent or as an adjunct to antibiotics and lytic phages, without requiring outer membrane permeabilizers, for therapeutic purposes. Moreover, because it originates from a bacteriophage, LysSA05 may exert lower selective pressure for resistance compared to traditional antibiotics, particularly when used in combination with phages targeting the same bacterial pathogen. However, several challenges remain for the clinical translation of LysSA05. Its stability, half-life, immunogenicity, and potential toxicity must be rigorously evaluated *in vivo* to ensure safety and efficacy. Nonetheless, this study contributes valuable advances in both endolysin characterization and phage purification techniques relevant to therapeutic development. By enriching ε15 particles free of endotoxins and cellular debris, this work moves a step closer to making phage therapy safer and more clinically viable. Highly purified phage preparations reduce the risk of inflammatory side effects associated with contaminants, thus supporting their potential for systemic administration. Furthermore, the high-resolution structural insights presented here offer a foundation for engineering hypothetical phage proteins and for deepening our understanding of the molecular mechanisms underlying phage infection. Looking ahead, the properties by LysSA05 provide a compelling framework for the discovery and development of novel phage-derived AMPs and enzybiotics. In summary, this study not only advances our understanding of phage structural biology but also supports ongoing efforts to develop phage-based therapeutics and enzybiotics to address the persistent global threat of MDR bacterial pathogens.

Data availability statement

The datasets presented in this study can be found in online repositories. The complete phage genome sequence of ε15 is available at GenBank under accession number NC_004775.2. Additional datasets, including raw data and analysis files, are provided in the Supplementary Material at: https://www.frontiersin.org/articles/10.3389/fcimb.2025.1643576/full#supplementary-material.

Author contributions

MK: Visualization, Formal analysis, Validation, Data curation, Methodology, Software, Writing – review & editing, Investigation, Conceptualization, Writing – original draft. JW: Funding acquisition, Supervision, Writing – review & editing, Resources, Formal analysis, Methodology, Conceptualization, Validation. SJ:

Formal analysis, Methodology, Conceptualization, Data curation, Writing – review & editing, Investigation. DT: Data curation, Validation, Writing – review & editing, Resources, Writing – original draft, Visualization. BS: Methodology, Data curation, Conceptualization, Investigation, Writing – review & editing, Formal analysis. SP: Writing – review & editing, Software, Methodology, Conceptualization, Data curation, Investigation. JZ: Conceptualization, Funding acquisition, Writing – review & editing, Resources, Project administration, Supervision. JY: Project administration, Supervision, Resources, Funding acquisition, Writing – review & editing, Visualization, Conceptualization, Validation.

Funding

The author(s) declare financial support was received for the research and/or publication of this article. We sincerely thank the Dalian Deng Feng Program for supporting this work through the Key Medical Specialties Construction Grant provided by the People's Government of Dalian Municipality (Grant No. 2021-243). We also acknowledge the China Scholarship Council (CSC) for providing the research support at Zhejiang University. The funding bodies had no role in the study design, data collection and analysis, decision to publish, or preparation of the manuscript.

Acknowledgments

We extend our sincere gratitude to the students of the Zhan Jinbiao and Tan laboratories for their insightful discussions and invaluable assistance throughout this study. We also thank Professor Xing Zhang and Zihui Huang for their support with cryo-EM facility access and data analysis. Additionally, we are grateful to the Second Affiliated Hospital of Zhejiang University School of Medicine for providing multidrug-resistant bacterial strains used in this work.

Conflict of interest

The authors declare that the research was conducted in the absence of any commercial or financial relationships that could be construed as a potential conflict of interest.

Generative AI statement

The author(s) declare that no Generative AI was used in the creation of this manuscript.

Publisher's note

Supplementary material

The Supplementary Material for this article can be found online at: https://www.frontiersin.org/articles/10.3389/fcimb.2025.1643576/full#supplementary-material

References

Authority, E. F. S and Prevention, E. C. F. D. & Control (2020). The European Union Summary Report on Antimicrobial Resistance in zoonotic and indicator bacteria from humans, animals and food in 2017/2018. *EFSA J.* 18, e06007. doi: 10.2903/j.efsa.2020.6007

Baker, M. L., Hryc, C. F., Zhang, Q., Wu, W., Jakana, J., Haase-Pettingell, C., et al. (2013). Validated near-atomic resolution structure of bacteriophage epsilon15 derived from cryo-EM and modeling. *Proc. Natl. Acad. Sci.* 110, 12301–12306. doi: 10.1073/pnas.1309947110

Blum, M., Andreeva, A., Florentino, L. C., Chuguransky, S. R., Grego, T., Hobbs, E., et al. (2025). InterPro: the protein sequence classification resource in 2025 mode longmeta? *Nucleic Acids Res.* 53, D444–D456. doi: 10.1093/nar/gkae1082

Chang, J. T., Schmid, M. F., Haase-Pettingell, C., Weigele, P. R., King, J. A., and Chiu, W. (2010). Visualizing the structural changes of bacteriophage Epsilon15 and its Salmonella host during infection. *J. Mol. Biol.* 402, 731–740. doi: 10.1016/j.jmb.2010.07.058

Chio, U. S., Palovcak, E., Smith, A. A., Autzen, H., Muñoz, E. N., Yu, Z., et al. (20242225). Functionalized graphene-oxide grids enable high-resolution cryo-EM structures of the SNF2h-nucleosome complex without crosslinking. *Nat. Commun.* 15, 2225. doi: 10.1038/s41467-024-46178-y

Cornelissen, A., Hardies, S. C., Shaburova, O. V., Krylov, V. N., Mattheus, W., Kropinski, A. M., et al. (2012). Complete genome sequence of the giant virus OBP and comparative genome analysis of the diverse ϕKZ-related phages. *J. Virol.* 86, 1844–1852. doi: 10.1128/JVI.06330-11

Daigle, F. (2021). Special issue "Salmonella: pathogenesis and host restriction". *Microorganisms.* 9 (2), 325. doi: 10.3390/microorganisms9020325

Davis, M. R. Jr, and Goldberg, J. B. (2012). Purification and visualization of lipopolysaccharide from Gram-negative bacteria by hot aqueous-phenol extraction. *J. visualized experiments: JoVE.* (63), 3916. doi: 10.3791/3916

Deng, S., Xu, Q., Fu, Y., Liang, L., Wu, Y., Peng, F., et al. (2021). Genomic analysis of a novel phage infecting the Turkey pathogen Escherichia coli APEC O78 and its endolysin activity. *Viruses* 13, 1034. doi: 10.3390/v13061034

Ding, Y., Zhang, Y., Huang, C., Wang, J., and Wang, X. (2020). An endolysin LysSE24 by bacteriophage LPSE1 confers specific bactericidal activity against multidrug-resistant Salmonella strains. *Microorganisms* 8, 737. doi: 10.3390/microorganisms8050737

Fan, H., and Sun, F. (2022). Developing graphene grids for cryoelectron microscopy. *Front. Mol. Biosci.* 9, 937253. doi: 10.3389/fmolb.2022.937253

Fernandes, S., and São-José, C. (2018). Enzymes and mechanisms employed by tailed bacteriophages to breach the bacterial cell barriers. *Viruses* 10, 396. doi: 10.3390/v10080396

Gasteiger, E., Hoogland, C., Gattiker, A., Duvaud, S. E., Wilkins, M. R., Appel, R. D., et al. (2005). Protein identification and analysis tools on the ExPASy server. *Proteomics Protoc. Handb.*, 571–607. doi: 10.1385/1-59259-890-0:571

Gautier, R., Douguet, D., Antonny, B., and Drin, G. (2008). HELIQUEST: a web server to screen sequences with specific α-helical properties. *Bioinformatics* 24, 2101–2102. doi: 10.1093/bioinformatics/btn392

Guichard, J. A., Middleton, P. C., and Mcconnell, M. R. (2013). Genetic analysis of structural proteins in the adsorption apparatus of bacteriophage epsilon 15. *World J. Virol.* 2, 152. doi: 10.5501/wjv.v2.i4.152

Guliy, O. I., and Evstigneeva, S. S. (2025). Bacteria-and phage-derived proteins in phage infection. *Front. Bioscience-Landmark* 30, 24478. doi: 10.31083/FBL24478

He, F. (2011). Laemmli-sds-page. *Bio-protocol* 1 (11), e80–e80. doi: 10.21769/BioProtoc.80

Hirst, J. C., and Hutchinson, E. C. (2025). Purification of influenza virions. *Methods Mol Biol*. 2890, 27-51. doi: 10.1007/978-1-0716-4326-6_2

Islam, M. M., Kim, D., Kim, K., Park, S.-J., Akter, S., Kim, J., et al. (2022). Engineering of lysin by fusion of antimicrobial peptide (cecropin A) enhances its antibacterial properties against multidrug-resistant Acinetobacter baumannii. *Front. Microbiol.* 13, 988522. doi: 10.3389/fmicb.2022.988522

Jayamanne, M. N., and Foddai, A. C. (2025). Use of bacteriophages for biocontrol of pathogens in food and food-contact surfaces: a systematic review of the literature. *Sustain. Microbiol.* 2, qvaf005. doi: 10.1093/sumbio/qvaf005

Jiang, W., Baker, M. L., Jakana, J., Weigele, P. R., King, J., and Chiu, W. (2008). Backbone structure of the infectious ε15 virus capsid revealed by electron cryomicroscopy. *Nature* 451, 1130–1134. doi: 10.1038/nature06665

Jiang, W., Chang, J., Jakana, J., Weigele, P., King, J., and Chiu, W. (2006). Structure of epsilon15 bacteriophage reveals genome organization and DNA packaging/injection apparatus. *Nature* 439, 612–616. doi: 10.1038/nature04487

Jończyk-Matysiak, E., Łodej, N., Kula, D., Owczarek, B., Orwat, F., Międzybrodzki, R., et al. (2019). Factors determining phage stability/activity: Challenges in practical phage application. *Expert Rev. anti-infective Ther.* 17, 583–606. doi: 10.1080/14787210.2019.1646126

Jones, D. T. (1999). Protein secondary structure prediction based on position-specific scoring matrices. *J. Mol. Biol.* 292, 195–202. doi: 10.1006/jmbi.1999.3091

Kelley, L. A., Mezulis, S., Yates, C. M., Wass, M. N., and Sternberg, M. J. (2015). The Phyre2 web portal for protein modeling, prediction and analysis. *Nat. Protoc.* 10, 845–858. doi: 10.1038/nprot.2015.053

Khan, M. S. I., Gao, X., Liang, K., Mei, S., and Zhan, J. (2021). Virulent drexlervirial bacteriophage MSK, morphological and genome resemblance with Rtp bacteriophage inhibits the multidrug-resistant bacteria. *Front. Microbiol.* 12, 706700. doi: 10.3389/fmicb.2021.706700

Kim, J., Liao, X., Zhang, S., Ding, T., and Ahn, J. (2025a). Application of phage-derived enzymes for enhancing food safety. *Food Res. Int.* 116318. doi: 10.1016/j.foodres.2025.116318

Kim, J., Son, S. M., Ahn, E., Park, H., and Ryu, S. (2025b). Surface charge of the C-terminal helix is crucial for antibacterial activity of endolysin against Gram-negative bacteria. *J. Biomed. Sci.* 32, 38. doi: 10.1186/s12929-025-01133-x

Kropinski, A. M., Kovalyova, I. V., Billington, S. J., Patrick, A. N., Butts, B. D., Guichard, J. A., et al. (2007). The genome of ε15, a serotype-converting, Group E1 Salmonella enterica-specific bacteriophage. *Virology* 369, 234–244. doi: 10.1016/j.virol.2007.07.027

Kumar, S., Stecher, G., Suleski, M., Sanderford, M., Sharma, S., and Tamura, K. (2024). MEGA12: Molecular Evolutionary Genetic Analysis version 12 for adaptive and green computing. *Mol. Biol. Evol.* 41, msae263. doi: 10.1093/molbev/msae263

Lai, M.-J., Lin, N.-T., Hu, A., Soo, P.-C., Chen, L.-K., Chen, L.-H., et al. (2011). Antibacterial activity of Acinetobacter baumannii phage ϕAB2 endolysin (LysAB2) against both gram-positive and gram-negative bacteria. *Appl. Microbiol. Biotechnol.* 90, 529–539. doi: 10.1007/s00253-011-3104-y

Lin, L., Zhu, Y., and Cui, H. (2018). Inactivation of Escherichia coli O157: H7 treated by poly-L-lysine-coated bacteriophages liposomes in pork. *J. Food Saf.* 38, e12535. doi: 10.1111/jfs.12535

Liu, Y., Grimm, M., Dai, W.-T., Hou, M.-C., Xiao, Z.-X., and Cao, Y. (2020). CB-Dock: a web server for cavity detection-guided protein–ligand blind docking. *Acta Pharmacologica Sin.* 41, 138–144. doi: 10.1038/s41401-019-0228-6

Lood, R., Winer, B. Y., Pelzek, A. J., Diez-Martinez, R., Thandar, M., Euler, C. W., et al. (2015). Novel phage lysin capable of killing the multidrug-resistant gram-negative bacterium Acinetobacter baumannii in a mouse bacteremia model. *Antimicrobial Agents chemotherapy* 59, 1983–1991. doi: 10.1128/AAC.04641-14

Lu, R., Liu, B., Wu, L., Bao, H., García, P., Wang, Y., et al. (2023). A broad-spectrum phage endolysin (LysCP28) able to remove biofilms and inactivate Clostridium perfringens strains. *Foods* 12, 411. doi: 10.3390/foods12020411

Medalla, F., Gu, W., Friedman, C. R., Judd, M., Folster, J., Griffin, P. M., et al. (2021). Increased incidence of antimicrobial-resistant nontyphoidal Salmonella infections, United States 2004–2016. *Emerging Infect. Dis.* 27, 1662. doi: 10.3201/eid2706.204486

Murray, E., Draper, L. A., Ross, R. P., and Hill, C. (2021). The advantages and challenges of using endolysins in a clinical setting. *Viruses* 13, 680. doi: 10.3390/v13040680

Nazir, A., Xu, X., Liu, Y., and Chen, Y. (2023). Phage endolysins: Advances in the world of food safety. *Cells* 12, 2169. doi: 10.3390/cells12172169

Oliveira, H., Vilas Boas, D., Mesnage, S., Kluskens, L. D., Lavigne, R., Sillankorva, S., et al. (2016). Structural and enzymatic characterization of ABgp46, a novel phage endolysin with broad anti-gram-negative bacterial activity. *Front. Microbiol.* 7, 208. doi: 10.3389/fmicb.2016.00208

Paradis-Bleau, C., Cloutier, I., Lemieux, L., Sanschagrin, F., Laroche, J., Auger, M., et al. (2007). Peptidoglycan lytic activity of the Pseudomonas aeruginosa phage φKZ gp144 lytic transglycosylase. *FEMS Microbiol. Lett.* 266, 201–209. doi: 10.1111/j.1574-6968.2006.00523.x

Park, Y., Lim, J. A., Kong, M., Ryu, S., and Rhee, S. (2014). Structure of bacteriophage SPN1S endolysin reveals an unusual two-module fold for the peptidoglycan lytic and binding activity. *Mol. Microbiol.* 92, 316–325. doi: 10.1111/mmi.12555

Penadés, J. R., Seed, K. D., Chen, J., Bikard, D., and Rocha, E. P. (2025). Genetics, ecology and evolution of phage satellites. *Nat. Rev. Microbiol.* 23 (7), 410-422. doi: 10.1038/s41579-025-01156-z

Peng, S.-Y., You, R.-I., Lai, M.-J., Lin, N.-T., Chen, L.-K., and Chang, K.-C. (2017). Highly potent antimicrobial modified peptides derived from the Acinetobacter baumannii phage endolysin LysAB2. *Sci. Rep.* 7, 11477. doi: 10.1038/s41598-017-11832-7

Potter, S. C., Luciani, A., Eddy, S. R., Park, Y., Lopez, R., and Finn, R. D. (2018). HMMER web server: 2018 update. *Nucleic Acids Res.* 46, W200–W204. doi: 10.1093/nar/gky448

Reindel, R., and Fiore, C. R. (2017). *Phage therapy: considerations and challenges for development* (Oxford University Press US). 64, 1589–1590. doi: 10.1093/cid/cix188

Rey, J., Murail, S., De Vries, S., Derreumaux, P., and Tuffery, P. (2023). PEP-FOLD4: A pH-dependent force field for peptide structure prediction in aqueous solution. *Nucleic Acids Res.* 51, W432–W437. doi: 10.1093/nar/gkad376

Robert, X., and Gouet, P. (2014). Deciphering key features in protein structures with the new ENDscript server. *Nucleic Acids Res.* 42, W320–W324. doi: 10.1093/nar/gku316

Scheres, S. H. (2016). Processing of structurally heterogeneous cryo-EM data in RELION. *Methods enzymology* 579, 125–157. doi: 10.1016/bs.mie.2016.04.012

Schorb, M., Haberbosch, I., Hagen, W. J., Schwab, Y., and Mastronarde, D. N. (2019). Software tools for automated transmission electron microscopy. *Nat. Methods* 16, 471–477. doi: 10.1038/s41592-019-0396-9

Shah, S., Das, R., Chavan, B., Bajpai, U., Hanif, S., and Ahmed, S. (2023). Beyond antibiotics: phage-encoded lysins against Gram-negative pathogens. *Front. Microbiol.* 14, 1170418. doi: 10.3389/fmicb.2023.1170418

Sievers, F., and Higgins, D. G. (2018). Clustal Omega for making accurate alignments of many protein sequences. *Protein Sci.* 27, 135–145. doi: 10.1002/pro.3290

Söding, J., Biegert, A., and Lupas, A. N. (2005). The HHpred interactive server for protein homology detection and structure prediction. *Nucleic Acids Res.* 33, W244–W248. doi: 10.1093/nar/gki408

Sui, B., Li, X., Li, N., Tao, Y., Wang, L., Xu, Y., et al. (2025). Synergistic action of mucoactive drugs and phages against Pseudomonas aeruginosa and Klebsiella pneumoniae. *Microbiol. Spectr.* 13, e01601–e01624. doi: 10.1128/spectrum.01601-24

Suleman, S., Schrubaji, K., Filippou, C., Ignatova, S., Hewitson, P., Huddleston, J., et al. (2022). Rapid and inexpensive purification of adenovirus vectors using an optimised aqueous two-phase technology. *J. Virological Methods* 299, 114305. doi: 10.1016/j.jviromet.2021.114305

Tadesse, D. A., Zhao, S., Tong, E., Ayers, S., Singh, A., Bartholomew, M. J., et al. (2012). Antimicrobial drug resistance in Escherichia coli from humans and food animals, United States 1950–2002. *Emerging Infect. Dis.* 18, 741. doi: 10.3201/eid1805.111153

Tan, L., and Grewal, P. S. (2002). Comparison of two silver staining techniques for detecting lipopolysaccharides in polyacrylamide gels. *J. Clin. Microbiol.* 40, 4372–4374. doi: 10.1128/JCM.40.11.4372-4374.2002

Thandar, M., Lood, R., Winer, B. Y., Deutsch, D. R., Euler, C. W., and Fischetti, V. A. (2016). Novel engineered peptides of a phage lysin as effective antimicrobials against multidrug-resistant Acinetobacter baumannii. *Antimicrobial Agents chemotherapy* 60, 2671–2679. doi: 10.1128/AAC.02972-15

Thomas, S., Karnik, S., Barai, R. S., Jayaraman, V. K., and Idicula-Thomas, S. (2010). CAMP: a useful resource for research on antimicrobial peptides. *Nucleic Acids Res.* 38, D774–D780. doi: 10.1093/nar/gkp1021

Wallace, A. C., Laskowski, R. A., and Thornton, J. M. (1995). LIGPLOT: a program to generate schematic diagrams of protein-ligand interactions. *Protein engineering design selection* 8, 127–134. doi: 10.1093/protein/8.2.127

Wang, D., Zhao, X., and Wang, H. (2023). Recent advances of bacteriophage-derived strategies for biofilm control in the food industry. *Food Bioscience* 54, 102819. doi: 10.1016/j.fbio.2023.102819

Wu, H., Chen, R., Li, X., Zhang, Y., Zhang, J., Yang, Y., et al. (2024). ESKtides: a comprehensive database and mining method for ESKAPE phage-derived antimicrobial peptides. *Database* 2024, baae022. doi: 10.1093/database/baae022

Wu, M., Hu, K., Xie, Y., Liu, Y., Mu, D., Guo, H., et al. (2019). A novel phage PD-6A3, and its endolysin Ply6A3, with extended lytic activity against Acinetobacter baumannii. *Front. Microbiol.* 9, 3302. doi: 10.3389/fmicb.2018.03302

Yang, H., Wang, M., Yu, J., and Wei, H. (2015). Antibacterial activity of a novel peptide-modified lysin against Acinetobacter baumannii and Pseudomonas aeruginosa. *Front. Microbiol.* 6, 168319. doi: 10.3389/fmicb.2015.01471

Yuan, Y., Li, X., Wang, L., Li, G., Cong, C., Li, R., et al. (2021). The endolysin of the Acinetobacter baumannii phage vB_AbaP_D2 shows broad antibacterial activity. *Microbial Biotechnol.* 14, 403–418. doi: 10.1111/1751-7915.13594

Zampara, A., Sørensen, M. C. H., Grimon, D., Antenucci, F., Vitt, A. R., Bortolaia, V., et al. (2020). Exploiting phage receptor binding proteins to enable endolysins to kill Gram-negative bacteria. *Sci. Rep.* 10, 12087. doi: 10.1038/s41598-020-68983-3

Zheng, S. Q., Palovcak, E., Armache, J.-P., Verba, K. A., Cheng, Y., and Agard, D. A. (2017). MotionCor2: anisotropic correction of beam-induced motion for improved cryo-electron microscopy. *Nat. Methods* 14, 331–332. doi: 10.1038/nmeth.4193

frontiers | Frontiers in Cellular and Infection Microbiology

TYPE Original Research
PUBLISHED 04 September 2025
DOI 10.3389/fcimb.2025.1610625

OPEN ACCESS

EDITED BY
Derry Keith Mercer,
INCATE, Switzerland

REVIEWED BY
Genyan Liu,
Nanjing Medical University, China
Mansura Sherif Mulani,
Savitribai Phule Pune University, India
Jamil Allen Fortaleza,
NU Fairview Incorporated, Philippines
Lin Gan,
Capital Institute of Pediatrics, China

*CORRESPONDENCE
Yongwei Li
lyw@hactcm.edu.cn

†These authors share first authorship

RECEIVED 12 April 2025
ACCEPTED 26 June 2025
PUBLISHED 04 September 2025

CITATION
Zhu R, Wang R, Fei B, Lu R, You X, Liu X, Wang C and Li Y (2025) *In vitro* and *in vivo* antibacterial efficacy of bacteriophage combined with tigecycline against carbapenem-resistant *Klebsiella pneumoniae* and characterization of phage resistant mutants. *Front. Cell. Infect. Microbiol.* 15:1610625. doi: 10.3389/fcimb.2025.1610625

In vitro and *in vivo* antibacterial efficacy of bacteriophage combined with tigecycline against carbapenem-resistant *Klebsiella pneumoniae* and characterization of phage resistant mutants

Rui Zhu[1†], Ruilin Wang[2†], Bing Fei[2†], Ruici Lu[2], Xiaojuan You[2], Xinwei Liu[1], Chunxia Wang[1] and Yongwei Li[1,2,3,4,5*]

[1]Henan Province Hospital of Traditional Chinese Medicine (The Second Affiliated Hospital of Henan University of Chinese Medicine), Zhengzhou, China, [2]The Second Clinical Medical College, Henan University of Chinese Medicine, Zhengzhou, China, [3]The Key Laboratory of Pathogenic Microbes and Antimicrobial Resistance Surveillance of Zhengzhou, Henan Province Hospital of Traditional Chinese Medicine, Zhengzhou, China, [4]Henan Engineering Research Center for Identification of Pathogenic Microbes, Henan Province Hospital of Traditional Chinese Medicine, Zhengzhou, China, [5]Henan Provincial Key Laboratory of Antibiotics-Resistant Bacterial Infection Prevention and Therapy with Traditional Chinese Medicine, Henan Province Hospital of Traditional Chinese Medicine, Zhengzhou, China

Carbapenem-resistant *Klebsiella pneumoniae* (CRKP) has emerged as a critical global public health threat, characterized by high infection rates, elevated mortality, and limited therapeutic options. In this study, we isolated and characterized a novel bacteriophage (phage), designated as HZJ31, which exhibited potent lytic activity against CRKP strains. Phylogenetic and genomic analyses revealed that phage HZJ31 belongs to the order *Caudovirales* and lacks virulence factors, antibiotic resistance genes, and lysogeny-related elements, supporting its suitability for therapeutic applications. Phage HZJ31 exhibits remarkable anti-biofilm activity by preventing biofilm formation and disrupting established biofilms, with bacterial reduction rates exceeding 70% ($P<0.05$). In combination with Tigecycline, it significantly enhanced bactericidal efficacy, delayed the emergence of phage resistant mutants, and improved survival rates in *Galleria mellonella* larvae infection models. Compared to the bacterial-infected group, which had 80% larval mortality at 96 h, treatment with HZJ31 or TGC alone led to 50% and 60% survival, while their combination improved survival to 70% ($P < 0.05$). Notably, the phage-resistant mutant, which emerged due to capsule loss, resulted in reduced growth and virulence, while regaining sensitivity to certain antibiotics (such as gentamicin), indicating a fitness cost associated with phage resistance. Collectively, these findings provide valuable insights into phage-antibiotic synergy and underscore the promising clinical potential of phage HZJ31 as a therapeutic agent against CRKP infections.

KEYWORDS

carbapenem-resistant Klebsiella pneumoniae, phage therapy, biofilm, phage resistance, Galleria mellonella infection model

1 Introduction

Antibiotic resistance is acknowledged as a critical threat to public health. Carbapenems, including imipenem and meropenem, are highly effective broad-spectrum β-lactam antibiotics used as a last resort against multidrug-resistant Gram-negative infections, particularly those caused by ESBL- and AmpC-producing *Klebsiella pneumoniae* (KP) strains (Bologna et al., 2024; Naghavi et al., 2024). The extensive clinical utilization of carbapenems has led to the global rise of carbapenem-resistant *Klebsiella pneumoniae* (CRKP) (Ding et al., 2023; Hu et al., 2024a). In 2024, according to the China Antimicrobial Surveillance Network (CHINET), KP strains ranked second among all clinical isolates, accounting for 13.9% (n=458271), second only to *Escherichia coli* at 18.2%. From 2014 to 2024, clinical KP isolates showed increased resistance to imipenem and meropenem, rising from 11.0% and 14.1% to 22.6% and 23.4%, respectively, indicating a concerning trend (Karampatakis et al., 2023). Infections with CRKP endure a significant fatality rate and are challenging to treat (Lou et al., 2022; Hu et al., 2024a). In 2017, WHO published the WHO Priority Pathogens List for R&D of New Antibiotics, where carbapenem-resistant Enterobacteriaceae (including CRKP) was categorized as a "Critical" priority level (Miller and Arias, 2024). Treatment options for CRKP infections are extremely restricted, emphasizing the urgent need for novel antibacterial strategies (Hu et al., 2024a; Xing et al., 2025).

Bacteriophages (phages) are viruses that specifically infect bacteria and cause lysis, characterized by their ubiquity, abundance, diversity, structural simplicity, and amenability to genetic manipulation. In light of the escalating global antimicrobial resistance crisis, phage therapy has garnered renewed interest from the scientific community (Goodridge, 2010; Jault et al., 2019; Patpatia et al., 2021; Uyttebroek et al., 2022). Phages are classified into lytic and lysogenic phages based on their life cycle and replication characteristics. Lytic phages exhibit specific adsorption to bacterial cells and release progeny phages through a five-stage process: adsorption, penetration, biosynthesis, maturation, and release (Suttle, 2007). Bacteriophages, whether administered as monotherapy or in combination regimens, have demonstrated potent bactericidal activity against KP strains (Martins et al., 2022; Mulani et al., 2022), emerging as a promising therapeutic modality for CRKP infections (Baqer et al., 2022; Gorodnichev et al., 2023; Kou et al., 2024). Phage therapy offers distinct advantages over antibiotics, such as effectiveness against multidrug-resistant bacteria, anti-biofilm capabilities, high specificity, potent bactericidal activity, and the potential for genetic engineering (Kortright et al., 2019; Xing et al., 2025). Phage therapy faces multiple challenges, including a restricted host range, the rapid emergence of phage-resistant mutants, possible clearance by the host immune system, the absence of standardized manufacturing protocols and robust clinical trial data (Strathdee et al., 2023) (Uyttebroek et al., 2022). Moreover, recent studies have highlighted the potential risk of horizontal gene transfer (HGT) mediated by phages, which may unintentionally contribute to the dissemination of virulence factors and antibiotic resistance genes among pathogenic bacteria (Colavecchio et al., 2017; Cui et al., 2024; Cook and Hynes, 2025; She et al., 2025). These limitations significantly impede its broader clinical application.

This study identified a newly isolated lytic phage, HZJ31, targeting CRKP, and evaluated its biology, genome, anti-biofilm activity, and antibacterial efficacy *in vitro* and *in vivo*, highlighting its potential as a novel antibacterial strategy for CRKP infections. Notably, the analysis of the phage-resistant strain sheds light on the dynamic interactions between phages and bacteria, while also offering valuable insights into the fitness costs associated with phage resistance.

2 Materials and methods

2.1 Bacterial strains and culture conditions

Clinical KP strains, including KPZ2 and its phage-resistant mutant KPZ2-R, were isolated from the clinical laboratory at Henan Provincial Hospital of Traditional Chinese Medicine and preserved in 25% glycerol at -80°C. The strains were identified using the IVD MALDI Biotyper mass spectrometer (Bruker Daltonik, Germany). Antimicrobial susceptibility testing was performed using the VITEK 2 Compact system (bioMérieux, France), and results were interpreted according to the Clinical and Laboratory Standards Institute (CLSI) guidelines. The strains were revived on blood agar plates and incubated overnight at 37°C with 5% CO_2. After that, one colony was added to Luria-Bertani broth and cultured at 37°C with shaking at 180 rpm until the OD600 reached 0.6–1.0, indicating the logarithmic growth phase.

2.2 Phage isolation and purification

Phages were isolated from untreated hospital wastewater using a modified enrichment protocol (Wang et al., 2024). To screen for lytic phages, several clinical KP isolates, including KPZ2, were randomly selected as candidate host strains. After being stored at 4°C for 2 h, untreated sewage samples were concentrated at 8000 rpm for 10 min and filtered through a 0.22 μm filter. The filtered sewage was then mixed with an equal volume of 2× LB broth and inoculated with a clinical isolate (OD600 = 0.5). The mixture was incubated overnight at 37°C with shaking at 120 rpm. The phage stock was obtained by collecting the supernatant after centrifuging and filtering the supernatant through a 0.22 μm filter. The double-layer agar plate approach was used to purify phages until a single type of phage morphology was observed.

2.3 Transmission electron microscopy

The agarose gel blocks containing phages were incubated in PBS at 4°C for 6 h, then centrifuged and filtered through a 0.22 μm filter to obtain phage suspension. The phage suspension was

concentrated with a 30 kDa ultrafiltration tube at 3000 × g and 4°C for 15 min. Phages were adsorbed onto the 200-mesh carbon-coated copper grid and stained with 2% phosphotungstic acid. Phage morphology was observed using a Hitachi HT7800.

2.4 Optimal multiplicity of infection

The optimal MOI for phage HZJ31 was determined with a modified protocol (Wang et al., 2024) by incubating it with KPZ2 at MOI values of 0.001, 0.01, 0.1, and 1 at 37°C with shaking at 200 rpm for 4 h. The mixture of cultures was centrifuged at 6000 rpm for 15 min and the supernatant passed through a 0.22 μm filter to remove bacterial cells. Phage titers were determined using the double-layer agar method.

2.5 One-step growth curve

The one-step growth curve of phage HZJ31 was evaluated using the method (Fei et al., 2023). Briefly, phages HZJ31(MOI=0.001) and KPZ2 were incubated at 37°C for 15 min to allow adsorption. The mixture was then centrifuged at 12,000 rpm for 5 min at 4°C, and the supernatant was removed. The pellet was resuspended in LB broth and incubated at 37°C with shaking at 200 rpm for 100 min. The samples were collected at 10-minute intervals, and phage titers were quantified to generate the growth curve. The burst size = (Final phage titer - Initial free phage titer)/Number of infected bacterial cells.

2.6 Host range of phage

The host range of phage HZJ31 was determined by the spot assay according to the protocol described previously (Wang et al., 2024). Clinical CRKP isolates were adjusted to an OD600 of 0.5 using PBS, and the bacterial suspensions were evenly spread on LB agar plates. Then, 10 μL of phage HZJ31 was immediately spotted onto the surface, followed by overnight incubation at 37°C. The host range was evaluated through plaque formation: ++ denotes clear plaques, + signifies faint plaques, and - indicates the absence of plaque. All experiments were conducted in triplicate for consistency.

2.7 The stability for temperature and pH

The stability of phage was carried out according to the published paper (Fei et al., 2023). The thermal stability of phage HZJ31 was tested by incubating the phage (1×10^{10} PFU/mL) at temperatures of 4, 25, 37, 50, 60, 70, and 80°C for 1 h. For pH stability, phage HZJ31 was mixed with SM buffer at pH values of 3, 5, 7, 9, 10, 11, and 13 in a 1:10 (v/v) ratio and incubated at 37°C for 1 h. Then, phage titers were determined.

2.8 Cytotoxicity of phage by CCK-8 assay

The procedures were performed according to the previous study with minor modifications (Wang et al., 2024). The cells were plated at a density of 1×10^{4} cells per well in a 96-well plate and differentiated with 200 ng/mL of phorbol 12-myristate 13-acetate (PMA) overnight at 37°C with 5% CO_2. Phage HZJ31 was diluted from 10^{8} to 10^{14} PFU/mL in RPMI-1640 with 10% FBS and incubated with cells at 37°C, 5% CO_2 for 24, 48, and 72 h. Following incubation, 100 μL of a CCK-8 premix (Beijing Solarbio, China) with 90% PBS was added to each well after the cells were washed twice with PBS. After an additional incubation for 3 h, absorbance at OD450 nm was detected.

2.9 Genomic extraction of phages

The Phage DNA was extracted utilizing the Viral Gene Extraction Kit (Takara Bio, China). A solution containing 200 μL Buffer VGB, 20 μL Proteinase K, one μL Carrier RNA, and 200 μL phage suspension (10^{8} PFU/mL) was incubated at 56°C for 10 min.200 μL of anhydrous ethanol was added and mixed before transferring to a spin column. The mixture was centrifuged at 12,000 rpm for 2 min, and the filtrate was discarded. Subsequently, 500 μL of Buffer RWA and 700 μL of Buffer RWB were added in sequence, centrifuged, and discarded, with Buffer RWB applied twice, followed by centrifugation at 12,000 rpm for 3 min. The spin column was then transferred to a new RNase-free tube, and 60 μL of RNase-free ddH2O was added to elute the DNA. This mixture was incubated for 5 min and centrifuged at 12,000 rpm for 5 min to collect the phage DNA.

2.10 Phage genome sequencing and annotation

The phage genome was sequenced using the Illumina HiSeq 2500 platform, yielding a high average sequencing depth of 24,068×. Raw reads were filtered and quality-checked using *fastp*, and *de novo* assembly was performed with *SPAdes*. The quality of the assembly was evaluated using *QUAST*, resulting in an N50 value of 40,624 bp, indicating good assembly continuity. The genome was uploaded to the National Center for Biotechnology Information (NCBI). It was then analyzed with BLASTn to identify similar phages in the GenBank database. The tRNA genes encoded by the phage were identified using tRNAscan-SE. Phage-encoded genes were annotated using the Prokaryotic Genome Annotation System (Prokka). Functional characterization of the predicted amino acid sequences of these genes was conducted using NCBI's BLASTp. Virulence factors and antibiotic resistance genes were identified using the VFDB and ARDB databases (thresholds of ≥70% identity and ≥70% coverage). The genomic map was visualized with CGview.

2.11 Phylogenetic analysis of phage HZJ31

The terminase large subunit sequences were used for phylogenetic analysis. The amino acid sequence of terminase large subunit of phage HZJ31 was entered into NCBI's BLASTp, resulting in the identification of ten homologous sequences with notable similarity. The basis for generating a phylogenetic tree using the ClustalW alignment tool within the MEGA 11.0 platform. Furthermore, the genome sequences of phage HZJ31 and the selected phage were analyzed by Easyfig.

2.12 Determination of minimum inhibitory concentration

The MICs of tigecycline (TGC) against KPZ2 were conducted by the broth dilution method. TGC was serially diluted in LB broth in twofold dilutions.100 μL of each antibiotic dilution was added to the corresponding wells of a 96-well plate. Negative control wells contained only medium without bacteria, while positive control wells contained bacteria without antibiotics. The KPZ2 bacterial suspension was diluted in LB broth to 5×10^5 CFU/mL from an initial McFarland 0.5 suspension. Then, 100 μL of the bacteria was added to each well. The plate was incubated for 18 h at 37°C. The MIC was determined as the lowest concentration of TGC that inhibited visible bacterial growth.

2.13 Bactericidal kinetics of the combined phage HZJ31 and tigecycline

The assay was performed according to a previously reported method (Wang et al., 2024), with minor modifications. The experimental design included the following groups: The KPZ2 group, The phage HZJ31 group (MOI = 0.001), The 1/2 MIC TGC group, and the phage HZJ31 with 1/2 MIC TGC group. The KPZ2 was standardized to 1×10^6 CFU/mL. 100 μL of the bacterial culture was added to the 96-well plate, followed by the addition of phage HZJ31 and/or TGC, according to group assignment. The plate was incubated at 37°C for 36 h, with OD600 measurements taken hourly to construct bactericidal kinetics curves to evaluate the inhibitory effects of phage and/or TGC on bacterial growth. Synergy was defined as a statistically significant enhancement of antibacterial activity in the combination group (phage + TGC) compared to each monotherapy group, based on OD600 values measured over time. Statistical analysis was performed using two-way ANOVA followed by Tukey's multiple comparison test ($P < 0.05$).

2.14 Antibacterial efficacy of phage HZJ31 and TGC in the *Galleria mellonella* infection model

The experiments were evaluated using a *Galleria mellonella* (*G.mellonella*)larvae infection model using a protocol modified from a previous study (Peng et al., 2025). The larvae, approximately 2–3 cm in length and weighing 250–300 mg, with a uniform milky white color and no gray spots, exhibiting high vitality, were selected for the experiments (purchased from Tianjin Huiyude Biotechnology Co., Ltd., China). To determine the optimal bacterial infection dose, we selected the concentration that resulted in approximately 80% larval mortality at 24 h post-infection as the target inoculum. Before experimentation, larvae were acclimated at 37°C for 1–2 h, and KPZ2 was cultured in LB broth to reach an OD600 of 0.8-1.0. The culture underwent centrifugation at 7,000 rpm for 10 min, followed by PBS washing and adjustment to concentrations of 10^5 to 10^9 CFU/mL. 10 μL bacterial suspension or PBS (as control) was administered into the last left proleg of the larvae. Larvae were incubated at 37°C with survival rates monitored every 12 h.

To evaluate the combined antibacterial efficacy of phage HZJ31 and TGC in the *G.mellonella* infection model, larvae were randomly assigned to five groups: the PBS control group, the KPZ2 group, the phage HZJ31 group, the TGC group, and the phage HZJ31 + TGC group. Except for the PBS control group (injected with an equal volume of PBS), each larva received 10 μL of KPZ2 suspension (at a concentration determined by preliminary experiments) into the last left proleg. After 1 h, 10 μL of the respective treatment was injected into the last right proleg of each larva: PBS (for the PBS control and KPZ2 group), phage HZJ31 (MOI = 0.001, HZJ31 group), 1/2 MIC TGC (TGC group), and a mixture of phage HZJ31 and 1/2 MIC TGC (combined treatment group). All larvae were incubated at 37°C and monitored every 12 h for 4 consecutive days. Survival status was recorded, and survival rates were calculated for each group to evaluate therapeutic efficacy.

2.15 Biofilm quantification by crystal violet assay

The biofilm quantification was performed using a modified protocol

(Wang et al., 2024). A 96-well plate was incubated at 37°C for 24 h, 48 h, and 72 h with KPZ2 suspension (10^6 CFU/mL) and phage HZJ31 (MOI =0.001). For biofilm disruption, another set of KPZ2 cultures was incubated for 48 h to form biofilms, which were then treated with phage HZJ31 (MOI = 0.01) for 6 h. After washing with PBS to remove planktonic cells, biofilms were fixed with methanol for 30 min and stained with 0.1% crystal violet solution (Shanghai Baisai, China) for 15 min. The residual stain was removed by PBS washing, and biofilm biomass was quantified by dissolving crystal violet in 200 μL of 30% glacial acetic acid. Absorbance at 595 nm was measured to assess biofilm biomass. All experiments were performed in triplicate.

2.16 Bactericidal activity in biofilms by XTT assay

The experiment was conducted with suitable modifications (Fei et al., 2023). KPZ2 suspension (10^6 CFU/mL) and phage HZJ31

(MOI = 0.001) were co-incubated in a 96-well plate at 37°C for 24 h, 48 h, and 72 h. For biofilm disruption, preformed 48 h biofilms were treated with HZJ31 (MOI = 0.01) for 6 h. After incubation, PBS was used to wash the plate to remove planktonic bacteria. Subsequently, 200 μL of LB broth and 20 μL of XTT solution (Shanghai Yuanye, China) were introduced into each well. The plate was then incubated at 37°C in the dark for 3 h, followed by absorbance measurement at OD490 nm. The inhibitory rate was calculated using the following formula:

$$\left[1-\frac{\mathbf{A}(\text{Experimental group})-\mathbf{A}(\text{Blank control group})}{\mathbf{A}(\text{Control group})-\mathbf{A}(\text{Blank control group})}\right]\times 100\,\%\,.$$

The experiment was repeated three times.

2.17 Screening of phage-resistant bacteria

The experiment was performed with some modifications based on a previous study (Wang et al., 2024). KPZ2 and phage HZJ31 (MOI =0.001) were incubated at 37°C with shaking at 200 rpm for 24 h. Cultures were streaked onto blood agar plates to isolate single colonies. The isolates were identified by the mass spectrometer. Phage resistance was confirmed by spot testing and double-layer agar assays. Resistant strains were designated KPZ2-R.

2.18 Scanning electron microscopy

KPZ2 and KPZ2-R were incubated at 37°C with shaking at 220 rpm for 6 h. The cultures were then centrifuged at 8000 rpm for 10 min to collect the pellets, which were subsequently washed with PBS. Pellets were fixed in 2.5% glutaraldehyde at room temperature for 5 h, followed by PBS washing and 15-minute dehydration using graded ethanol concentrations (30%, 50%, 70%, 90%, 100%). After dehydration, the samples were dried, gold-coated, and observed under the SEM Hitachi SU8100 to capture morphology.

2.19 Antibiotic susceptibility testing

Antibiotic susceptibility of KPZ2 and KPZ2-R was determined using the VITEK-2 Compact system (BioMérieux, France). The KPZ2 and KPZ2-R were standardized to a 0.5 McFarland scale. The prepared bacterial suspension was loaded along with the AST-GN card into the VITEK-2 Compact system for automatic inoculation and determination. The results were analyzed following the guidelines of the Clinical and Laboratory Standards Institute (CLSI).

2.20 Phage adsorption efficiency

The assay was performed using a modified protocol (Wang et al., 2024). KPZ2 and KPZ2-R were incubated with phage HZJ31 (MOI =0.001) at 37°C, with samples collected at 0, 5, 10, 15, and 20 min. The samples were centrifuged at 11000 rpm for 8 min at 4°C. The supernatants were filtered (0.22 μm), and then the phage titer was determined. The Adsorption Efficiency = [(Initial Phage Titer - Phage Titer in Supernatant)/Initial Phage Titer] × 100%.

2.21 Bacterial growth rates

KPZ2 and KPZ2-R were adjusted to 1.0×10^6 CFU/mL. The 96-well plate was prepared with 200 μL of bacterial suspension in each test well and 200 μL of LB broth in the control wells. The plate was incubated at 37°C for 24 h with hourly OD600 measurements.

2.22 Comparison of virulence using the *G.mellonella* infection model

The concentrations of KPZ2 and KPZ2-R were adjusted to 10^6 and 10^7 CFU/mL, respectively. Each *G.mellonella* larvae received an injection of 10 μL bacterial suspension (PBS as a control) into the last left proleg. Larvae were incubated at 37°C with survival monitored every 12 h over 4 days.

2.23 Bacterial whole-genome sequencing

Genomic DNA of strains KPZ2 and KPZ2-R was extracted using a whole-genome extraction kit (Sangon Biotech, China) according to the manufacturer's instructions. Briefly, 5 mL of overnight bacterial culture was centrifuged to collect the cells, followed by the addition of lysis buffer and incubation at 65 °C for 1 h to lyse the cells. Subsequently, Buffer PB was added, mixed thoroughly, and briefly incubated at −20 °C. After centrifugation, the supernatant was transferred, isopropanol was added, mixed well, and centrifuged again to pellet the DNA. The DNA pellet was washed with 75% ethanol, dried after removing the ethanol, and then dissolved in TE buffer. DNA concentration and integrity were assessed using a Qubit 4.0 fluorometer (Thermo Fisher Scientific, China). The extracted DNA was either used for subsequent experiments or stored at −20°C.

The genomes of strains KPZ2 and KPZ2-R were sequenced using the BGI MGISEQ 2000 platform. The extracted DNA was enzymatically fragmented, end-repaired, ligated with adaptors, and amplified by PCR to construct sequencing libraries. Library concentration was quantified using a Qubit fluorometer, and fragment size distribution was assessed using the Agilent 2100 Bioanalyzer; libraries with a main peak around 500 bp were considered qualified. The libraries were then denatured, circularized, and purified before sequencing. Raw sequencing data were subjected to quality control to remove adaptors and low-quality reads. The filtered reads were assembled using SPAdes (v3.13.0). Based on alignment results, ANGSD (v0.940) was used to reconstruct the genome sequences, and genome completeness and contamination were evaluated using CheckM (v1.2.2).

The K-locus types of KPZ2 and KPZ2-R were identified using the Kaptive Web tool (https://kaptive-web.erc.monash.edu/).

Genome assemblies in FASTA format were uploaded, and typing was based on sequence coverage, identity, and completeness. Confidence levels were recorded for each result.

2.24 Statistical analysis

All statistical analyses were conducted using GraphPad Prism 9.2. One-way or two-way analysis of variance (ANOVA) followed by Tukey's multiple comparisons test was employed to undertake multiple group comparisons. Survival curves for *G.mellonella* were analyzed using the log-rank (Mantel-Cox) test. Statistical significance was indicated by $^{*}P$ <0.05, $^{**}P$ <0.01, $^{***}P$ < 0.001, and $^{****}P$ <0.0001.

3 Results

3.1 Isolation and characterization of phage HZJ31

Phage HZJ31 was isolated using strain KPZ2 as the host bacterium from wastewater. TEM revealed the phage had an icosahedral head approximately 80 nm in diameter and a short tail measuring 10 nm (Figure 1A). The plaques were large, clear, and uniform, reaching up to 4.0 mm in diameter, with a halo of approximately 7.2 mm, which indicates the high efficiency (Figure 1B). Phage HZJ31 was classified within the *Caudovirales* based on its morphological characteristics.

The double-layer agar plate method was employed to determine the optimal MOI, one-step growth, and stability of phage HZJ31. Phage titer of HZJ31 remained largely stable across MOIs from 0.1 to 0.0001, peaking at an MOI of 0.001, which was chosen for further experiments (Figure 1C). The one-step growth curve showed a 10-minute latent period, followed by a rapid exponential rise in phage population between 10 and 70 min, culminating in a plateau phase. The estimated burst size was 374 PFU/cell, suggesting that HZJ31 possesses a highly efficient host cell lysis capability (Figure 1D).

The environmental stability of phage HZJ31 was further assessed under varying pH and temperature conditions. Phage HZJ31 exhibited stable titers between pH 5 and 9, with the highest stability observed around neutral pH. In contrast, the phage titer drastically decreased under highly alkaline (pH > 9) and acidic (pH < 5) conditions, becoming nearly undetectable at pH 3 (Figure 1E). The thermal stability of HZJ31 was robust between 4°C and 50°C, but its titer began to decrease beyond 50°C, and complete inactivation occurred at 80°C (Figure 1F). The stability of HZJ31 indicates its potential suitability for phage therapy applications. Phage HZJ31 demonstrates strong host specificity, with a lysis rate of 23.33% (7/30) against clinical CRKP isolates and only 13.33% (4/30) achieving complete lysis (Table 1). Furthermore, CCK-8 assays showed that co-culturing THP-1 cells with HZJ31 at concentrations ranging from 10^8 to 10^{11} PFU/mL for 24 h and 48 h did not significantly affect cell viability compared to the untreated control (mean ± SD, n=6, Figure 1G), confirming the cellular safety of HZJ31 for therapeutic applications.

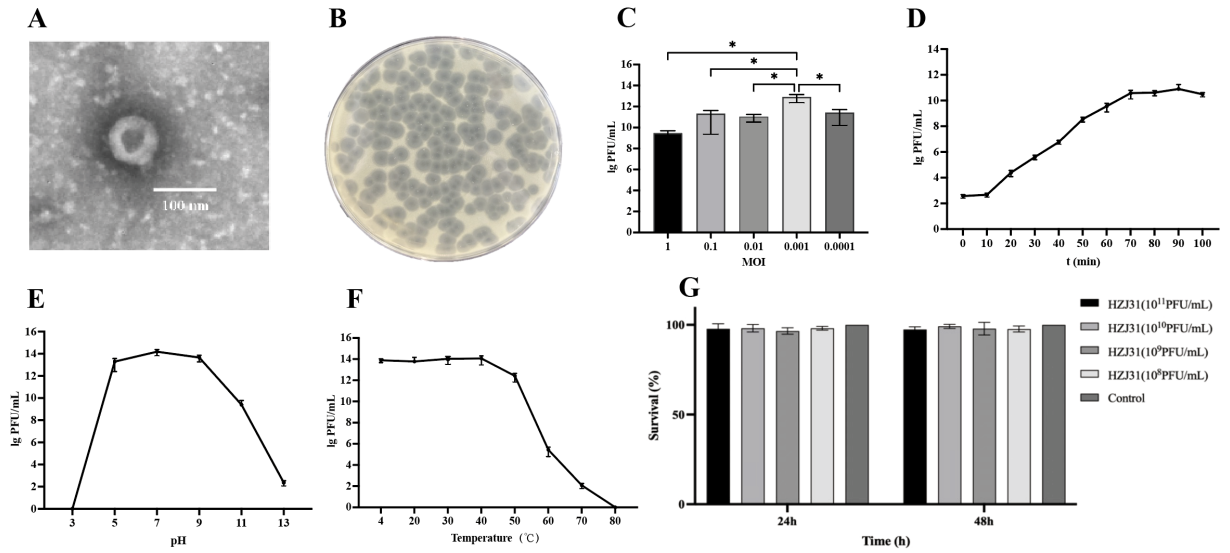

FIGURE 1
Biological characteristics, stability and cytotoxicity of phage HZJ31. **(A)** TEM morphology of phage HZJ31, revealing an icosahedral head (~80 nm) and short tail (~10 nm), consistent with *Caudovirales*. **(B)** Plaque morphology of phage HZJ31 on a double-layer agar plate. **(C)** The optimal MOI of phage HZJ31, the highest titer was observed at MOI = 0.001, mean ± SD. **(D)**The one-step growth curve of phage HZJ31, mean ± SD. **(E)** The pH stability of phage HZJ31, the phage remained stable between pH 5–9 but was inactivated under extreme acidic or alkaline conditions. mean ± SD. **(F)** Thermal stability of phage HZJ31. phage activity was maintained up to 50 °C and declined at higher temperatures, with complete inactivation at 80 °C. mean ± SD. **(G)** Cytotoxicity assessment of phage HZJ31 on THP-1 cells by CCK-8 assay. no significant cytotoxicity was observed after 24 h and 48 h exposure to phage HZJ31 at various concentrations (10^8 to 10^{11} PFU/mL). mean ± SD. $^{*}P < 0.05$.

10.3389/fcimb.2025.1610625

TABLE 1 The host range of phage HZJ31.

Strain	Type	Source	Lysis capability
KPZ2	CRKP	Sputum	++
154	CRKP	Sputum	–
156	CRKP	Sputum	–
159	CRKP	Sputum	–
160	CRKP	Ascites	–
168	CRKP	Urine	–
172	CRKP	Sputum	–
173	CRKP	Pus secretion	–
294	CRKP	Sputum	+
302	CRKP	Rectal Swab	–
303	CRKP	Urine	+
309	CRKP	Sputum	+
312	CRKP	Sputum	–
314	CRKP	Sputum	–
316	CRKP	Rectal Swab	–
318	CRKP	Sputum	–
322	CRKP	Sputum	–
323	CRKP	Sputum	–
328	CRKP	Rectal Swab	–
329	CRKP	Sputum	–
341	CRKP	Urine	–
344	CRKP	Sputum	–
488	CRKP	Sputum	++
662	CRKP	Sputum	–
665	CRKP	Urine	–
682	CRKP	Sputum	-
692	CRKP	Sputum	–
693	CRKP	Blood	–
L8	hv-CRKP	Sputum	++
L9	hv-CRKP	Blood	++

'++' denotes clear plaques, '+' signifies faint plaques, and '-' indicates the absence of plaque

3.2 Genomic analysis of phage HZJ31

The genome of Phage HZJ31 (GenBank: OR050820.1) was sequenced using Illumina HiSeq 2500 platform, identifying a circular dsDNA molecule of 40,624 bp with a GC content of 53.16%. The genomic map was constructed using GCview (Figure 2A). Annotation using Prokka identified 48 ORFs, of which 33 were functionally annotated and classified into four major categories: structural proteins, DNA replication and metabolism, lysis mechanisms, and genome packaging (Table 2). In the structural module, ORF1 encodes a major capsid protein (98.84% identity with phage IME264), and ORF4 encodes a host adsorption protein (100% identity with phage K11), both essential for host recognition and infection. Tail-associated proteins such as ORF40 and ORF41 (tail fiber proteins) contribute to phage structural assembly. Replication-related genes include ORF12 (DNA polymerase I) and ORF16 (primase/helicase), while ORF30 encodes a DNA-directed RNA polymerase, suggesting the phage can replicate and transcribe independently of the host. Lysis functions are attributed to ORF20, encoding an amidase/lysin, and ORF39, encoding a holin, which together facilitates host cell wall degradation and phage release. Packaging proteins ORF36 and ORF38 encode the large and small terminase subunits, respectively, responsible for DNA cleavage and encapsidation. Overall, HZJ31 harbors a complete set of functional modules characteristic of a lytic phage, supporting its potential as a therapeutic agent against CRKP infections.

The absence of virulence or antibiotic resistance genes in the VFDB and ARDB databases highlights the phage's biosafety for therapeutic use. Genomic analysis using BLASTn revealed that phage HZJ31 exhibits 94.84% sequence identity with Klebsiella phage 066012 (GenBank: MW042787.1) with 94% coverage. The terminase large subunit gene of HZJ31 was found to be highly conserved, and phylogenetic analysis based on this gene positioned HZJ31 in close relation to Klebsiella phage SH-KP152226 (QDF14649.1) (Figures 2B, C). These findings collectively indicate that HZJ31 represents a novel Klebsiella-specific phage, expanding our understanding of phage diversity and potential for therapeutic exploitation.

3.3 Antibacterial efficacy of phage HZJ31 and TGC *in vitro* and *in vivo*

The schematic diagrams of the in vitro bactericidal kinetics assay and the G. mellonella infection model are shown in Figures 3A and 3B, respectively. In this study, the combined antibacterial effect of phage HZJ31 and TGC was first evaluated *in vitro*. Prior to combination testing, the MIC of TGC against strain KPZ2 was determined to be 1.0 μg/mL. Then the bactericidal kinetics of phage HZJ31(MOI = 0.001), TGC (1/2 MIC, 0.5 μg/mL), and their combination against strain KPZ2 were evaluated over a 36-h period (Figure 3C). During the initial 6 h, the bacterial growth among all groups was generally consistent, with no significant differences in OD600. In the HZJ31 group, although the OD600 values gradually increased after 7 h, they remained significantly lower than those of the KPZ2 group throughout the entire experiment. In the 1/2 MIC TGC group, bacterial growth was also delayed, with OD600 increasing at a slower rate than in the HZJ31 group, reaching approximately 0.45 at 36 h. In the HZJ31 combined with the 1/2 MIC TGC group, no significant increase in OD600 was observed during the first 10 h, followed by a slight increase thereafter. However, the OD600 of the HZJ31 with 1/2 MIC TGC group remained at a low level (< 0.3) throughout the 36-h period, significantly lower than those in

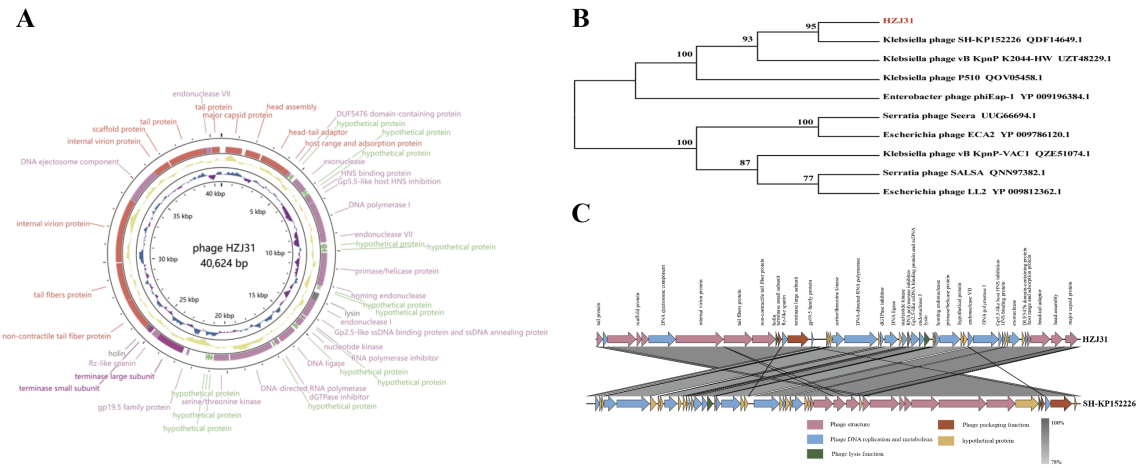

FIGURE 2
Genomic analysis of phage HZJ31. **(A)** Gene map of Phage HZJ31. **(B)** Phylogenetic tree phage HZJ31 based on terminase large subunit. **(C)** Genomic comparative of phage HZJ31 and *Klebsiella* phage SH-KP152226.

all other groups ($P < 0.05$), indicating a synergistic antibacterial effect of the combined treatment.

Given the significant similarities between the innate immune responses of *G.mellonella* larvae and vertebrates, the *G.mellonella* model is widely used as an alternative to evaluating bacterial virulence and *in vivo* antimicrobial efficacy. We then evaluated the bactericidal efficacy of phage HZJ31 and TGC in the *G.mellonella* infection model. In this study, we established an infection model by injecting *G.mellonella* larvae with varying concentrations of bacteria, determining that an optimal inoculum of 10^7 CFU/mL for KPZ2 resulted in an 80% mortality rate at 24 h (Figure 3D). Significant differences were observed in the survival curves among the groups (log-rank test, $P < 0.05$). Compared to the KPZ2 group, the survival rates at 96 h were 50% and 60% for the phage HZJ31 and TGC treatments, respectively, while the survival rate for larvae treated with the combination of phage HZJ31 and TGC was 70% (Figure 3E). In summary, phage HZJ31 effectively controlled KPZ2 infection *in vivo*.

3.4 The antibiofilm activity of phage HZJ31

The results showed that phage HZJ31 significantly inhibited KPZ2 biofilm formation at 24 h, 48 h, and 72 h ($P < 0.05$, Figure 4A). The inhibitory effect of phage HZJ31 on bacterial growth within the KPZ2 biofilm was assessed, showing a 59.45% inhibition rate at 72 h ($P < 0.05$) (Figure 4C). When phage HZJ31 was co-cultured with preformed KPZ2 biofilm for 6 h, significant disruption of the biofilm was observed (Figure 4B), with bacterial inhibition within the biofilm exceeding 70% ($P < 0.05$, Figure 4D). These findings demonstrate that phage HZJ31 effectively inhibits the formation of KPZ2 biofilms and disrupts preformed biofilms, exerting a substantial inhibitory effect on the bacteria within the biofilm.

3.5 Fitness cost of phage resistance in KPZ2-R: impaired capsule, growth, and virulence

After 24 h of co-culturing KPZ2 with phage HZJ31 (MOI = 0.001), the culture appeared visibly turbid, suggesting the emergence of phage-resistant mutants. Subsequent plating on LB agar and purification on blood agar yielded colonies that were no longer susceptible to phage HZJ31, as confirmed by both the double-layer agar method and spot assay, which showed no lysis zones. Mass spectrometry analysis identified all resistant colonies as *Klebsiella pneumoniae*, excluding the possibility of contamination. One phage-resistant isolate (designated KPZ2-R) was randomly selected from these colonies for further comparison with the wild-type strain. KPZ2 exhibited a slightly faster growth rate in LB broth than KPZ2-R, as measured by OD600 (Figure 5A). The phage adsorption efficiency of KPZ2 was 65.82% at 5 min, significantly higher than that of KPZ2-R (24.24%), and continued to increase over time, reaching 88.00% at 15 min. Conversely, the adsorption efficiency of KPZ2-R remained low throughout the incubation period (Figure 5B).

We also compared the virulence of KPZ2 and KPZ2-R using the *G.mellonella* infection model. At 10^6 and 10^7 CFU/mL of KPZ2, the survival rates of larvae at 48 h were 40% and 20%, respectively, whereas larvae injected with the same doses of KPZ2-R had survival rates of 70% and 50% (Figure 5C). Overall, KPZ2-R demonstrated lower virulence than KPZ2 *in vivo*. We further compared the antibiotic susceptibility of KPZ2 and KPZ2-R (shown in Table 3). Among all antibiotics tested, KPZ2 was only susceptible to TGC, polymyxin B, and ceftazidime/avibactam, while resistant to the others. In contrast, KPZ2-R showed increased susceptibility, shifting from resistance (R) to susceptibility (S) to piperacillin and gentamicin.

On blood agar, KPZ2 formed large, smooth, plump, and moist colonies with a milky white appearance (Figure 5D), while the

10.3389/fcimb.2025.1610625

TABLE 2 Functional gene annotation of phage HZJ31 (GenBank:OR050820.1).

Function	No.	Start position	Stop position	Strand	Predicted function	Similar species	Identified
Phage structure	ORF1	1288	254	–	major capsid protein	Klebsiella phage IME264	98.84%
	ORF2	2466	1516	–	head assembly	Klebsiella phage VLCpiA3d	96.84%
	ORF3	4177	2570	–	head-tail adaptor	Klebsiella phage K5	98.50%
	ORF4	4449	4189	–	host range and adsorption protein	Klebsiella phage K11)	100%
	ORF40	27480	25555	–	non-contractile tail fiber protein	Klebsiella phage P560	98.44%
	ORF41	29880	27499	–	tail fibers protein	Klebsiella phage IME304	98.99%
	ORF42	33908	29943	–	internal virion protein	Klebsiella phage vB_KpnP_ZK2	98.86%
	ORF44	36770	36180	–	internal virion protein	Klebsiella phage KN4-1	100%
	ORF45	37183	36773	–	scaffold protein	Klebsiella phage P560	100%
	ORF46	39632	37257	–	tail protein	Klebsiella phage 2044-307w	97.85%
	ORF48	40516	40022	–	tail protein	Klebsiella phage vB_KpnP_IME205	99.39%
Phage DNA replication and metabolism	ORF5	4672	4451	–	DUF5476 domain-containing protein	Klebsiella phage vB_KpnP_IME205	100%
	ORF7	6005	5100	–	exonuclease	Klebsiella phage vB_KpnP_IME205	99.34%
	ORF10	6583	6374	–	HNS binding protein	Klebsiella phage vB_Kp1	100%
	ORF11	6864	6580	–	Gp5.5-like host HNS inhibition	Klebsiella phage SH-Kp 152410	95.74%
	ORF12	9009	6883	–	DNA polymerase I	Klebsiella phage vB_KpnP_BIS33	96.75%
	ORF13	9442	8990	–	endonuclease VII	Klebsiella phage vB_KpnP_BIS33	98.00%
	ORF16	11818	10100		primase/helicase protein	Klebsiella phage NL_ZS_1	99.48%
	ORF17	12158	11793		homing endonuclease	Klebsiella phage IME304	100%
	ORF21	13542	13093	–	endonuclease I	Klebsiella phage KMI1	98.66%
	ORF22	14237	13542	–	Gp2.5-like ssDNA binding protein and ssDNA annealing protein	Klebsiella phage vB_KpnP_IME205	100%
	ORF23	14446	14297	–	RNA polymerase inhibitor	Klebsiella phage K11	91.84%
	ORF25	14955	14527	–	nucleotide kinase		97.18%

(Continued)

TABLE 2 Continued

Function	No.	Start position	Stop position	Strand	Predicted function	Similar species	Identified
						Klebsiella phage vB_KpnP1	
	ORF27	16410	15328	–	DNA ligase	Klebsiella phage Tokugawa	97.50%
	ORF28	16768	16511	–	dGTPase inhibitor	Klebsiella phage VLCpiA3b	97.65%
	ORF30	19768	17048	–	DNA-directed RNA polymerase	Klebsiella phage vB_KpnP_FZ12	99.01%
	ORF31	20799	19840	–	serine/threonine kinase	Enterobacter phage ENC14	86.35%
	ORF43	36180	33925	–	DNA ejectosome component	Klebsiella phage P560	99.20%
	ORF47	39999	39598	–	endonuclease VII	Klebsiella phage KP32_isolate 195	95.49%
Phage lysis function	ORF20	13090	12635	–	amidase/lysin	Klebsiella phage vB_Kp_IME531	95.36%
	ORF39	25545	25342	–	holin	Klebsiella phage VLCpiA3a	100%
Phage packaging	ORF36	24541	22784	–	terminase large subunit	Klebsiella phage P560	99.83%
	ORF38	25338	25081	–	terminase small subunit	Klebsiella phage vB_KpnP_KpV767	98.82%

phage-resistant mutant KPZ2-R formed smaller, gray, semi-transparent colonies, but no obvious difference in diameter (Figure 5H). SEM revealed that the surface of KPZ2 appeared smooth, dense, and uniform, exhibiting a full and thick structure without visible indentations (Figures 5E, F). In contrast, KPZ2-R displayed a rough, uneven surface with wrinkles or depressions, a comparatively thinner structure, and showed evident structural defects in the capsule (Figures 5I, J). TEM further confirmed these differences, revealing a prominent, well-defined capsule surrounding KPZ2 (Figure 5G), while KPZ2-R exhibited a significantly reduced and poorly defined capsule with only a faint or nearly absent surrounding layer (Figure 5K), indicating impaired capsule formation in the resistant mutant.

Consistent with these observations, Kaptive-based analysis revealed that both KPZ2(GenBank: CP178862.1) and its phage-resistant mutant KPZ2-R (GenBank: CP192283.1) matched the KL47 capsular locus with 99.67% sequence identity (Figures 5L, M). KPZ2 exhibited complete locus coverage (99.98%) and intact capsule biosynthesis genes. However, KPZ2-R was classified as "capsule null" due to a truncated *wcaJ* gene (51.58% identity), suggesting the loss of capsule synthesis capability is associated with phage resistance.

4 Discussion

In recent years, CRKP has rapidly spread worldwide, resulting in high mortality rates and limited treatment options, and has become a serious public health concern (Karampatakis et al., 2023). Therefore, there is an urgent need to explore alternative therapeutic strategies (Chang et al., 2022). Amid the growing challenge of antimicrobial resistance, phage therapy has emerged as a promising antibacterial approach (Hatfull et al., 2022; Kou et al., 2024). Numerous preclinical studies and clinical case reports have demonstrated the therapeutic potential of phages in treating KP infections (Kou et al., 2024; Xing et al., 2025).

Phage HZJ31 demonstrated stability across pH values ranging from 5 to 9 and temperatures from 4°C to 50°C. This robust stability profile facilitates its activity under diverse environmental conditions, simplifying storage and transportation logistics. Following a 48 co-culture of phage HZJ31 with THP-1 cells, the CCK-8 assay yielded no detectable cytotoxicity, indicating biocompatibility. Genomic sequencing further disclosed an absence of genes conferring toxicity or antibiotic resistance, offering initial assurance of its safety for therapeutic applications. These findings underpin the promising clinical potential of phage HZJ31.

Biofilms significantly contribute to recurrent medical device-associated chronic infections and play a pivotal role in bacterial adaptive resistance and evasion of host immune surveillance (Chadha et al., 2022). These complicated microbial communities are composed of bacteria that are embedded within a self-produced matrix of extracellular polymers (EPS) consisting of extracellular polysaccharides, proteins, and extracellular DNA (eDNA) (Flemming et al., 2016). The biofilm-forming ability of KP is

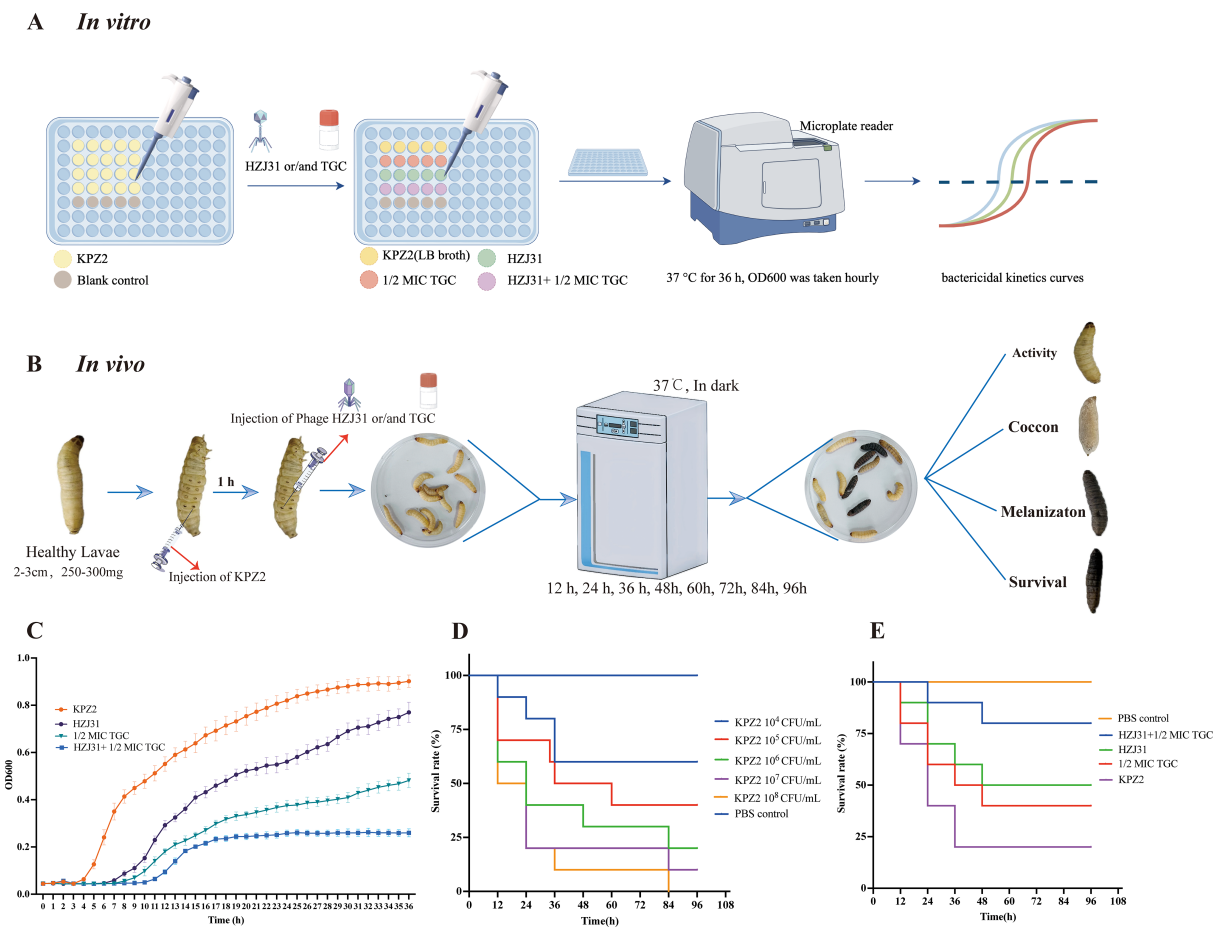

FIGURE 3
Antibacterial efficacy of phage HZJ31 and TGC against KPZ2 in Vivo and in Vitro. **(A)** Schematic of the *in vitro* bactericidal kinetics assay. KPZ2 was cultured in a 96-well plate and treated with phage HZJ31 (MOI = 0.001), 1/2 MIC TGC, or their combination. OD600 values were measured hourly over 36 hours at 37 °C using a microplate reader to generate bactericidal kinetics curves. **(B)** Schematic of the bactericidal efficacy in the *G.mellonella* infection model. Larvae were injected with KPZ2 (10 μL) into the last left proleg and incubated for 1 h, followed by injection of phage HZJ31, 1/2 MIC TGC, or their combination into the last right proleg. Larvae were monitored at 12-h intervals for survival over 96 hours. **(C)** *In vitro* bactericidal activity of phage HZJ31 and TGC against KPZ2 strain, mean ± SD. **(D)** Survival curves of *G.mellonella* larvae injected with different concentrations of KPZ2 to determine the optimal bacterial inoculum. An inoculum of 1×10^7 CFU/mL resulted in approximately 80% mortality at 24 h, mean ± SD. **(E)** Therapeutic efficacy of HZJ31 and TGC in *G.mellonella* infection model, mean ± SD.

closely associated with the expression of virulence factors such as capsular polysaccharides and outer membrane proteins (Sauer et al., 2022) (Li et al., 2024). KP strains with robust biofilm-forming capabilities exhibit heightened virulence, suggesting more severe infections and adverse outcomes (Zheng et al., 2018; Tang et al., 2024). Phage therapy has emerged as a promising strategy to combat biofilm-associated infections. In this study, phage HZJ31 effectively inhibited KPZ2 biofilm formation at 24 h, 48 h, and 72 h and compromised the structural integrity of preformed biofilms, resulting in efficient bacterial lysis within the biofilms.

Phages can encode enzymes, such as depolymerase, endolysin and holin, that degrade biofilm matrices, including polymers and capsular polysaccharides, thus facilitating the disruption of bacterial biofilm integrity, which is a key mechanism of phage action against bacterial biofilms (Lin et al., 2014; Topka-Bielecka et al., 2021; Lendel et al., 2024; Zhao et al., 2024a). The effectiveness of HZJ31 in overcoming bacterial biofilm defenses presents a new avenue for the treatment of refractory infections. A total of 48 ORFs were identified in the genome of phage HZJ31 through Prokka annotation, of which 33 were functionally characterized. Notably, ORF 20 and ORF 39 were predicted to encode a lysin and a holin protein, respectively. In addition, 15 ORFs were annotated as hypothetical proteins, suggesting that some of them may encode previously uncharacterized enzymes involved in biofilm matrix degradation. Further structural and functional analyses are required to elucidate their potential roles.

Phage-antibiotic combination therapy emerges as a promising strategy for combating antibiotic-resistant infections. This therapeutic approach harnesses the distinct antimicrobial mechanisms of phages and antibiotics to expand the host range, augment antibacterial potency, and retard the development of phage resistance. Furthermore, it has the potential to diminish the necessary antibiotic dosages, alleviate associated side effects, and optimize treatment efficacy in complex infections (Van

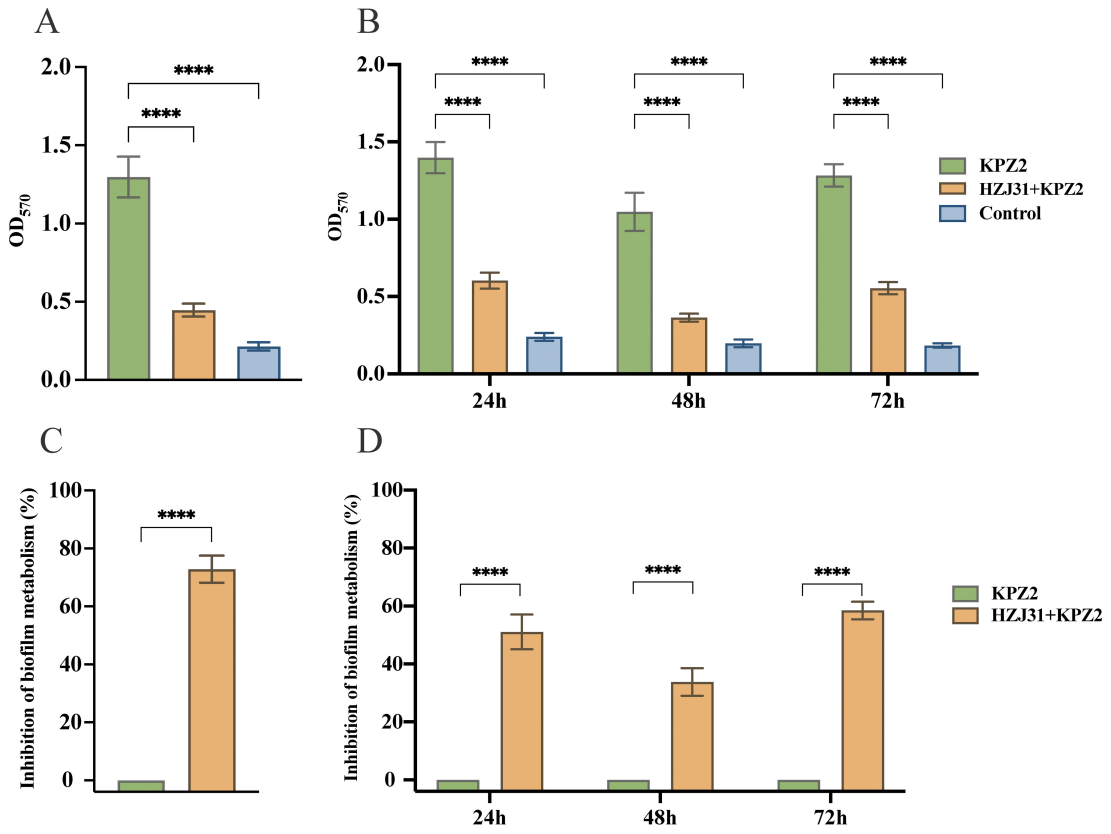

FIGURE 4
The antibiofilm activity of phage HZJ31.The crystal violet assay was used to quantify biofilm biomass and assess the disruptive effect of phage HZJ31 on pre-formed biofilms **(A)**and its inhibitory effect on biofilm formation **(B).** The XTT assay measured bacterial viability within biofilms to assess the disruptive **(C)** and inhibitory effects **(D)** of phage HZJ31. All data are shown as mean ± SD. ****P <0.0001.

Nieuwenhuyse et al., 2021; Ashworth, 2024). In our study, tigecycline was selected for combination therapy based on susceptibility testing, which showed that KPZ2 was resistant to most antibiotics but remained sensitive to TGC, polymyxin B, and ceftazidime-avibactam (Table 3). TGC, a tetracycline derivative, manifests broad-spectrum antimicrobial properties and an extended half-life by impeding protein synthesis in a spectrum of pathogens, including antibiotic-resistant bacteria and biofilms (Giamarellou and Poulakou, 2011). Both monotherapy of TGC and its synergistic combinations with other antibiotics have shown promising treatment efficacies against CRKP infections (Park et al., 2024; Xie et al., 2024). In this study, the bactericidal kinetics data revealed that phage HZJ31 and TGC exhibited distinct antimicrobial effects when applied individually or in combination against KPZ2. The phage HZJ31 group demonstrated a moderate inhibitory effect, with OD600 values rising after 7 h but remaining significantly lower than those of the untreated control throughout the 36-h observation period. This indicates that phage HZJ31 can delay bacterial proliferation and partially suppress growth, though phage resistance may emerge over time. Notably, the combination of phage HZJ31 with 1/2 MIC TGC achieved superior bacterial suppression, suggesting a synergistic interaction between phage HZJ31 and sub-inhibitory concentrations of TGC in both augmenting bactericidal efficacy and delaying the emergence of resistant strains. In addition to TGC, other antibiotics such as polymyxin B, colistin, and ceftazidime-avibactam may also be considered for phage-antibiotic combination strategies (Wang et al., 2021; Han et al., 2022; Cristinziano et al., 2024), depending on the antibiotic susceptibility profile and infection context (Diallo and Dublanchet, 2022) (Morrisette et al., 2020; Zhao et al., 2024b).

In the *G.mellonella* infection model, larvae treated with phage HZJ31 or TGC alone had survival rates of 50% and 60%, respectively, after 96 h, while the HZJ31-TGC combination exhibited a significantly improved survival rate (70%). These results demonstrate that the phage HZJ31-TGC combination enhances antibacterial activity both *in vitro and in vivo*. Furthermore, the phage-antibiotic combination exhibited synergistic effects in biofilm degradation. The therapeutic efficacy of phage-antibiotic combination therapy is contingent upon a multitude of factors, such as the specific types of phages and antibiotics employed, the order of administration, dosages, and the duration of treatment. It is noteworthy that certain phage-antibiotic combinations may exhibit antagonistic interactions. In light of the absence of standardized protocols for phage-antibiotic therapy, there is an imperative need for systematic experimentation to ascertain the most efficacious combinations. These experiments should also carefully monitor the emergence of resistant strains during treatment. Highly personalized treatment regimens should

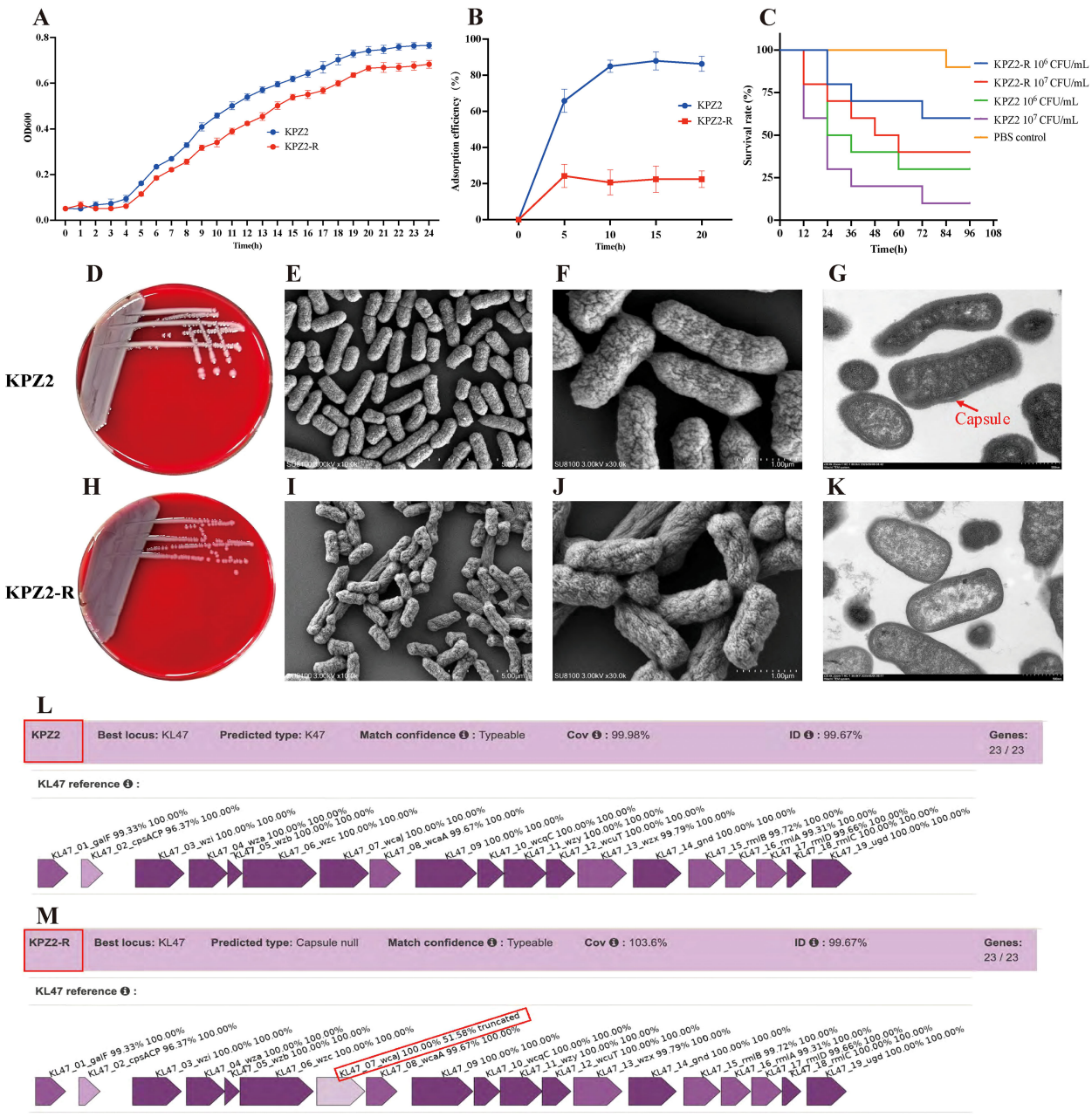

FIGURE 5
Characterization of phage-resistant strain KPZ2-R. **(A)** Growth curves of KPZ2 and KPZ2-R in LB broth measured by OD600, mean ± SD. **(B)** Comparison of adsorption efficiency between KPZ2 and KPZ2-R, mean ± SD. **(C)** Comparison of virulence between KPZ2 and KPZ2-R in the *G.mellonella* infection model. **(D, H)** Colony morphology of the strain KPZ2 and KPZ2-R on blood agar plates. **(E, F, I, J)** SEM images of KPZ2 **(E, F)** and KPZ2-R **(I , J)**. KPZ2 showed a smooth, dense, and uniform surface with a thick structure. In contrast, KPZ2-R had a rough, uneven surface with wrinkles or depressions and a thinner structure, along with evident capsule defects. **(G, K)** TEM images of KPZ2 **(G)** and KPZ2-R **(K)**. KPZ2 exhibited a well-defined, prominent capsule surrounding the cell, whereas KPZ2-R displayed a significantly reduced and poorly defined capsule. **(L, M)** Kaptive-based capsular locus analysis. Both strains matched the KL47 capsular type with 99.67% identity. KPZ2 showed complete locus coverage (99.98%) with intact capsule biosynthesis genes, while KPZ2-R was classified as "capsule null" due to a truncated wcaJ gene (51.58% identity).

be designed to maximize therapeutic efficacy while minimizing adverse reactions (Hong et al., 2024) (Fungo et al., 2023).

In monophage therapy, bacteria rapidly develop resistance to phages under selective pressure, which limits the application of phage therapy (Strathdee et al., 2023; Laanto, 2024; Pal et al., 2024). The mechanisms of phage resistance are complex and diverse, including preventing phage adsorption, blocking phage DNA injection, cleaving the phage genome, abortive infection, and quorum sensing, among others (Laanto et al., 2020). Adsorption is the initial step of phage infection of bacteria and a crucial factor determining the success of phage therapy. Bacteria can block phage adsorption through several mechanisms: mutation or modification of the phage receptor, extracellular matrix interference with the receptor, and competitive inhibition by receptor analogs (Laanto

TABLE 3 The antibiotic susceptibility of KPZ2 and KPZ2-R.

Antibiotics	KPZ2		KPZ2-R	
	MIC	S/I/R	MIC	S/I/R
Tigecycline	≤1	S	≤1	S
Polymyxin B	≤0.05	S	≤0.05	S
Ceftazidime-avibactam	≤4	S	≤4	S
Piperacillin	≥128	R	≤32	S
Gentamycin	≥16	R	≤4	S
Phosphomycin	≥64	R	≥64	R
Ceftazidime	≥64	R	≥64	R
Ampicillin	≥32	R	≥32	R
Tobramycin	≥16	R	≥16	R
Imipenem	≥16	R	≥16	R
Ciprofloxacin	≥4	R	≥4	R
Cefuroxime sodium	≥64	R	≥64	R
Levofloxacin	≥8	R	≥8	R
Cefazolin	≥64	R	≥64	R
Cefoperazone/Sulbactam	≥64	R	≥64	R
Meropenem	≥16	R	≥16	R
Cotrimoxazole	≤20	S	≤20	S
Amikacin	≥64	R	≥64	R
Ceftriaxone	≥64	R	≥64	R
Cefotetan	≥64	R	≥64	R
Piperacillin/tazobactam	≥128	R	≥128	R
Ampicillin/sulbactam	≥32	R	≥32	R
Aztreonam	≥64	R	≥64	R
Cefuroxime	≥64	R	≥64	R

S, Sensitivity; I, Intermediary; R, Resistance.

et al., 2020). Capsular polysaccharides, outer membrane proteins, and lipopolysaccharides serve as the adsorption receptors for KP phages, and their loss or mutation can lead to phage resistance (Camprubí, 1991; Henrici De Angelis et al., 2021; Cai et al., 2022; Fang and Zong, 2022; Geng et al., 2023). The capsule often masks the bacterial receptors, preventing direct binding between the phage and the receptor (Samson et al., 2013). In this study, we observed that KPZ2 developed phage resistance under selective pressure from phage HZJ31 by losing its capsule, resulting in a significant decrease in the phage's adsorption efficiency to the resistant mutant KPZ2-R. Moreover, we observed a significant trade-off phenomenon — KPZ2-R exhibited altered colony morphology, slower growth rate, and reduced virulence, which could increase its susceptibility to immune clearance during actual infections. Interestingly, KPZ2-R regained sensitivity to piperacillin and gentamicin, a phenomenon not uncommon in bacterial resistance mechanisms (Hu et al., 2024b). Although bacteria may escape phage infection by altering or shedding their capsule and outer membrane proteins, this adaptation can inadvertently compromise their defense against antibiotics, consequently rendering them susceptible once again (Gordillo Altamirano et al., 2021; Nang et al., 2024). The employment of a phage cocktail comprising both capsule-dependent and -independent phages, or a strategic sequence of phage and antibiotic administration, may yield superior therapeutic outcomes, offering innovative strategies and perspectives for phage therapy.

This study has several limitations that should be acknowledged. First, the host range of phage HZJ31 was assessed using 30 clinical CRKP isolates through spot assays. The limited number of isolates may not fully represent the genetic and phenotypic diversity of CRKP in clinical settings. Moreover, most strains were collected from a single hospital, raising the possibility of strain clustering and potential bias toward nosocomial infection types. Future studies will include a broader and more diverse set of CRKP isolates from multiple geographic and clinical sources to enhance the accuracy and generalizability of the host range evaluation. Second, the antibacterial and antibiofilm effects of phage HZJ31 were evaluated only against a single CRKP strain, without investigating potential cross-species or cross-strain activity. Additionally, the synergistic antibacterial activity was tested only in combination with TGC, to which the tested strain was already susceptible. Expanding the evaluation to include multiple antibiotics and additional strains will provide a more comprehensive understanding of its synergistic potential. The *in vivo* antibacterial efficacy was limited to the *G.mellonella* model and has not yet been validated in advanced mammalian models, which restricts the generalizability of the study. Lastly, the biosafety of phage HZJ31 was only preliminarily assessed at the genetic and cellular levels. Further evaluation in mammalian models is necessary to comprehensively assess its safety and therapeutic efficacy.

In conclusion, we successfully isolated a novel lytic phage, HZJ31, which has demonstrated high environmental stability and biocompatibility. Furthermore, the synergistic application of HZJ31 with TGC showed a markedly enhanced antibacterial activity in both *in vitro* and the *G.mellonella* infection model. These findings provide theoretical support for the potential clinical application of phage HZJ31.

Data availability statement

The datasets presented in this study can be found in online repositories. The names of the repository/repositories and accession number(s) can be found in the article/supplementary material.

Ethics statement

The manuscript presents research on animals that do not require ethical approval for their study.

Author contributions

RZ: Conceptualization, Data curation, Funding acquisition, Software, Validation, Visualization, Writing – original draft, Writing – review & editing. RW: Investigation, Methodology, Software, Writing – original draft. BF: Investigation, Methodology, Writing – original draft. RL: Data curation, Methodology, Writing – original draft. XY: Investigation, Software, Writing – review & editing. XL: Project administration, Software, Supervision, Writing – original draft. CW: Conceptualization, Resources, Supervision, Writing – review & editing. YL: Conceptualization, Funding acquisition, Project administration, Writing – review & editing.

Funding

The author(s) declare that financial support was received for the research and/or publication of this article. The work was supported by the Henan Provincial Science and Technology Research Project (No. 242102310148), the Natural Science Foundation of Henan Province (No.242300420437), the Key Scientific Research Project of Henan Higher Education Institutions (No.24A310007), and Wu Jieping Medical Foundation (NO.320.6750.2024-03-27).

Conflict of interest

The authors declare that the research was conducted in the absence of any commercial or financial relationships that could be construed as a potential conflict of interest.

Generative AI statement

The author(s) declare that no Generative AI was used in the creation of this manuscript.

Publisher's note

References

Ashworth, E. A., Wright, R. C. T., Shears, R. K., Wong, J. K. L., Hassan, A., Hall, J. P. J., et al. (2024). Exploiting lung adaptation and phage steering to clear pan-resistant Pseudomonas aeruginosa infections *in vivo*. *Nat. Commun.* 15 (1), 1547. doi: 10.1038/s41467-024-45785-z

Baqer, A. A., Fang, K., Mohd-Assaad, N., Adnan, S. N. A., and Md Nor, N. S. (2022). *In vitro* activity, stability and molecular characterization of eight potent bacteriophages infecting carbapenem-resistant klebsiella pneumoniae. *Viruses* 15, 117. doi: 10.3390/v15010117

Bologna, E., Licari, L. C., Manfredi, C., Ditonno, F., Cirillo, L., Fusco, G. M., et al. (2024). Carbapenem-resistant enterobacteriaceae in urinary tract infections: from biological insights to emerging therapeutic alternatives. *Medicina (Mex.)* 60, 214. doi: 10.3390/medicina60020214

Cai, R., Deng, H., Song, J., Zhang, L., Zhao, R., Guo, Z., et al. (2022). Phage resistance mutation triggered by OmpC deficiency in Klebsiella pneumoniae induced limited fitness costs. *Microb. Pathog.* 167, 105556. doi: 10.1016/j.micpath.2022.105556

Camprubí, S. (1991). Isolation and characterization of bacteriophage FC3–10 from Klebsiella spp. *FEMS Microbiol. Lett.* 83, 291–297. doi: 10.1016/0378-1097(91)90491-R

Chadha, J., Harjai, K., and Chhibber, S. (2022). Revisiting the virulence hallmarks of *Pseudomonas aeruginosa* : a chronicle through the perspective of quorum sensing. *Environ. Microbiol.* 24, 2630–2656. doi: 10.1111/1462-2920.15784

Chang, R. Y. K., Nang, S. C., Chan, H.-K., and Li, J. (2022). Novel antimicrobial agents for combating antibiotic-resistant bacteria. *Adv. Drug Deliv. Rev.* 187, 114378. doi: 10.1016/j.addr.2022.114378

Colavecchio, A., Cadieux, B., Lo, A., and Goodridge, L. D. (2017). Bacteriophages contribute to the spread of antibiotic resistance genes among foodborne pathogens of the enterobacteriaceae family - A review. *Front. Microbiol.* 8. doi: 10.3389/fmicb.2017.01108

Cook, B. W. M., and Hynes, A. P. (2025). Re-evaluating what makes a phage unsuitable for therapy. *NPJ Antimicrob. Resist.* 3, 45. doi: 10.1038/s44259-025-00117-z

Cristinziano, M., Shashkina, E., Chen, L., Xiao, J., Miller, M. B., Doligalski, C., et al. (2024). Use of epigenetically modified bacteriophage and dual beta-lactams to treat a Mycobacterium abscessus sternal wound infection. *Nat. Commun.* 15, 10360. doi: 10.1038/s41467-024-54666-4

Cui, L., Watanabe, S., Miyanaga, K., Kiga, K., Sasahara, T., Aiba, Y., et al. (2024). A comprehensive review on phage therapy and phage-based drug development. *Antibiot. Basel Switz.* 13, 870. doi: 10.3390/antibiotics13090870

Diallo, K., and Dublanchet, A. (2022). Benefits of combined phage-antibiotic therapy for the control of antibiotic-resistant bacteria: A literature review. *Antibiot. Basel Switz.* 11, 839. doi: 10.3390/antibiotics11070839

Ding, L., Shen, S., Chen, J., Tian, Z., Shi, Q., Han, R., et al. (2023). *Klebsiella pneumoniae* carbapenemase variants: the new threat to global public health. *Clin. Microbiol. Rev.* 36, e00008–e00023. doi: 10.1128/cmr.00008-23

Fang, Q., and Zong, Z. (2022). Lytic Phages against ST11 K47 Carbapenem-Resistant Klebsiella pneumoniae and the Corresponding Phage Resistance Mechanisms. *mSphere* 7, e00080–e00022. doi: 10.1128/msphere.00080-22

Fei, B., Li, D., Liu, X., You, X., Guo, M., Ren, Y., et al. (2023). Characterization and genomic analysis of a broad-spectrum lytic phage HZ2201 and its antibiofilm efficacy against Pseudomonas aeruginosa. *Virus Res.* 335, 199184. doi: 10.1016/j.virusres.2023.199184

Flemming, H.-C., Wingender, J., Szewzyk, U., Steinberg, P., Rice, S. A., and Kjelleberg, S. (2016). Biofilms: an emergent form of bacterial life. *Nat. Rev. Microbiol.* 14, 563–575. doi: 10.1038/nrmicro.2016.94

Fungo, G. B. N., Uy, J. C. W., Porciuncula, K. L. J., Candelario, C. M. A., Chua, D. P. S., Gutierrez, T. A. D., et al. (2023). Two is better than one": the multifactorial nature of phage-antibiotic combinatorial treatments against ESKAPE-induced infections. *PHAGE* 4, 55–67. doi: 10.1089/phage.2023.0007

Geng, H., Song, L., Yang, X., Xing, S., Wang, R., Xu, Y., et al. (2023). Resistance of Klebsiella pneumoniae to Phage hvKpP3 Due to High-Molecular Weight Lipopolysaccharide Synthesis Failure. *Microbiol. Spectr.* 11, (3), e0438422. doi: 10.1128/spectrum.04384-22

Giamarellou, H., and Poulakou, G. (2011). Pharmacokinetic and pharmacodynamic evaluation of tigecycline. *Expert Opin. Drug Metab. Toxicol.* 7, 1459–1470. doi: 10.1517/17425255.2011.623126

Goodridge, L. D. (2010). Designing phage therapeutics. *Curr. Pharm. Biotechnol.* 11, 15–27. doi: 10.2174/138920110790725348

Gordillo Altamirano, F., Forsyth, J. H., Patwa, R., Kostoulias, X., Trim, M., Subedi, D., et al. (2021). Bacteriophage-resistant Acinetobacter baumannii are resensitized to antimicrobials. *Nat. Microbiol.* 6, 157–161. doi: 10.1038/s41564-020-00830-7

Gorodnichev, R. B., Kornienko, M. A., Malakhova, M. V., Bespiatykh, D. A., Manuvera, V. A., Selezneva, O. V., et al. (2023). Isolation and characterization of the first zobellviridae family bacteriophage infecting klebsiella pneumoniae. *Int. J. Mol. Sci.* 24, 4038. doi: 10.3390/ijms24044038

Han, M.-L., Nang, S. C., Lin, Y.-W., Zhu, Y., Yu, H. H., Wickremasinghe, H., et al. (2022). Comparative metabolomics revealed key pathways associated with the synergistic killing of multidrug-resistant Klebsiella pneumoniae by a bacteriophage-polymyxin combination. *Comput. Struct. Biotechnol. J.* 20, 485–495. doi: 10.1016/j.csbj.2021.12.039

Hatfull, G. F., Dedrick, R. M., and Schooley, R. T. (2022). Phage therapy for antibiotic-resistant bacterial infections. *Annu. Rev. Med.* 73, 197–211. doi: 10.1146/annurev-med-080219-122208

Henrici De Angelis, L., Poerio, N., Di Pilato, V., De Santis, F., Antonelli, A., Thaller, M. C., et al. (2021). Phage resistance is associated with decreased virulence in KPC-producing klebsiella pneumoniae of the clonal group 258 clade II lineage. *Microorganisms* 9, 762. doi: 10.3390/microorganisms9040762

Hong, Q., Chang, R. Y. K., Assafiri, O., Morales, S., and Chan, H.-K. (2024). Optimizing *in vitro* phage-ciprofloxacin combination formulation for respiratory therapy of multi-drug resistant Pseudomonas aeruginosa infections. *Int. J. Pharm.* 652, 123853. doi: 10.1016/j.ijpharm.2024.123853

Hu, F., Pan, Y., Li, H., Han, R., Liu, X., Ma, R., et al. (2024a). Carbapenem-resistant Klebsiella pneumoniae capsular types, antibiotic resistance and virulence factors in China: a longitudinal, multi-centre study. *Nat. Microbiol.* 9, 814–829. doi: 10.1038/s41564-024-01612-1

Hu, Q., Huang, L., Yang, Y., Xiang, Y., and Liu, J. (2024b). Essential phage component induces resistance of bacterial community. *Sci. Adv.* 10, eadp5057. doi: 10.1126/sciadv.adp5057

Jault, P., Leclerc, T., Jennes, S., Pirnay, J. P., Que, Y.-A., Resch, G., et al. (2019). Efficacy and tolerability of a cocktail of bacteriophages to treat burn wounds infected by Pseudomonas aeruginosa (PhagoBurn): a randomised, controlled, double-blind phase 1/2 trial. *Lancet Infect. Dis.* 19, 35–45. doi: 10.1016/S1473-3099(18)30482-1

Karampatakis, T., Tsergouli, K., and Behzadi, P. (2023). Carbapenem-resistant klebsiella pneumoniae: virulence factors, molecular epidemiology and latest updates in treatment options. *Antibiotics* 12, 234. doi: 10.3390/antibiotics12020234

Kortright, K. E., Chan, B. K., Koff, J. L., and Turner, P. E. (2019). Phage therapy: A renewed approach to combat antibiotic-resistant bacteria. *Cell Host Microbe* 25, 219–232. doi: 10.1016/j.chom.2019.01.014

Kou, X., Yang, X., and Zheng, R. (2024). Challenges and opportunities of phage therapy for Klebsiella pneumoniae infections. *Appl. Environ. Microbiol.* 90, e0135324. doi: 10.1128/aem.01353-24

Laanto, E. (2024). "Overcoming bacteriophage resistance in phage therapy," in *Bacteriophages*. Ed. E. Tumban (Springer US, New York, NY), 401–410. doi: 10.1007/978-1-0716-3549-0_23

Laanto, E., Mäkelä, K., Hoikkala, V., Ravantti, J. J., and Sundberg, L.-R. (2020). Adapting a phage to combat phage resistance. *Antibiotics* 9, 291. doi: 10.3390/antibiotics9060291

Lendel, A. M., Antonova, N. P., Grigoriev, I. V., Usachev, E. V., Gushchin, V. A., and Vasina, D. V. (2024). Biofilm-disrupting effects of phage endolysins LysAm24, LysAp22, LysECD7, and LysSi3: breakdown the matrix. *World J. Microbiol. Biotechnol.* 40, 186. doi: 10.1007/s11274-024-03999-9

Li, L., Gao, X., Li, M., Liu, Y., Ma, J., Wang, X., et al. (2024). Relationship between biofilm formation and antibiotic resistance of Klebsiella pneumoniae and updates on antibiofilm therapeutic strategies. *Front. Cell. Infect. Microbiol.* 14. doi: 10.3389/fcimb.2024.1324895

Lin, T.-L., Hsieh, P.-F., Huang, Y.-T., Lee, W.-C., Tsai, Y.-T., Su, P.-A., et al. (2014). Isolation of a bacteriophage and its depolymerase specific for K1 capsule of klebsiella pneumoniae: implication in typing and treatment. *J. Infect. Dis.* 210, 1734–1744. doi: 10.1093/infdis/jiu332

Lou, T., Du, X., Zhang, P., Shi, Q., Han, X., Lan, P., et al. (2022). Risk factors for infection and mortality caused by carbapenem-resistant Klebsiella pneumoniae: A large multicentre case–control and cohort study. *J. Infect.* 84, 637–647. doi: 10.1016/j.jinf.2022.03.010

Martins, W. M. B. S., Li, M., Sands, K., Lenzi, M. H., Portal, E., Mathias, J., et al. (2022). Effective phage cocktail to combat the rising incidence of extensively drug-resistant *Klebsiella pneumoniae* sequence type 16. *Emerg. Microbes Infect.* 11, 1015–1023. doi: 10.1080/22221751.2022.2051752

Miller, W. R., and Arias, C. A. (2024). ESKAPE pathogens: antimicrobial resistance, epidemiology, clinical impact and therapeutics. *Nat. Rev. Microbiol.* 22, 598–616. doi: 10.1038/s41579-024-01054-w

Morrisette, T., Kebriaei, R., Lev, K. L., Morales, S., and Rybak, M. J. (2020). Bacteriophage therapeutics: A primer for clinicians on phage-antibiotic combinations. *Pharmacother. J. Hum. Pharmacol. Drug Ther.* 40, 153–168. doi: 10.1002/phar.2358

Mulani, M. S., Kumkar, S. N., and Pardesi, K. R. (2022). Characterization of novel *klebsiella* phage PG14 and its antibiofilm efficacy. *Microbiol. Spectr.* 10, e01994–e01922. doi: 10.1128/spectrum.01994-22

Naghavi, M., Vollset, S. E., Ikuta, K. S., Swetschinski, L. R., Gray, A. P., Wool, E. E., et al. (2024). Global burden of bacterial antimicrobial resistance 1990–2021: a systematic analysis with forecasts to 2050. *Lancet* 404, 1199–1226. doi: 10.1016/S0140-6736(24)01867-1

Nang, S. C., Lu, J., Yu, H. H., Wickremasinghe, H., Azad, M. A. K., Han, M., et al. (2024). Phage resistance in Klebsiella pneumoniae and bidirectional effects impacting antibiotic susceptibility. *Clin. Microbiol. Infec.* 30 (6), 787–794. doi: 10.1016/j.cmi.2024.03.015

Pal, N., Sharma, P., Kumawat, M., Singh, S., Verma, V., Tiwari, R. R., et al. (2024). Phage therapy: an alternative treatment modality for MDR bacterial infections. *Infect. Dis.* 56 (10), 785–817. doi: 10.1080/23744235.2024.2379492

Park, S., Choi, J., Shin, D., Kwon, K. T., Kim, S.-H., Wi, Y. M., et al. (2024). Conversion to colistin susceptibility by tigecycline exposure in colistin-resistant Klebsiella pneumoniae and its implications to combination therapy. *Int. J. Antimicrob. Agents* 63, 107017. doi: 10.1016/j.ijantimicag.2023.107017

Patpatia, S., Yilmaz, O., Ylänne, M., and Kiljunen, S. (2021). Isolation and Genomic Analysis of the Phage vB_PaeP_fHoPae04 Infecting Pseudomonas aeruginosa. *Microbiol. Resour. Announc.* 10, e00076–e00021. doi: 10.1128/MRA.00076-21

Peng, X., Chang, J., Zhang, H., Li, X., Zhang, C., Jiao, S., et al. (2025). Isolation, characterization, and genomic analysis of a novel bacteriophage vB_Kp_XP4 targeting hypervirulent and multidrug-resistant Klebsiella pneumoniae. *Front. Microbiol.* 16. doi: 10.3389/fmicb.2025.1491961

Samson, J. E., Magadán, A. H., Sabri, M., and Moineau, S. (2013). Revenge of the phages: defeating bacterial defences. *Nat. Rev. Microbiol.* 11, 675–687. doi: 10.1038/nrmicro3096

Sauer, K., Stoodley, P., Goeres, D. M., Hall-Stoodley, L., Burmølle, M., Stewart, P. S., et al. (2022). The biofilm life cycle: expanding the conceptual model of biofilm formation. *Nat. Rev. Microbiol.* 20, 608–620. doi: 10.1038/s41579-022-00767-0

She, T., Tan, D., Balcazar, J. L., Friman, V., Wang, D., Zhu, D., et al. (2025). Phage-mediated horizontal transfer of *Salmonella enterica* virulence genes with regulatory feedback from the host. *iMeta*, e70042. doi: 10.1002/imt2.70042

Strathdee, S. A., Hatfull, G. F., Mutalik, V. K., and Schooley, R. T. (2023). Phage therapy: From biological mechanisms to future directions. *Cell* 186, 17–31. doi: 10.1016/j.cell.2022.11.017

Suttle, C. A. (2007). Marine viruses — major players in the global ecosystem. *Nat. Rev. Microbiol.* 5, 801–812. doi: 10.1038/nrmicro1750

Tang, M., Zhao, D., Zhang, Y., Qian, C., Chen, H., Chen, L., et al. (2024). Impact of LuxS on virulence and pathogenicity in Klebsiella pneumoniae exhibiting varied mucoid phenotypes. *Infect. Immun.* 92, e0001224. doi: 10.1128/iai.00012-24

Topka-Bielecka, G., Dydecka, A., Necel, A., Bloch, S., Nejman-Faleńczyk, B., Węgrzyn, G., et al. (2021). Bacteriophage-derived depolymerases against bacterial biofilm. *Antibiotics* 10, 175. doi: 10.3390/antibiotics10020175

Uyttebroek, S., Chen, B., Onsea, J., Ruythooren, F., Debaveye, Y., Devolder, D., et al. (2022). Safety and efficacy of phage therapy in difficult-to-treat infections: a systematic review. *Lancet Infect. Dis.* 22, e208–e220. doi: 10.1016/S1473-3099(21)00612-5

Van Nieuwenhuyse, B., Galant, C., Brichard, B., Docquier, P.-L., Djebara, S., Pirnay, J.-P., et al. (2021). A Case of *In Situ* Phage Therapy against Staphylococcus aureus in a Bone Allograft Polymicrobial Biofilm Infection: Outcomes and Phage-Antibiotic Interactions. *Viruses* 13, 1898. doi: 10.3390/v13101898

Wang, X., Loh, B., Gordillo Altamirano, F., Yu, Y., Hua, X., and Leptihn, S. (2021). Colistin-phage combinations decrease antibiotic resistance in *Acinetobacter baumannii* via changes in envelope architecture. *Emerg. Microbes Infect.* 10, 2205–2219. doi: 10.1080/22221751.2021.2002671

Wang, R., You, X., Liu, X., Fei, B., Li, Y., Wang, D., et al. (2024). Characterization of phage HZY2308 against Acinetobacter baumannii and identification of phage-resistant bacteria. *Virol. J.* 21 (1), 283. doi: 10.1186/s12985-024-02556-y

Xie, M., Ye, L., Chen, K., Xu, Q., Yang, C., Chen, X., et al. (2024). Clinical use of tigecycline may contribute to the widespread dissemination of carbapenem-resistant hypervirulent Klebsiella pneumoniae strains. *Emerg. Microbes Infect.* 13, 2306957. doi: 10.1080/22221751.2024.2306957

Xing, J., Han, R., Zhao, J., Zhang, Y., Zhang, M., Zhang, Y., et al. (2025). Revisiting therapeutic options against resistant klebsiella pneumoniae infection: Phage therapy is key. *Microbiol. Res.* 293, 128083. doi: 10.1016/j.micres.2025.128083

Zhao, R., Jiang, S., Ren, S., Yang, L., Han, W., Guo, Z., et al. (2024a). A novel phage putative depolymerase, Depo16, has specific activity against K1 capsular-type Klebsiella pneumoniae. *Appl. Environ. Microbiol.* 90, e0119723. doi: 10.1128/aem.01197-23

Zhao, M., Li, H., Gan, D., Wang, M., Deng, H., and Yang, Q. E. (2024b). Antibacterial effect of phage cocktails and phage-antibiotic synergy against pathogenic Klebsiella pneumoniae. *mSystems*. 9, e0060724. doi: 10.1128/msystems.00607-24

Zheng, J.-X., Lin, Z.-W., Chen, C., Chen, Z., Lin, F.-J., Wu, Y., et al. (2018). Biofilm Formation in Klebsiella pneumoniae Bacteremia Strains Was Found to be Associated with CC23 and the Presence of wcaG. *Front. Cell. Infect. Microbiol.* 8. doi: 10.3389/fcimb.2018.00021

frontiers | Frontiers in Cellular and Infection Microbiology

TYPE Perspective
PUBLISHED 22 October 2025
DOI 10.3389/fcimb.2025.1690404

OPEN ACCESS

EDITED BY
Mercedes Gonzalez Moreno,
Hans Knoll Institute, Germany

REVIEWED BY
Kilian Vogele,
Invitris GmbH, Germany

*CORRESPONDENCE
Sahan B. W. Liyanagedera
sahan@biophoundry.com

RECEIVED 21 August 2025
ACCEPTED 29 September 2025
PUBLISHED 22 October 2025

CITATION
Kulkarni V, Laohakunakorn N and Liyanagedera SBW (2025) Synthetic cells for phage therapy: a perspective. *Front. Cell. Infect. Microbiol.* 15:1690404. doi: 10.3389/fcimb.2025.1690404

Synthetic cells for phage therapy: a perspective

Vishwesh Kulkarni[1,2], Nadanai Laohakunakorn[3] and Sahan B. W. Liyanagedera[3,4]*

[1]School of Biomedical Engineering and Imaging Sciences, King's College London, London, United Kingdom, [2]SUSTech-King's School of Medicine, Shenzhen, China, [3]Institute of Quantitative Biology, Biochemistry and Biotechnology, University of Edinburgh, Edinburgh, United Kingdom, [4]Biophoundry Inc., Chapel Hill, NC, United States

A synthetic cell is a membrane-bound vesicle that encapsulates cell-free *transcription/translation* (TXTL) systems. It represents a transformative platform for advancing bacteriophage therapy. Building on experimental work that demonstrates (i) modular genome assembly, (ii) high-yield phage TXTL systems, and (iii) smart hydrogel encapsulation, we explore how synthetic cells can address major limitations in phage therapy. The promising advances include point-of-care phage manufacturing, logic-responsive antimicrobial biomaterials, and new chassis to dissect the dynamics of phage-host interactions. We also propose a roadmap for the deployment of synthetic cells as programmable and evolvable tools in the context of laboratory research and translational clinical adoption.

KEYWORDS

cell-free protein synthesis, transcription/translation (TXTL), synthetic cells, bacteriophages, phage therapy, hydrogel

1 Introduction

Phage therapy refers to the therapeutic use of bacteriophages—viruses that specifically infect and kill bacteria—to treat bacterial infections (Skurnik et al., 2025). Although it has been practiced for over a century in limited clinical settings, its widespread authorized adoption remains restricted, with most applications occurring under compassionate use or experimental frameworks (Yang et al., 2023). This is largely due to regulatory uncertainty, challenges in large-scale manufacturing and robust engineering methods for personalized phage cocktail design (Zalewska-Piątek 2023).

However the recent resurgence of phage therapy, catalyzed by advances in synthetic biology, has equipped us with an expanding arsenal of engineered bacteriophages to combat the *antimicrobial resistance* (AMR) crisis (Sawa et al., 2024). It is now possible to reprogram the phage-host range (Ando et al., 2015), enhance lytic activities (Son et al., 2021), and even assemble entire phage particles at clinically relevant titres *in vitro* through the use of cell-free transcription-translation (TXTL) systems (Garenne et al., 2021; Liyanagedera et al., 2022b; Levrier et al., 2024). However, the next great leap in phage therapeutics may not lie solely in the phage itself, but in the platforms used to produce,

deploy, and study them. *Synthetic cells*, defined here as vesicles that encapsulate the TXTL machinery, offer exciting opportunities (Garamella et al., 2019a). Our exposition in this paper goes beyond the *in vitro* use of cell-free TXTL systems and is inspired by early work in the fields of artificial life and synthetic cells [see (Adamala et al., 2017; Bayoumi et al., 2017; Lentini et al., 2017; Majumder et al., 2017; Rampioni et al., 2018; Sakamoto et al., 2018; Tang et al., 2018)]. We propose that programmable modular synthetic cells capable of assembly of infectious phage particles or phage-associated proteins (i.e., lysins/de-polymerases) could serve as a powerful enabling technology for advanced phage therapy. Positioned as a conduit for *artificial intelligence* (AI) driven phage discovery, synthetic cells can provide the essential experimental infrastructure to generate large, diverse, and discrete datasets suitable for training the underlying machine learning models (Figure 1). For example, such an experimental platform capable of high-throughput screening could generate data sets to predict phage-host interactions, enabling forward engineering of phage therapies against bacterial pathogens. Thus, synthetic cells can serve as a platform that will not only enable new therapeutic strategies, but also unlock new ways to probe the fundamental biology of the interactions between phage and host (Rothschild et al., 2024).

2 Cell-free TXTL and synthetic cells

Cell-free TXTL is an *in vitro* platform that reconstitutes the core molecular machinery of cellular transcription and translation, supported by energy regeneration and co-factor recycling, without the constraints of a cell membrane (Noireaux et al., 2003). This technology uses a cytoplasmic extract, typically derived from *Escherichia coli* (*E. coli*), which provide the core transcription-translation machinery, including RNA polymerase, ribosomes and translation factors, along with endogenous enzymes that support energy regeneration and central metabolism. By supplementing this extract with exogenous DNA template(s) and energy sources, TXTL enables robust synthesis of proteins and complex genetic circuits in a one-pot reaction, offering unparalleled speed, flexibility, and control for synthetic biology, functional genomics, and bio-manufacturing.

Synthetic cell construction integrates cell-free protein synthesis and liposome technology to create artificial bioreactors that replicate cellular phenomena. An increasingly large number of studies have recently demonstrated how synthetic cell technology has reached a level of complexity that could make them useful as actuators and mediators of signal transduction (Adamala et al., 2017; Bayoumi et al., 2017; Lentini et al., 2017; Majumder et al., 2017; Rampioni et al., 2018; Sakamoto et al., 2018; Tang et al., 2018). Quite a few recent studies demonstrate cell-free expression-mediated communication between synthetic cells and bacteria (Lentini et al., 2017; Rampioni et al., 2018), as well as between synthetic cells themselves (Adamala et al., 2017; Bayoumi et al., 2017; Tang et al., 2018). Most of such studies have established robust and replicable unidirectional communication. However, a study has also described bidirectional communication; where synthetic cells 'translated' chemical signals that cannot be sensed naturally, into perceivable inputs for *E. coli* (Lentini et al., 2014). Furthermore, membrane channels, such as alpha-hemolysin pores, can be used to decorate the phospholipid bilayer of the liposome.

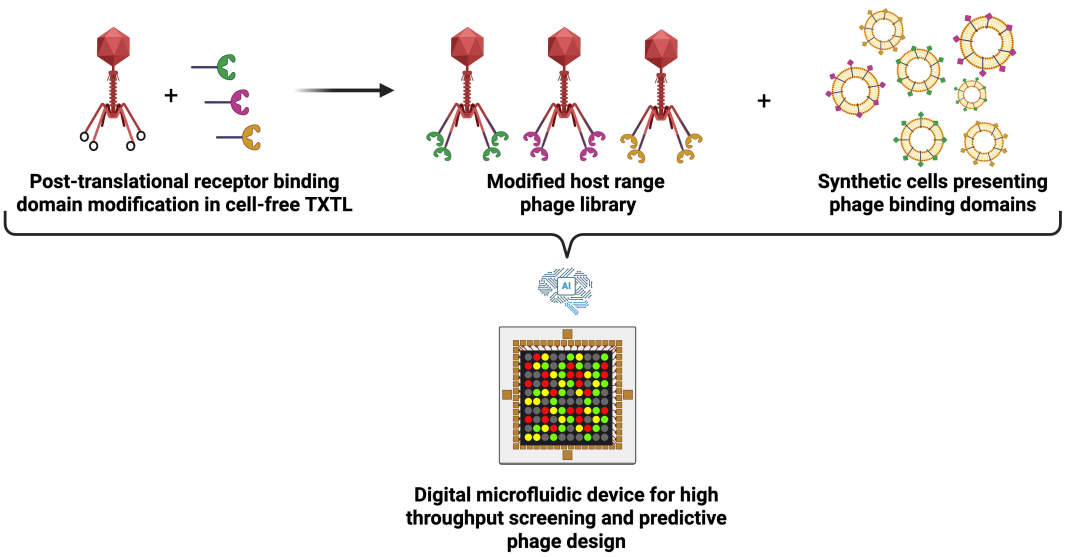

FIGURE 1
High-throughput synthetic cell and engineered phage interaction platform for predictive phage design. Schematic overview of a proposed library on library screening framework. Scaffold phage are assembled in TXTL and post-translationally decorated with receptor binding domain modifications to create a modified host range phage library. Synthetic cells, each engineered to express and present distinct receptor landscapes are combined with diverse host range phage library using combinatorial digital microfluidics. These high throughput experiments generate large interaction data sets that capture receptor-phage compatibility and infection outcomes. Data sets can be used to train advanced machine learning models for predictive phage design.

Such channels can either be incorporated during the construction of the liposome or be expressed *in situ* in response to a defined stimulus (Majumder et al., 2017). As such, through the coupling of synthetic genetic regulatory mechanisms to protein production, synthetic cells can be made to perform as highly programmable units of artificial life (Adamala et al., 2017).

3 Synthetic cells as phage research models

By recreating selected features of natural infection cycles in a controlled environment, synthetic cells provide a tractable platform to dissect phage-host interactions, test mechanistic hypotheses, and build a modular toolkit for phage research. This research-oriented perspective positions synthetic cells as reductionist experimental models to explore fundamental questions in virology and synthetic biology. A key advance in the use of synthetic cells for phage therapy is the recent demonstration of a fully synthetic cell-free phage infection cycle as reported in (Levrier et al., 2025). Here, the researchers created liposome-based synthetic cells encapsulating an *E. coli* cell-free TXTL system, with a *lipopolysaccharide* (LPS) outer shell. The LPS outer shell enabled T7 phage attachment, infection and delivery of the T7 phage genome into the synthetic cell. Following infection, the encapsulated TXTL machinery was able to act on the delivered phage genome and produce phage particles within synthetic cells. This "all-cell-free viral cycle" effectively mimics phage infection by facilitating attachment, viral genome replication, and phage production within discrete synthetic compartments. In this platform, the progeny of the phages was released via osmotic shock, an external trigger that disrupted the synthetic cell membrane, liberating the newly assembled virions. To advance toward truly autonomous systems, programmable lysis mechanisms are required, and here the bacteriophage holin proteins could be the key.

Holin proteins are an integral part of the lytic cycle and function as a "molecular clock" to time the lysis of the host (Schwarzkopf et al., 2024). These proteins, which when expressed from the phage genome, progressively accumulate in the membrane of the bacteria and undergo a sudden oligomerization to form large holes in the cytoplasmic membrane, thus providing access to phage-encoded endolysins to attack the cell wall. These coordinated events result in instantaneous lysis of the bacterial host, thus releasing the now assembled phage particles to enable another round of the lytic cycle.

A liposome-based single bilayer synthetic cell can be considered as a model of the cytoplasm and the cytoplasmic membrane of the bacterium (or a bacterium without a cell wall). In fact, early work on putative holin characterization used classical liposome fluorescence leakage assays to determine the lytic potential of the protein in question (Smith et al., 1998). Taking inspiration from the natural mechanisms of holing function, proof of concept studies have attempted programmable triggered release of phage assembled within synthetic cells. For example, initial attempts encapsulated TXTL systems capable of K1F phage assembly in synthetic cells based on single bilayer liposomes produced by the emulsion transfer technique (Liyanagedera 2022a). In this approach, the purified K1F phage genomes were co-encapsulated with the cell-free TXTL machinery during vesicle formation, rather than being introduced by infection. These synthetic cells exhibited dramatic loss of vesicles after 12 hours of incubation, likely due to premature holin-mediated lysis before phage assembly was complete. In contrast, controls with transcription inhibited by rifampicin remained morphologically stable. Consistent with this, plaque assays revealed that while bulk TXTL reactions produced phages, encapsulated systems did not, highlighting the challenge of synchronizing phage assembly with timed release. In addition, protein expression yields achieved per particle in encapsulated cell-free reactions are typically lower than those of bulk systems, likely reflecting the limited energy reserves within individual compartments (Noireaux and Libchaber 2004; Gonzales et al., 2022). This constraint becomes particularly relevant for larger phages, such as those typically used in phage therapy, whose assembly places greater energetic demands on the encapsulated system (Mahmoudabadi et al., 2017).

Despite these advances, significant challenges remain before synthetic cells can serve as robust models of phage infection. Current systems are constrained by their reliance on *E. coli*-derived TXTL, restricting applicability to *E. coli*-infecting phages (Garenne et al., 2021). To broaden the scope, it is necessary to develop non-model cell-free systems derived from other bacteria capable of phage assembly, which would allow the study and production of phages that infect diverse hosts (Brooks et al., 2023; Emslander et al., 2022). Similarly, while LPS coated vesicles enable T7 infection, many phages depend on alternative receptors such as outer membrane proteins or capsular polysaccharides, as exemplified by K1F phage (Liyanagedera et al., 2022b. Addressing this limitation may involve membrane engineering approaches, such as functionalizing synthetic cell membranes with purified receptors (Elani 2016) or integrating *outer membrane vesicles* (OMVs) from non-model bacteria to recreate authentic attachment environments (Bali et al., 2023).

4 Smart antimicrobial materials

Synthetic cells are emerging as minimalist and programmable bioreactors for the *de novo* synthesis and delivery of biological drugs (Monck et al., 2024). This approach goes beyond traditional drug delivery by creating systems capable of sensing, decision making, and autonomous action at the infection site (Gispert and Elani 2025).

Although synthetic cells show promise as standalone antimicrobial agents, their therapeutic potential is magnified when integrated into structured materials. The smart antimicrobial material, i.e. a material that can (i) sense a bacterial threat, (ii) synthesize phage on demand, and (iii) release those phages at the site of infection, is a compelling goal for phage therapy (Beth et al., 2023; El-Husseiny et al., 2022). Its foundation lies at the convergence of smart materials and artificial life.

The bottom-up design of synthetic cells and their translation into the creation of smart antimicrobial materials is reliant on

compartmentalized electrical or chemical signal transduction in which the complex tissue is realized by interconnecting the "blocks" or "compartments" of well-characterized synthetic biological circuits (Rothschild et al., 2024). From the perspective of a smart material, the compartmentalization of synthetic biology modules allows spatial and temporal control over the properties of the material, thus enabling the same material to have defined regions with different capabilities (Kusters et al., 2011; Lentini et al., 2016; Stadler et al., 2009).

Critical innovation would arise from the incorporation of genetic circuits designed to respond to pathogenic stimuli. These circuits are engineered to detect quorum-sensing molecules (e.g. acyl-homoserine lactones from Gram-negative bacteria), virulence factors, or specific microenvironmental pH changes associated with biofilm formation. An envisioned use case is as follows. Upon detection of these *pathogen associated molecular patterns* (PAMPs), the genetic circuit of the synthetic cell will be activated, thereby triggering the expression and synthesis of bacteriophage, *antimicrobial peptides* (AMPs), or bacteriolytic enzymes (e.g., lysins) directly within the synthetic compartment. AMPs, such as melittin or defensin analogs, are particularly suited for this application because of their broad-spectrum activity and the difficulty pathogens face in developing resistance against them. The synthesized AMPs can accumulate within the vesicle until membrane lysis releases a bolus, or they can be secreted through engineered pore proteins (e.g., alpha-hemolysin nanopores) for sustained controlled release. The "smart" functionality would be embedded in the feedback and regulatory mechanisms of the genetic circuitry. Several excellent results are available on the design of such circuits [see (Brophy and Voigt 2014; Nielsen et al., 2016; Palacios et al., 2025), and references therein].

A more advanced application involves programming synthetic cells for the synthesis and self-assembly of antimicrobial nanostructures. This could involve the expression of enzymes that catalyze the precipitation of toxic metal ions (e.g., silver) into nanoparticles directly on the bacterial membrane or the production of self-assembling peptide nanofibers that disrupt biofilm integrity. The primary challenges remain to optimize the stability, yield, and kinetic parameters of the encapsulated TXTL system, preventing immune recognition *in vivo*, and scaling production.

Building on these seminal works, we can envision a proof-of-concept for a smart antimicrobial hydrogel material wherein a population of synthetic cells could be engineered to sense the presence of bacteria and, in response, produce and release a cell-free assembled phage (Figure 2). To mitigate the challenge of autolysis of synthetic cells producing phage outlined previously, one could exercise holin expression control using antisense ssDNA to silence translation, allowing tunable delays in lysis (Vogele et al., 2021). Trigger plasmids could offer further control by releasing silenced mRNA in response to stimuli, such as quorum-sensing molecules, enabling infection-responsive executioner cells (Garamella et al., 2019b). Such strategies would enable the ultimate aim of the construction of autonomous antimicrobial modules capable of both sensing bacterial presence and responding with a precise therapeutic payload (Liyanagedera 2022a). Furthermore, they could allow the implementation of prolonged smart functionality that does not require a gel-sol transition (semi-solid gel to liquid-like sol) and thus preserve intelligence and material integrity.

Nonetheless, a significant technical challenge in the construction of any smart material is the movement of molecules within it (Badeau et al., 2018). This directly impacts the embedding of TXTL circuitry within a material. Specifically, a hydrogel architecture would have to strike a balance between the permeation of signal inputs and the leaching out of the TXTL machinery, as well as any desired structural properties of the hydrogel. Methods for the encapsulation of logic circuitry in extracellular compartments are not available today but synthetic cells that compartmentalize cell-free reactions might resolve this difficulty (Adamala et al., 2017).

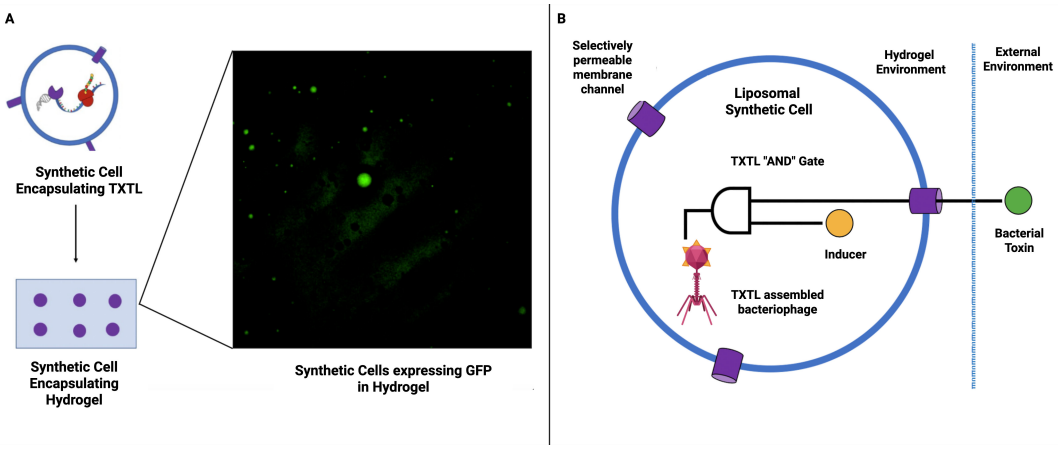

FIGURE 2
Synthetic cells for smart antimicrobial materials. **(A)** Synthetic cells expressing GFP immobilized within hydrogel (Liyanagedera (2022a). These synthetic cells are immobilized within a hydrogel matrix, thus paving the way for the utilization of synthetic cells to create smart hydrogel-based materials. **(B)** Schematic representation of smart antimicrobial material proof of concept. A hydrogel-based material is used to encapsulate synthetic cells containing a simple TXTL "AND" gate. The circuit will produce an output (cell-free assembled bacteriophage) when activated by an inducer molecule (trapped inside the synthetic cell) and a bacterial toxin which enters through a selectively permeable membrane.

5 Future directions: a unified platform for phage therapy

In light of the continued progress of synthetic biology research, synthetic cells could soon be engineered to support the entire phage life cycle *in vitro*. By modularly integrating genome assembly cassettes, capsid display systems, and programmable lysis circuits, researchers can reconstruct phage behavior from the ground up. These platforms would enable systematic investigation of key parameters such as tail fiber specificity, lysis timing, and CRISPR evasion within a fully defined, controllable context. For phage therapy, these synthetic cells will offer a highly useful platform to investigate fundamental questions in phage biology (Rothschild et al., 2024; Sampson et al., 2024).

A promising direction is the development of a modular synthetic cell library that features a variety of bacterial surface receptors. This would enable high-throughput compatibility testing with engineered phage libraries, facilitating large-scale screening of phage–host interactions. Even today it is known that beyond the facilitation of simple binding assays, these synthetic cells also offer a unique opportunity to dissect the molecular mechanics of infection (van den Berg et al., 2022). For example we envision that the *internal capsid protein* (ICP) ejection process, which is central to the delivery of the phage genome and has been exploited for diagnostic applications, can be explored in isolation. By co-encapsulating purified "sentinel" phages with bacterial components such as membrane receptors or cell wall fragments, researchers can pinpoint precise triggers for DNA and ICP release, all without the complexity of live cell systems.

These platforms could be combined with minimal TXTL systems such as the PURE (Protein synthesis Using Recombinant Elements) system, and further optimized with metabolic intermediates identified through virocell profiling, to enable fine-tuned emulation of host-like conditions (Yadav et al., 2025; Emslander et al., 2022). This bottom-up approach can help us answer fundamental questions such as, '*What is the minimal set of host factors required to assemble a phage?*' The solution to this question will accelerate the development of GMP-compliant, minimal TXTL systems optimized for therapeutic phage production (Liyanagedera et al., 2022b).

Local expression of therapeutic payloads within synthetic cells offers advantages beyond serving merely as release vehicles: it enables on-demand co-synthesis of phages with unstable or short-lived compounds, provides precise spatiotemporal control of drug release (Monck et al., 2024), and reduces the risk of premature drug degradation prior to delivery (Kim et al., 2025). Nonetheless, in the context of *in vivo* therapeutic applications, additional challenges arise around stability, immunogenicity, and delivery of the synthetic cells themselves (Kim et al., 2025). In particular, early work on intratumoral protein synthesis using synthetic cells highlighted immunogenic risks associated with extract-derived endotoxin release (Krinsky et al., 2018), but recent advances in developing endotoxin free cell-free systems and advanced liposomal stabilisation strategies, are helping to mitigate these concerns (Wilding et al., 2019; Beltrán-Gracia et al., 2019; Meyer et al., 2025).

The power of synthetic cells will emerge when the capabilities of therapeutic production and mechanistic investigation are combined. Such a platform will not only manufacture a therapeutic phage but also test its efficacy and study its infection dynamics, establishing a rapid, iterative design–build–test–learn cycle entirely *in vitro*. A novel phage genome could be designed *in silico*, the corresponding DNA parts synthesized, assembled, encapsulated and introduced into a synthetic cell library that mimics various host profiles, all within a single modular framework.

The true programmability will be determined by what else is included in the encapsulated TXTL reaction. By co-encapsulating a scaffold phage genome with plasmids encoding various different *receptor binding domains* (RBDs) or other therapeutic payloads, it would be possible to dictate the final form of the phage post-translationally, thereby turning each synthetic cell into a bespoke production line (Liyanagedera et al., (2022b). Then, a single scaffold genome can yield a multitude of phenotypically distinct phage variants, with the final output determined simply by the "instruction set" of DNA parts included in the initial reaction.

With the incorporation of artificial intelligence (AI) and microfluidics, this vision can be scaled further: library-on-library interactions between engineered phages and synthetic cells that feature variable receptor landscapes could be rapidly screened (York 2025). The resulting data would make it feasible to build reliable and powerful machine learning models for predictive phage design, enabling automated workflows for personalized and precision-engineered phage therapies, as noted in (Keith et al., 2024).

Seminal work recently demonstrated that generative genome language models can design completely new phages with improved fitness and the ability to overcome resistance (King et al., 2025). Synthetic cells could provide an important complement to such AI-driven therapeutic phage design, providing reductionist experimental platforms for generating training data for phage-host interactions that remain unrepresented in public genome collections. Such approaches could fill a gap by providing experimentally validated data sets in areas where models otherwise face sparse or biased training data. Looking forward, ensuring that such interaction data sets are made publicly available - for example through national initiatives such as the UK's open data programs for biomedical AI - will be critical in accelerating progress towards predictive phage therapy.

Data availability statement

The original contributions presented in the study are included in the article/supplementary material. Further inquiries can be directed to the corresponding author.

Author contributions

VK: Writing – review & editing. NL: Writing – review & editing. SL: Conceptualization, Writing – original draft, Writing – review & editing.

Funding

The author(s) declare financial support was received for the research and/or publication of this article. SL is supported by NL's UKRI Future Leaders Fellowship (MR/V027107/1). SL is additionally supported by Biophoundry Inc.

Acknowledgments

The figures in this manuscript were created with BioRender.com.

Conflict of interest

Author SL was employed by the company Biophoundry Inc.

The remaining authors declare that the research was conducted in the absence of any commercial or financial relationships that could be construed as a potential conflict of interest.

Generative AI statement

The author(s) declare that no Generative AI was used in the creation of this manuscript.

Any alternative text (alt text) provided alongside figures in this article has been generated by Frontiers with the support of artificial intelligence and reasonable efforts have been made to ensure accuracy, including review by the authors wherever possible. If you identify any issues, please contact us.

Publisher's note

References

Adamala, K. P., Martin-Alarcon, D. A., Guthrie-Honea, K. R., and Boyden, E. S. (2017). Engineering genetic circuit interactions within and between synthetic minimal cells. *Nat. Chem.* 9, 431–439. doi: 10.1038/nchem.2644

Ando, H., Lemire, S., Pires, D. P., and Lu, T. K. (2015). Engineering modular viral scaffolds for targeted bacterial population editing. *Cell Syst.* 1, 187–196. doi: 10.1016/j.cels.2015.08.013

Badeau, B. A., Comerford, M. P., Arakawa, C. K., Shadish, J. A., and DeForest, C. A. (2018). Engineered modular biomaterial logic gates for environmentally triggered therapeutic delivery. *Nat. Chem.* 10, 251–258. doi: 10.1038/nchem.2917

Bali, K., McCoy, R., Lu, Z., Treiber, J., Savva, A., Kaminski, C. F., et al. (2023). Multiparametric sensing of outer membrane vesicle-derived supported lipid bilayers demonstrates the specificity of bacteriophage interactions. *ACS Biomater. Sci Eng.* 9, 3632–3642. doi: 10.1021/acsbiomaterials.3c00021

Bayoumi, M., Bayley, H., Maglia, G., and Sapra, K. T. (2017). Multi-compartment encapsulation of communicating droplets and droplet networks in hydrogel as a model for artificial cells. *Sci. Rep.* 7, 45167. doi: 10.1038/srep45167

Beltrán-Gracia, E., López-Camacho, A., Higuera-Ciapara, I., Velázquez-Fernández, J. B., and Vallejo-Cardona, A. A. (2019). Nanomedicine review: Clinical developments in liposomal applications. *Cancer Nanotechnol.* 10, 11. doi: 10.1186/s12645-019-0055-y

Beth, M., Monroe, B., and Fikhman, D. A. (2023). Mini-review antimicrobial smart materials: the future's defense against wound infections. *Front. Biomater. Sci* 2. doi: 10.3389/fbiom.2023.1285386

Brooks, R., Morici, L., and Sandoval, N. (2023). Cell free bacteriophage synthesis from engineered strains improves yield. *ACS Synthetic. Biol.* 12, 2418–2431. doi: 10.1021/acssynbio.3c00239

Brophy, J. A. N., and Voigt, C. A. (2014). Principles of genetic circuit design. *Nat. Methods* 11, 508–520. doi: 10.1038/nmeth.2926

Elani, Y. (2016). Construction of membrane-bound artificial cells using microfluidics: a new frontier in bottom-up synthetic biology. *Biochem. Soc. Trans.* 44, 723–730. doi: 10.1042/bst20160052

El-Husseiny, H. M., Mady, E. A., Hamabe, L., Abugomaa, A., Shimada, K., Yoshida, T., et al. (2022). Smart/stimuli-responsive hydrogels: Cutting-edge platforms for tissue engineering and other biomedical applications. *Mater. Today Bio* 13, 100186. doi: 10.1016/j.mtbio.2021.100186

Emslander, Q., Vogele, K., Braun, P., Stender, J., Willy, C., Joppich, M., et al. (2022). Cell-free production of personalized therapeutic phages targeting multidrug-resistant bacteria. *Cell Chem. Biol.* 29, 1434–1445.e6. doi: 10.1016/j.chembiol.2022.06.003

Garamella, J., Garenne, D., and Noireaux, V. (2019a). TXTL-based approach to synthetic cells. *Methods Enzymol.* 617, 217–239. doi: 10.1016/bs.mie.2018.12.015

Garamella, J., Majumder, S., Liu, A. P., and Noireaux, V. (2019b). An adaptive synthetic cell based on mechanosensing, biosensing, and inducible gene circuits. *ACS Synthetic. Biol.* 8, 1913–1920. doi: 10.1021/acssynbio.9b00204

Garenne, D., Thompson, S., Brisson, A., Khakimzhan, A., and Noireaux, V. (2021). The All-E. coli TXTL toolbox 3.0: new capabilities of a cell-free synthetic biology platform. *Synthetic. Biol.* 6, ysab017. doi: 10.1093/synbio/ysab017

Gispert, I., and Elani, Y. (2025). Synthetic cell preservation strategies enable their storage and activation at the point of use. *Chem. Commun.* 61, 8359–8362. doi: 10.1039/d5cc00826c

Gonzales, D. T., Yandrapalli, N., Robinson, T., Zechner, C., and Tang, T. Y. D. (2022). Cell-free gene expression dynamics in synthetic cell populations. *ACS Synthetic. Biol.* 11, 205–215. doi: 10.1021/acssynbio.1c00376

Keith, M., de la Torriente, A. P., Chalka, A., Vallejo-Trujillo, A., McAteer, S. P., Paterson, G. K., et al. (2024). Predictive phage therapy for Escherichia coli urinary tract infections: Cocktail selection for therapy based on machine learning models. *Proc. Natl. Acad. Sci.* 121, e2313574121. doi: 10.1073/pnas.2313574121

Kim, W., Han, J., Chauhan, S., and Lee, J. W. (2025). Cell-free protein synthesis and vesicle systems for programmable therapeutic manufacturing and delivery. *J. Biol. Eng.* 19, 52. doi: 10.1186/s13036-025-00523-x

King, S. H., Driscoll, C. L., Li, D. B., Guo, D., Merchant, A. T., Brixi, G., et al. (2025). Generative design of novel bacteriophages with genome language models. *bioRxiv*. doi: 10.1101/2025.09.12.675911

Krinsky, N., Kaduri, M., Zinger, A., Shainsky-Roitman, J., Goldfeder, M., Benhar, I., et al. (2018). Synthetic cells synthesize therapeutic proteins inside tumors. *Adv. Healthcare. Mater.* 7, 1701163. doi: 10.1002/adhm.201701163

Kusters, I., Mukherjee, N., de Jong, M. R., Tans, S., Kocer, A., and Driessen, A. J. (2011). Taming membranes: functional immobilization of biological membranes in hydrogels. *PloS One* 6, e20435. doi: 10.1371/journal.pone.0020435

Lentini, R., Martín, N. Y., Forlin, M., Belmonte, L., Fontana, J., Cornella, M., et al. (2017). Two-way chemical communication between artificial and natural cells. *ACS Cent. Sci* 3, 117–123. doi: 10.1021/acscentsci.6b00330

Lentini, R., Santero, S. P., Chizzolini, F., Cecchi, D., Fontana, J., Marchioretto, M., et al. (2014). Integrating artificial with natural cells to translate chemical messages that direct E. coli behaviour. *Nat. Commun.* 5, 4012. doi: 10.1038/ncomms5012

Lentini, R., Yeh Martin, N., and Mansy, S. S. (2016). Communicating artificial cells. *Curr. Opin. Chem. Biol.* 34, 53–61. doi: 10.1016/j.cbpa.2016.06.013

Levrier, A., Karpathakis, I., Nash, B., Bowden, S. D., Lindner, A. B., and Noireaux, V. (2024). PHEIGES: all-cell-free phage synthesis and selection from engineered genomes. *Nat. Commun.* 15, 2370. doi: 10.1038/s41467-024-46585-1

Levrier, A., Soudier, P., Garenne, D., Izri, Z., Bowden, S., Lindner, A. B., et al. (2025). A synthetic cell phage cycle. *bioRxiv*. doi: 10.1101/2025.06.14.659709

Liyanagedera, S. B. W. (2022a). *Optimisation of cell-free transcription/translation systems for phage therapy* (University of Warwick). Available at: http://webcat.warwick.ac.uk/record=b3877449~S15.

Liyanagedera, S. B. W., Williams, J., Wheatley, J. P., Biketova, A. Y., Hasan, M., Sagona, A. P., et al. (2022b). SpyPhage: A cell-free TXTL platform for rapid engineering of targeted phage therapies. *ACS Synthetic. Biol.* 11, 3330–3342. doi: 10.1021/acssynbio.2c00244

Mahmoudabadi, G., Milo, R., and Phillips, R. (2017). Energetic cost of building a virus. *Proc. Natl. Acad. Sci.* 114, E4324–E4333. doi: 10.1073/pnas.1701670114

Majumder, S., Garamella, J., Wang, Y.-L., DeNies, M., Noireaux, V., and Liu, A. P. (2017). Cell-sized mechanosensitive and biosensing compartment programmed with DNA. *Chem. Commun.* 53, 7349–7352. doi: 10.1039/c7cc03455e

Meyer, C., Arizzi, A., Henson, T., Aviran, S., Longo, M. L., Wang, A., et al. (2025). Designer artificial environments for membrane protein synthesis. *Nat. Commun.* 16, 4363. doi: 10.1038/323s41467-025-59471-1

Monck, C., Elani, Y., and Ceroni, F. (2024). Genetically programmed synthetic cells for thermo responsive protein synthesis and cargo release. *Nat. Chem. Biol.* 20, 1380–1386. doi: 10.1038/s41589-024-01673-7

Nielsen, A. A. K., Der, B. S., Shin, J., Vaidyanathan, P., Paralanov, V., Strychalski, E. A., et al. (2016). Genetic circuit design automation. *Science* 352, aac7341. doi: 10.1126/science.aac7341

Noireaux, V., Bar-Ziv, R., and Libchaber, A. (2003). Principles of cell-free genetic circuit assembly. *Proc. Natl. Acad. Sci.* 100, 12672–12677. doi: 10.1073/pnas.2135496100

Noireaux, V., and Libchaber, A. (2004). A vesicle bioreactor as a step toward an artificial cell assembly. *Proc. Natl. Acad. Sci.* 101, 17669–17674. doi: 10.1073/pnas.0408236101

Palacios, S., Collins, J. J., and Del Vecchio, D. (2025). Machine learning for synthetic gene circuit engineering. *Curr. Opin. Biotechnol.* 92, 103263. doi: 10.1016/j.copbio.2025.103263

Rampioni, G., D'Angelo, F., Messina, M., Zennaro, A., Kuruma, Y., Tofani, D., et al. (2018). Synthetic cells produce a quorum sensing chemical signal perceived by Pseudomonas aeruginosa. *Chem. Commun.* 54, 2090–2093. doi: 10.1039/c7cc09678j

Rothschild, L. J., Averesch, N. J. H., Strychalski, E. A., Moser, F., Glass, J. I., Cruz Perez, R., et al. (2024). Building synthetic cells—From the technology infrastructure to cellular entities. *ACS Synthetic. Biol.* 13, 974–997. doi: 10.1021/acssynbio.3c00724

Sakamoto, R., Noireaux, V., and Maeda, Y. T. (2018). Anomalous scaling of gene expression in confined cell-free reactions. *Sci. Rep.* 8, 8081. doi: 10.1038/s41598-018-25532-3

Sampson, K., Sorenson, C., and Adamala, K. P. (2024). Preparing for the future of precision medicine: synthetic cell drug regulation. *Synthetic. Biol.* 9, ysae004. doi: 10.1093/synbio/ysae004

Sawa, T., Moriyama, K., and Kinoshita, M. (2024). Current status of bacteriophage therapy for severe bacterial infections. *J. Intensive Care* 12, 34. doi: 10.1186/s40560-024-00759-7

Schwarzkopf, J. M. F., Mehner-Breitfeld, D., and Brüser, T. (2024). A dimeric holin/antiholin complex controls lysis by phage T4. *Front. Microbiol.* 15. doi: 10.3389/fmicb.2024.1419106

Skurnik, M., Alkalay-Oren, S., Boon, M., Clokie, M., Sicheritz-Pontén, T., Dabrowska, K., et al. (2025). Phage therapy. *Nat. Rev. Methods Primers* 5, 1–21. doi: 10.1038/s43586-024-00377-5

Smith, D. L., Struck, D. K., Scholtz, J. M., and Young, R. (1998). Purification and biochemical characterization of the lambda holin. *J. Bacteriol.* 180, 2531–2540. doi: 10.1128/jb.180.9.2531-2540.1998

Son, B., Kong, M., Lee, Y., and Ryu, S. (2021). Development of a novel chimeric endolysin, lys109 with enhanced lytic activity against staphylococcus aureus. *Front. Microbiol.* 11. doi: 10.3389/fmicb.2020.615887

Stadler, B., Price, A. D., Chandrawati, R., Hosta-Rigau, L., Zelikin, A. N., and Caruso, F. (2009). Polymer hydrogel capsules: en route toward synthetic cellular systems. *Nanoscale* 1, 68–73. doi: 10.1039/b9nr00143c

Tang, T. D., Cecchi, D., Fracasso, G., Accardi, D., Coutable-Pennarun, A., Mansy, S. S., et al. (2018). Gene-mediated chemical communication in synthetic protocell communities. *ACS Synthetic. Biol.* 7, 339–346. doi: 10.1021/acssynbio.7b00306

van den Berg, B., Silale, A., Baslé, A., Brandner, A. F., Mader, S. L., and Khalid, S. (2022). Structural basis for host recognition and superinfection exclusion by bacteriophage T5. *Proc. Natl. Acad. Sci.* 119, e2211672119. doi: 10.1073/pnas.2211672119

Vogele, K., Falgenhauer, E., von Schonberg, S., Simmel, F. C., and Pirzer, T. (2021). Small antisense DNA-based gene silencing enables cell-free bacteriophage manipulation and genome replication. *ACS Synthetic. Biol.* 10, 459–465. doi: 10.1021/acssynbio.0c00402

Wilding, K. M., Hunt, J. P., Wilkerson, J. W., Funk, P. J., Swensen, R. L., Carver, W. C., et al. (2019). Endotoxin-Free E. coli-Based Cell-Free Protein Synthesis: Pre-Expression Endotoxin Removal Approaches for on-Demand Cancer Therapeutic Production. *Biotechnol. J.* 14, e1800271. doi: 10.1002/biot.201800271

Yadav, S., Perkins, A. J. P., Liyanagedera, S. B. W., Bougas, A., and Laohakunakorn, N. (2025). ATP regeneration from pyruvate in the PURE system. *ACS Synthetic. Biol.* 14, 247–256. doi: 10.1021/acssynbio.4c00697

Yang, Q., Le, S., Zhu, T., and Wu, N. (2023). Regulations of phage therapy across the world. *Front. Microbiol.* 14. doi: 10.3389/fmicb.2023.1250848

York, A. (2025). Predicting phage–host specificity: Viral infection. *Nat. Rev. Microbiol.* 23, 5. doi: 10.1038/s41579-024-01132-z

Zalewska-Piątek, B. (2023). Phage therapy—Challenges, opportunities and future prospects. *Pharmaceuticals* 16, 1638. doi: 10.3390/ph16121638

frontiers | Frontiers in Cellular and Infection Microbiology

TYPE Review
PUBLISHED 29 October 2025
DOI 10.3389/fcimb.2025.1631359

OPEN ACCESS

EDITED BY
Derry Keith Mercer,
INCATE, Switzerland

REVIEWED BY
Bob Gordon Blasdel,
Vesale Pharma, Belgium
Holger Loessner,
Paul-Ehrlich-Institut (PEI), Germany

*CORRESPONDENCE
Anja Duechting
anja.duechting@bfarm.de

RECEIVED 19 May 2025
ACCEPTED 15 October 2025
PUBLISHED 29 October 2025

CITATION
Fuerst-Wilmes M, Respondek V, Schramm M, Lilienthal N, Buss K and Duechting A (2025) Regulation of phage therapy medicinal products: developments, challenges, and opportunities. *Front. Cell. Infect. Microbiol.* 15:1631359. doi: 10.3389/fcimb.2025.1631359

Regulation of phage therapy medicinal products: developments, challenges, and opportunities

Miriam Fuerst-Wilmes, Vanessa Respondek, Michael Schramm, Nils Lilienthal, Katrin Buss and Anja Duechting*

Federal Institute for Drugs and Medical Devices, Bonn, Germany

Due to their biological properties, bacteriophages represent a regulatory specialty and, at the same time, a challenge with regard to medicinal product approval. Established European guidelines on pharmaceutical quality, preclinical development, and clinical development are only partially applicable. The growing threat posed by infections with multidrug-resistant bacteria has not only boosted the development of bacteriophages for the treatment of bacterial infections in recent years but has also led to substantial progress in adapting regulatory requirements. In 2024, harmonized quality criteria for phage therapy medicinal products and active substances were implemented for the first time in the European Pharmacopoeia. Future European pharmaceutical legislation and recent national acts such as the German Medical Research Act are intended to enable exemptions that address the specific characteristics of phage therapeutics and open new regulatory pathways. Increasing amounts of data on clinical use of phage therapeutics are being published; however, the anticipated breakthrough in the form of a demonstration of efficacy in randomized controlled clinical trials has not yet been achieved. Growing experience with innovative phage preparations has been utilized to adjust regulatory requirements. On the path to approval of a defined phage therapy medicinal product, the evidence-based demonstration of efficacy and safety in randomized controlled clinical trials is the next and decisive step.

KEYWORDS

bacteriophages, phage therapy medicinal products, regulatory advice, antimicrobial resistance, antibacterial treatment, non-traditional product

Introduction

Bacteriophages (phages, for short) are one of the most promising tools in combating infections caused by multidrug-resistant bacteria. Although the first (documented) clinical applications of phage preparations date back nearly 100 years and they have been continuously used in Eastern Europe to this day, there is still a lack of established

standards for defining the pharmaceutical quality, safety, and efficacy of these preparations (Summers, 1999; Strathdee et al., 2023; Palma and Qi, 2024). In response to the growing threat posed by multidrug-resistant bacteria, numerous funding initiatives have been launched in recent years which have spurred the development of bacteriophages as medicinal products (2025). One of the challenges has always been to incorporate phage therapy medicinal products (PTMPs), with their unique biological properties and modes of action, into the existing regulatory framework or to adapt the latter accordingly. Requirements for the quality, safety, and efficacy of phage preparations have evolved in recent years both on a national level in Germany and across Europe. This article aims to provide an overview of these developments and to depict the current state of regulatory requirements for PTMPs in Europe and, in particular, in Germany.

Quality aspects

Manufacture and application of PTMPs

In Europe, bacteriophages for therapeutic use in humans are considered biological medicinal products pursuant to Article 1 (2) and (3) in conjunction with Annex I, Part 1, 3.2.1.1 (b) Sentences 3 and 4 of Directive 2001/83/EC). In Germany, they are classified as medicinal products by function pursuant to Section 2 (1) in conjunction with Section 3 No. 4 of the Medicinal Products Act (*Arzneimittelgesetz*, AMG). Prior to use in patients, they generally require either a marketing authorization or an authorization for use as investigational medicinal product in a clinical trial.

Currently, PTMPs are manufactured and applied via two distinct pathways:

1. Standardized phage preparations (often mixtures of various phages) are produced industrially in advance and used in the context of a clinical trial. These medicinal products are subject to the obligation to obtain a marketing authorization and manufacturing authorization. They can, in principle, be assessed for their quality, efficacy, and safety through clinical trials and ultimately be approved under the existing regulatory pathways. As authorized medicinal products, they would then be available to all patients in accordance with the approved indication. However, current regulatory requirements—for example, for changes in the composition of approved PTMPs—present challenges for these products (e.g., replacement or adaptation of phages in the medicinal product due to resistance development of the bacterial pathogens – "moving targets"). Future European pharmaceutical legislation could establish more suitable structures and regulatory concepts in this regard.
2. Phage preparations are manufactured as individual magistral formulations (referred to as *formula magistralis* in Directive 2001/83/EC) specifically for the individual patient based on a physician's prescription, usually in a (hospital) pharmacy, shortly before application. These products are exempted from the obligations to obtain a marketing and manufacturing authorization, as they do not fall within the scope of Directive 2001/83/EC pursuant to Article 3 (1). In Germany, the obligation to obtain a marketing authorization under Section 21 (1) AMG applies to finished medicinal products (as defined in Section 4 (1) Sentence 1 AMG), but not to individual magistral formulations, as these are not manufactured "beforehand" according to the definition in Section 4 (1) No. 1 AMG, but rather "in the pharmacy in particular cases on the basis of a prescription or other request by an individual person (…)," as specified in Section 1a (8) of the Ordinance on the Operation of Pharmacies (*Apothekenbetriebsordnung*, ApBetrO). Use of phage preparations typically occurs under the conditions of an attempt to restore health or alleviate suffering for an individual patient (cf. Section 37 of the Declaration of Helsinki). Modifications to PTMPs exempted from the obligation to obtain a marketing authorization can be implemented more flexibly and quickly, since regulatory steps for approval of the changes are not required. However, this "last-resort" treatment is only available to a small number of patients in exceptional cases.

Quality of PTMPs

Pursuant to Section 55 (8) AMG, all medicinal products must be manufactured in accordance with recognized pharmaceutical rules. In accordance with Section 55 (1) AMG, these rules are laid down in the German pharmacopoeia. They include, among others, the quality of medicinal products and the substances used in their manufacture. The rules of the pharmacopoeia provide recognized common standards for the quality of medicinal products and their components, thereby ensuring patient safety. In March 2024, during its 178th session, the European Pharmacopoeia Commission adopted the general chapter "Phage therapy medicinal products (5.31)". The chapter was published in July 2024 in Supplement 11.6 of the European Pharmacopoeia (Ph. Eur.) and came into force in January 2025. This chapter becomes legally binding once it is referenced in a monograph (or in another general chapter that is in turn referenced in a monograph). For the first time, this chapter defines quality criteria for PTMPs and active substances that are harmonized across Europe. It encompasses both human and veterinary medicinal products subject to as well as exempt from the obligation to obtain a marketing authorization. In order to accommodate the wide range of highly diverse products, the chapter establishes fundamental requirements while allowing sufficient flexibility.

This framework of requirements addresses, among others:

- Specifications for bacterial and phage banks, including critical quality attributes (e.g. identity, purity, activity).

- Production process and purification steps, including in-process controls.
- Specifications for active substances and drug products, including relevant quality attributes (e.g. identity, microbial quality, activity).

A critical quality attribute of all PTMPs is the biological activity, which is typically determined using a plaque assay. However, this method has not yet been standardized. At its 176th session in June 2023, the European Pharmacopoeia Commission decided to draft a new general chapter (2.7.38) on the determination of bacteriophage potency, with the aim of providing harmonized provisions for the conduct, standardization, and validation of the assay. A draft version of this chapter was published for public consultation in April 2025.

To address the requirements for PTMPs subject to the obligation to obtain a marketing authorization, the European Medicines Agency (EMA) has issued specific guidelines. For veterinary medicinal products, the "Guideline on quality, safety and efficacy of veterinary medicinal products specifically designed for phage therapy" (EMA/CVMP/NTWP/32862/2022) has been published. A corresponding guideline for human phage therapeutics is currently under development ("Guideline on quality aspects of phage therapy medicinal products", EMA/CHMP/BWP/1/2024). Relevant aspects (also considering Ph. Eur. Chapter 5.31) of this latter guideline include, among others:

- Quality of starting materials, excipients, and active substances.
- Manufacture and specifications of bacterial and phage banks.
- Characterization of the active substance and its impurities (e.g., endotoxins).
- Manufacturing process, including process development, validation, and controls.
- Specifications of the active substance and finished product, including analytical and validation.
- Reference standards and stability.

Publication of the draft guideline for public consultation is scheduled for November 2025. In addition, the principles of existing EMA and ICH guidelines for biotech products are, where applicable, also relevant for PTMPs. These include, for example, guidelines on the characterization of cell banks (ICH Q5D), stability (ICH Q5C), specifications (ICH Q6B), analytical methods (ICH Q2, Q14), as well as further topics (ICH Q8 – Q11). Particularly relevant for phage products as investigational medicinal products in clinical trials is the "Guideline on the requirements for quality documentation concerning biological investigational medicinal products in clinical trials" (EMA/CHMP/BWP/534898/2008 Rev. 2).

Furthermore, a S2k-guideline is currently being developed by the Association of the Scientific Medical Societies in Germany (*Arbeitsgemeinschaft der Wissenschaftlichen Medizinischen Fachgesellschaften*, AWMF), with finalization planned for December 2025. This guideline will provide recommendations on the personalized manufacture and therapeutic application of bacteriophages and address legal and logistical considerations specific to Germany. Through its consensus-based development process and the involvement of several medical societies, the guideline will yield a harmonized set of recommendations of varying evidence levels, providing guidance and a framework for, among others, the manufacture of personalized PTMPs, including their quality attributes and quality control measures.

The multitude of ongoing activities in the area of the quality and manufacturing of PTMPs underscores the potential of these products, even though clinical efficacy has not yet been conclusively demonstrated in randomized controlled clinical trials (RCTs). Nonetheless, systematic case observations increasingly suggest that phage therapy (most likely in combination with antibiotics) may represent a viable treatment option for infections caused by antibiotic-resistant bacteria (Pirnay et al., 2024). The above-described regulatory developments have introduced and continue to establish specific requirements for this special class of medicinal products, with the aim of ensuring a consistently high and harmonized quality across Europe—ultimately in the interest of patient safety.

Manufacturing authorization and good manufacturing practice

In principle, the manufacture of medicinal products on a commercial basis in Europe is subject to an obligation to obtain a manufacturing authorization (Art. 40 of Directive 2001/83/EC; Section 13 (1) AMG) and requires compliance with the principles and guidelines of Good Manufacturing Practice (GMP). This compliance is verified as part of the procedure for granting a manufacturing authorization (Section 1 (1) in conjunction with Section 2 (3) and Section 13 (1) of the Ordinance on the Manufacture of Medicinal Products and Active Substances (*Arzneimittel- und Wirkstoffherstellungsverordnung*, AMWHV)).

The personalized manufacture of medicinal products in a pharmacy, within the ordinary course of pharmacy operations, based on a medical prescription for a specific patient is exempted from the obligation to obtain a manufacturing authorization (Section 13 (2) sentence 1 AMG). However, also in this case, manufacture must conform to the recognized pharmaceutical rules (Section 55 (8) AMG), and the quality of both starting materials and the finished product must be ensured (Section 6 (1) in conjunction with Section 11 of the ApBetrO). The decision whether the preparation of individualized PTMPs constitutes the "ordinary course of pharmacy operations" lies within the responsibility of the competent authority (in Germany, that of the federal state in which the pharmacy is located). If this classification is not granted, the preparation is subject to the obligation to obtain a manufacturing authorization pursuant to Section 13 (1) AMG.

Personalized preparation of PTMPs may, in principle, also be carried out by physicians ("directly under his/her professional responsibility for personal use by a specific patient"; Section 13

(2b) sentence 1 AMG). If a GMP-compliant phage active substance is used for PTMP preparation, this activity is exempted from the obligation to obtain a manufacturing authorization under Section 13 (2b) AMG (although it must be notified under Section 67 (2) AMG). However, the preparation of a phage active substance by a physician in order to manufacture a PTMP is subject to the obligation to obtain a manufacturing authorization pursuant to Section 13 (1) sentence 3 AMG.

The manufacture of genetically modified or recombinantly produced PTMPs—defined as Advanced Therapy Medicinal Products (ATMPs)—is in any case subject to the obligation to obtain a manufacturing authorization (Section 13 (1) AMG). Furthermore, the provisions of directives 2001/18/EC and 2009/41/EC should be taken into account for genetically modified phages, as applicable.

With the enactment of the Medical Research Act (*Medizinforschungsgesetz*), which amends both the AMG and the AMWHV accordingly, the specific requirements of individualized phage therapeutics are taken into account. Under the newly introduced Section 14 (6) AMG, "the competent higher federal authority can publish recommendations on the interpretation of the principles and guidelines of good manufacturing practice." Furthermore, pursuant to the new Section 14 (7) AMG, on application by a competent authority, the competent higher federal authority may prepare and publish "an opinion on the interpretation of the principles and guidelines of good manufacturing practice for the medicinal products". The AMWHV has been amended accordingly in Section 3 (2) by reference to Section 14 (6) AMG.

These regulatory amendments allow for individual and risk-based adaptations of the general GMP requirements to the specific circumstances of PTMP manufacture, while ensuring consistent high quality and safety of these products. This enables the GMP framework to better account for the particular characteristics of phages as medicinal products. Publication of the recommendations pursuant to Section 14 (6) AMG is planned for end of 2025. These recommendations are not legally binding for the competent authorities, but any deviation from them should be justified.

Outlook on regulation of PTMPs

The current regulatory framework cannot fully accommodate the specific requirements of PTMPs. Challenges arise particularly in relation to marketing authorization or subsequent modification of PTMPs in order to introduce new or replace existing phage (-strains) in response to resistance development, without requiring a separate marketing authorization for each (new) phage. The use of a platform technology and the possibility of authorizing PTMPs with (partially) variable composition could provide a viable solution by enabling regulatory grouping of the manufacture (including manufacturing authorization) and approval of various phage(-strains).

In the adopted proposals for a new Directive and a new Regulation (cf. documents 2023/0132 (COD) and 2023/0131 (COD)), which revise and replace the existing general pharmaceutical legislation (Directive 2001/83/EC and Regulation (EC) No. 726/2004), the European Commission addresses PTMPs (subject to the obligation to obtain a marketing authorization), as well as the aforementioned regulatory challenges(2025). The proposals introduce new concepts such as "adapted frameworks" (Article 28 of the proposal for a new EU Directive) and a "regulatory sandbox" (Articles 113–115 of the proposed new EU Regulation), which provide for "adapted, enhanced, waived or deferred requirements". Moreover as forward looking legal frameworks, they establish new pathways for the approval of medicinal products "comprised of a fixed component and a variable component that is pre-defined in order to, where appropriate, target different variants of an infectious agent ('platform technology')" (Article 15 of the proposed new EU Directive). These new and flexible regulatory mechanisms could prove highly beneficial, enabling a pragmatic approach to both initial marketing authorization and subsequent modifications of the products, thereby granting all patients access to PTMPs as a therapeutic option.

Preclinical aspects

The following outlines the assumptions underlying the considerations for the preclinical development program: Bacteriophages are biologicals that do not replicate in eukaryotic cells and exert no direct pharmacological effects within them. Therefore, virulent phages are considered non-hazardous (non-toxic) to humans. Both animals and humans are constantly and naturally exposed to large quantities of bacteriophages (Clokie et al., 2011; Salmond and Fineran, 2015).

Sections of the "Guideline on the evaluation of medicinal products indicated for treatment of bacterial infections" (CPMP/EWP/558/95 Rev. 3) can be applied to PTMPs (Section 4.1: Non-clinical assessment of anti-bacterial activity), and the guideline for veterinary phage products (EMA/CVMP/NTWP/32862/2022) also includes guidance relevant to the preclinical program. While currently no specific guideline exists for the development of PTMPs for human use—and hence no dedicated description of preclinical requirements, the aforementioned guidelines provide an initial orientation regarding regulatory expectations. It is widely acknowledged that regulatory requirements for new medicinal products should be proportionate to the risks associated with their intended use. Based on this principle, deviations from or reductions in the standardized set of preclinical investigations expected for newly developed medicinal products—such as *pharmacology, pharmacodynamics, pharmacokinetics (PK), repeated-dose toxicity, genotoxicity, carcinogenicity, reproductive toxicity*, and other toxicological endpoints like *local tolerance*—can be scientifically justified. Nevertheless, applicants should address the safety of the selected phages (and the final lots/batches) in terms of toxicity endpoints and support the non-clinical dossier of a marketing authorization application with corresponding information and discussions.

Potential safety concerns may arise from the presence of microbiological contaminants, such as endotoxins and other potent pro-inflammatory substances released as a consequence of bacterial lysis during phage propagation (Liu et al., 2021). Endotoxins and exotoxins as potential microbiological contaminants are critical quality attributes of the product. These and other bacterial components have to be controlled in phage products. Current experience in this area indicates that product quality (purity) is a key determinant of safety (see section Quality Aspects).

In vitro susceptibility studies should demonstrate efficacy of the phages against the targeted bacterial pathogens. Such studies should be conducted under conditions that closely resemble those at the site of infection (e.g., presence of a biofilm). When using phage combinations, compatibility among the phages with respect to a representative clinical isolate has to be ensured. Even though conventional studies of absorption, distribution, metabolism, and excretion (PK) are considered unsuitable for phage products, the applicant should investigate or discuss—based also on literature data—the absorption at the site of administration, distribution, and expected degradation pathways of the phages. Depending on the intended route of administration (e.g., inhalational or intravenous), different PK data are required.

Due to antibiotic resistance, antibiotics are sometimes investigated in combination with phages. Potential antagonistic or synergistic interactions between phages and antibiotics should be considered in the development of a PTMP. Reports indicate that the outcome of phage–antibiotic interactions depends on several factors, including the class of antibiotic, type of phage, and pairing stoichiometry (Gu Liu et al., 2020). Additionally, resistance mechanisms and phage-induced immune responses may be relevant for phage monotherapy and/or phage–antibiotic combination therapy (Krut and Bekeredjian-Ding, 2018; Doub, 2020). These aspects should also be discussed or explored early in the development process.

Regarding the above aspects, there is currently no requirement for conducting *in vivo* animal studies. Rather, it is the responsibility of the applicant to demonstrate the efficacy of the selected phages against the target bacteria, to establish the safety of the phage product, and to determine the safe and effective dose in humans.

The Federal Institute for Drugs and Medical Devices (*Bundesinstitut für Arzneimittel und Medizinprodukte*, BfArM), as the competent authority for (non-genetically modified) phages in Germany, does not expect stand-alone studies on reproductive and developmental toxicity for PTMPs. It is assumed that virulent bacteriophages do not interact directly with eucaryotic DNA or other chromosomal material. Consequently, the standard test battery to assess genotoxicity and carcinogenicity studies may also be omitted.

In conclusion, an effectively designed preclinical program for phage PTMPs can meet the regulatory requirements for safe drug development when targeted adaptations and exceptions are scientifically justified.

Clinical aspects

Phages have been used to treat bacterial infections for more than 100 years. However, evidence-based proof of the efficacy of phage therapy based on a sufficiently large and well-designed RCT (conducted in line with current standards), which would be a prerequisite for marketing authorization of a PTMP, is still lacking. From a regulatory perspective, efficacy data from Phase 2 and Phase 3 RCTs are urgently needed in order to establish phage therapy as an effective therapeutic option and to adapt regulatory requirements. Data on the efficacy and safety of phages originate primarily from individual applications in patients with limited treatment options and uncontrolled studies. In the few RCTs conducted and published so far that included at least 20 patients (only Phase 1/2 and Phase 2 studies; see Table 1), in most cases, the efficacy of phage therapy could not be sufficiently demonstrated (Sarker et al., 2016; Jault et al., 2019; Leitner et al., 2021).

In a recently published retrospective observational study by Pirnay et al (Pirnay et al., 2024), 100 cases of personalized phage treatment were described. Personalized phage treatment led to clinical improvement in 77% of cases and to eradication of targeted bacteria in 61% of cases. However, the quality of evidence cannot be considered similar to that of a RCT as there was no control group and the efficacy (and safety) of the phage application was not assessed on the basis of objective, predefined criteria but only by the physician´s assessment. In addition, phages were applied for various indications (in 70% of cases in combination with an antibiotic) and in different ways leading to very small numbers of treated patients per indication and method of administration meaning that these study results do not have any statistical power. Nevertheless, the experience gained from these and other personalized phage applications can be incorporated into the design of RCTs (e.g., with regard to phage dose, method of administration and duration of treatment).

At present, there are no specific guidelines for the clinical development program of PTMPs for human use. However, the "Guideline on the evaluation of medicinal products indicated for treatment of bacterial infections" (CPMP/EWP/558/95 Rev 3) is largely applicable (e.g., Section 5: General considerations for clinical programs).

Based on experience from published RCTs and scientific advice procedures at German national and EU level, the following aspects should be considered from a regulatory perspective for the planning of Phase 2 and Phase 3 studies and the demonstration of efficacy of PTMPs:

Indication

Phage preparations could be used for both treatment of bacterial infections and prevention (by eradication of a potential pathogen in a specific body region). However, the phage-host specificity excludes a broad indication as many authorized

TABLE 1 Examples of published randomized controlled clinical trials (phase 1/2 and 2 with n ≥20) in which, among other things, the efficacy of phages was investigated (as of 10/2025)*.

Study	Study description	Included patients	Phage product/ application/dosage	Result in terms of efficacy	Reference
Phase 1/2	Randomized, placebo-controlled, double-blind study in adult patients with chronic otitis media caused by *Pseudomonas aeruginosa*	n = 24	Fixed cocktail of 6 phages; topical application; Single dose of 6x 10^5 PFU	• Significant clinical improvement • Reduction of bacterial load • Replication of the applied phages	(Wright et al., 2009)
	Randomized, placebo-controlled study in hospitalized children (6–24 months of age) with acute bacterial diarrhea caused by *Escherichia coli*	n = 120	Fixed cocktail of 11 phages or commercial product from Russia (of at least 17 phages); oral application; 3.6x 10^8 PFU or 1.4x 10^9 PFU over 4 days	• No clinical improvement • No replication of phages in the intestine Reasons for negative study result: • only 60% of the included patients had a proven *E. coli* infection • Insufficient coverage of the phage cocktail • Lower *E. coli* titer than expected • pH stability of the phage cocktail unclear	(Sarker et al., 2016)
	Randomized, placebo-controlled, double-blind, multicenter study in adult patients with *Pseudomonas aeruginosa*-infected burns (PhagoBurn)	n = 27	Fixed cocktail of 12 phages; topical application; 1x 10^6 PFU/ml for 7 days	• Study was terminated early due to insufficient recruitment and lack of efficacy Reasons for negative study result: • Instability of the phage cocktail and therefore too low phage concentration applied	(Jault et al., 2019)
	Randomized, placebo-controlled, double-blind monocenter study in adults with chronic wound infections (mono- and polybacterial infections)	n = 60	Individualized phage cocktail; topical application, 0.5x 10^9 PFU on alternate days for up to 3 months in addition to standard of care	• Improvement of various wound parameters over time • 93.3% of the wounds became sterile in 39 days (median sterility time), followed by complete healing by the end of 90 days	(Karn et al., 2024)
Phase 2	Randomized, placebo-controlled, double-blind study for the treatment of urinary tract infections (caused by *Enterococcus* spp., *E. coli*, *Proteus mirabilis*, *P. aeruginosa*, *Staphylococcus* spp., *Streptococcus* spp.) in men with planned transurethral resection of the prostate	n= 113	Commercial phage cocktail from Georgia; topical application (intravesical); 2x daily for 7 days	• No difference in efficacy between the treatment arms Reasons for negative study result: • Indication too broad • High spontaneous healing rate for uncomplicated urinary tract infections	(Leitner et al., 2021)

*Further published RCTs (e.g. the recently published study by Weiner et al (Weiner et al., 2025)) are not included in the Table because of the small number of patients recruited and hence very limited informative value in the present context.
The results of these studies (negative and positive) should be considered when planning further studies (phase 2 and phase 3) in order to provide the outstanding proof of efficacy of phage therapy.

antibiotics have. Particularly suitable for a proof-of-concept (PoC) study (Phase 2) are (acute) infections that are caused exclusively or predominantly by a single bacterial species (monobacterial infections) and for which phages can be applied locally.

The study design of a pivotal study (Phase 3) primarily depends on whether the phage product is intended to be used alone or in combination with antibiotics. Particularly in cases of severe and/or chronic infections, a combination therapy of phages and antibiotics could be reasonable. In this case, superiority of the combination therapy over the standard of care has to be demonstrated. For less severe infections, non-inferiority of the PTMP to standard antibiotic therapy (or placebo, if no standard of care exists) should be demonstrated.

Dosage and method of administration

For a successful therapy, a sufficiently high number of phages has to reach the site of infection. The replication of the phages with subsequent lysis of the target bacteria is key in the so-called "active therapy" (Payne et al., 2000). However, the pharmacokinetics of phages are still insufficiently understood, and it remains unresolved whether a high concentration always correlates with a better therapeutic outcome. Furthermore, phage replication depends on the bacterial load at the site of infection (Danis-Wlodarczyk et al., 2021; Nang et al., 2023; Pirnay et al., 2024).

Nevertheless, local applications (e.g., topical or inhalative) can achieve higher phage concentrations at the infection site.

Experience from personalized phage applications particularly in regard to phage concentration, dosing interval, and duration of therapy should be incorporated into the design of RCTs. Moreover, it is highly recommended to test phage replication at the infection site in a RCT.

Diagnostics

In contrast to most antibiotics, phages are highly specific for a single bacterial species, meaning that the causative pathogen must be identified before the start of phage therapy. Thus, adequate microbiological diagnostics are required.

We highly recommend susceptibility testing prior to patient inclusion in a clinical study, although it is not necessarily required (e.g., in the case of a fixed phage cocktail with a high coverage rate). However, the susceptibility of the bacterial isolate to individual phages or to the phage cocktail should definitely be tested during the clinical study in order to enable correlation of the results of the susceptibility test with therapeutic outcome. In a pivotal study, the primary analysis should be based on all patients with phage-susceptible bacteria ("microbiological Intention-To-Treat population"; CPMP/EWP/558/95 Rev 3). Susceptibility testing at certain time points of the clinical study can provide information on potential resistance development and, depending on the study design, can also be used to adjust the treatment.

Endpoints

For a PoC study, a microbiological primary endpoint (e.g., reduction of bacterial load) can be selected as a surrogate parameter for efficacy. However, it is recommended that, already in a PoC study, clinical endpoints are investigated to allow estimations of the clinical benefit of phage therapy. Relevant clinical endpoints could be time to clinical improvement of symptoms, duration of hospitalization, need for (or duration of) additional antibiotic therapy, frequency of reinfections, or infection rate (in case of prophylactic application).

Patient population

The patient population to be included in a study should be clearly defined in line with the intended indication. For this, the prevalence of a specific pathogen in a given indication should be taken into account in order to be able to recruit a sufficiently large number of patients. Furthermore, based on the potential risk of phage therapy, it should be considered which patients would most likely benefit from phage therapy and in which patient population efficacy can likely be demonstrated (benefit-risk analysis).

In general, a favorable safety profile has been described for the use of phages in clinical studies (Rhoads et al., 2009; Wright et al., 2009; Sarker et al., 2016; Jault et al., 2019) as well as in personalized phage applications in patients with limited treatment options (Uyttebroek et al., 2022; Pirnay et al., 2024). In a systematic review published in 2022 comprising 52 studies on the safety and efficacy of phage therapy in difficult-to-treat infections, adverse events were reported in 33 (7%) of 441 patients receiving phage therapy and in 37 (15%) of 249 patients in the control group (Uyttebroek et al., 2022). In general, these adverse events were mild in nature and resolved after discontinuation of phage therapy. Since phage therapy appears to be safe and well tolerated, it may represent an advantage over antibiotic therapy (in terms of benefit-risk-ratio), especially for those antibiotics associated with severe side effects. In the long term, a systematic investigation of efficacy in specific patient populations, such as the pediatric population or immunosuppressed patients, would also be desirable.

Further aspects

Neutralization of phages by antibodies has already been described in the literature and may dependent on the duration of therapy, the immune status of the patient, and the route of administration (e.g., intravenous administration) (Dedrick et al., 2021; Nang et al., 2023; Pirnay et al., 2024). Additional data on neutralizing antibodies and the correlation between antibody detection and efficacy are needed and should be systematically studied in clinical trials. To enhance/maintain therapeutic efficacy, adaptation of the phages in the medicinal product to the patient's bacterial isolate is conceivable, e.g., in the form of so-called "phage training" or by means of genetic/synthetic modification of the phages (Bleriot et al., 2024; Ngiam et al., 2024).

Conclusion

With regard to the regulation of phage therapeutics, various developments have recently taken place. The publication of guidelines for harmonized quality criteria for PTMPs at the European level and the adaptation of German national and European pharmaceutical legislation to the specific characteristics of phage therapeutics show how dynamic this field currently is and that important hurdles have been overcome. However, the overall aim of the marketing authorization of a first PTMP has not yet been achieved. Crucial to this will be learning from the mistakes of previously conducted clinical studies in order to design high-quality clinical studies capable of demonstrating the efficacy and safety of defined PTMPs. Regular discussions with regulators (e.g. through scientific advice meetings) are highly recommended to streamline PTMP development in accordance with regulatory requirements.

Author contributions

MF-W: Writing – original draft. VR: Writing – original draft. MS: Writing – review & editing. NL: Writing – review & editing. KB: Writing – review & editing. AD: Writing – original draft.

Funding

The author(s) declare financial support was received for the research and/or publication of this article. This work was funded by the German Federal Ministry of Research, Technology and Space (grants no. 03LW0314 and HZI2020Z36).

Conflict of interest

The authors declare that the research was conducted in the absence of any commercial or financial relationships that could be construed as a potential conflict of interest.

Generative AI statement

The author(s) declare that no Generative AI was used in the creation of this manuscript.

Any alternative text (alt text) provided alongside figures in this article has been generated by Frontiers with the support of artificial intelligence and reasonable efforts have been made to ensure accuracy, including review by the authors wherever possible. If you identify any issues, please contact us.

Publisher's note

References

(2025). (Zugegriffen). Available online at: https://www.bundestag.de/resource/blob/1034900/795cde9dc6330445565942231494a553/WD-8-081-24-pdf.pdf (Accessed Feburary 2, 2025).

(2025). (Zugegriffen). Available online at: https://health.ec.europa.eu/publications/proposal-regulation-laying-down-union-procedures-authorisation-and-supervision-medicinal-products_en (Accessed Feburary 2, 2025).

Bleriot, I., Pacios, O., Blasco, L., Fernández-García, L., López, M., and Ortiz-Cartagena, C.. (2024). Improving phage therapy by evasion of phage resistance mechanisms. *JAC Antimicrob. Resist.* 6, dlae017. doi: 10.1093/jacamr/dlae017

Clokie, M. R., Millard, A. D., Letarov, A. V., and Heaphy, S. (2011). Phages in nature. *Bacteriophage* 1, 31–45. doi: 10.4161/bact.1.1.14942

Danis-Wlodarczyk, K., Dabrowska, K., and Abedon, S. T. (2021). Phage therapy: the pharmacology of antibacterial viruses. *Curr. Issues Mol. Biol.* 40, 81–164. doi: 10.21775/cimb.040.081

Dedrick, R. M., Freeman, K. G., Nguyen, J. A., Bahadirli-Talbott, A., Smith, B. E., and Wu, A. E.. (2021). Potent antibody-mediated neutralization limits bacteriophage treatment of a pulmonary Mycobacterium abscessus infection. *Nat. Med.* 27, 1357–1361. doi: 10.1038/s41591-021-01403-9

Doub, J. B. (2020). Bacteriophage therapy for clinical biofilm infections: parameters that influence treatment protocols and current treatment approaches. *Antibiotics-Basel* 9 (11), 799. doi: 10.3390/antibiotics9110799

Gu Liu, C., Clark, J. R., Salazar, K. C., and Terwilliger, A. L.. (2020). Phage-antibiotic synergy is driven by a unique combination of antibacterial mechanism of action and stoichiometry. *mBio* 11, e01462-20. doi: 10.1128/mBio.01462-20

Jault, P., Leclerc, T., Jennes, S., Pirnay, J. P., Que, Y.-A., and Resch, G. (2019). Efficacy and tolerability of a cocktail of bacteriophages to treat burn wounds infected by Pseudomonas aeruginosa (PhagoBurn): a randomised, controlled, double-blind phase 1/2 trial. *Lancet Infect. Dis.* 19, 35–45. doi: 10.1016/S1473-3099(18)30482-1

Karn, S. L., Bhartiya, S. K., Pratap, A., Saroj, S. K., Kumar, R., and Sahu, M.. (2024). A randomized, placebo-controlled, double-blind clinical trial of bacteriophage cocktails in chronic wound infections. *Int. J. Low Extrem Wounds* 17, 15347346231226342. doi: 10.1177/15347346231226342

Krut, O., and Bekeredjian-Ding, I. (2018). Contribution of the immune response to phage therapy. *J. Immunol.* 200, 3037–3044. doi: 10.4049/jimmunol.1701745

Leitner, L., Ujmajuridze, A., Chanishvili, N., Goderdzishvili, M., Chkonia, I., and Rigvava, S.. (2021). Intravesical bacteriophages for treating urinary tract infections in patients undergoing transurethral resection of the prostate: a randomised, placebo-controlled, double-blind clinical trial. *Lancet Infect. Dis.* 21, 427–436. doi: 10.1016/S1473-3099(20)30330-3

Liu, D., Van Belleghem, J. D., de Vries, C. R., Burgener, E., Chen, Q., and Manasherob, R.. (2021). The safety and toxicity of phage therapy: A review of animal and clinical studies. *Viruses* 13, 1268. doi: 10.3390/v13071268

Nang, S. C., Lin, Y.-W., Petrovic Fabijan, A., Chang, R. Y. K., Rao, G. G., and Iredell, J.. (2023). Pharmacokinetics/pharmacodynamics of phage therapy: a major hurdle to clinical translation. *Clin. Microbiol. Infect.* 29, 702–709. doi: 10.1016/j.cmi.2023.01.021

Ngiam, L., Weynberg, K., and Guo, J. (2024). Evolutionary and co-evolutionary phage training approaches enhance bacterial suppression and delay the emergence of phage resistance. *ISME Commun.* 4, ycae082. doi: 10.1093/ismeco/ycae082

Palma, M., and Qi, B. (2024). Advancing phage therapy: A comprehensive review of the safety, efficacy, and future prospects for the targeted treatment of bacterial infections. *Infect. Dis. Rep.* 16, 1127–1181. doi: 10.3390/idr16060092

Payne, R., Phil, D., and Jansen, V. (2000). Phage therapy: the peculiar kinetics of self-replicating pharmaceuticals. *Clin. Pharmacol. Ther.* 68, 225–230. doi: 10.1067/mcp.2000.109520

Pirnay, J. P., Djebara, S., Steurs, G., Griselain, J., Cochez, C., and De Soir, S.. (2024). Personalized bacteriophage therapy outcomes for 100 consecutive cases: a multicentre, multinational, retrospective observational study. *Nat. Microbiol.* 9, 1434–1453. doi: 10.1038/s41564-024-01705-x

Rhoads, D. D., Wolcott, R. D., Kuskowski, M. A., Wolcott, B. M., Ward, L. S., and Sulakvelidze, A. (2009). Bacteriophage therapy of venous leg ulcers in humans: results of a phase I safety trial. *J. Wound Care* 18, 237–238, 240-233. doi: 10.12968/jowc.2009.18.6.42801

Salmond, G. P., and Fineran, P. C. (2015). A century of the phage: past, present and future. *Nat. Rev. Microbiol.* 13, 777–786. doi: 10.1038/nrmicro3564

Sarker, S. A., Sultana, S., Reuteler, G., Moine, D., Descombes, P., and Charton, F. (2016). Oral phage therapy of acute bacterial diarrhea with two coliphage preparations: A randomized trial in children from Bangladesh. *EBioMedicine* 4, 124–137. doi: 10.1016/j.ebiom.2015.12.023

Strathdee, S. A., Hatfull, G. F., Mutalik, V. K., and Schooley, R. T. (2023). Phage therapy: From biological mechanisms to future directions. *Cell* 186, 17–31. doi: 10.1016/j.cell.2022.11.017

Summers, W. C. (1999). *Félix d'Herelle and the origins of molecular biology* (New Haven: Yale University Press).

Uyttebroek, S., Chen, B., Onsea, J., Ruythooren, F., Debaveye, Y., and Devolder, D.. (2022). Safety and efficacy of phage therapy in difficult-to-treat infections: a systematic review. *Lancet Infect. Dis.* 22, e208–e220. doi: 10.1016/S1473-3099(21)00612-5

Weiner, I., Kahan-Hanum, M., Buchstab, N., Zelcbuch, L., Navok, S., and Sherman, I.. (2025). Phage therapy with nebulized cocktail BX004 – A for chronic Pseucomonas aeruginosa infections in cystic fibrosis: a randomized first-in-human trial. *Nat. Commun.* 16, 5579. doi: 10.1177/15347346231226342

Wright, A., Hawkins, C. H., Anggard, E. E., and Harper, D. R. (2009). A controlled clinical trial of a therapeutic bacteriophage preparation in chronic otitis due to antibiotic-resistant Pseudomonas aeruginosa; a preliminary report of efficacy. *Clin. Otolaryngol.* 34, 349–357. doi: 10.1111/j.1749-4486.2009.01973.x

frontiers | Frontiers in Cellular and Infection Microbiology

TYPE Original Research
PUBLISHED 25 November 2025
DOI 10.3389/fcimb.2025.1597805

OPEN ACCESS

EDITED BY
Silke Alt,
German Center for Infection Research (DZIF), Germany

REVIEWED BY
Robert Ramirez-Garcia,
Imperial College London, United Kingdom
Deborah M. Hinton,
National Institutes of Health (NIH), United States

*CORRESPONDENCE
Flor I. Arias-Sánchez
flor-ines.arias-sanchez@charite.de

RECEIVED 21 March 2025
ACCEPTED 01 September 2025
PUBLISHED 25 November 2025

CITATION
Ning Y, González-Tortuero E, Wagemans J and Arias-Sánchez FI (2025) Hard to jump: host shifts appear unlikely in a T4-like phage evolved in the lab.
Front. Cell. Infect. Microbiol. 15:1597805.
doi: 10.3389/fcimb.2025.1597805

Hard to jump: host shifts appear unlikely in a T4-like phage evolved in the lab

Yu Ning[1], Enrique González-Tortuero[2], Jeroen Wagemans[3] and Flor I. Arias-Sánchez[1,4]*

[1]BIH Center for Regenerative Therapies (BCRT), Charité - Universitätsmedizin Berlin, Berlin, Germany, [2]School of Science, Engineering and Environment, University of Salford, Salford, United Kingdom, [3]Department of Biosystems, Katholieke Universiteit (KU) Leuven Kulak, Kortrijk, Belgium, [4]Institute of Integrative Biology, ETH Zürich, Zürich, Switzerland

Introduction: Bacteriophage therapy is emerging as a promising alternative to antibiotics, particularly in the face of rising antimicrobial resistance. However, concerns remain regarding host shifts, where therapeutic phages could evolve to infect and harm beneficial commensal bacteria. Understanding how frequently host shifts occur and what evolutionary constraints shape them is critical to assessing the safety of phage therapy.

Methods: We investigated the evolutionary potential for host shifts using Escherichia coli-infecting phage BW-1. Experimental evolution was conducted under controlled conditions that favored adaptation, using both non-permissive (unable to infect) and semi-permissive (low infectivity) bacterial strains. Virulence was assayed across hosts, and whole-genome sequencing was used to identify mutations associated with adaptation.

Results: Host shifts were found to be rare, with no significant increases in virulence observed in non-permissive hosts. In contrast, adaptation occurred in semi-permissive hosts and was linked to trade-offs, where increased virulence in one host reduced infectivity in others. Whole-genome sequencing revealed a single convergent regulatory SNP across all phages adapted to the semi-permissive host, indicating constrained evolutionary pathways during host adaptation.

Discussion: Our findings suggest that phages exhibit high host specificity, which limits the risk of host shifts to commensal bacteria. Although adaptation to semi-permissive hosts is possible, it is constrained and associated with fitness trade-offs across host ranges. These results indicate that therapeutic phages are unlikely to negatively impact intestinal microbiota, supporting their potential as safe and effective alternatives to antibiotics.

KEYWORDS

phage therapy, host shifts, virulence, infection, phage therapeutics

Introduction

When they shift to a new host, parasites can overcome their overall specificity and gain access to new environments. Although host shifts are beneficial to the parasite, they can be highly detrimental to the novel host, as demonstrated by the number of human pandemics (like HIV, malaria and influenza) that are caused by newly acquired parasites (Liu et al., 2010; Mollentze and Streicker, 2020; Sharp and Hahn, 2010; Webby and Webster, 2001). Despite our knowledge of host shifts as natural events that tend to occur among closely related species (Lee, 2024; Longdon et al., 2014; Seal et al., 2021; Woolhouse et al., 2005), understanding what drives and constrains host shifts remains elusive. We lack information about how frequently they happen and whether they tend to be associated with increased virulence in the new or old hosts.

A better understanding of the conditions that facilitate or constrain viral host shifts and high levels of virulence might also be crucial for the success of new treatments like phage therapy. If host shifts are facilitated among closely related hosts, using phages to treat infections in complex communities such as the gut might result in undesirable host shifts to commensal bacteria. Although patterns of phage-bacterial infection in complex communities such as those in the gastrointestinal tract are still poorly understood (Mirzaei and Maurice, 2017; Shkoporov and Hill, 2019), many factors predicted to be essential for host shifts are inherent to the host. These include CRISPR/Cas systems (Angermeyer et al., 2021; Sorek et al., 2008), the presence of particular proteins like phage receptors (Bertozzi Silva et al., 2016; Kim et al., 2023), horizontally transferred elements like plasmids (Jalasvuori et al., 2011; Shan et al., 2023), or just general phenotypic similarity to existing hosts, which would be reflected in phylogenetic distance effect (Longdon et al., 2011; Walsh et al., 2023).

Here, we looked at host shifts using a microbial system comprised of a lytic bacteriophage (virus infecting bacteria) and 8 strains of *Escherichia coli*. As a species, *E. coli* is a highly versatile continuum that ranges from commensal strains living in the gut to pathogenic strains causing urinary tract infections or severe gut infections (Kaper et al., 2004; Siniagina et al., 2021; Tenaillon et al., 2010). Phages infecting *E. coli* are specific for particular strains (Allen et al., 2017; Li et al., 2022; Michel et al., 2010). Past work shows that phages infecting *E. coli* and other bacteria can rapidly adapt to increase their infectivity against bacterial hosts and sometimes adapt to new host strains (Benmayor et al., 2009; Bohannan and Lenski, 2000; Koskella et al., 2022), but the outcomes can be highly variable. Despite this variability, few studies have addressed host shifts systematically in a controlled evolutionary framework. Our study is one of the first to experimentally approach this question using a phage with known host range variability and a rationally chosen set of diverse *E. coli* strains. We, therefore, hypothesized that a phage would be able to adapt to some novel hosts from a collection of natural and clinical isolates. We made the additional prediction that adaptation to new hosts would be most likely for hosts more genetically similar to the set of known host genotypes that the phage could already infect (native host range). To test this, we evolved a phage in the presence of various novel hosts that the phage could not infect (non-permissive host). We controlled the experimental conditions to favor host shifts. BW1 was selected as the focal phage because it exhibited diversity in its infectivity across strains, suggesting evolutionary potential in its host range. The *E. coli* strains were drawn from the well-characterized ECOR collection and were selected to represent different phylogenetic backgrounds and ecological sources, thereby maximizing diversity within a tractable number of hosts. This experimental system, while limited in scope, provides a strategic balance between complexity and control, enabling detailed insight into the repeatability and constraints of host range evolution. At the end of the experiment, we tested for Reductions in Bacterial Growth (RBG) after phage exposure, which we take as a measure of phage virulence (Hall et al., 2011; Poullain et al., 2008; Wendling et al., 2022). In cases where phages evolved virulence against a host they could not previously infect, we interpret this as a host shift. We also included hosts that the phage could infect but only cause small reductions in bacterial growth (semi-permissive hosts) compared to other hosts found to be highly susceptible to the same phage. By evolving phage with semi-permissive hosts, we aimed to test for (1) increases in phage virulence with hosts they could already infect and (2) whether this also resulted in altered virulence against non-permissive hosts (that is, the possibility of host shifting as a 'side-effect' of adaptation to other hosts).

Materials and methods

Organisms and culture conditions

We used different *E. coli* strains and *Escherichia* phage BW-1 (Ackermann and Krisch, 1997), a lytic T4-like phage from the *Straboviridae* family and Tevenviridae subfamily. This phage produces clear plaques (<0.1mm) and was found in a previous study to infect a relatively large number of natural and clinical *E. coli* isolates compared to other phages tested in the same study (Allen et al., 2017) (Figure 1A). Evidence suggests parasites with broader host ranges are more likely to infect new hosts (Cleaveland et al., 2001; Thines, 2019). Therefore, we assumed *Escherichia* phage BW-1 was a favorable candidate for host shifts. Its intermediate host range made it particularly suitable for assessing both potential for adaptation and constraints on host range expansion under selection. As bacterial hosts, we selected eight strains from the *E. coli* (ECOR) collection (Ochman and Selander, 1984). The strains varied in their level of susceptibility to ancestral *Escherichia* phage BW-1 infection, as measured by the level of Reduction in Bacterial Growth (RBG, described in more detail below) (Figure 1B). We included five strains where we detected little or no reduction in bacterial growth caused by ancestral *Escherichia* phage BW-1 compared to phage-free cultures (RBG equal or close to zero; Figure 1B). Hereafter, we refer to these strains as non-permissive hosts. For four of these strains, we also detected no evidence of plaque formation by *Escherichia* phage BW-1 when spotted on an

agar lawn of the bacteria. As semi-permissive hosts, we included three strains with a significant reduction in bacterial growth caused by *Escherichia* phage BW-1. However, this reduction was at an intermediate level compared to that observed for ancestral *Escherichia* phage BW-1 across a wide range of natural and clinical isolates, as estimated in a previous study that also included the isolates used here (Allen et al., 2017). Note that the reduction in bacterial growth caused by ancestral *Escherichia* phage BW-1 on each strain in this previous study was strongly correlated with that in our experiment ($r^2 = 0.81$, $F_{1,7} = 29.3$, $P = 0.001$). We also found that ancestral *Escherichia* phage BW-1 formed plaques on all these semi-permissive hosts. The strains were selected to maximize phylogenetic and ecological diversity within the species, while still allowing experimental tractability across replicates and time points. We chose strains from various phylogenetic subgroups of *E. coli*, as inferred previously from whole-genome sequence data (Allen et al., 2017)(Figure 1C). Finally, we included *E. coli* K12-MG1655 in our experiments, which is highly susceptible to *Escherichia* phage BW-1 infection (Figure 1C). All experiments were performed at 37 °C in lysogeny broth (LB) medium supplemented with 10mM $MgSO_4$ and 10mM Tris HCL, hereafter referred to as LBMT.

Phage evolution experiment

We set up our evolution experiment to simulate a tough but realistic situation in which phages would need to evolve to infect new bacterial hosts in order to survive. To test whether host shifts (significant increase in RBG after evolution in hosts where RBG of ancestral *Escherichia* phage BW-1 equals zero) and/or high levels of virulence could be selected for, we evolved *Escherichia* phage BW-1 in non-evolving populations of each non-permissive or semi-permissive host (see diagram in Figure 1D). For each bacterial host ($n = 8$), we experimentally evolved three independent populations ($n = 24$ evolved phage lines). We initiated each phage line by adding 10^5 plaque-forming units (PFU) ancestral *Escherichia* phage BW-1 particles to mixed bacterial populations (6mL cultures) consisting of 1% permissive host (*E. coli* K12-MG1655) and 99% of either non-permissive or semi-permissive host (ECOR strain) (Figure 1D). This initial ratio was specifically chosen to impose strong selection for host-range expansion while maintaining minimal access to a permissive host, preventing immediate phage extinction. Culturing phages in mixed bacterial populations (Benmayor et al., 2009; Borin et al., 2021) helps to maintain phage population turnover while keeping a large number of susceptible cells for any phage mutant that can infect the new host. To prevent any cumulative shift in bacterial strain frequencies, each 24-hour transfer cycle was initiated using fresh overnight cultures prepared from frozen bacterial stocks, and the 1%:99% ratio of MG1655 to test host has re-established at the start of every transfer. This ensured that any within-transfer overrepresentation of MG1655 did not carry over across passages and allowed us to preserve a consistent and reproducible selective environment for all evolving phage lines. We extracted phage after 24h (Transfer-1 phage lysates), adding 10% chloroform to each culture, vortexing for 1 min, and centrifuging at 13,000 rpm for 2 min (Buckling and Rainey, 2002). We transferred 50µl of each phage lysate to new non-evolving mixed bacterial populations (stocks from the freezer), meaning that bacterial hosts were not allowed to evolve in our experiment. We incubated and extracted phage as described above for a total of 14 transfers, which we expected to be enough time for the emergence of virulent mutants under strong selection based on previous work with other phage species (Benmayor et al., 2009; Borin et al., 2021; Hall et al., 2011). To verify phage presence in every transfer, we spotted 3.5µl of phage lysate onto a lawn of the susceptible host (*E. coli* K12-MG1655) and incubated overnight to look for clear spots or plaques. At the end of the experiment (transfer 14), we plated serial dilutions and estimated phage titers in each phage line (Figures 1D, 2A). For phage lines that did not go extinct, we tested for variation in final phage population size (titer in PFU/mL) among populations evolved with different host strains. To do this, we used one-way ANOVA with titer as the response variable (mean of 3 replicate measurements for each of 3 phage lines per host strain) and host strain during the evolution experiment as a factor. We then tested for pairwise differences in phage population densities per host strain, correcting for multiple comparisons using Tukey's Honest significant difference (Figure 2A).

Measuring changes in virulence

We quantified virulence differences among the ancestral and evolved phage lines by estimating the reduction in bacterial growth (RBG) due to phage infection after 24h (Hall et al., 2011; Poullain et al., 2008; Wendling et al., 2022). We did a cross-infection experiment, testing the ancestral phage and all evolved phage lines against all hosts, including the ones they evolved with and the ones they did not. Independent bacterial populations ($n = 6$) of each host ($n = 9$) were exposed to either ancestral phage, an evolved phage line ($n = 18$) or phage-free conditions (control) in microcosms containing fresh media supplemented with phage titers adjusted to reach the same multiplicity of infection in all populations (MOI = 10). The basic setup was 10^4 bacterial cells + 10^5 PFU particles in volume of 100µl where at least 90% was fresh LBMT. After 24h, we measured bacterial biomass as optical density (OD24h) in each population (n=1080) using an Infinite M200 spectrophotometer (Tecan, USA). All measurements were corrected by subtracting the mean score of sterile medium (OD = 0.045). We calculated the RBG (Reduction in Bacterial Growth) values for each bacterial population in the experiment with the equation:

$$\mathrm{RBG} = 1 - \frac{OD24h\ \ with\ \ phage}{mean(OD24h\ \ without\ \ phage)}$$

For each host strain, we tested whether evolved phage populations showed altered virulence (RBG) compared to the ancestral phage using pairwise Welch's *t*-tests, which allow for

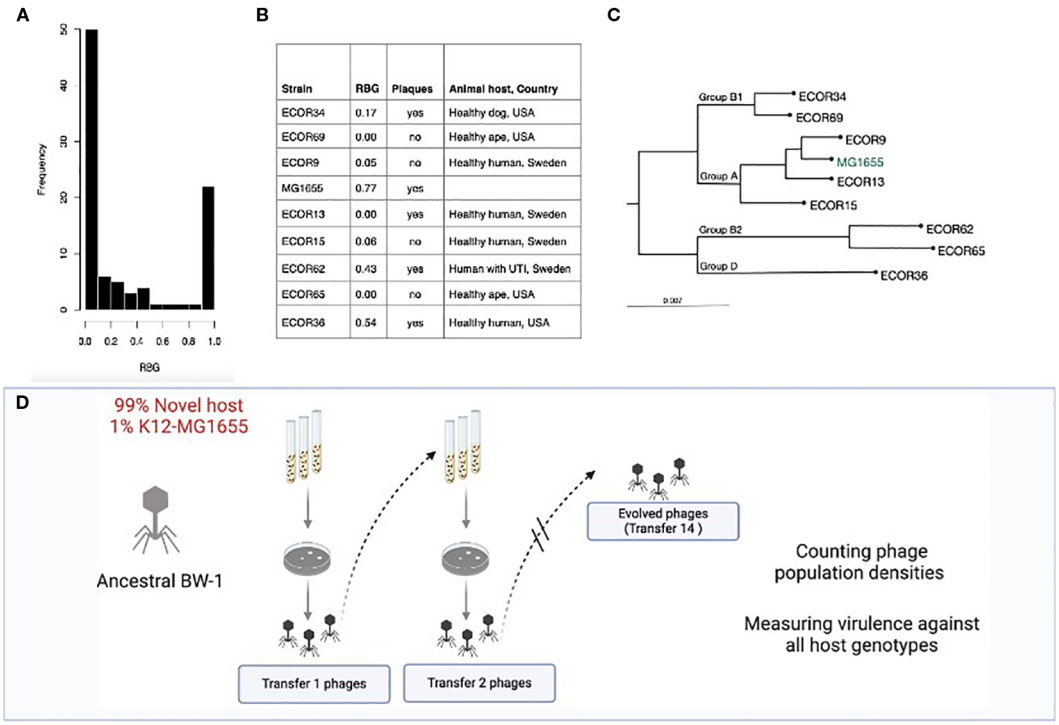

Strain	RBG	Plaques	Animal host, Country
ECOR34	0.17	yes	Healthy dog, USA
ECOR69	0.00	no	Healthy ape, USA
ECOR9	0.05	no	Healthy human, Sweden
MG1655	0.77	yes	
ECOR13	0.00	yes	Healthy human, Sweden
ECOR15	0.06	no	Healthy human, Sweden
ECOR62	0.43	yes	Human with UTI, Sweden
ECOR65	0.00	no	Healthy ape, USA
ECOR36	0.54	yes	Healthy human, USA

FIGURE 1
E. coli hosts used in the evolution experiment. **(A)** Histogram of Reduction in Bacterial Growth (RBG) caused by ancestral *Escherichia* phage BW-1 against 94 different natural and clinical isolates of *E. coli* (Allen et al., 2017). **(B)** List of bacterial hosts used in this study, with average RBG data observed in our experiments after 24h of exposure to ancestral *Escherichia* phage BW-1, plaque formation data and additional details about strain origins. **(C)** Phylogenetic tree of *E. coli* isolates from different sub-species groups used in this study. Details of how the tree was produced are provided as Supplementary Information. **(D)** Diagram representation of the evolution experiment for phage BW-1 and one bacterial host. Note that the ancestral phage was serially passaged in co-cultures containing 99% novel host (either permissive or semi-permissive) and 1% K12-MG1655. In this way, we included a selective pressure that would allow adaptation to the new host, but preventing phage extinction by including a small percentage of cells that the ancestral phage could infect.

unequal variances as observed in some of our comparisons. In cases where we tested multiple evolved populations against the same control, we corrected for multiple testing by sequential Bonferroni adjustment (Figure 2B). Virulence gain was estimated with respect to Reductions in Bacterial Growth (RBG) of evolved phage versus ancestral phage (i.e. evolved RBG-ancestral RBG). Positive values indicate an increase in virulence after evolution, and negative values indicate reduced virulence. In Figure 2B, each data point represents the virulence gain for an evolved line. Statistically significant changes in virulence are shown as arrows, with the arrowhead positioned at the exact level of virulence gain or loss (Figure 2B; RGB data for this figure can be found in Supplementary Figures S2 and S3). Non-significant changes are shown as simple dots. This visual distinction highlights where meaningful evolutionary shifts in virulence occurred.

Estimation of genetic distance to native host range

In order to determine whether the host strains in our experiment were relatively closely or distantly related to host strains against which ancestral *Escherichia* phage BW-1 is highly virulent, we computed the average genetic distance of each non-permissive and semi-permissive host to a set of host strains found previously to be highly susceptible to *Escherichia* phage BW-1 (Allen et al., 2017). These data show that susceptibility to *Escherichia* phage BW-1 is bimodal among these isolates (Figure 1A). We therefore took all isolates (n = 94) where RBG>0.5 as being relatively highly susceptible. We then calculated the average genetic distance for each strain used in our experiment to this set of highly susceptible strains. We estimated the genetic distance between a given pair of strains as patristic difference using the *adephylo* package (Jombart et al., 2010). This is the sum of the branch lengths between the two strains, where branch length is the expected number of nucleotide changes per base pair across the 1424 loci used for phylogenetic reconstruction (Supplementary Information S1). For each strain used in our experiment we calculate these distances to each of the highly susceptible strains, and then take the average as a measure of genetic distance to the native host range of *Escherichia* phage BW-1. We then tested whether genetic distance to the native host range was correlated with the change in virulence over the course of selection (*mean*(*RBGevolved*) – *mean*(*RBGancestral*)) for each group of three replicates evolved with the same host). All statistical analyses were conducted in R 3.1.1 (R Core Team, 2015).

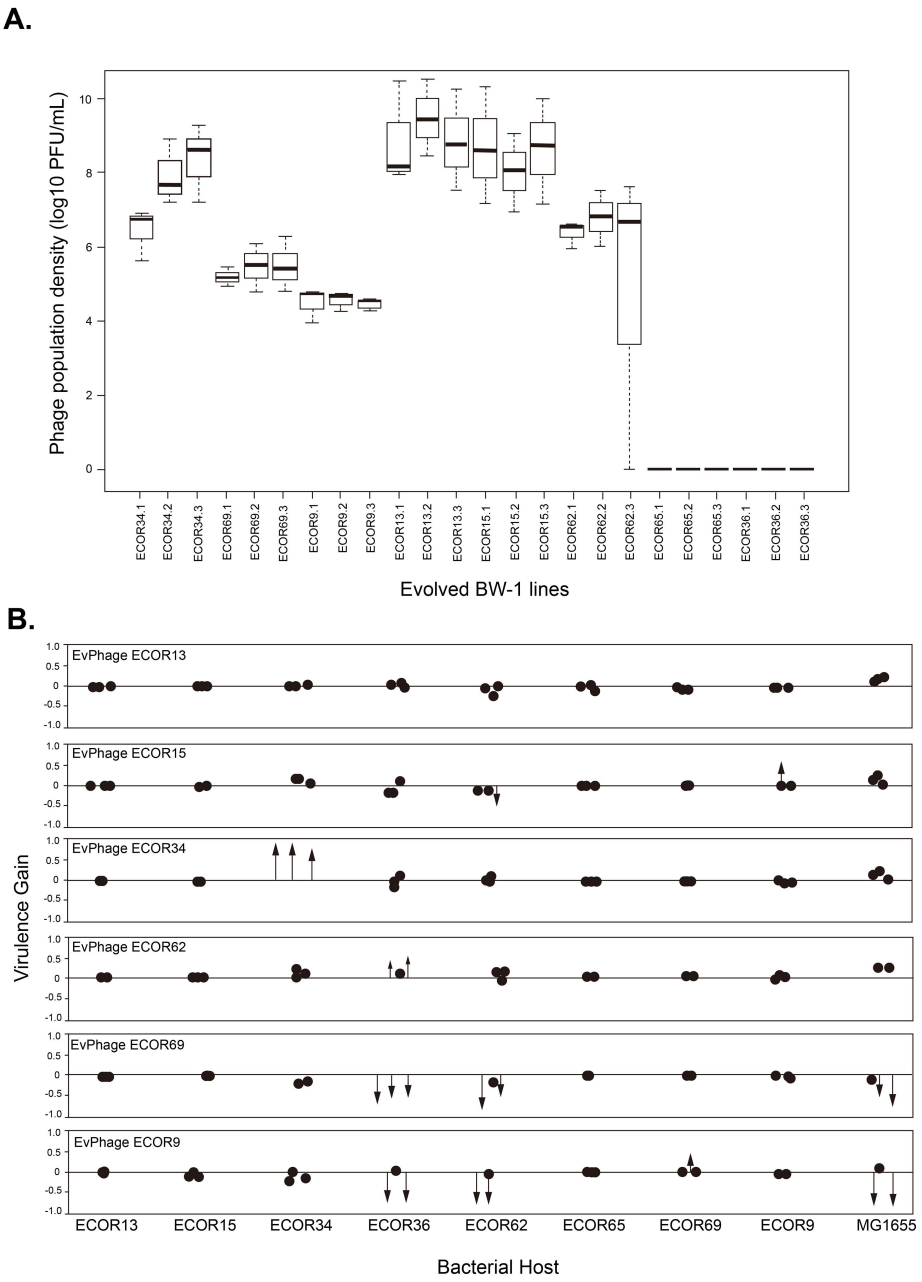

FIGURE 2
(A) Phage population densities of evolved *Escherichia* phage BW-1 lines at the end of the evolution experiment (Transfer 14). The name of each evolved BW-1 line (*x*-axis) indicates which bacterial host was present during the evolution experiment. Replicate selection lines are differentiated with numbers (1-3), and each box shows the results of three replicate assays. **(B)** Changes in virulence after evolving bacteriophage BW-1 on different *E. coli* hosts. Virulence gain was estimated as the difference in Reductions in Bacterial Growth (RBG) between evolved and ancestral phage for each bacterial host. Positive values indicate an increased virulence, and negative values indicate decreased virulence following evolution. Each point represents an individual evolved line. Statistically significant changes in virulence are shown as arrows, with the arrowhead marking the exact magnitude of virulence gain or loss. Non-significant changes are shown as simple dots. RGB data for this figure can be found in Supplementary Figures S2 and S3.

Phage genomic extraction, sequencing, and annotation

Phage genome isolation was performed as previously described (Green and Sambrook, 2012). Briefly: 1 mL of phage stock was treated with ten µg DNaseI and 50 µg RNaseA (Roche Diagnostics; Mannheim, Germany) in the presence of MgCl2 to degrade the bacterial DNA that is still present after phage production, followed by 50 µg/mL of proteinase K (Thermo Scientific, Waltham, MA, USA), 20 mM EDTA and 0.5% SDS treatment to inactivate the DNaseI/RNaseA and to disrupt the phage capsid proteins.

Subsequently, extraction by phenol-chloroform (Carl Roth GmbH, Karlsruhe, Germany) was performed to remove debris. The nucleic acid pellet was precipitated (14,000× g, 20 min) in the

presence of absolute alcohol (Merck KGaA, Darmstadt, Germany) and washed with 70% alcohol before being suspended in deionized distilled water. Nanodrop measurements (Peqlab; Erlangen, Germany) were done to determine concentration and purity (260/230 ratio). Sequencing was performed on an Illumina (San Diego, CA, USA) MiniSeq instrument. The Nextera Flex DNA library kit (Illumina) was used for library preparation. Long reads were generated using an Oxford Nanopore MinION (Oxford, UK) device with an R.9.4.1 flow cell. The latter library was prepared with Rapid barcoding. Sequence quality was examined with FastQC (https://www.bioinformatics.babraham.ac.uk/projects/fastqc/). Low-quality reads and adapter removal from the paired ends for all sequences were filtered by Trim Galore v. 0.6.6 (https://www.bioinformatics.babraham.ac.uk/projects/trim_galore/) using a Phred quality cutoff of 30. Then, human reads were discarded by mapping them against the Genome Consortium Human Build 38(GRCh38; Schneider et al., 2017) using Bowtie2 v. 2.4.2 (Langmead and Salzberg, 2012) with default parameters. For the *de novo* assembly, metaSPAdes v. 3.15.0 (Bankevich et al., 2012; Nurk et al., 2017) with default parameters was executed as recommended in previous publications (Sutton et al., 2019). The resulting contigs were annotated using VIGA 0.11.1 (Gonzalez-Tortuero et al., 2022; González-Tortuero et al., 2018) using the RefSeq Viral Database (Brister et al., 2015), the Viral Orthologs Groups(VOGs; Marz et al., 2014), the Viral DataBase (RVDB v. 21.0; Bigot et al., 2020) and the Prokaryotic virus Remote Homologous Groups (PHROGS v. 4; Terzian et al., 2021) for the functional prediction. Variant calling between the evolved Escherichia phages and the ancestral one was performed using Snippy v. 4.6 (https://github.com/tseemann/snippy).

Comparative genomic analysis and visualization

To investigate the potential regulatory or functional impact of SNP 164264, a 1,000 bp region centered on the SNP was extracted from the assembled BW1 genome and aligned to the homologous region in the Escherichia phage T4 (reference genome NC_000866.4). Protein-coding open reading frames (ORFs) in the BW1 region were predicted using VIGA v.0.12.0 (González-Tortuero et al., 2018), by scanning all putative reading frames using the bacterial genetic code (11) and a minimum threshold of 60bp for ORF length. Gene annotations for T4 were retrieved from GenBank and the noncoding RNAs rnaC and rnaD (also known as species 1 and 2 RNAs) were mapped based on the coordinates described by Miller et al. (2003). A comparative figure was generated to visualize the gene architecture, the SNP position, and the local sequence context. Features displayed include directional gene arrows, codon context (highlighting the T-C transition at the SNP), putative BW-1 specific ORFs, and the location of predicted regulatory elements. All visualizations were constructed using SnapGene v. 8.1.1 and in Python v. 3.12.1 using the matplotlib 3.8.2 library.

Virulence assay against ECOR collection strains

To test whether gains in virulence after evolution affected virulence patterns towards other *E. coli* strains, we performed a fully factorial cross infection experiment, using the evolved phages where we observed a consistent increase in virulence across the 3 replicate lines against all members of the ECOR collection. We tested virulence differences of the evolved phages against all 72 strains in ECOR collection as compared to the virulence observed in the ancestral phage. The overnight cultures (corresponding to approx. 10^8 CFU/mL) were then mixed with either ancestral phage, an evolved phage line (n = 3) or phage-free conditions (control) at MOI = 10 (10^5 PFU/mL) after diluted to 10^4 CFU/mL and incubated at 37°C. After 24h, the bacterial biomass was measured as optical density (OD_{600}24h) in each population (3 replicates per experimental condition for an overall total of n=1080) using an Infinite M200 spectrophotometer (Tecan, USA). All measurements were corrected by subtracting the mean score of sterile media (OD = 0.0495). The reduction in bacterial growth (RBG values) were calculated for each population, as mentioned before. For each host strain, we tested whether evolved phage populations showed altered virulence (RBG) compared to the ancestral phage using pairwise Welch's t-tests, which allow for unequal variances as observed in some of our comparisons. In cases where we tested multiple evolved populations against the same control, we corrected for multiple testing by sequential Bonferroni adjustment.

Results

Variation in phage population densities at the end of the evolution experiment

Evolving with new hosts had a significant effect on phage population densities by the end of the experiment. Despite continued mixed-host culturing until the final transfer in all phage lines (n = 24), we observed phage extinction in lines that evolved with one non-permissive host (ECOR65) and one semi-permissive host (ECOR36) (Figure 2A). Extinctions happened early in the evolution experiment. We had no phage detection after transfer 2 in all phage lines that evolved with ECOR36 and two phage lines that evolved with ECOR65 (the third phage line went extinct at transfer 3). As for the phage lines where phage did not go extinct, we found significant differences in average phage population densities depending on the host they evolved with ($F_{5,12}$ = 24.42, P<0.0001 by one-way ANOVA). Phage lines that evolved with ECOR9, ECOR69, and ECOR62 had significantly lower average phage population densities than phage lines that evolved with ECOR15 and ECOR13 (Tukey HSD for all pairwise comparisons P<0.05) (Figure 2A).

Virulence increases in evolved phages are rare and confined to semi-permissive hosts, with host shifts remaining unconfirmed

The majority of evolved phage lines did not show significant changes in virulence compared to the ancestral phage. Specifically, in 12 out of the 18 cases tested, we observed no significant differences in relative bacterial growth (RBG) ($P > 0.05$ in all cases by Welch's t-test corrected with sequential Bonferroni; see black dots in Figure 2B; RBG values in Supplementary Figures S2, S3). However, we identified some cases where virulence increased, and these gains were primarily observed in phages that evolved with semi-permissive hosts. Notably, phage lines evolved with the semi-permissive host ECOR34 showed substantial increases in virulence, with an average RBG value of 0.98 ± 0.02 compared to 0.17 for the ancestral phage ($P < 0.05$; see red arrows in Figure 2B; Supplementary Figure S3). By contrast, none of the phages evolved with non-permissive hosts exhibited any significant gains in virulence (Figure 2B; Supplementary Figure S2).

Additionally, we found one intriguing data point suggesting a possible host shift. Specifically, phage lines evolved with ECOR69 appeared to increase infectivity based on RBG data, but when we spot-plated these phage lines on ECOR69 agar plates, they failed to form plaques, providing no evidence of successful infection on this host. Conversely, phage lines evolved with ECOR15 were able to form plaques on ECOR15 agar plates despite showing no significant increase in virulence in liquid culture ($P > 0.05$ in all cases). These results highlight that while virulence increases were rare and primarily restricted to semi-permissive hosts, liquid culture infectivity does not necessarily correlate with plaque formation on agar surfaces.

First, we asked whether evolved phage lines were more virulent towards their corresponding bacterial host (the host strain they were exposed to during experimental evolution, shown in Figure 2B). We found significant gains in virulence ($P<0.05$ in pairwise comparisons against the ancestral phage using Welch's *t*-test corrected with sequential Bonferroni) in six phage lines corresponding to three hosts (see red arrows in Figure 2B). None of the phage lines that evolved with non-permissive host had significant gains in virulence. However, in one specific case (evolution with the semi-permissive host ECOR34) phage lines showed a considerable gain in virulence (average RBG for evolved phage lines=0.98 ± 0.02; RBG for the ancestral phage=0.17) (Supplementary Figure S3), highlighting that changes can occur under permissive conditions. For the remaining phage lines ($n = 12$) we observed no significant virulence differences from the ancestor ($P>0.05$ in all cases by Welch's *t*-test corrected with sequential Bonferroni) (see black dots in Figure 2B and RGB values in S2&S3). In short, our RBG data shows that while phage BW-1 can increase virulence under certain permissive conditions (as seen with host ECOR34), it did not evolve the ability to infect any of the non-permissive hosts tested, suggesting that full host shifts remain unlikely in this system.

Adaptation to one host can be costly in terms of virulence profiles towards other hosts

We further asked whether evolution influenced phage virulence towards hosts other than the ones encountered during the evolution experiment. For two semi-permissive hosts (ECOR36 & ECOR62) (Figure 2B; S3), multiple evolved phage lines that had been evolved with other hosts had altered virulence relative to the ancestor, and for two non-permissive hosts (ECOR9 & ECOR69) (Figure 2B; S2), we observed small increases in virulence in a single evolved phage line. Specifically, we observed that replicate phage lines that evolved with hosts ECOR9 and ECOR69 (at least two phage lines in each case) lost virulence against both hosts ECOR36 (mean RBG for all phage lines different from an ancestor that evolved with host ECOR9 = 0.211 ± 0.333, with host ECOR69 = 0.008 ± 0.003 *vs* mean RBG ancestral phage=0.544) and ECOR62 (mean RBG for all phage lines different from ancestor that evolved with host ECOR9 = 0.137 ± 0.238, with host ECOR69 = 0.101 ± 0.090 *vs* mean RBG ancestral phage=0.434). In comparison, phage lines that evolved with ECOR62 (2 out of 3 phage lines) had significant gains in virulence against ECOR36 (mean RBG for all phage lines different from an ancestor that evolved with host ECOR62 = 0.867 ± 0.121, *vs* RBG ancestral phage=0.544) (Supplementary Figure S3).

We also tested for changes in virulence against the permissive host K12-MG1655 (Supplementary Figure S4), finding that phage lines that evolved with ECOR9 and ECOR69 (2 out of 3 phage lines in both cases) had lost virulence (RBG) as compared to the ancestral phage (mean RBG for all phage lines different from an ancestor that evolved with host ECOR9 = 0.303 ± 0.465, with host ECOR69 = 0.379 ± 0.327 *vs* mean RBG ancestral phage= 0.767). In summary, phage lines that evolved with the non-permissive host ECOR69 did not gain the ability to infect the new host and still, paid the expense of losing virulence towards multiple hosts. By contrast, phages that had adapted to increase their virulence on the semi-permissive host ECOR34 did not incur a reduction in virulence on other hosts. (Supplementary Figures S2, S3).

No evidence that adaptation is more likely when hosts are closely related to the native host range

The only case where we found evidence of adaptation resulting in increased virulence (ECOR34) is the strain with the highest genetic distance to the set of highly susceptible host isolates identified in a previous study (Allen et al., 2017; Supplementary Figure S1) (Figure 3A). This was also true when we used alternative cut-off values for classifying host isolates as highly susceptible (tested for RBG = 0.3, 0.7 & 0.9). This provides no support for the idea that adaptation resulting in increased virulence is more likely in host strains that are closely related to the current host range of the pathogen.

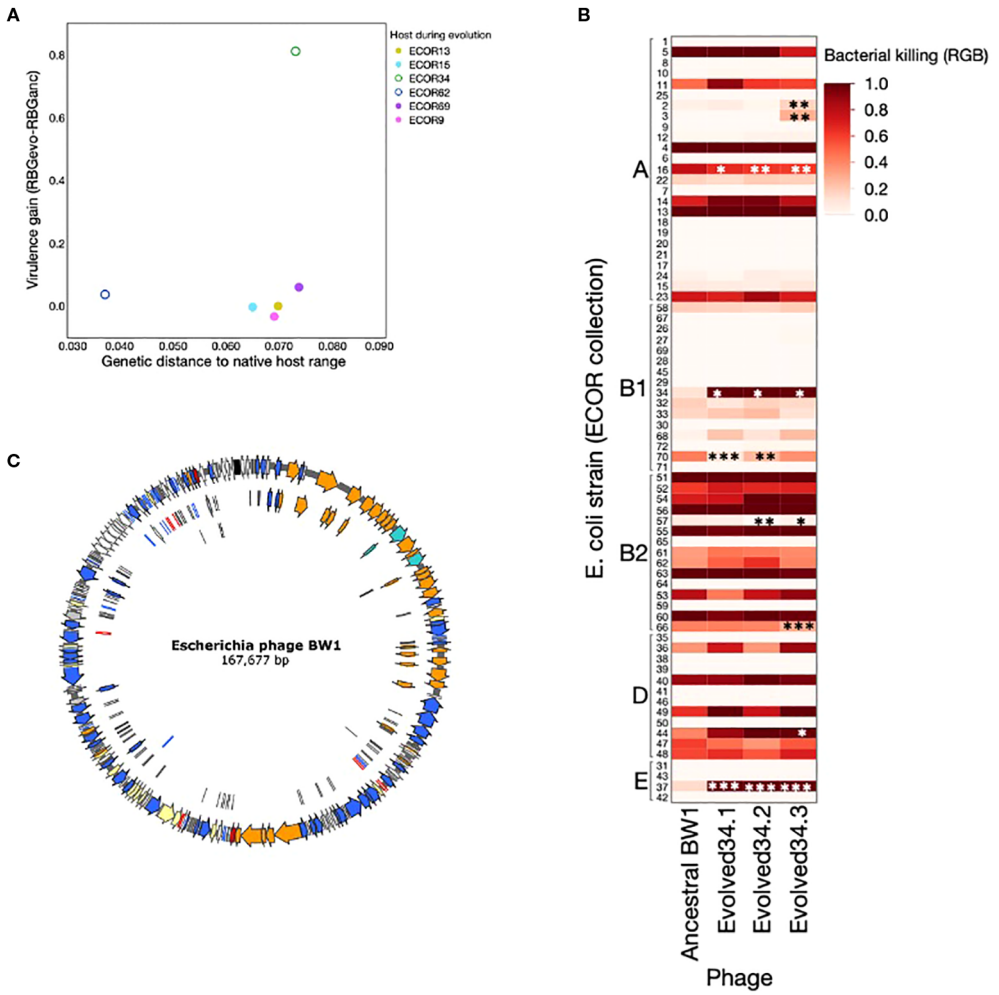

FIGURE 3
(A) Virulence gain (difference between average RBG for evolved phage lines and RBG for ancestral *Escherichia* phage BW-1) as a function of the genetic distance to native host range (calculated as described in methods). Each dot represents the average virulence gain for the three independent lines evolved with each host. Phage lines evolved with non-permissive hosts are shown as full circles, and phage lines evolved with semi-permissive hosts are shown as empty circles. **(B)** Phages evolved with ECOR34 tested against a set of 72 *E. coli* strains from the ECOR collection. Asterisks indicate cases where the evolved phage shows a statistically significant difference in virulence compared to the ancestral BW1 phage. This figure shows that increased virulence toward ECOR34 does not lead to widespread changes in virulence across other hosts—most strains show no significant change, and where changes do occur, they are primarily losses of virulence (except ECOR37). **(C)** Genome annotation of Escherichia phage BW-1. Colors indicate gene function based on viral gene classification proposed by Moura de Souza et al. (2021). Orange: structural, turquis: packaging, blue: DNA metabolism, red: lysis, yellow: regulation, white: hypothetical, black: tRNAs, grey: miscellaneous. See annotation details in Supplementary Table S1).

Convergent evolution in phage adaptation: a regulatory SNP drives adaptation to semi-permissive *E. coli* host

To gain deeper insight into the genetic changes underlying increased phage virulence, we performed whole-genome sequencing on phages evolved with the semi-permissive host ECOR34. Based on prior studies of T4-like phages such as BW-1, we anticipated identifying multiple polymorphisms, particularly in genes involved in host specificity, such as those encoding the distal regions of the long tail fibers (Miller et al., 2003; Taslem Mourosi et al., 2022). The C-terminal region of gp37, known to be hypervariable (Hashemolhosseini et al., 1994; Montag et al., 1990; Taslem Mourosi et al., 2022)and implicated in host range expansion, was of particular interest (Chen et al., 2017). However, sequencing revealed surprisingly limited genetic changes across three independent evolution experiments. A single, shared single-nucleotide polymorphism (SNP) was consistently identified in all evolved populations, located within a non-coding regulatory region between two hypothetical genes (Figure 4).

Further inspection revealed that this region corresponds to the reverse strand and aligns with two adjacent noncoding RNAs described in phage T4: rnaC and rnaD (Miller et al., 2003). These small RNAs, though of unknown function, are transcribed sequentially and occupy the genomic coordinates 164080–164336 in our phage BW1, with *rnaC* (~138 bp) located upstream of *rnaD*

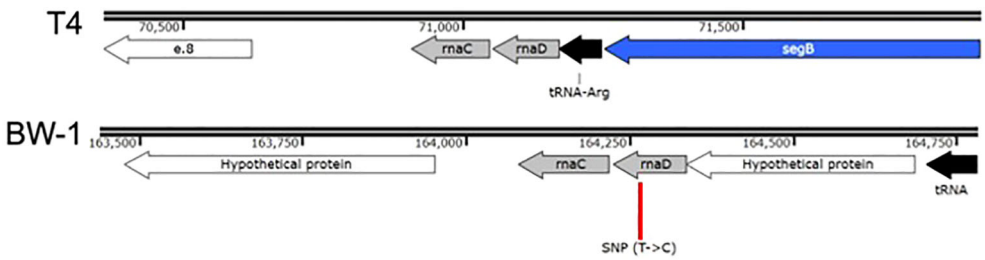

FIGURE 4
Genomic context of the convergent SNP (position 164264) found in all phage lines evolved with ECOR34. This SNP lies in a noncoding intergenic region on the reverse strand of the BW1 genome, between two hypothetical protein-coding genes. Comparative analysis reveals homology with a well-described region of phage T4 that contains two small noncoding RNAs: rnaC and rnaD (Miller et al., 2003). In BW1, rnaC (~138 bp) is more conserved, while rnaD (~118 bp) is more degenerated relative to T4. The SNP occurs within the 3′ region of rnaD, at approximately position 41 of the predicted transcript.

(~118 bp). The SNP lies within the 3′ end of *rnaD*, approximately at position 41 of the predicted transcript. While *rnaC* appears to be well conserved (90% conservation), *rnaD* is more degenerated in BW1 compared to its T4 counterpart. RNAfold predictions suggested that the BW1 rnaD region may adopt a somewhat more stable secondary structure than the corresponding region in T4. The presence of the SNP did not appear to drastically alter the overall fold in these preliminary predictions, but its potential impact on local stability remains to be fully tested. No additional consistent mutations were detected across the three populations, suggesting that adaptive changes during co-evolution with ECOR34 were constrained and focused on this regulatory locus (See Supplementary Tables S2-S4). While the functional implications of this mutation remain to be fully elucidated, its convergence across all replicates strongly suggests a potential role in the phage's adaptation to the semi-permissive host ECOR34. This finding highlights the specificity of genomic changes associated with host shifts under controlled laboratory conditions.

Discussion

We used a controlled experimental framework to investigate the evolution of bacteriophage host shifts and changes in virulence. Our study focused on a single phage BW1 and a carefully selected panel of eight *E. coli* strains, allowing us to probe the dynamics of host shifts with high experimental resolution. While this narrow scope limits broad generalizations, it enabled us to test evolutionary outcomes under tightly controlled and reproducible conditions.

Our finding that evolved phages had increased virulence in just a limited number of cases is consistent with the overall expectation that although host shifts can happen, they are rare and limited events (Benmayor et al., 2009; De Sordi et al., 2017; Hall et al., 2011; Marchi et al., 2023; Scanlan et al., 2013). Of the hosts where we observed adaptation, changes were only found in the semi-permissive hosts, demonstrating that phages primarily adapt to hosts they can already infect to some degree. Whole-genome sequencing of the evolved phage lines with ECOR34 revealed a single shared SNP located in a non-coding intergenic region of the reverse strand. Further analysis revealed that this region aligns with the rnaC–rnaD noncoding RNA cluster described in phage T4 (Miller et al., 2003). These two adjacent ncRNAs have unknown functions but are thought to play regulatory roles. In BW1, *rnaC* appears to be relatively conserved, whereas *rnaD* is more degenerated. The SNP in question lies within the 3′ end of *rnaD*, around position 41 of the predicted transcript. Using RNAfold, we found that the rnaD region in BW1 (with and without the SNP) appears to adopt more stable secondary structures than the corresponding region in phage T4, which is more structurally flexible. This increased structural stability in BW1 may reflect reduced regulatory flexibility, potentially affecting the timing or expression of downstream genes. We emphasize that these predictions are exploratory, and the precise structural and functional consequences of this SNP remain to be fully determined.

The lack of host shifts might be explained by their cost. Phages that evolved with ECOR69, when compared to the ancestral phage, displayed loss of virulence towards other hosts. These results suggest that a host shift might be more costly than beneficial in complex bacterial communities. Such hypothesis might explain the results of our experiment: acquiring a mutation that allows infection of other hosts may be so costly in terms of virulence that such mutants are not able to replicate fast enough in our experiments and therefore we were unable to detect them. Cost expressed as reduced virulence have been observed previously in bacteriophages infecting *Pseudomonas fluorescens* (Poullain et al., 2008; Wang et al., 2024). The genomic constraint observed in our WGS data further supports the idea that evolutionary paths toward broader host range may be both rare and deeply bounded by trade-offs or lack of mutational accessibility.

Our data also suggests that host shifts are not simply determined by genetic similarity of the new host to the pathogen's native host. Although our data do not have sufficient statistical power (due to a limited number of hosts) to test this definitively, it was not the case that hosts closely related to the native host range were easier to adapt to. In fact, the host where we observed adaptation (ECOR34) is the most distant to the native host range. An alternative hypothesis is that adaptation to new hosts is driven by the presence of specific components, like phage receptors (Bertozzi Silva et al., 2016; Burmeister et al., 2021) or plasmids (Jalasvuori et al., 2011; Shan et al., 2023), which can be transmitted

horizontally (Tzipilevich et al., 2017) and independently of phylogeny. The observed SNP in a regulatory region across all ECOR34-adapted phages may reflect subtle tuning of gene expression in response to these specific host factors, rather than structural changes in host-recognition proteins.

Our results have several implications for phage therapy. Our data support the prevailing view that host shifts are rare events due to high specificity of phages, and suggest that the risk of unintended phage activity on commensal bacteria is low, even under experimental conditions designed to promote such shifts. Nevertheless, host shifts are still possible events, and our data show that adaptation to one host can result in either loss or gain of virulence towards different hosts. A recent study with *in vitro* and *in vivo* experiments using mice (De Sordi et al., 2017) found that intermediate hosts from gut microbiota are important for phage host shifts, but even in these cases, host shifts were observed only in 20% of the cases. These complementary findings imply that future studies looking at the safety of phages need to incorporate the complexity of the gut microbiota. A future study could perform *in vitro* evolution experiments like ours but using greater numbers of intermediate hosts (mixed bacterial communities) in the experimental regime.

It is important to note, however, that the virulence assays used in our study rely on RGB signal reduction in liquid cultures, which may reflect not only bacterial lysis but also general growth inhibition or metabolic suppression. This contrasts with traditional agar plate assays, which provide a more direct measure of lytic activity. While our approach offers a scalable and high-throughput alternative, it is limited in its ability to distinguish between these different modes of bacterial suppression. Previous authors have noted that observations of phage-bacteria interactions in liquid and on agar surfaces sometimes differ (Hyman and Abedon, 2010; Koskella and Meaden, 2013). Future studies could address this limitation by conducting comparative virulence analyses using both agar plate and liquid culture methods. This would help clarify whether observed reductions in bacterial growth are due to true lysis or other inhibitory effects. This is an important distinction, especially considering that a phage might still reduce bacterial growth despite being unable to lyse the host effectively through its ancestral mechanisms. Additionally, characterizing the physiological and genetic mechanisms that enable or constraint host shifts, including regulatory regions like the one identified in our study, could help map the distribution of potential host-switching pathways across the microbiota. Identifying key elements such as phage receptors or mobile plasmids, and assessing their prevalence and transferability, would provide valuable insights into the dynamics and risks of host range evolution in therapeutic contexts.

Data availability statement

The datasets generated and analyzed in this study are available in the Zenodo repository at https://zenodo.org/records/17353398.

Ethics statement

Ethical approval was not required for this study because no experiments were conducted on animals or humans. All experiments were performed in vitro using bacterial strains, some of which were isolated from animal sources. No work was performed directly on animals.

Author contributions

YN: Investigation, Writing – review & editing, Methodology, Writing – original draft, Data curation. EG-T: Writing – original draft, Software, Formal Analysis, Visualization, Data curation, Writing – review & editing. JW: Writing – review & editing, Methodology, Writing – original draft, Resources. FA-S: Software, Writing – original draft, Methodology, Investigation, Data curation, Formal Analysis, Resources, Funding acquisition, Writing – review & editing, Supervision, Project administration, Conceptualization, Visualization.

Funding

The author(s) declare financial support was received for the research and/or publication of this article. FA-S was funded by the German Science Foundation Principal Investigator grant DFG AR1359/1-1. YN was funded by the China Scholarship Council (Grant Number 202106910002).

Acknowledgments

We acknowledge Prof. Alex R. Hall for his input during the early stages of this work.

Conflict of interest

The authors declare that the research was conducted in the absence of any commercial or financial relationships that could be construed as a potential conflict of interest.

Generative AI statement

The author(s) declare that Generative AI was used in the creation of this manuscript. Generative AI was used as a tool to improve the grammar and clarity of the final text, as the majority of the authors are not native English speakers. Generative AI was not used to create any of the data in this manuscript.

Any alternative text (alt text) provided alongside figures in this article has been generated by Frontiers with the support of artificial

intelligence and reasonable efforts have been made to ensure accuracy, including review by the authors wherever possible. If you identify any issues, please contact us.

Publisher's note

All claims expressed in this article are solely those of the authors and do not necessarily represent those of their affiliated organizations, or those of the publisher, the editors and the reviewers. Any product that may be evaluated in this article, or claim that may be made by its manufacturer, is not guaranteed or endorsed by the publisher.

Supplementary material

The Supplementary Material for this article can be found online at: https://www.frontiersin.org/articles/10.3389/fcimb.2025.1597805/full#supplementary-material

References

Ackermann, H.-W., and Krisch, H. M. (1997). A catalogue of T4-type bacteriophages. *Arch. Virol.* 142, 2329–2345. doi: 10.1007/s007050050246

Allen, R. C., Pfrunder-Cardozo, K. R., Meinel, D., Egli, A., and Hall, A. R. (2017). Associations among antibiotic and phage resistance phenotypes in natural and clinical Escherichia coli isolates. *MBio* 8, e01341–17. doi: 10.1128/mBio.01341-17

Angermeyer, A., Hays, S. G., Nguyen, M. H. T., Johura, F. T., Sultana, M., Alam, M., et al. (2021). Evolutionary sweeps of subviral parasites and their phage host bring unique parasite variants and disappearance of a phage CRISPR-cas system. *MBio* 13, e0308821. doi: 10.1128/mbio.03088-21

Bankevich, A., Nurk, S., Antipov, D., Gurevich, A. A., Dvorkin, M., Kulikov, A. S., et al. (2012). SPAdes: A new genome assembly algorithm and its applications to single-cell sequencing. *J. Comput. Biol.* 19, 455–477. doi: 10.1089/cmb.2012.0021

Benmayor, R., Hodgson, D. J., Perron, G. G., and Buckling, A. (2009). Host mixing and disease emergence. *Curr. Biol.* 19, 764–767. doi: 10.1016/j.cub.2009.03.023

Bertozzi Silva, J., Storms, Z., and Sauvageau, D. (2016). Host receptors for bacteriophage adsorption Downloaded from. *FEMS Microbiol. Lett.* 363, fnw002. Available online at: http://femsle.oxfordjournals.org/ (Accessed September 02, 2018).

Bigot, T., Temmam, S., Pérot, P., and Eloit, M. (2020). RVDB-prot, a reference viral protein database and its HMM profiles. *F1000Research* 8, 1–12. doi: 10.12688/f1000research.18776.2

Bohannan, B. J. M., and Lenski, R. E. (2000). Linking genetic change to community evolution: insights from studies of bacteria and bacteriophage. *Ecol. Lett.* 3, 362–377. doi: 10.1046/j.1461-0248.2000.00161.x

Borin, J. M., Avrani, S., Barrick, J. E., Petrie, K. L., and Meyer, J. R. (2021). Coevolutionary phage training leads to greater bacterial suppression and delays the evolution of phage resistance. *Proc. Natl. Acad. Sci. United States America* 118, e2104592118. doi: 10.1073/pnas.2104592118

Brister, J. R., Ako-Adjei, D., Bao, Y., and Blinkova, O. (2015). NCBI viral Genomes resource. *Nucleic Acids Res.* 43, D571–D577. doi: 10.1093/nar/gku1207

Buckling, A., and Rainey, P. B. (2002). 2002 The role of parasites in sympatric and allopatric host diversification.pdf. *Nature* 420, 496–499. doi: 10.1038/nature01164

Burmeister, A. R., Sullivan, R. M., Gallie, J., and Lenski, R. E. (2021). Sustained coevolution of phage lambda and escherichia coli involves inner- as well as outer-membrane-Defences and counter-Defences. *Microbiol. (United Kingdom)* 167, 001063. doi: 10.1099/MIC.0.001063

Chen, M., Zhang, L., Abdelgader, S. A., Yu, L., Xu, J., Yao, H., et al. (2017). Alterations in gp37 expand the host range of a T4-like phage. *Appl. Environ. Microbiol.* 83, e01576–17. doi: 10.1128/AEM.01576-17

Cleaveland, S., Laurenson, M. K., and Taylor, L. H. (2001). Diseases of humans and their domestic mammals: Pathogen characteristics, host range and the risk of emergence. *Philos. Trans. R. Soc. B* 356, 991–999. doi: 10.1098/rstb.2001.0889

De Sordi, L., Khanna, V., and Debarbieux, L. (2017). The gut microbiota facilitates drifts in the genetic diversity and infectivity of bacterial viruses. *Cell Host Microbe* 22, 801–808.e3. doi: 10.1016/j.chom.2017.10.010

Gonzalez-Tortuero, E., Krishnamurthi, R., Goodhead, I., Allison, H., and James, C. (2022). Improving phage genome annotation to understand phage biology: the case of Pseudomonas aeruginosa LES prophages. *Access Microbiol.* 4, 277509. doi: 10.1099/acmi.ac2021.po0318

González-Tortuero, E., Sean Sutton, T. D., Velayudhan, V., Shkoporov, A. N., Draper, L. A., Stockdale, S. R., et al. (2018). VIGA: A sensitive, precise and automatic *de novo* VIral Genome Annotator. *BioRxiv*. doi: 10.1101/277509

Green, M. R., and Sambrook, J. (2012). "Molecular cloning: A laboratory manual," in *Dong wu xue yan jiu = Zoological research/"Dong wu xue yan jiu" bian ji wei yuan hui bian ji*, vol. 1. (Yunnan, China: Cold Spring Harbor Laboratory Press). doi: 10.3724/sp.j.1141.2012.01075

Hall, A. R., Scanlan, P. D., and Buckling, A. (2011). Bacteria-phage coevolution and the emergence of generalist pathogens. *Am. Nat.* 177, 44–53. doi: 10.1086/657441

Hashemolhosseini, S., Montag, D., Kramer, L., and Henning, U. (1994). Determinants of receptor specificity of coliphages of the T4 family. A chaperone alters the host range. *J. Mol. Biol.* 241, 524–533. doi: 10.1006/jmbi.1994.1529

Hyman, P., and Abedon, S. T. (2010). "Bacteriophage host range and bacterial resistance," in *Advances in Applied Microbiology*, *1st ed*, vol. 70. (Amsterdam, The Netherlands: Elsevier Inc). doi: 10.1016/S0065-2164(10)70007-1

Jalasvuori, M., Friman, V. P., Nieminen, A., Bamford, J. K. H., and Buckling, A. (2011). Bacteriophage selection against a plasmid-encoded sex apparatus leads to the loss of antibioticresistance plasmids. *Biol. Lett.* 7, 902–905. doi: 10.1098/rsbl.2011.0384

Jombart, T., Balloux, F., and Dray, S. (2010). adephylo: New tools for investigating the phylogenetic signal in biological traits. *Bioinformatics* 26, 1907–1909. doi: 10.1093/bioinformatics/btq292

Kaper, J. B., Nataro, J. P., and Mobley, H. L. T. (2004). Pathogenic escherichia coli. *Nat. Rev. Microbiol.* 2, 123–140. doi: 10.1038/nrmicro818

Kim, M. J., Bae, H. E., Kwon, S., Park, M. K., Yong, D., Kang, M. J., et al. (2023). Phage-targeting bimetallic nanoplasmonic biochip functionalized with bacterial outer membranes as a biorecognition element. *Biosensors Bioelectronics* 238, 115598. doi: 10.1016/j.bios.2023.115598

Koskella, B., Hernandez, C. A., and Wheatley, R. M. (2022). Understanding the impacts of bacteriophage viruses: from laboratory evolution to natural ecosystems. *Annu. Rev. Virol.* 9, 57–78. doi: 10.1146/annurev-virology-091919-075914

Koskella, B., and Meaden, S. (2013). Understanding bacteriophage specificity in natural microbial communities. *Viruses* 5, 806–823. doi: 10.3390/v5030806

Langmead, B., and Salzberg, S. L. (2012). Fast gapped-read alignment with Bowtie 2. *Nat. Methods* 9, 357–359. doi: 10.1038/nmeth.1923

Lee, C.-Y. (2024). Exploring potential intermediates in the cross-species transmission of influenza A virus to humans. *Viruses* 16, 1129. doi: 10.3390/v16071129

Li, L., Wu, Y., Ma, D., Zhou, Y., Wang, L., Han, K., et al. (2022). Isolation and characterization of a novel Escherichia coli phage Kayfunavirus ZH4. *Virus Genes* 58, 448–457. doi: 10.1007/s11262-022-01916-6

Liu, W., Li, Y., Learn, G. H., Rudicell, R. S., Robertson, J. D., Keele, B. F., et al. (2010). Origin of the human malaria parasite Plasmodium falciparum in gorillas. *Nature* 467, 420–425. doi: 10.1038/nature09442

Longdon, B., Brockhurst, M. A., Russell, C. A., Welch, J. J., and Jiggins, F. M. (2014). The evolution and genetics of virus host shifts. *PLoS Pathog.* 10, e1004395–8. doi: 10.1371/journal.ppat.1004395

Longdon, B., Hadfield, J. D., Webster, C. L., Obbard, D. J., and Jiggins, F. M. (2011). Host phylogeny determines viral persistence and replication in novel hosts. *PLoS Pathog.* 7, e1002260. doi: 10.1371/journal.ppat.1002260

Marchi, J., Zborowsky, S., Debarbieux, L., and Weitz, J. S. (2023). The dynamic interplay of bacteriophage, bacteria and the mammalian host during phage therapy. *IScience* 26, 106004. doi: 10.1016/j.isci.2023.106004

Marz, M., Beerenwinkel, N., Drosten, C., Fricke, M., Frishman, D., Hofacker, I. L., et al. (2014). *bioinformatics%2Fbtu105.pdf*. (Oxford, England), 1–7.

Michel, A., Clermont, O., Denamur, E., and Tenaillon, O. (2010). Bacteriophage PhiX174's ecological niche and the flexibility of its escherichia coli lipopolysaccharide receptor. *Appl. Environ. Microbiol.* 76, 7310–7313. doi: 10.1128/AEM.02721-09

Miller, E. S., Kutter, E., Mosig, G., Arisaka, F., Kunisawa, T., and Rüger, W. (2003). Bacteriophage T4 genome. *Microbiol. Mol. Biol. Rev.* 67, 86–156. doi: 10.1128/mmbr.67.1.86-156.2003

Mirzaei, M. K., and Maurice, C. F. (2017). Ménage à trois in the human gut: Interactions between host, bacteria and phages. *Nat. Rev. Microbiol.* 15, 397–408. doi: 10.1038/nrmicro.2017.30

Mollentze, N., and Streicker, D. G. (2020). Viral zoonotic risk is homogenous among taxonomic orders of mammalian and avian reservoir hosts. *Proc. Natl. Acad. Sci. United States America* 117, 9423–9430. doi: 10.1073/pnas.1919176117

Montag, D., Hashemolhosseini, S., and Henning, U. (1990). Receptor-recognizing proteins of T-even type bacteriophages. The receptor-recognizing area of proteins 37 of phages T4 TuIa and TuIb. *J. Mol. Biol.* 216, 327–334. doi: 10.1016/S0022-2836(05)80324-9

Moura de Souza, J. A., Pfeifer, E., Touchon, M., and Rocha, E. P. C. (2021). Causes and consequences of bacteriophage diversification via genetic exchanges across lifestyles and bacterial taxa. *Mol. Biol. Evol.* 38, 2497–2512. 10.1093/molbev/msab044

Nurk, S., Meleshko, D., Korobeynikov, A., and Pevzner, P. A. (2017). MetaSPAdes: A new versatile metagenomic assembler. *Genome Res.* 27, 824–834. doi: 10.1101/gr.213959.116

Ochman, H., and Selander, R. K. (1984). Standard reference strains of Escherichia coli from natural populations. *J. Bacteriology* 157, 690–693. doi: 10.1128/jb.157.2.690-693.1984

Poullain, V., Gandon, S., Brockhurst, M. A., Buckling, A., and Hochberg, M. E. (2008). The evolution of specificity in evolving and coevolving antagonistic interactions between a bacteria and its phage. *Evolution* 62, 1–11. doi: 10.1111/j.1558-5646.2007.00260.x

R Core Team (2015). *R: A Language and Environment for Statistical Computing* (Vienna, Austria: R Foundation for Statistical Computing). 2014. R Foundation for Statistical Computing. *R Foundation for Statistical Computing, Vienna, Austria.*, 2, 2019.

Scanlan, P. D., Hall, A. R., Burlinson, P., Preston, G., and Buckling, A. (2013). No effect of host-parasite co-evolution on host range expansion. *J. Evolutionary Biol.* 26, 205–209. doi: 10.1111/jeb.12021

Schneider, V. A., Graves-Lindsay, T., Howe, K., Bouk, N., Chen, H. C., Kitts, P. A., et al. (2017). Evaluation of GRCh38 and *de novo* haploid genome assemblies demonstrates the enduring quality of the reference assembly. *Genome Res.* 27, 849–864. doi: 10.1101/gr.213611.116

Seal, S., Dharmarajan, G., and Khan, I. (2021). Evolution of pathogen tolerance and emerging infections: A missing experimental paradigm. *ELife* 10, 68874. doi: 10.7554/eLife.68874

Shan, X., Szabo, R. E., and Cordero, O. X. (2023). doi: 10.1038/s41467-023-37512-x

Sharp, P. M., and Hahn, B. H. (2010). The evolution of HIV-1 and the origin of AIDS. *Philos. Trans. R. Soc. B* 365, 2487–2494. doi: 10.1098/rstb.2010.0031

Shkoporov, A. N., and Hill, C. (2019). Bacteriophages of the human gut: the "Known unknown" of the microbiome. *Cell Host Microbe* 25, 195–209. doi: 10.1016/j.chom.2019.01.017

Siniagina, M. N., Markelova, M. I., Boulygina, E. A., Laikov, A. V., Khusnutdinova, D. R., Abdulkhakov, S. R., et al. (2021). Diversity and adaptations of escherichia coli strains: Exploring the intestinal community in crohn's disease patients and healthy individuals. *Microorganisms* 9, 1299. doi: 10.3390/microorganisms9061299

Sorek, R., Kunin, V., and Hugenholtz, P. (2008). CRISPR - A widespread system that provides acquired resistance against phages in bacteria and archaea. *Nat. Rev. Microbiol.* 6, 181–186. doi: 10.1038/nrmicro1793

Sutton, T. D. S., Clooney, A. G., Ryan, F. J., Ross, R. P., and Hill, C. (2019). Choice of assembly software has a critical impact on virome characterisation. *Microbiome* 7, 1–15. doi: 10.1186/s40168-019-0626-5

Taslem Mourosi, J., Awe, A., Guo, W., Batra, H., Ganesh, H., Wu, X., et al. (2022). Understanding bacteriophage tail fiber interaction with host surface receptor: the key "Blueprint" for reprogramming phage host range. *Int. J. Mol. Sci.* 23, 12146. doi: 10.3390/ijms232012146

Tenaillon, O., Skurnik, D., Picard, B., and Denamur, E. (2010). The population genetics of commensal Escherichia coli. *Nat. Rev. Microbiol.* 8, 207–217. doi: 10.1038/nrmicro2298

Terzian, P., Olo Ndela, E., Galiez, C., Lossouarn, J., Pérez Bucio, R. E., Mom, R., et al. (2021). PHROG: Families of prokaryotic virus proteins clustered using remote homology. *NAR Genomics Bioinf.* 3, 1–12. doi: 10.1093/nargab/lqab067

Thines, M. (2019). An evolutionary framework for host shifts – jumping ships for survival. *New Phytol.* 224, 605–617. doi: 10.1111/nph.16092

Tzipilevich, E., Habusha, M., and Ben-Yehuda, S. (2017). Acquisition of phage sensitivity by bacteria through exchange of phage receptors. *Cell* 168, 186–199.e12. doi: 10.1016/j.cell.2016.12.003

Walsh, S. K., Imrie, R. M., Matuszewska, M., Paterson, G. K., Weinert, L. A., Hadfield, J. D., et al. (2023). The host phylogeny determines viral infectivity and replication across Staphylococcus host species. *PLoS Pathog.* 19, e1011433. doi: 10.1371/journal.ppat.1011433

Wang, J., Wang, X., Yang, K., Lu, C., Fields, B., Xu, Y., et al. (2024). Phage selection drives resistance–virulence trade-offs in Ralstonia solanacearum plant-pathogenic bacterium irrespective of the growth temperature. *Evol. Lett.* 8, 253–266. doi: 10.1093/evlett/qrad056

Webby, R. J., and Webster, R. G. (2001). Emergence of influenza A viruses. *Philos. Trans. R. Soc. B* 356, 1817–1828. doi: 10.1098/rstb.2001.0997

Wendling, C. C., Lange, J., Liesegang, H., Sieber, M., Pöhlein, A., Bunk, B., et al. (2022). Higher phage virulence accelerates the evolution of host resistance. *Proc. R. Soc. B* 289, 20221070. doi: 10.1098/rspb.2022.1070

Woolhouse, M. E. J., Haydon, D. T., and Antia, R. (2005). Emerging pathogens: The epidemiology and evolution of species jumps. *Trends Ecol. Evol.* 20, 238–244. doi: 10.1016/j.tree.2005.02.009

Frontiers in
Cellular and Infection Microbiology

Investigates how microorganisms interact with their hosts

Explores bacteria, fungi, parasites, viruses, endosymbionts, prions and all microbial pathogens as well as the microbiota and its effect on health and disease in various hosts.

Discover the latest Research Topics

See more →

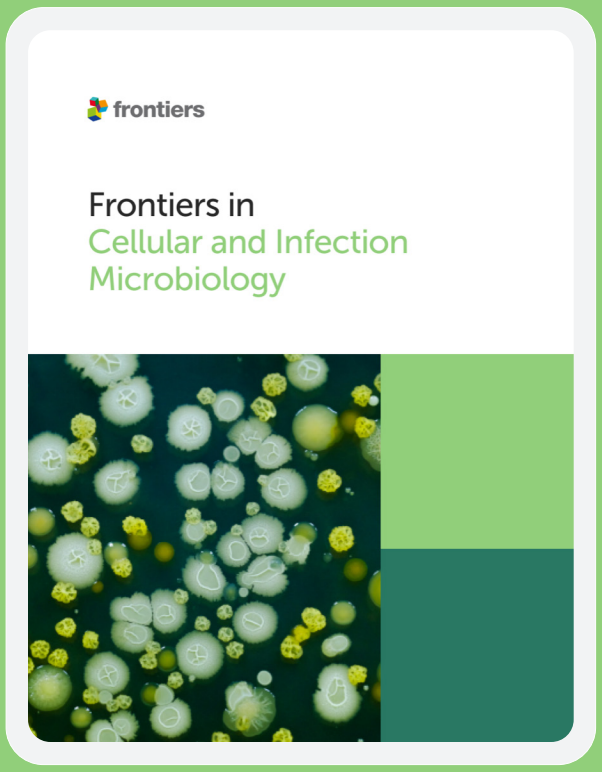

Frontiers

Avenue du Tribunal-Fédéral 34
1005 Lausanne, Switzerland
frontiersin.org

Contact us

+41 (0)21 510 17 00
frontiersin.org/about/contact